SOME MAGNETIC PROPERTIES OF DILUTE RARE - EARTH ALLOYS

Thesis submitted for the Degree of Doctor of Philosophy of the University of London.

by

GWYN WILLIAMS

Physics Department

Imperial College of Science and Technology

London, S.W.7

October, 1967

ACKNOWLEDGEMENTS

I would like to offer my sincere thanks to Professor B.R.Coles for his enthusiasm and guidance in all matters which arose during the course of this work, which was carried out at his suggestion and under his supervision. I am greatly indebted to Dr. L.L.Hirst for innumerable discussions, particularly during the fitting of the experimental data. Finally, I would like to offer my thanks to Dr. D. Griffiths for handing on the susceptibility balance with which this investigation was made; for his help during the design and construction of the servo-system, and for allowing me to make use of some of his unpublished e.p.r. data.

Financial support from the Science Research Council is also acknowledged.

ABSTRACT

The magnetic susceptibility of some dilute alloys has been measured between 2 and 300°K by a force method. The investigation has been concerned mainly with solid solutions of 1 at.% or less of the elements of the second half of the rare-earth series in silver or gold, in order to study local moments on the impurity ions. The observed departures of the susceptibility from a Curie-Weiss behaviour can be understood and fitted primarily in terms of crystal field effects. In some of the more concentrated alloys the effects of inter impurity interactions can be seen.

Measurements have also been made on Pd and Pd based alloys, in particular on some PdNi alloys in view of the recent theoretical and experimental interest in this system.

CONTENTS

	Page No.
ABSTRACT	3
INTRODUCTION	9
CHAPTER 1 - THE SUSCEPTIBILITY OF DIA AND PARAMAGNETS	
1. Introduction.	11
2. Alignment of permanent moments, Van Vleck paramagnetism and Core diamagnetism.	12
3. Pauli spin paramagnetism.	15
4. Conduction electron diamagnetism.	16
5. Effects of nuclear spin.	19
6. Saturation effects.	20
CHAPTER 2 - IMPURITY STATES IN DILUTE ALLOYS	
1. Introduction.	23
2. The impurity potential.	24
(a) Weak potential.	24
(b) Strong potential.	25
(c) Intermediate strength potential.	27
3. Screening	32
(a) Static screening.	34
(b) Screening of a strong potential.	37

Page No.

CHAPTER 3 - INTERACTIONS BETWEEN MAGNETIC IMPURITIES

1. Molecular field model. 44

2. Collective electron model. 46

3. Coupling mechanisms in dilute alloys. 48

(a) Zener 49

(b) Yosida 49

(c) Indirect interaction between virtual states. 54

4. Treatment of interaction effects. 58

CHAPTER 4 - GROUP THEORETICAL BACKGROUND; ITS APPLICATION TO THE PRESENT PROBLEM.

Background summary:

1. Finite groups - Matrix representations. 62

2. Application to quantum mechanics. 65

3. Continuous groups. 66

4. Point groups. 73

Crystal fields: 75

1. Strong fields. 76

2. Intermediate fields. 76

Page No.

3. Weak fields. 76

(a) Integral J 77

(b) Half integral J. 78

CHAPTER 5 - REVIEW OF PREVIOUS WORK.

1. Electrical resistivity 85

2. Magneto resistance 87

3. Specific heat 89

4. Thermopower. 91

5. Magnetic susceptibility 91

CHAPTER 6 - EXPERIMENTAL DETAILS

1. General 94

2. The magnetic balance. 95

3. Temperature measurements. 99

4. Calibrations: 102

(a) Magnet 102

(b) Temperature. 104

5. Experimental procedure. 105

6. Errors in measurements. 109

7. The servo-system. 110

8. Servo-performance. 117

Page No.

CHAPTER 7* - EXPERIMENTAL RESULTS

General: 120

1. The Ag Gd system. 121

2. The Ag Tb system. 137

3. The Ag Dy system. 141

4. The Ag Ho system. 149

5. The Ag Er system. 157

6. The Ag Tm system. 165

7. The Ag Yb system. 169

8. The Au Er system. 172

9. The Au Tm system. 176

10. The Au Yb system. 180

CHAPTER 8* - DISCUSSION

1. S-State impurities. 184

2. Non S-state impurities. 188

3. Introduction. 188

4. Fitting the experimental data. 190

5. Concluding remarks. 207

Page No.

CHAPTER 9* - RESULTS AND DISCUSSION ON Pd AND SOME Pd BASED ALLOYS.

1. Dilute Pd-Rare-earth alloys 219

2. Pd and Pd-Ni alloys. 229

3. Pd-Pt. 242

APPENDICES 246

REFERENCES 272

ACKNOWLEDGEMENTS 2

* Some of the results in this section have been reported at the 1967 International Magnetism Conference (Boston, September 1967), and will appear in its Proceedings, to be published in J.App.Phys.

INTRODUCTION

Over the past decade much theoretical and experimental effort has been directed towards investigating the changes in electronic structure which occur when an impurity atom is introduced into a metallic host. Typically, in the case of dilute alloys of noble metals containing impurities from the 3d transition series, the bulk of the experimental evidence indicates that the inherent screening of the excess or defect charge of the impurity is accomplished by electrons in 'virtual' states. In spite of this, many theoretical approaches still regard the situation as being similar to that of a paramagnetic ion in an insulating matrix, where the impurity has a well defined magnetic moment associated with it. Such an approach is more likely to be applicable to the same solvents containing rare-earth impurities.

For such a model, the most influencial factor effecting the magnetic properties of the dilute alloy will be the cubic crystalline field of the noble metal host. This will raise the angular momentum degeneracy of the impurity f-electron terms, an

immediate consequence of which will be that the susceptibility associated with all non S-state impurities should exhibit departures from a Curie-law behaviour in some temperature range.

Data showing such characteristics are presented in this thesis, the interpretation of which is indeed discussed primarily in terms of empirically fitted cubic crystal field parameters.

CHAPTER 1

FACTORS CONTRIBUTING TO THE SUSCEPTIBILITY OF PARA AND DIAMAGNETIC MATERIALS.

1. Magnetic susceptibility

The most natural way to classify the magnetic properties of a material is by its response to an applied magnetic field. This response is characterised by the susceptibility χ in the relation

$$\underline{M} = \chi \underline{H} \qquad 1.1$$

where $\underline{M}$ is the magnetisation and $\underline{H}$ the applied field. In general χ can be a function of both $\underline{H}$ and the temperature T. If the material is magnetically isotropic, $\underline{M}$ and $\underline{H}$ are parallel and χ is a scalar; for magnetically anisotropic materials χ is a tensor. As equation (1.1) indicates, when the magnetisation is a linear function of the applied field the susceptibility will be independent of the field.

The experimentally determined susceptibility of dia and paramagnetic materials is the result of several contributing factors, these are listed below:-

(i) The alignment of permanent moments by the applied field.

(ii) The "Van-Vleck" term, arising from the perturbing effects of the applied field.

(iii) Core diamagnetism.

(iv) Pauli spin paramagnetism.

(v) Conduction electron diamagnetism.

2. The Hamiltonian for an atomic system in a magnetic field

On a simple basis, the Hamiltonian $\underline{H}$ for a free atomic system may be written, in the usual notation, as

$$\underline{H} = \sum_{\substack{i=1 \\ \text{electrons}}}^{n} \left(-\frac{\hbar^2}{2m_i}\nabla_i^2\right) + V \qquad 1.2$$

where V is some potential function. The application of a magnetic field to such a system can be taken into account by replacing the operator $(-i\nabla)$ by $(-i\nabla - e\underline{A}/c)$, where $\underline{A}$ is the vector potential[1]. Using this, equation (1.2) becomes :

$$\underline{H} = \sum_{\substack{i=1 \\ \text{electrons}}}^{n} \left(-\frac{\hbar^2}{2m_i}\nabla_i^2 - \frac{i e_i}{2M_i c}(\underline{A}\nabla_i + \nabla_i\underline{A}) + \frac{e_i^2 A^2}{2M_i c^2}\right) + V \qquad 1.3$$

When the applied field is along $\underline{z}$, and with a suitable choice of vector potential, equation (1.3) becomes[2] :

$$\underline{H} = \sum_{\substack{i=1 \\ \text{electrons}}}^{n} \left[-\frac{\hbar^2}{2m_i}\nabla_i^2 - \frac{ie_i\hbar}{2m_i c} H\left(y_i\frac{\partial}{\partial x_i} - x_i\frac{\partial}{\partial y_i}\right) + \frac{e_i^2 H^2}{8m_i c^2}(x_i^2+y_i^2)\right] + V \qquad 1.4$$

Assuming that the extra terms in this Hamiltonian can be treated by perturbation theory, and that a series development of the field strength dependent energy E_n is applicable, i.e. :

$$E_{njm} = E^o_{njm} + HE^{(1)}_{njm} + H^2E^{(2)}_{njm} \qquad 1.5$$

Van Vleck[2] has shown that the average magnetic moment, $\bar{m}_{Hnjm}$, associated with a given stationary state, the average being defined

as :

$$\bar{m}_{Hnjm} = \langle n,j,m \mid m_H \mid n,j,m \rangle = -\frac{\partial E_{njm}}{\partial H}$$

is given by :

$$\bar{m}_{Hnjm} = \langle n,j,m, \mid m_H^o \mid n,j,m \rangle + 2H \sum_{n'j'm' \neq njm} \frac{|\langle njm \mid m_H^o \mid n'j'm' \rangle|^2}{E_{n'j'm'} - E_{njm}}$$

$$- H \langle n,j,m \mid \sum_i \frac{e_i^2}{4m_i c^2} (x_i^2 + y_i^2) \mid n,j,m \rangle \qquad 1.6$$

The total magnetisation is the statistical mean over all eigenstates weighed according to the Boltzman factor $e^{-Enjm/kT}$, and multiplied by the number N of atoms per unit volume (to give the volume magnetisation M, say)

$$M = N \sum_{njm} \frac{\langle n,j,m \mid m_H \mid n,j,m \rangle e^{-Enjm/kT}}{\sum_{njm} e^{-Enjm/kT}} \qquad 1.7$$

Considering only that part of the susceptibility which is independent of the field strength, the development of equations (1.6) and (1.7) lead, in Van Vleck's notation, to

$$\chi = \frac{B}{kT} \sum_{jm} |\langle jm \mid m_H \mid jm \rangle|^2 e^{-E^o njm/kT}$$

$$+ 2B \sum_{jm \neq j'm'} \frac{|\langle jm \mid \mu_H \mid j'm' \rangle|^2 e^{-E^o njm/kT}}{E^o_{n'j'm'} - E^o_{njm}}$$

$$+ 2B \sum_{\substack{jmn'j'n' \\ (n' \neq n)}} \frac{|\langle njm \mid m_H^o \mid n'j'n \rangle|^2 e^{-E^o njm/kT}}{E^o_{n'j'm'} - E^o_{njm}} - \frac{Ne^2}{6mc^2} \Sigma(\bar{r^2}) \qquad 1.8$$

The first term in equation (1.8) corresponds to (i) in the list of factors contributing to the susceptibility, the magnitude of its contribution will depend on the temperature and on the distribution of moments over the various states. The second and third terms in (1.8) correspond to (ii); again the magnitude of their contribution depends on the detailed nature of the system, however at sufficiently high temperature its contribution is zero. The final term in equation (1.8) corresponds to (iii) in the previous list; as this equation indicates the evaluation of the diamagnetic contribution from the core requires an estimate of $(\bar{r^2})$, the time averaged value of the square of the radius of the electronic orbit. A typical magnitude for this term is 10^{-7} e.m.u/gm.

For later application it is instructive to consider the modification of equation (1.8) in situations where energy changes associated with changes in the quantum numbers n and j are very much larger than thermal energies (kT). Neglecting the diamagnetic terms this restriction reduces (1.8) to:

$$\chi = \frac{B}{kT} \sum_m |\langle jm|\mu_H|jm\rangle|^2 e^{-E^o njm/kT} + 2B \sum_{m\neq m'} \frac{|\langle njm|m^o H|njm'\rangle|^2 e^{-E^o njm/kT}}{E^o njm' - E^o njm} \qquad 1.9$$

If the further restriction that energy changes associated with changes in the quantum number m are very small compared with kT

is added, then the previous equation becomes:

$$\chi = \frac{Ng^2\beta^2 J(J+1)}{3kT} \qquad 1.10$$

where g is the Lande factor, β the Bohr magneton and J the total angular momentum quantum number.

This equation is often used to define an effective moment μ_{eff}, as:

$$\chi = \frac{N\mu_{eff}^2 \beta^2}{3kT} \qquad \text{thus } \mu_{eff} = \sqrt{\frac{3k}{N\beta^2}\, C}$$

where C is the slope of the ($\frac{1}{\chi}$ vs T) plot in the high temperature region. If the susceptibility per mole is used, then

$$\mu_{eff} = 2.839 \sqrt{C} \text{ Bohr magnetons.} \qquad 1.11$$

3. Pauli spin paramagnetism

The application of a magnetic field to a free electron gas causes a redistribution of electrons between the spin up and spin down states, as a result of the energy difference of $2\beta H$ induced by the field between the two spin orientations. This redistribution results in an excess number of electrons being oriented parallel to the applied field, H, producing a magnetisation per unit volume, M, given by[3]:

$$M = \frac{3M\beta}{4} \left(\frac{T}{T_f}\right)^{3/2} \left[F_{\frac{1}{2}}\left(\frac{\alpha+\beta H}{kT}\right) - F_{\frac{1}{2}}\left(\frac{\alpha-\beta H}{kT}\right)\right] \qquad 1.12$$

where Tf is the "degeneracy temperature", α the chemical potential, N the number of electrons per unit volume and $F_k(\eta)$ the

appropriate Fermi-Dirac integral.

At low temperatures equation (1.12) reduces to :

$$\chi_{\text{volume}} \approx \frac{3N\beta^2}{2kT_f} \qquad 1.13$$

(this is roughly equivalent to 10^{-7} e.m.u/gm for the noble metals). While in the classical, high temperature, limit:

$$\chi_{\text{Volume}} \approx \frac{N\beta^2}{kT} \qquad 1.14$$

For the case of electrons in metals, obeying Fermi-Dirac statistics, the volume susceptibility at temperature T not too large compared with T_f may be written[4]:

$$\chi_{\text{volume}} \approx 2\beta N(E_f)\left[1+ \frac{(\Pi kT)^2}{6}\left\{ \frac{d^2}{dE^2} (\log N(E))\right\}_{E:E_f}\right] \qquad 1.15$$

where $N(E)$ is the generalised density of states per unit volume. Equation (1.15) reduces to (1.13) when $N(E)$ is taken as the free electron density of states.

4. Conduction electron diamagnetism

If the conduction electrons are treated as a free electron gas, then application of classical mechanics indicates that the diamagnetic susceptibility is zero[5]. This result rests essentially on the fact that the magnetic forces do no work and hence the energy (or more generally the free energy F) must be field independent. Consequently the magnetic moment, which depends on

the derivative of F with respect to H, is zero. Indeed, on the classical basis the combined effects of the Curie-like paramagnetism and the core diamagnetism can be shown to vanish at all field strength.

On a quantum mechanical basis the situation is quite different. The application of a magnetic field to a free electron gas results in the electrons moving in quantized orbits about the field direction. Under these conditions, whether the electron gas is treated as degenerate or non-degenerate, the magnetic moment μ given by:

$$\mu = - \left(\frac{\partial F}{\partial H}\right)_{T,V} \qquad 1.16$$

is non-vanishing. For the non-degenerate case, in the classical, high temperature limit, the volume susceptibility can be written[6]:

$$\chi_{\text{volume}} \approx - \frac{1}{3} \frac{N\beta^2}{kT} \qquad 1.17$$

which is exactly one third of the Pauli spin contribution, equation (1.14), in the same limit.

When the electron gas is regarded as degenerate, and consequently treated with Fermi-Dirac statistics, the volume susceptibility becomes:

$$\chi_{\text{volume}} = - \frac{4\pi m}{3h^2} \left(\frac{3N}{\pi}\right)^{1/3} \beta^2 \qquad 1.18$$

where m is the electronic mass. This is the Landau formula; its magnitude is of the order of 10^{-7} e.m.u/gm.

The type of modification likely to be introduced by the periodic lattice field has been investigated by Peierls[7]; using wave functions obtained from the tight binding approach this author has obtained an expression for the volume susceptibility which, when the electronic energy E can be written as:

$$E = \frac{\hbar^2}{2m}\left(ak_x^2 + bk_y^2 + c\,k_z^2\right) \qquad 1.19$$

has the form:

$$\chi_{volume} = -\frac{4\pi m}{3h^2}\left(\frac{3N}{\pi}\right)^{1/3}\left[\frac{(ab)^2}{c}\right]^{1/3}\beta^2 \qquad 1.20$$

For free electrons equation (1.20) reduces to (1.18). The above equation indicates that the conduction electron diamagnetic susceptibility can depend strongly on the position of the Fermi surface relative to the zone boundaries.

The diamagnetism of Bloch electrons has been considered in some detail by Hebborn et al[8], who have considered a system of non interacting Bloch electrons subject to a magnetic field $\underline{H}$ given by:

$$\underline{H} = (0,\ 0,\ H_o \cos Ky)$$

with an associated vector potential

$$\underline{A} = \left(-\frac{H_o}{K}\sin Ky,\ 0,\ 0\right) \qquad 1.21$$

Using this form of vector potential in equation (1.3) shows that the Hamiltonian for the probelm can be expressed in the form:

where $\underline{H}_o$ is the field free Bloch Hamiltonian, and $\underline{H}_1$ and $\underline{H}_2$ are the magnetic perturbing terms given by:

$$\underline{H}_1 = 2i\beta\frac{Ho}{K} \sin Ky \frac{\partial}{\partial x} \quad \text{and} \quad \underline{H}_2 = \frac{2m}{h^2} \frac{\beta^2 Ho^2}{K^2} \sin^2 Ky$$

Using Maxwell-Boltzmann statistics the field independent susceptibility is calculated by using the term in $\underline{H}_o^2$ in the expansion of the energy-trace exp.$(-\underline{H}/kT)$ - in powers of $\underline{H}_1$ and $\underline{H}_2$[9]. At the end of the calculation K is allowed to tend to infinity so that the response to a steady field is examined. In addition a transformation from classical to quantum statistics is employed. The resulting susceptibility has four contributing terms; one of these is the analogue of the Landau-Peierls diamagnetism, having a form similar to the expression given by Peierls; a second term corresponds to atomic diamagnetism (including a "Van Vleck" like term), while the remaining contributions are "mixed terms", numerical estimates of which have not been made.

5. Effects of nuclear spin

The effect of including nuclear spin, represented by the quantum number I and possessing an associated magnetic moment μ_I defined by:

$$\mu_i = g_I I\beta; \quad g_I \text{ - the "nuclear g factor"} \qquad 1.22$$

is to introduce an additional contribution to the susceptibility.

Provided that the width of the hyperfine multiplet is small compared with thermal energies (kT), then it can be shown, using arguments similar to those used by Van Vleck to discuss the breakdown of "LS" coupling and its attendant effects, that the form of the nuclear contribution to the susceptibility is the same in either case of J and I remaining coupled or becoming decoupled. The inclusion of this contribution into equation (1.10) modifies the latter to:

$$\chi = \frac{N\beta^2}{3kT}\left[g_J^2 J(J+1) + g_I^2 I(I+1)\right] \qquad 1.23$$

A typical value of g_I defined in equation (1.22) is 10^{-3}, and hence its contribution in this approximation is vanishingly small.

In the opposite approximation, in which only the lowest hyperfine level is occupied, the contribution to the susceptibility depends to some extent on whether hyperfine coupling is valid. This situation will be discussed more fully later.

6. Saturation effects

Within the frame work of the assumptions leading to equation (1.10), the general expression for the magnetisation, equation (1.7), becomes

$$M = N\sum_{mj} \frac{m_J g_J \beta e^{m_J g \beta H/kT}}{\sum_{mj} e^{m_J g \beta H/kT}} \qquad 1.24$$

This expression may be evaluated in a closed form, giving[10]

$$M = NJg_J\beta\, B_J\left(\frac{Jg_J\beta H}{kT}\right) \qquad 1.25$$

where $B_J(y)$ is the well known Brillouin function defined by:

$$B_J(y) = \frac{(2J+1)}{2J}\coth\left[\frac{(2J+1)y}{2J}\right] - \frac{1}{2J}\coth\left(\frac{y}{2J}\right) \qquad 1.26$$

The saturation moment predicted by equation (1.26) is $Jg_J\beta$. The Brillouin curve for $Gd^{+++}(^8S_{7/2})$ is drawn in figure (1.1), the example of an S-state ion has been choosen so that the effects of crystalline fields can, for many practical considerations, be neglected. The curve departs from linearity at a value of HT^{-1} equal to 1.93K oersted per ^oK, i.e. at 4.2^oK the magnetisation should become non linear in the magnetic field for fields of the order of 8K oersted. Such deviations are of some importance in connection with later discussion.

FIG(1:1). BRILLOUIN CURVE FOR Gd.

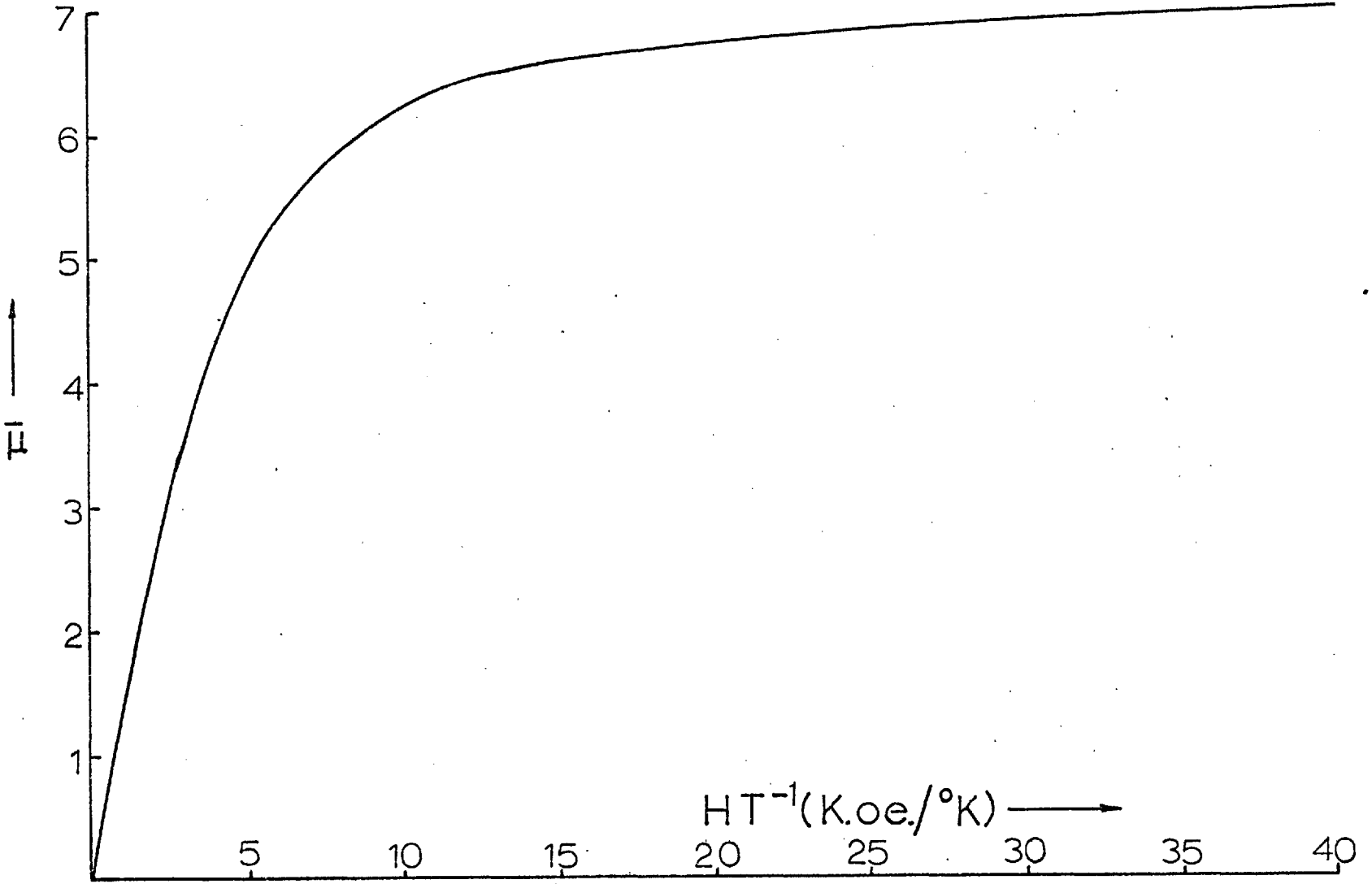

CHAPTER 2

A SUMMARY OF THE PERTURBING POTENTIALS ASSOCIATED WITH, AND THE CONDUCTION ELECTRON SCREENING OF IMPURITIES IN A DILUTE ALLOY.

1. Dilute alloys

Impurity atoms dissolved in some matrix are said to form a dilute metallic solid solution when the binary system is homogeneous and retains the crystal structure of the host metal. Further, the concentration of impurity atoms should be such that their mutual interaction is weak. Under these conditions the properties of the alloy will depend on the original electronic structure of the impurity and host materials, together with the modifications of these structures resulting from the interaction of the impurity with its nearest neighbour solvent atoms, caused by the overlap of their outer electronic wavefunctions.

On entering the host, the impurity will donate its valence electrons to the conduction band. If the number of electrons donated by the impurity is different from the number donated by each individual atom of the host, then a charge singularity will exist at the impurity lattice site. The two most important aspects of this situation are:-

(i) The correct description of the perturbing potential associated with the impurity site. This arises due to the departure from periodicity of the lattice field due to the presence of the impurity, with a consequent scattering of Bloch electrons.

(ii) The redistribution of conduction electron charge density around the impurity so that the associated charge singularity is screened.

2. The impurity potential

A discussion of the impurity perturbing potential may be conveniently subdivided according to whether this potential constitutes a weak, strong or intermediate strength perturbation of the system.

(a) Weak potential - The rigid band approximation

Under these conditions the effect of the impurity can be ascertained by using perturbation theory[11]. This indicates that ΔE, the first order change in energy of Bloch conduction electrons, given by the expectation value of the perturbing potential V_p, is independent of the wave vector $\underline{k}$ labelling the conduction $\psi_{\underline{k}}(\underline{r})$ electron states, provided that the associated state function can be written as

$$\psi_{\underline{k}}(\underline{r}) = \psi_o(\underline{r})\, e^{i\underline{k}.\underline{r}} \qquad 2.1$$

with $\psi_o(\underline{r})$ showing little dependence on $\underline{k}$, and that Vp varies slowly in distances of the order of k^{-1}. Under these conditions the energy of every state in the band is changed by the same amount. Consequently the relationship between the density of states in the alloy Na(E) and in the pure metal $N_m(E)$ is :

$$Na(E) = N_m(E \pm \Delta E) \qquad 2.2$$

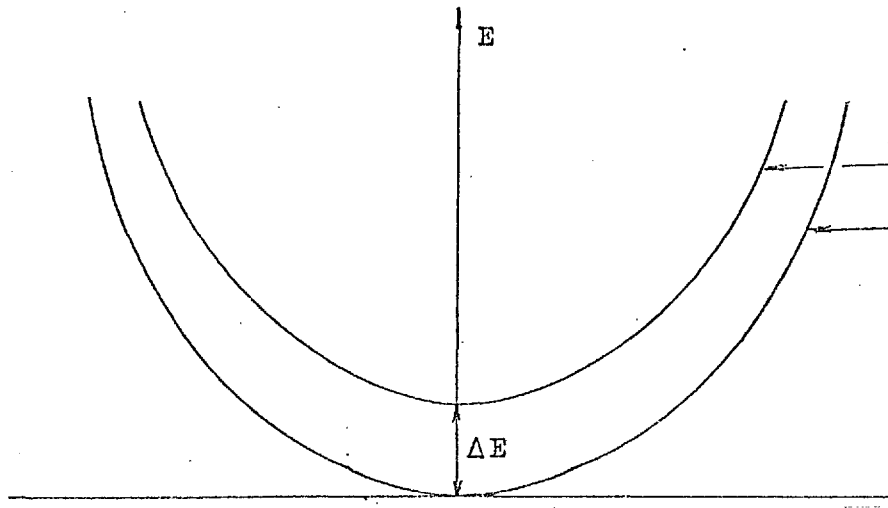

Fig.(2:1)

From Ref. 12.

(b) Strong potential

The effects of a strong impurity potential have been treated by Koster and Slater[13]. These authors have investigated the case of a perturbation localised on one lattice site, and have calculated its effects on the wavefunctions of a single band in a simple cubic lattice using a Green's function technique. The energies of the unperturbed lattice were taken as :

$$E = E(o) + 2E(1)[\cos k_x R + \cos k_y R + \cos k_z R] \qquad 2.3$$

The results of the calculation indicated that a bound state is removed from the top or bottom of the band, depending on the sign of the perturbation, when the expectation value of the perturbing potential exceeds $\Delta E(1)$. The state function of this bound state in the region outside the potential well of the impurity having the

form

$$\frac{e^{-\alpha r}}{r} \qquad 2.4$$

where α is a parameter depending on the energy difference between the bound state and the bottom (or top) of the well. Equation (2.4) indicates that as the depth of the well increases the state function of the bound state becomes increasingly confined to the well; falling off increasingly rapidly in the exponential region outside. Consequently, for an extremely deep well the state function becomes negligible outside the well while inside it becomes idential with that of a true bound state of the impurity.

When the impurity excess charge is positive with respect to the matrix, and the potential of sufficient strength, a bound state will be formed below the bottom of the conduction band. This state will be filled by an electron from the band. In the opposite situation, with a state pushed above the Fermi level, it becomes energetically unfavourable for an electron to remain in this state and this will consequently be donated to the band. In each case the charge difference between the impurity and the matrix will be reduced by one.

This concept of the emptying of a bound state pushed above the Fermi level has been used by Friedel[11] to explain the difference in average impurity moment of Cr and Mn in Ni.

(c) Intermediate strength potentials

As the strength of the impurity potential, initially strong enough to remove a bound state below the conduction band, is reduced, the state rises in energy and, according to equation (2.4) becomes spacially more extended. If the impurity potential is sufficiently reduced in strength, this state crosses the bottom of the conduction band and merges into the continuum of extended band states. Interaction can then take place between the state and the conduction band states of the same energy and appropriate symmetry, causing the former to become broadened in space and energy - it becomes what Friedel terms a virtual bound state.

This situation is analogous to the virtual binding of a particle of energy E incident on a double potential barrier of height $V_b > E$[14]. The situation is depicted in figure (2.2). The usual spatial variation of the state-function is shown in figure (2.2a), but for certain values of the incident energy the variation shown in figure (2.2b) can occur, which corresponds to the situation above. The oscillatory nature of the state-function over all space outside the well corresponds to the fact that in "real" situations, having entered the conduction band, the state can no longer be described as truly bound since it is characterised by positive kinetic energy throughout the whole lattice.

In reality, potential barriers of the kind represented in

FIG(2:2a)

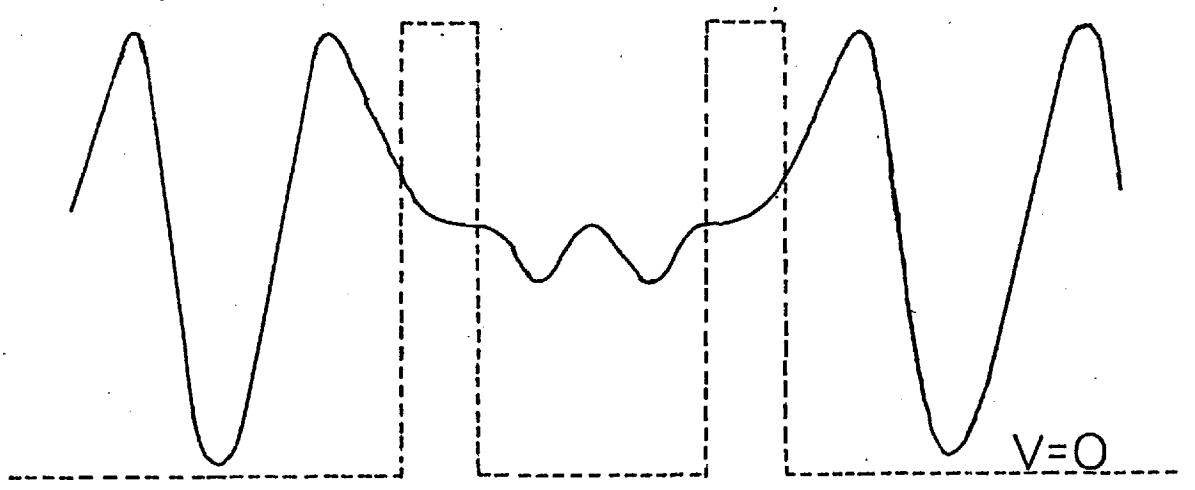

FIG(2:2b)

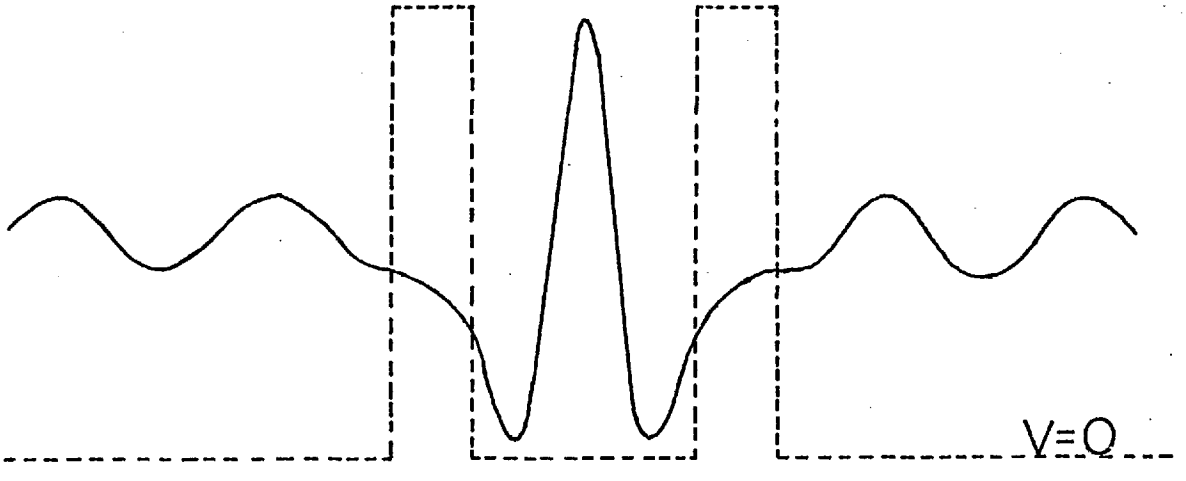

FIG(2:3)

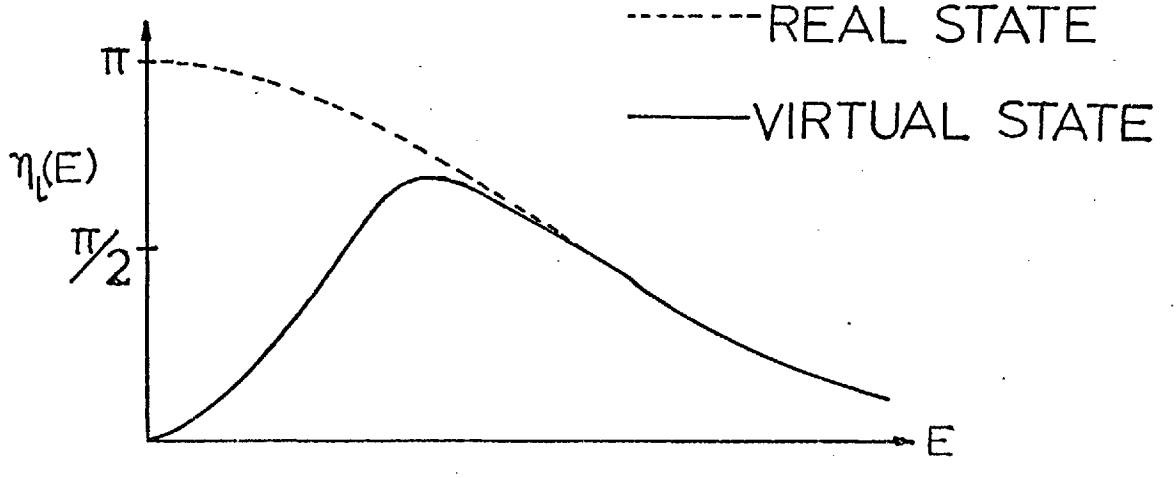

figure (2.2) can arise from the modification of some attractive potential function V(r) by the centrifugal potential term appearing in the radial wave equation for a partial wave of angular momentum $\ell\hbar > 0$.

The finite lifetime of a virtual state, a consequence of its energy broadening, implies a trapping and subsequent delayed scattering of conduction electrons. This effect is particularly strong for conduction electron states of the right energy and symmetry since these have a large amplitude in the vicinity of the impurity - figure (2.2b). The scattering can be investigated by examining the phase shift η_ℓ of that component of the extended conduction band state of angular momentum $\ell\hbar$. Figure (2.3) shows schematically the phase shift $\eta_\ell(E)$ for a real and a virtual bound state, and typifies the numerical calculations of Blandin and Friedel[15]. The density of states in energy for the virtual state is obtained by differentiating equation (2.19) with respect to energy, giving :

$$n_v(E) = dZ/dE = \frac{2}{\pi} \sum_\ell (2\ell+1) \frac{d\eta_\ell}{dE} \qquad 2.5$$

thus showing that the maximum density of the virtual state, $n(E_o)$, occurs at the point where the $(\eta_\ell(E) - E)$ curve has a point of inflexion. E_o, thus defined, can be taken as the centre of the state. Further, the width, in energy, can be defined as the difference $E_1 - E_2$ where

$$(E_1) = \tfrac{1}{2}\eta\,(E_o) \quad : \quad (E_2) = 3/2\eta\,(E_o)$$

The properties of the virtual states so defined may be summarised as follows:-

(i) The symmetry is determined by that of the bound state from which it was derived.

(ii) The large amplitude of the resonating conduction band states, when summed over the virtual state, is approximately equal to that of the original bound state, and is related to its excess charge.

(iii) At a given energy E_o, the width of the state increases as the amount of conduction band state of the same energy and symmetry increases. Thus for a given E_o the width decreases with increasing angular momentum $\ell\hbar$.

(iv) For a given value of ℓ, the width is roughly proportional to the energy Eo, measured from the top of the 'well'.

Figure (2.3) indicates that the variation of phase shift with electron energy near the centre of the virtual level is quite rapid. Thus the properties of an alloy having its Fermi level in this region is highly sensitive to electron concentration. Indeed, a small change in average electron concentration can sweep the Fermi level through the virtual state; this is precisely the mechanism used by Friedel[16] to explain the variation in residual resistivity of first row transition impurities in Al. The broad peak around

Cr being attributed to resonant scattering of the Fermi electrons of Al by the broadened d shell of the impurity as the level crosses the Fermi level.

The concept of a virtual state split by exchange interaction into spin up and spin down substates was qualitatively introduced by Friedel[16], and has since received mathematical treatment by several authors. Closely associated with this concept is that of a magnetised virtual state formed when one of the spin states is full and the other, overlapping the Fermi level, is partly empty. The approach of Wolff[17] to this situation is perhaps best suited to normal metal impurities in other normal metals, while that of Anderson[18] to transition metal impurities in normal metals.

As this thesis is primarily concerned with the magnetic properties of noble metals containing small amounts of rare earth impurities, it seems appropriate, following the above discussion, to formulate a preliminary description of the rare earth impurity states in these matrices. Many properties of the rare earths - typically chemical bonding - indicate that the 4f shell, although unfilled, is energetically low lying compared with the 5d and 6s shells, and its electronic wavefunctions are well localised within these shells. This suggests that in alloys of the above type the 4f electrons would exist in real bound states below the bottom of the conduction band, in which case their associated wavefunctions would not be unlike atomic 4f wavefunctions, or

in rather narrow virtual states near the bottom of the band. This last conclusion is indicated by the Anderson approach which would seem particularly applicable in view of the well localised nature of the 4f wavefunctions. In most chemical compounds the rare earth's appear as tripositive ions, and in this configuration the number of 4f electrons, for the later half of the series, increases uniformly from $4f^7$ in Gd to $4f^{14}$ in Lu. Consequently one would expect these real or virtual states to accommodate a number of electrons consistent with these figures.

One final comment, Yb which occurs immediately before the end of the series has the $4f^{13}$ configuration when it occurs as a tripositive ion. In some circumstances it appears as a divalent ion indicating that it is sometimes energetically more favourable for it to complete its 4f shell. Effects of this type could occur in the alloy system of interest here, and would be clearly evident from the magnetic properties of the alloy.

3. Screening

One approach to investigating the redistribution of conduction electron charge density around an impurity so that its excess charge is screened is to examine the conduction electron response to a time dependent perturbation, $\Delta\mu(\underline{r},t)$, of frequency w, wave vector $\underline{q}$, growing slowly with time constance α[19,20] :

$$\Delta\mu(\underline{r},t) = \mu e^{i\underline{q}\cdot\underline{r}} . e^{iwt} . e^{\alpha t} \qquad 2.6$$

This perturbation causes the state $|\underline{k}\rangle = e^{i\underline{k}\cdot\underline{r}}$ to become mixed with the state $|\underline{k}+\underline{q}\rangle$, its wavefunction becoming:

$$\psi_{\underline{k}}(\underline{r},t) = |\underline{k}\rangle + \frac{\langle \underline{k}+\underline{q}|\Delta\mu|\underline{k}\rangle}{E(\underline{k})-E(\underline{k}+\underline{q})+\hbar w-i\hbar\alpha} |\underline{k}+\underline{q}\rangle \qquad 2.7$$

The modification of the wavefunction results in a change in charge density, $\Delta\rho(\underline{r},t)$, given by:

$$\Delta\rho(\underline{r},t) = e \sum_{\substack{\underline{k} \\ \text{occupied states}}} \left\{ |\psi_{\underline{k}}(\underline{r},t)|^2 - 1 \right\} \qquad 2.8$$

This approach can be generalised to cover real perturbations by including the complex conjugate in equation (2.6), and further by introducing the occupation function $f^o(\underline{k})$, the Fermi-Dirac function, which measures the probability of state $|\underline{k}\rangle$ being occupied in the unperturbed situation. The resulting $\Delta\rho(\underline{r},t)$ has an associated potential $\Delta\Phi(\underline{r},t)$, to which it is related via Poisson's Equation. Provided $\Delta\Phi(\underline{r},t)$ has the same space and time variation as $\Delta\rho(\underline{r},t)$, this equation can be solved for $\Delta\Phi(\underline{r},t)$ and hence, in analogy with equation (2.6), for Φ . However, this potential also effects the conduction electrons, hence to make the calculation self consistent the assumed perturbation $\Delta\mu(\underline{r},t)$ should contain $\nabla\Phi(\underline{r},t)$ so that

$\Delta\mu(\underline{r},t) = \Delta\Phi(\underline{r},t) + \Delta V(\underline{r},t)$, where $\Delta V(\underline{r},t) = Ve^{i\underline{q}\cdot\underline{r}} . e^{iwt} . e^{\alpha t} + c.c.$

is the externally applied perturbation. With this modification

$$\mu = \frac{V}{\varepsilon(\underline{q},w)} \quad \text{where} \quad \varepsilon(\underline{q},w) = 1 + \frac{4e^2\pi}{q^2} \sum_{\text{all}\underline{k}} \frac{f^o(\underline{k}) - f^o(\underline{k}+\underline{q})}{E(\underline{k})-E(\underline{k}+\underline{q})+\hbar w-i\alpha} \qquad 2.9$$

which indicates that the effective potential, μ, acting on the electrons is not the applied potential V, but the latter divided by a dielectric function $\varepsilon(\underline{q},w)$.

Finally for the case of several Fourier components, such that

$$\Delta V(\underline{r},t) = \iint V(\underline{q},w) e^{i\underline{q}\cdot\underline{r}} e^{iwt} \, d\underline{q}dw \qquad 2.10$$

$$\text{then } \Delta\mu(\underline{r},t) = \iint \frac{V(\underline{q},w)}{(\underline{q},w)} e^{i\underline{q}\cdot\underline{r}} e^{iwt} d\underline{q}dw$$

4. Static screening

In the case of static potential w=0. Confining attention to the region of small $\underline{q}$, such that

$$E(\underline{k}-\underline{q})-E(\underline{k}) \approx \underline{q}\cdot\nabla_{\underline{k}} E(\underline{k}) \quad \text{and} \quad f^o(\underline{k}) - f^o(\underline{k}+\underline{q}) = -q\frac{\partial f^o}{\partial E}\nabla_{\underline{k}} E(\underline{k})$$

then the expression for $\varepsilon(\underline{q},o)$ becomes, on replacing the sum in equation (2.9) first an integral over $\underline{k}$, and then transforming to one over E and approximating $(\frac{-\partial f^o}{\partial E})$ to a delta function at the Fermi level:

$$\varepsilon(\underline{q},o) \longrightarrow 1 + \frac{4e^2\pi}{q^2} n(E_f) \qquad 2.11$$

where $n(E_f)$ is the density of states at the Fermi level.

Applying these results to the problem of the screening of an impurity of excess charge Ze yields the following expression for the special dependence of the screened perturbation:

$$\Delta\mu(\underline{r}) = \frac{Ze^2}{r} \exp.(-\lambda r) \qquad 2.12$$

where $\lambda = 4\pi e^2 n(E_f)$. This is the same result as obtained by Mott[4,11,21] using the Thomas-Fermi approach. Equation (2.12) shows that screening occurs in a distance of order λ^{-1}, hence indicating that a high density of states at E_f is conducive to effective screening.

Equation (2.11) is, of course, approximate, being confined to small values of q, i.e. to potentials that are spacially slowly varying. To investigate the screening for all values of q it is necessary to evaluate explicitly the sum in equation (2.9), which would require a detailed knowledge of $E(\underline{k})$. Within the free electron model, at $0^{\circ}K$, the sum becomes an integral over $\underline{k}$ and leads to:

$$\varepsilon(\underline{q},o) = 1 + \frac{4\pi e^2}{q^2} n(E_f)\left[\tfrac{1}{2} + \frac{4k_f^2-q^2}{8k_f q} .\log\left|\frac{2k_f+q}{2k_f-q}\right|\right] \qquad 2.13$$

where k_f is the Fermi wave vector. When the screened potential of a point charge Ze is calculated in this scheme, its spacial dependence is given by

$$\mu(\underline{r}) = 4\pi Ze^2 \int \left\{ q^2 + 4\pi e^2 n(E_f)\left[\tfrac{1}{2} + \frac{4k_f^2-q^2}{8k_f q} .\log\left|\frac{2k_f+q}{2k_f-q}\right|\right]\right\}^{-1} e^{i\underline{q}.\underline{r}} d\underline{q} \qquad 2.14$$

The singularity in $\varepsilon(\underline{q},o)$, given in equation (2.13), at $q=2k_f$, will show up as a contribution to $\mu(\underline{r})$ and will modify the smooth exponential decay of the screening charge density, given by equation (2.12), into a form containing oscillations of wave vector $2k_f$[19], which, at large distances will have the form $r^{-3}\cos 2k_f r$. This long range oscillation is a common feature of different models set up to examine the problem of impurity screening. Several of these models are discussed below.

1. Friedel[11]

As indicated above, any approach to the problem of impurity screening which is based on a Thomas-Fermi type of approximation requires the perturbing potential Vp to vary slowly in a distance of the order of an electron wavelength. Friedel has performed a calculation in which this restriction has been removed, and shows that the introduction of a thin spherical potential well, of depth Vo and radius b, into a free electron gas results in a modification of electron density. Provided $k_f.b$ and $b.(2Vo)^{\frac{1}{2}} \ll \pi$ the change in electron density, $\Delta\rho(\underline{r})$, as a function of the distance r from the centre of the well can be written, in atomic units, as:

$$\Delta\rho(r) = \frac{-16b^3k_f^4Vo}{3\pi^2} \cdot F(2k_f r) \qquad 2.15$$

where $F(x) = X^{-4}(x\cos x - \sin x)$.

At large distances $F(x) = x^{-3}\cos x$, which, although decreasing as x^{-3}, oscillates in sign and indicates a comparatively long range oscillatory behaviour. In addition to this the preceding example shows that 'corrections' to the Thomas-Fermi approximation should spread the screening charge somewhat.

Screening of a strong potential[11,22]

The screening charge density around a strong potential has been examined by Friedel by treating the conduction electrons as free and being scattered only from the perturbing potential. The latter is assumed to be spherically symmetric and, within the framework of a partial wave analysis, manifests itself via a phase shift η_ℓ in the scattered partial wave component of angular momentum ℓ. The electron gas is pictured within a large sphere of radius R, while the calculation shows that the number of screening charges per unit k, N(k), is :

$$N(k) = \int_0^R 4\pi r^2 \frac{d}{dk}(\Delta\rho(r)dr = \frac{2}{\pi}\sum_\ell (2\ell+1)[\frac{d\eta_\ell}{dk} - \frac{1}{k}\sin\eta_\ell \cdot \cos(2kR + \eta_\ell - \ell\pi)] \qquad 2.16$$

The total number of screening charges, N, is given by:

$$N = \int_0^{k_f} N(k)dk = \frac{2}{\pi}\sum_\ell (2\ell+1)\int_0^{k_f}[\frac{d\eta_\ell}{dk} - \frac{\sin\eta_\ell}{k}\cos(2kR + \eta_\ell - \ell\pi)] \qquad 2.17$$

yielding:

$$N = \frac{2}{\pi} \sum_{\ell} (2\ell+1)\, \eta_{\ell}(k_f) + \text{oscillating term} \qquad 2.18$$

The contribution of this oscillating term to N has been calculated using a W.K.B. approximation[22], and shown to be negligible.

The screening problem can be made self consistent by equating N, the total screening charge introduced below the Fermi level by the perturbation, to Z, the excess charge on the impurity. This leads to the Friedel Sum Rule:

$$Z = \frac{2}{\pi} \sum_{\ell} (2\ell+1)\, \eta_{\ell}(k_f) \qquad 2.19$$

In the case of large r, equation (2.16) gives:

$$\underset{\text{large } r}{\Delta\rho} = \frac{1}{\pi 2 r^2} \sum_{\ell} (2\ell+1) \int_0^{k_f} \sin\eta_{\ell} \sin(2kr + \eta_{\ell} - \ell\pi)\, dk =$$

$$\frac{A \cos(2k_f r + \phi)}{r^3} \qquad 2.20$$

where:

$$A = \frac{1}{2\pi^2 r^3}\left[\left\{\sum_{\ell} (2\ell+1)(-\sin\eta_{\ell} \cos(\eta_{\ell} - \ell\pi)\right\}^2 + \left\{\sum_{\ell} (2\ell+1)(-\sin\eta_{\ell} \sin(\eta_{\ell} - \ell\pi))\right\}^2\right]^{\frac{1}{2}}$$

and

$$\phi = \tan^{-1}\left\{\frac{\sum_{\ell} (2\ell+1)\sin\eta_{\ell}\cos(\eta_{\ell} - \ell\pi)}{\sum_{\ell} (2\ell+1)\sin\eta_{\ell}\sin(\eta_{\ell} - \ell\pi)}\right\}$$

Calculations of residual resistivities based on this model are in good agreement with experiment in situations where it is realistic to consider the scattering potential as real i.e. non magnetic impurities[23].

Kohn and Vosko[24]

These authors extend the above approach by considering Bloch electrons scattered by a real potential $V(\underline{r})$ which is derived from a self consistent calculation and includes the effects of screening. In the asymptotic limit solutions $\psi_{\underline{k}}(\underline{r})$ of the scattering problem are sought which correspond to an incident Bloch wave and an outgoing scattered wave i.e.

$$\psi_{\underline{k}}(\underline{r}) = \phi_{\underline{k}}(\underline{r}) + \frac{1}{r} f(\underline{k},\underline{k}')\, \phi_{\underline{k}'}(\underline{r}) \qquad 2.21$$

Since the potential is real the scattering is elastic and $|\underline{k}| = |\underline{k}'|$, consequently $f(\underline{k},\underline{k}')$ depends only on the magnitude of $\underline{k}$, and on the angle θ between $\underline{k}$ and $\underline{k}'$. Hence[25]

$$f_k(\theta) = \frac{1}{2ik} \sum_{\ell=0} (2\ell+1)(e^{2i\eta_\ell(k)} - 1)\, P_\ell(\cos\theta) \qquad 2.22$$

In this approximation the excess electron density $\Delta\rho_k(\underline{r})$ associated with $\psi_{\underline{k}}(\underline{r})$ is:

$$\Delta\rho_k(\underline{r}) = \left\{ |\psi_{\underline{k}}(\underline{r})|^2 - |\phi_{\underline{k}}(\underline{r})|^2 \right\}$$

and the total excess density at $\underline{r}$, $\Delta\rho(\underline{r})$, including the effect of spin is:

$$\Delta\rho(\underline{r}) = 2\sum_{\underline{k}} \Delta\rho_k(\underline{r}) = \frac{2}{(2\pi)^3} \int_0^{k_f} \Delta\rho_k(\underline{r})\, d\underline{k}$$

which, the authors show, becomes in this asymptotic limit:

$$\Delta\rho(\underline{r}) = \frac{-1}{4\pi^2 r^3} \left\{ e^{2ik_f r} f_k(\pi)\, (\mu_{k_f}(\underline{r}))^2 k_f + \text{c.c.} \right\} \qquad 2.23$$

$u_{k_f}(\underline{r})$ being the periodic modulation of the plane wavestate $e^{i\underline{k}_f \cdot \underline{r}}$ induced by including the effects of the lattice field.

In the case of plane waves equation (2.23) reduces to equation (2.20), the Friedel result.

Kohn and Vosko then evaluate the electric field gradient q produced at a solute nucleus at $\underline{r}_n$ by this excess charge density and arrive at

$$q = \alpha \cdot \frac{8}{3} \frac{A \cos(2k_f r_n + \phi)}{r_n^3} \qquad 2.24$$

where α is an enhancement factor which measures the increase of q over its value in a plane wave theory without antishielding, the latter arising out of core polarization effects[26]. The resulting expressions are finally applied to the problem of the broadening of the nuclear magnetic resonance line in Cu due to the presence of impurities which set up oscillating electric field gradients with which the Cu nuclear quadrupole moment interacts. The parameters A and ϕ, which depend on the partial wave phase shifts η_ℓ, are estimated from the observed residual resistivities of the particular impurity in Cu, and from the sum rule. The enhancement factor α, for Cu, is estimated to be about 26.

The field gradients obtained in this manner are in very good agreement with those estimated by Rowlands[27] as necessary to produce his experimentally observed broadenings.

March and Murray[28]

Rather than consider electronic wavefunctions, these authors use the more general density matrix approach[29], the diagonal elements of which give the electron density. They show that the full density matrix can be generated by perturbation theory to infinite order and illustrate that for a slowly varying potential the associated series can be summed, and yields the usual result for the excess density, c.f. equation (2.12).

In situations where the potential is not varying slowly, March and Murray treat the case of a point charge in a free electron gas, an exact self-consistent solution to first order in perturbation theory is given. The associated equations are solved numerically and the results indicate that the asymptotic form of the excess electron density is accurately represented by the equation:

$$\Delta\rho(\underline{r}) = \frac{ZA(k)}{8\pi k} \cos\frac{2kr}{r^3} \qquad 2.25$$

where Z is the excess point charge and A(k) is a slowly varying function of k. The amplitude of the oscillations in excess electron density associated with equation (2.25) are in excellent agreement with those obtained by Kohn and Vosko.

To summarise, the fact that a variety of approaches to the problem of impurity screening all lead to oscillations in the

FIG(2:4) EXCESS CHARGE DENSITY vs. kr

------ is $4\pi r^2 \Delta\rho(r)$

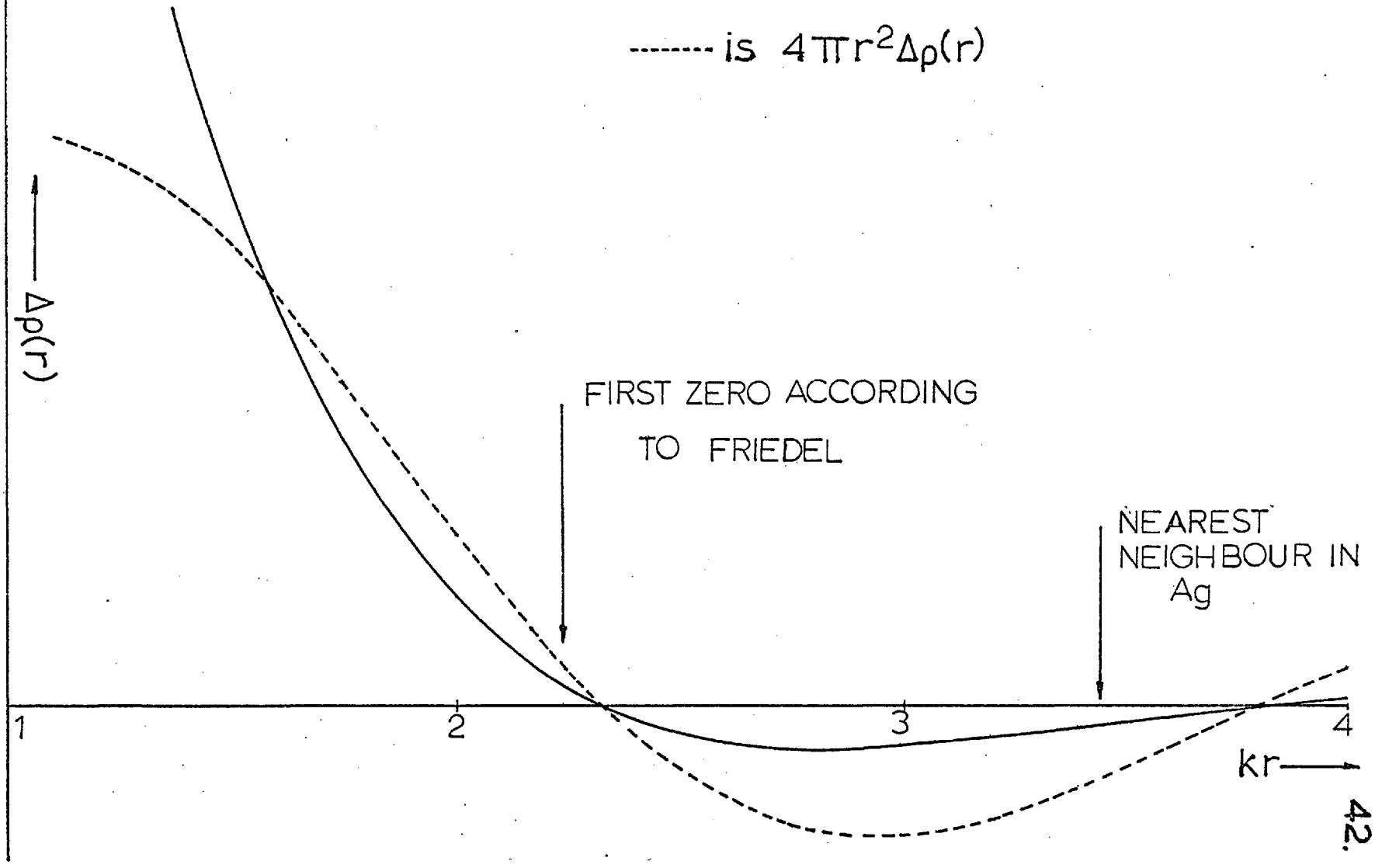

long range electronic screening charge density implies that these oscillation are not a peculiarity of a particular model. Experimentally, the work of Rowlands provides strong evidence in support of their existence. Perhaps the most important role played by such oscillations is that they afford a mechanism by which impurity atoms, separated by relatively large distances, can couple with one another. This mechanism is discussed in the next chapter.

CHAPTER 4

INTERACTION EFFECTS BETWEEN MAGNETIC ATOMS.

1. Molecular field model

The simplest way of treating the interaction between magnetic atoms in some solid lies in considering only one such atom, and replacing its interaction with the remaining atoms in the system by an effective field. Historically such an approach was first introduced by Weiss[30], who also introduced the assumption that this field was proportional to the average magnetisation, M, of the system. The field He acting on any atom is then :

$$He = H + \lambda M \qquad 3.1$$

where H is the applied field and λ the molecular field constant. The magnetic carriers can be envisaged as capable of assuming any orientation relative to the applied field, or these orientations can be assumed to be quantised. In either case this approach predicts a cooperative transition below some characteristic temperature, θ, the transition being characterised by a finite value of the magnetisation in zero applied field.

The fitting of experimental data in the high temperature region enables an estimate of to be made, and in the ferromagnetic elements (Fe, Ni, etc.) it is typically of the order of 10^3. This value is far too high to be attributed to magnetic dipole interactions, and, as is now well know, the interaction is quantum

mechanical in origin. Dirac[31] has shown that in the special case of localised electrons in orthogonal orbits the effect of the Pauli Exclusion Principle leads to a spin dependent contribution to the energy, which, for some purposes, may be regarded as arising from two body spin - spin interactions of the form:

$$\underline{H}_H = -2 \sum_{i<j} J_{ij} \, \underline{S_i} . \underline{S_j} \qquad 3.2$$

where Jij is the exchange energy between two electrons in states i and j. Supposing that nearest neighbour interactions alone are important, then for a single atom the 'Heisenberg' term, from equation (3.2), becomes:

$$\underline{H}_H = -2J \, \underline{Si} \sum_{j=1}^{n} \underline{Sj} \qquad 3.3$$

where the sum is over the n nearest neighbours of the ith atom. In a system in which the magnetic moment arises from spin alone, and replacing the interaction represented in equation (3.3) by an effective field, i.e.

$$\underline{H}_H = -g\beta \underline{Si} . \underline{H}_{eff} \qquad 3.4$$

thus

$$\underline{H}_{eff} = \frac{2J}{g\beta} \sum_{j=1}^{n} \underline{Sj} \qquad 3.5$$

Within the framework of the Weiss approach, each $\underline{Sj}$ is replaced by its average value $\langle \underline{Sj} \rangle$. Assuming all magnetic atoms are equivalent, $\langle \underline{Sj} \rangle$ is related to the total magnetic moment of the system by:

$$\underline{M} = Ng\beta \langle \underline{Sj} \rangle \quad , \text{ hence } \underline{H}_{eff} = \frac{2nJ}{Ng^2\beta^2} \underline{M} \qquad 3.6$$

On the basis of these equations the susceptibility , at high temperatures, is

$$\chi = \frac{Ng^2\beta^2 S(S+1)}{3k(T-\Theta)} \quad \text{where } \Theta = \frac{2nJS(S+1)}{3k} \qquad 3.7$$

Clearly the sign of Θ and λ (equation 3.6) depend on the sign of J, which must be positive for ferromagnetism to exist below Θ, the Curie temperature.

2. Collective electron model

The above application of the molecular field approach has been to localised magnetic carriers. Stoner[32] has applied this same approach to itinerant electrons, subject to Fermi-Dirac statistics. Using equation (3.1) the energy of a carrier becomes:

$$\varepsilon \pm \beta (H + \lambda M) \qquad 3.8$$

Defining a relative magnetisation $\zeta = M/M_{sat}$, equation (3.8) becomes:

$$\varepsilon \pm \beta H \pm \beta \lambda \zeta \cdot M_{sat} \qquad 3.9$$

As $\beta \lambda M_{sat}$ has the dimensions of energy per particle, it can be replaced by $k\Theta'$, where Θ' is a measure of the interaction strength. Using a parabolic density of states curve Stoner has shown that:

$$= \frac{F_{\frac{1}{2}}(\mu + \gamma + \gamma') - F_{\frac{1}{2}}(\mu - \gamma - \gamma')}{F_{\frac{1}{2}}(\mu + \gamma + \gamma') + F_{\frac{1}{2}}(\mu - \gamma - \gamma')} \qquad 3.10$$

where $F_k(\mu)$ are the appropriate Fermi-Dirac integrals, kT the chemical potential, $\gamma = \beta H/kT$ and $\gamma' = \theta'\zeta/T$. Stoner's analysis shows that the properties of such a system depend critically on the interaction strength $k\theta'$.

(i) For $3k\theta' < 2\varepsilon_f$ there is no ferromagnetism.

(ii) For $2/3 < k\theta'/\varepsilon_f < 0.79$ there is ferromagnetism below some Curie temperature θ (where $\theta=\theta'$ in the classical limit), but the magnetisation at absolute zero, is not saturated.

(iii) For $k\theta' > 0.79\varepsilon_f$ saturated ferromagnetism occurs.

Above the Curie temperature (for all temperatures if $3k\theta' < 2\varepsilon_f$), the inverse susceptibility is given by:

$$\frac{1}{\chi} = \frac{1}{\chi(\theta'=0)} - \frac{k\theta'}{N\beta^2} \qquad 3.11$$

Below the Curie temperature the temperature variation of the spontaneous magnetisation is given by equation (3.10) with $\gamma=0$, it is in reasonably good agreement with experiment except in the low temperature region.

Proceeding in the same manner as Stoner, Wolfarth[33] has examined the situation in which the density of states in energy has a rectangular form. The most marked difference between the predicted properties of the two models concerns the behaviour of the spontaneous magnetisation as a function of θ', the interaction strength. From such a comparison, Wolfarth however, concludes that the thermal properties would be rather more sensitive

to the assumed band form than the magnetic properties, since the former exhibit a dependence on this form even in the classical limit, whereas the latter do not.

The collective electron approach to antiferromagnetism, an extension of the above example in the case of negative exchange energy, has been examined by Lidiard[34].

A complete review of the various effective field models has been given by Smart[35], the previous examples may be regarded as illustrating the concept.

3. Coupling mechanisms in dilute alloys

The interaction mechanism invoked in the above models to explain the cooperative transitions was based on direct exchange between the electrons concerned. On a localised model the radial form of the direct exchange integral is similar to that for the wavefunction of the participating electrons and hence decreases exponentially with increasing separation of the interacting centres. In a dilute alloy, containing less than say 1 At.% impurity, the mean distance between impurities is much greater than the nearest neighbour distance and consequently direct exchange can no longer be regarded as an active coupling mechanism. There is, however, ample experimental evidence that cooperative phenomena occur in dilute alloy systems and so some indirect coupling mechanism must be operative.

Indirect interaction via "s-d" exchange

1. Zener[36]

Zener has suggested that the spin of an incomplete d shell is strongly coupled to the spin of the conduction electrons via exchange. This results in a uniform polarization of the conduction band. This polarization can then cause indirect interaction between two incomplete d shells via their mutual coupling to the conduction electron spins, and can result in a ferromagnetic alignment of the d spins.

2. Yosida[37]

This qualitative suggestion of an indirect coupling via "s-d" exchange has been examined by Yosida using an "s-d" interaction of the form discussed by Kasuya[38] and by Mitchell[39].

The diagonal elements of this interaction can be written:

$$- N^{-1} J(o)(n_+ - n_-) \sum_n S_n^Z \qquad 3.12$$

where N is the number of lattice points in the system, $J(\underline{k}-\underline{k}')$ the exchange integral between a conduction electron, with wave vectors $\underline{k}$ and $\underline{k}'$, and an impurity spin, Sn being the impurity spin operator at Rn. Equation (3.12) indicates that the energy is reduced as $(n_+ - n_-)$ increases, and tends therefore to polarise the conduction electrons. Using (3.12) as a perturbation from which the first order energies of spin up and spin down electrons can be calculated, and assuming a spherical Fermi surface,

Yosida shows:

$$n(\pm) = n \pm (3n/2E_f)N^{-1}J(o)\sum_n S_n^Z \qquad 3.13$$

E_f being the unperturbed Fermi energy and 2n the total number of electrons. The polarisation given by equation (3.13) is the same as that given by Frӧhlich[40] and by Zener. However, Yosida has pointed out that the difference between the first order perturbed wavefunctions for spin up and spin down electrons contributes a comparable polarisation to that in equation (3.13), and its inclusion leads to a density of spin up (or down) electrons at large distances r from the impurity given by:

$$\rho(\pm)(r) = \frac{n}{V} \pm \frac{3n}{8E_fVN}\sum_q J(q)f(q)\sum_n [e^{iq.(r-Rn)} + e^{-iq.(r-Rn)}]S_n^Z \qquad 3.14$$

where $q = k - k'$, V is the volume of the system, and

$$f(q) = 1 + \frac{4k_f^2 - q^2}{4k_fq}\log\left|\frac{2k_f + q}{2k_f - q}\right|$$

The final form of $\rho(\pm)(r)$ depends critically on $J(q)$, if this is assumed to be independent of q, then:

$$\rho(\pm)(r) = \frac{n}{V} \mp \frac{18n^2\pi}{VE_f}J(o)N^{-1}\sum_n F(2k_f|r - Rn|)S_n^Z \qquad 3.15$$

F(x) being defined in equation (2.15). However if $J(q)$ is taken to satisfy:

$$J(q)f(q) = 2J(o) \text{ for } q < 2k_f: = 0 \text{ for } q > 2k_f, \text{ then:}$$

$$P_{(\pm)}(r) = \frac{n}{V} \mp \frac{36n^2}{VE_f} J(o)N^{-1} \sum_n 2k_f|\underline{r}-\underline{Rn}|F(2k_f|\underline{r}-\underline{Rn}|)S_n^Z \qquad 3.16$$

At large distances the density given by equation (3.15) decreases as $|\underline{r}-\underline{Rn}|^{-3}$, while that in equation (3.16) decreases as $|\underline{r}-\underline{Rn}|^{-2}$. However, this latter equation is physically more acceptable since it remains finite at $\underline{r} = \underline{Rn}$, whereas the other does not.

The interaction, via "s-d" exchange, of a second spin at $\underline{Rm}$ with the modified conduction electron density produced by the first spin at $\underline{Rn}$ results in an indirect coupling between the two spins. Using the spin density given in equation (3.15), the interaction energy of the two spins, at large distances, is:

$$\frac{9}{16}\pi \left(\frac{2n}{N}\right)^2 \frac{J(o)^2}{E_f} \frac{\cos(2k_f|\underline{Rn}-\underline{Rm}|)}{(k_f|\underline{Rn}-\underline{Rm}|)^3} S(S+1)\underline{Un}.\underline{Um} \qquad 3.17$$

where the U's are unit vectors in the spin direction. This result has the same form as that obtained by Ruderman and Kittel[41] for the indirect coupling between nuclear spins via conduction electron polarisation. Equation (3.17) is often referred to as the RKY interaction.

As Freeman and Watson[42] have pointed out, Yosida's approach is rather restricted since it deals entirely with linear response i.e. in terms linear in the exchange. Further the expression for the exchange matrix elements used by the same author is appropriate only when the associated wavefunctions are orthogonal. To demonstrate with a practical example, Freeman and Watson used

wavefunctions appropriate to a spherical, half filled 4f shell in Gd^{+++}, representing the conduction electrons by single plane waves orthogonalised to the 4f and closed shell Gd^{+++} ion core. They calculated the $\underline{q}$ ($=\underline{k}-\underline{k}'$) dependence of $J(\underline{q})$, with $|\underline{k}|=kf$ and a varying $\underline{k}'$, and showed that far from being constant $J(\underline{q})$, although initially positive, exhibited an oscillatory dependence on $\underline{q}$. The resulting spin density, calculated from equation (3.14) is typified in figure (3.1) and has two features which are characteristic of the RKY approach. Firstly, for large values of r, the density displays "Friedel type" oscillations. Secondly, the average spin density is positive, reflecting the sign of J(o) (associated with which is the Zener term). The difference lie in the fact that the bulk of the induced positive spin density is not centred at the nucleus, but some 2 a.u. away, while $\rho(o)$ can be positive or negative, smaller or larger than the density at the nearest neighbour, depending on kf. This is in complete contrast to the RKY result where $\rho(o)$ is always large and positive. The behaviour of $\rho(o)$ and the associated outward shift of the region of net induced density is

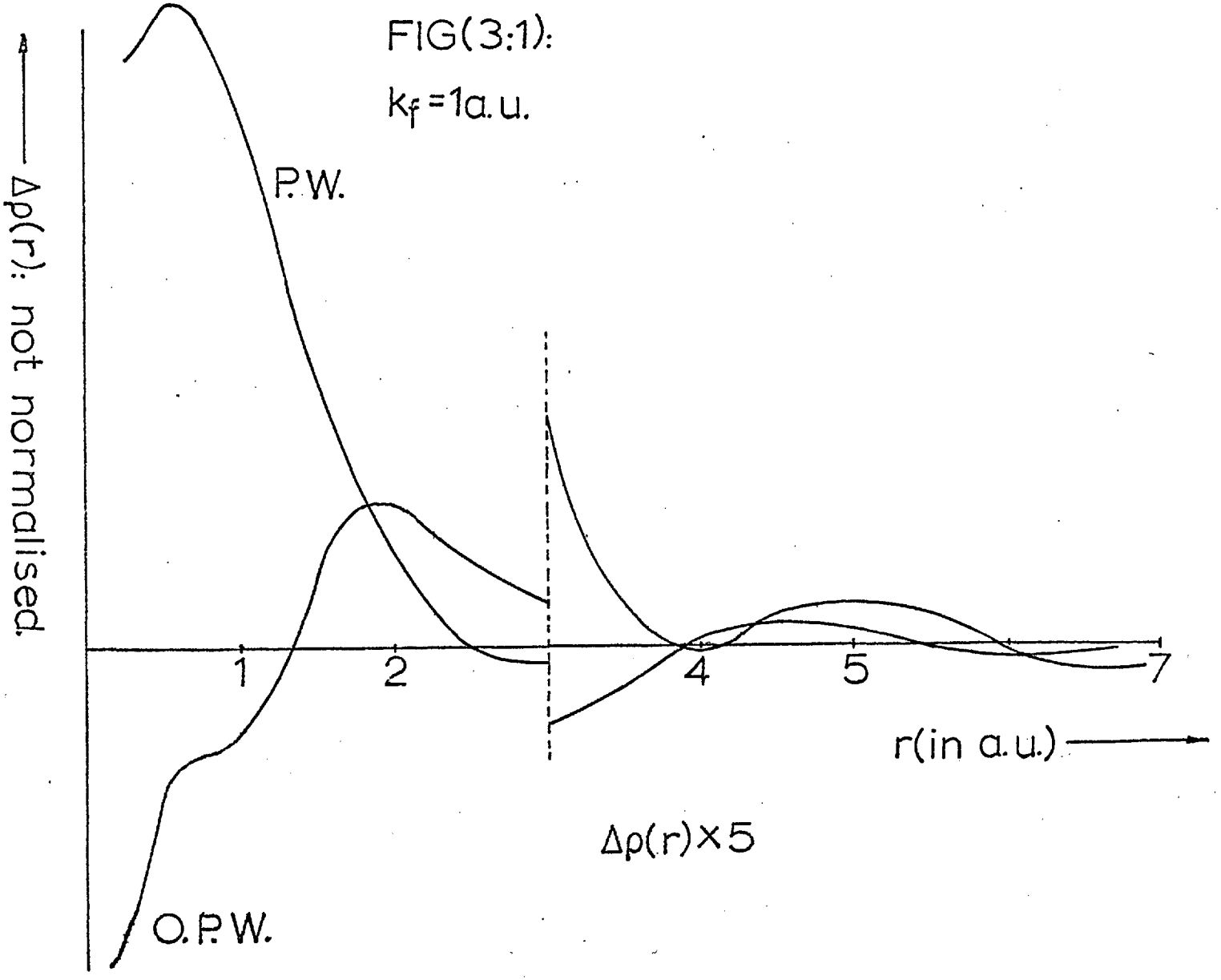
FIG(3:1):
k_f = 1a.u.
P.W.
O.P.W.
Δρ(r): not normalised
r(in a.u.)
1
2
4
5
7
Δρ(r)×5

also reflectedin the increased radii for the onset of Friedel type oscillation; this, coupled with the reduced $\rho(o)/\rho(n.n.)$ ratios greatly improve the theory's qualitative position with regard to experiment[43].

One final comment, both the above approaches assume that the conduction electrons have an infinite mean free path. De Gennes[44] has pointed out that a finite mean free path could affect this interaction since it will modify the polarisation distribution set up by a single spin. Further the temperature dependence of the mean free path could similarly lead to a temperature dependent RKY interaction.

Indirect interaction between virtual states

Blandin and Friedel[45] argue that when the spin degeneracy of a virtual state is lifted, the phase shifts for the spin up and spin down electrons, $\eta_{\uparrow}$ and $\eta_{\downarrow}$, are different. The result is that an oscillating spin density is associated with the "original" oscillating charge density, figure (3.2). Long range coupling can then occur since such an excess or deficiency of spin density at the site of a second virtual state can, via "s-d" exchange, cause the spin on the latter to align either parallel

FIG(3:2)

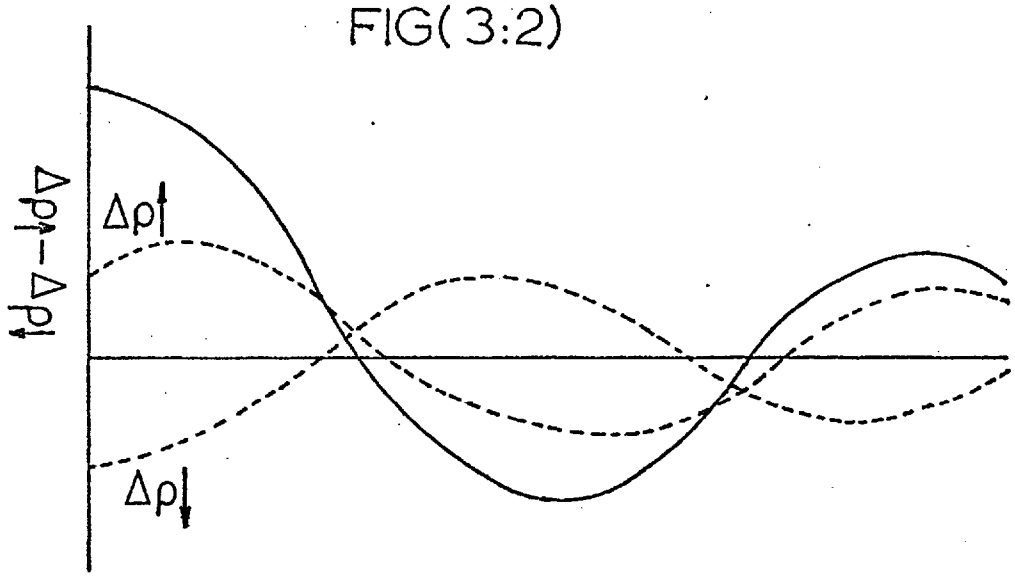

FIG(3:3)

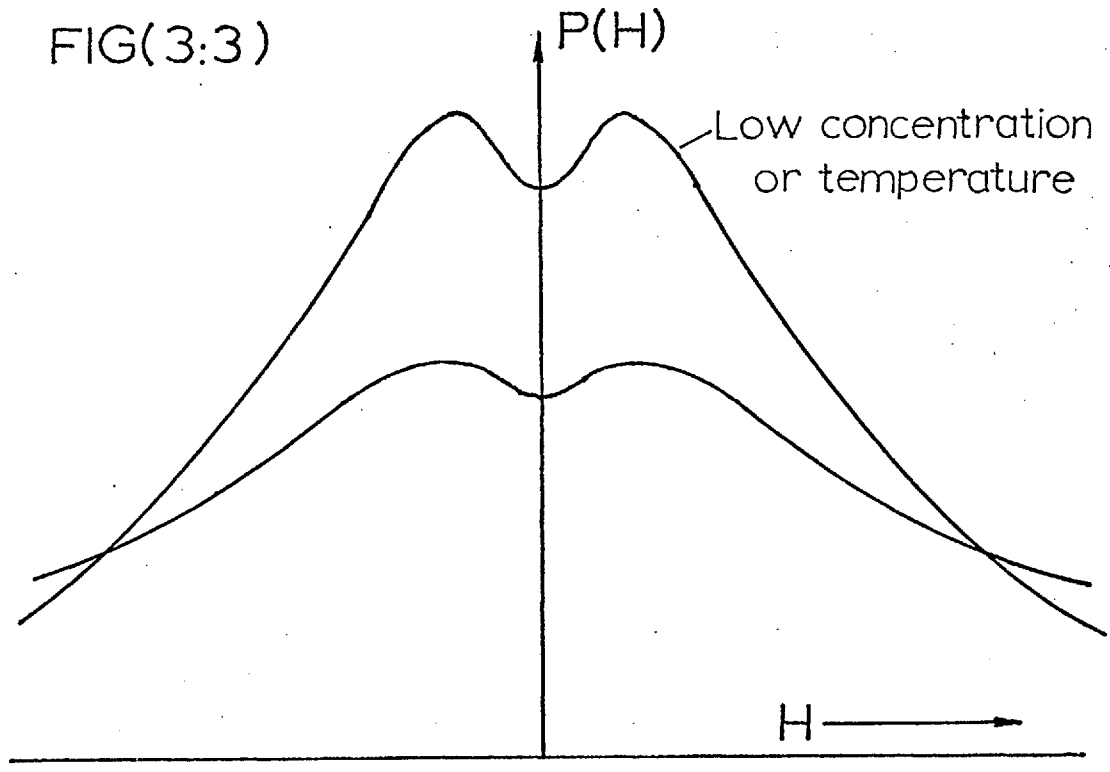

or antiparallel to the first.

When the spin decoupling is complete, and such that the spin down (say) state lies above and the spin up below the Fermi level, and assuming only the ℓ^{th} partial wave is significantly perturbed, then $\Delta\rho_-(r)=0$ and $\Delta\rho_+(r)$ is obtained from equation (2.20) with a spin index. In the case of large r this gives:

$$\Delta\rho_+(r) = \frac{(2\ell+1)}{4\pi^2} k_f^3 \sin\eta_{\ell+} \frac{\cos(2k_f r+\eta_{\ell+}(k_f))}{(k_f r)^3} \qquad 3.18$$

The interaction of a second impurity spin $\underline{S}$ at R with this spin density, via exchange, results in an interaction energy of the form[46] :-

$$E_{int} = \frac{3(2\ell+1)}{4} J \left\{\frac{2n}{N}\right\} \sin\eta_{\ell+}(k_f) \frac{\cos(2k_f R+\eta_{\ell+}(k_f))}{(k_f R)^3} S_{u_1}\cdot S_{u_2} \qquad 3.19$$

This type of coupling is somewhat hybrid, being of resonance type on one atom and exchange on the second.

The possibility also exists of interaction through resonant coupling to the conduction electrons at both sites. According to Caroli[46], the interaction energy between two identical $(2\ell+1)$ fold degenerate

virtual states at a large distance R from each other has the form:

$$E_{int} = \frac{(2\ell+1)}{2\pi} E_f \sin^2\eta_\ell(k_f) \frac{\cos(2k_fR+2\eta_\ell(k_f))}{(k_fR)^3} \underline{u}_1 \cdot \underline{u}_2 \qquad 3.20$$

The double resonance coupling would seem to be useful in accounting for the strong coupling of pairs of impurity atoms close to each other in the alloy.

Typically, taking $E_f = 7_{ev}$, $J = 0.1_{ev}$, $2n/N = 1$, $S = 2$ and $\eta_2 = \pi/5$ i.e. $\ell = 2$ partial waves only in CuMn, then:

$$E(int)(Yosida) \approx 10^{-2} \frac{\cos 2k_fR}{(k_fR)^3} \underline{u}_1 \cdot \underline{u}_2 \text{ e.v.}$$

$$E(int)(Blandin) \approx 4.5\times10^{-1} \frac{\cos(2k_fR+\pi/5)}{(k_fR)^3} \underline{u}_1 \cdot \underline{u}_2 \text{ e.v.}$$

$$E(int)(Caroli) \approx 9 \frac{\cos(2k_fR+2\pi/5)}{(k_fR)^3} \underline{u}_1 \cdot \underline{u}_2 \text{ e.v.}$$

thus, although each interaction seems roughly an order of magnitude larger than the previous one, allowance must be made for the fact that the sum of two phase shifts is involved in the argument of the cosine in Caroli's approach, one phase is involved in Blandin's approach, while no phase shift is involved in Yosida's

double "s-d" exchange coupling.

Treatment of interaction effects

Within the framework of the traditional molecular field approach, the effective field experienced by each 'magnetic atom' was taken to be the same, and proportional to the bulk magnetisation of the system The results derived in previous sections on coupling mechanisms in dilute alloys indicate that a random distribution of solute atoms means an interaction of varying strength and sign. This immediately precludes the use of the usual Molecular Field method from a realistic discussion of the properties of such a system.

Sato[48] has approached this problem by examining the properties of a cluster of atoms, and makes some attempt to take the effect of atoms outside the cluster into consideration. However, nearest neighbour interactions are still regarded as dominating and in this respect the approach is rather restricted.

Blandin and Friedel[45] have used the statistical method of Opechowski[49] to obtain a series expansion for the susceptibility in terms of $(\frac{1}{T})$ in the high

temperature (T) limit. Identifying the Curie temperature θ with the coefficient of the $(\frac{1}{T^2})$ term yields an expression which, in a dilute alloy where double 's-d' coupling is operative, becomes:

$$\theta = \frac{S(S+1)}{3k} 9\pi \left\{ \frac{2n}{N} \right\}^2 \frac{J(o)^2}{E_f} \sum_{\substack{\text{impurities} \\ o \neq i}} F(2k_f R_{oi}) \qquad 3.21$$

Doniach[50] has shown that on performing an ensemble average over possible impurity positions, the above equation becomes:

$$\theta = \frac{\pi S(S+1)}{3k} 9 \left\{ \frac{2n}{N} \right\}^2 \frac{J(o)^2}{E_f} c \sum_{\substack{\text{all sites} \\ o \neq j}} F(2k_f R_{oj}) \qquad 3.22$$

where c is the impurity concentration. Of particular interest in this thesis are alloys of the noble metals containing the heavier rare earths as impurities. In the second half of the rare earth series Russell Saunders spin-orbit coupling of total L to total S these being determined by Hund's rule, is operative, and the coupling, parallel. Thus:

$$\theta = \frac{(g_{R.E.}-1)^2}{3k} J(J+1) \cdot 9\pi \left\{ \frac{2n}{N} \right\}^2 \frac{J(o)^2}{E_f} c \cdot \sum_{\substack{\text{all sites} \\ o \neq j}} F(2k_f R_{oj}) \qquad 3.23$$

This equation predicts that in alloys containing the same small concentration of rare earth, provided J(o) remains constant, θ should vary as $(g_{R.E.}-1)^2 J(J+1)$[51].

Perhaps the most realistic approach yet made to the problem of treating interactions in a dilute alloy is to attempt to account for their varying magnitude and sign by some distribution of effective fields acting at the lattice points. The concept of a probability function P(H) for the magnitude of these fields was a natural consequence of the formalism of Overhauser's[52] spin density wave model for a dilute alloy, although Overhauser's approach has been criticised by Marshall[53].

This latter author has derived the general shape for the P(H,T) distribution in a dilute alloy using qualitative arguments. More recently Marshall's conclusions have been confirmed by the more rigorous approach of Klein and Brout[54,55], the general form of their conclusions about the P(H,T) curves are summarised in figure (3.3). Although this approach has had some success in predicting the correct general trend of the low temperature specific heat in alloys like CuMn, a detailed treatment of interactions in dilute alloys is

lacking, particularly in its relation to such properties as magnetic susceptibility.

CHAPTER 4

GROUP THEORETICAL BACKGROUND, AND IT'S APPLICATION TO THE PRESENT PROBLEM

BACKGROUND SUMMARY

1. Finite groups - Matrix representation

A representation is generally defined as any set of elements obeying the multiplication table of the group, they need not be distinct. Here it's form is rather more restrictive, namely, a set of square matrices, which, when placed in correspondence with the elements of the group, obey it's multiplication table. Γ_α denotes such a matrix set obeying the multiplication table of some finite group of order g. $\Gamma_\alpha(R)$ is the particular matrix in Γ_α which 'represents' the group element R, while $\Gamma_\alpha(R)_{ij}$ denotes the ij^{th} element of this particular matrix; n is the dimensionality of the matrices comprising

The character $\chi_\alpha(R)$ of a particular element R in the α representation is defined as:

$$\chi_\alpha(R) = \text{Trace}\ \Gamma_\alpha(R)$$

Since the trace of any matrix product is invariant under cyclic permutation of that product, then:

$$\text{Trace } S^{-1}\Gamma_\alpha S = \text{Trace } SS^{-1}\Gamma_\alpha = \text{Trace } \Gamma_\alpha$$

Hence the character of all equivalent representations are the same, the definition of the latter being obvious. Similarly if A, X and B are members of some group, and are related by:

$$A = X^{-1}BX$$

then A and B are conjugate and form all or part of a class. Clearly the character of each member of a class is the same.

A reducible representation is one in which every matrix can be put in the form:

$$\Gamma(R) = \begin{matrix} \Gamma_1(R) & 0 \\ 0 & \Gamma_2(R) \end{matrix} \qquad 4.1$$

where Γ_1 and Γ_2 are square, but not necessarily of the same dimension, they are also representations since they can be shown to obey the multiplication table. A reducible representation thus 'contains' more than one representation. This process of generating new representations can be continued until one is arrived at which cannot be placed in the form of equation (4.1) i.e. it cannot be expressed in terms of representations

of lower dimensionality. The condition that a representation be irreducible is:

$$\sum_R \left| \chi_\alpha (R) \right|^2 = g; \quad \text{where } g = \sum_\alpha n_\alpha^2 \qquad 4.2$$

For unitary irreducible representations Γ_α and Γ_β the following orthogonality relations hold:

$$\sum_{\substack{i=1 \\ \text{classes}}}^{r} hi \chi_\alpha(Ci)\, \chi_\beta(Ci) = g\, \delta_{\alpha\beta} \qquad 4.3a$$

$$\sum_{\substack{i=1 \\ \text{irreducible reps.}}}^{r'} hi\, \chi_\alpha(Ci)\, \chi_\alpha(Cj)^* = g\, \delta_{ij} \qquad 4.3b$$

hi is the number of elements in the class Ci.

From equations (4.3a,b) it can be shown that the number of classes is equal to the number of irreducible representations.

A reducible unitary representation Γ with character $\chi(R)$ can be transformed into the reduced form:

$$\Gamma = p_1\Gamma_1 + p_2\Gamma_2 + \ldots\ldots + p_n\Gamma_n \qquad 4.4$$

The right hand side of this equation has character $\sum_\alpha p_\alpha \chi_\alpha$, and since this is invariant under transformation:

$\chi(R) = \sum_\alpha p_\alpha \chi_\alpha(R)$, from which:

$$p_\alpha = 1/g \sum_R \chi(R)\, \chi_\alpha(R)^* \qquad 4.5$$

2. Application to quantum mechanics

Frequently in quantum mechanics the group of interest is the group of symmetry operators which leave the Hamiltonian invariant. Consider an ℓ fold degenerate level of the Hamiltonian $\underline{H}$, ofenergy En, with which the orthonormal set of function $\psi_i^{(n)}$ is associated.

$$\underline{H}\,\psi_i^{(n)} = E_n \psi_i^{(n)}: \quad i = 1 \ldots\ldots \ell.$$

Clearly if an operator leaves $\underline{H}$ invariant it is immaterial whether it appears to the left or right of $\underline{H}$, i.e. they commute. The set of all such operators are said to form the group of the Schroedinger equation. If R is a member of this group, and P(R) defined in Wigner's convention[56], then:

$$P(R)\underline{H}\psi_i^{(n)} = \underline{H}\,P(R)\psi_i^{(n)} = E_n P(R)\psi_i^{(n)}$$

This implies that $P(R)\psi_i^{(n)}$ is another function with energy E_n, and thus may be expanded as a linear sombination of thecomplete set of orthonormal functions associated with the degenerate level:

$$P(R)\psi_j^{(n)} = \sum_{i=1}^{\ell} \Gamma^{(n)}(R)_{ij}\,\psi_i^{(n)} \qquad 4.6$$

where $\Gamma^{(n)}(R)_{ij}$ is an array of coefficients. In fact the set of ℓ degenerate eigen functions $\psi_i^{(n)}$ of energy

E_n are the partners in a basis for an ℓ dimensional irreducible representation $\Gamma^{(n)}$ of the group of the Schroedinger equation. A knowledge of such representations enables very useful theorems to be invoked concerning the matrix elements of the Hamiltonian. However, matrix elements coupling states often arise from perturbations having a symmetry different from that of the Hamiltonian. Under these circumstances, labelling the functions $\psi_{n\alpha i}$ where n is some series index, α implying that the irreducible representation involved is Γ_α, and i labels partners, and noting that an arbitrary perturbation M can be decomposed linearly into terms $M_{\beta j}$, the latter transforming according to the jth row of Γ_β, an irreducible representation of the group involved in the states $\psi_{n\alpha i}$, then

$$\langle \psi_{n\alpha i} | M_{\beta j} | \psi_{n'\alpha' i'} \rangle = 0 \qquad 4.7$$

unless $\Gamma_\alpha^* \times \Gamma_\beta \times \Gamma_{\alpha'}$ contains the trivial representation Γ_1

3, Continuous groups

The continuous group of rotations in two and three dimensions are essential for the description of atoms, both free and in crystalline surroundings. The axial

rotation group consists of all rotations ϕ about some fixed axis. It is obviously commutative and has only one dimensional irreducible representations, i.e. $\chi(\phi)$ is both the character and the representation.

$\chi(\phi_1)\,\chi(\phi_2) = \chi(\phi_1+\phi_2)$, and $\chi(2\pi) = \chi(0) = 1$

hence the representations are:

$$\chi(\phi) = e^{im\phi},\ m = 0, \pm 1, \pm 2 \qquad 4.8$$

The irreducible representations of the three dimensional rotation group, the rotation symmetry group of an atom in free space, can be obtained by considering a set of functions which is invariant under this group. The set of all rotations in three dimensions obviously forms an infinite group, with an infinite number of classes. All rotations through the same angle about whatever axis belong to the same class because another rotation of the group connects the two rotation axes. Although finite rotations behave in quite a different manner, infinitesimal rotations add vectorially, this is reflected inthe fact that the infinitesimal rotation operator about some k axis, specified by direction cosines α_1 and α_2 and α_3, can be written:

$$I_k = \alpha_1 I_x + \alpha_2 I_y + \alpha_3 I_z$$

where I_x, I_y and I_z are the three infinitesimal Cartesian rotation operators. It can be shown that a finite rotationof angle α about some k axis can be written as:

$$R_{\alpha_k} = 1 + i\alpha I_k + \frac{(i\alpha I_k)^2}{2!} + \ldots = e^{i\alpha I_k} \qquad 4.9$$

Defining stepping operators by: $I \pm = I_x \pm iI_y$ 4.10

which obey the usual commutation relations:

$$I_z I\pm - I\pm I_z = \pm I\pm \quad : \quad I+I_- - I_-I+ = 2I_z \qquad 4.11$$

then following the previous discussion, it is clear that the irreducible representations of the full rotation group can be obtained by considering a set of functions which is invariant under $I\pm$, I_z, since any rotation can be built from them. Such a set offunctions are the spherical harmonics. The angular part of the Laplacian operator is invariant under rotation, hence it's eigen functions - the spherical harmonics, form bases of representations of the full rotation group. Operating on these functions with the stepping operators, and using their commutation relations, reveals that the dimensionality of the representation thus obtained is $(2\ell+1)$. Further the $(2\ell+1)$ dimensional space composed of

$$Y_\ell^\ell \; , \; Y_\ell^{\ell-1} \quad \ldots\ldots Y_\ell^{-\ell}$$

is invariant under $I_{\pm}$, I_z and hence under all rotations; it is also irreducible. This confirms that the spherical harmonics form bases for the $(2\ell+1)$ dimensional irreducible representations $D^{(\ell)}$ of the full rotation group. Thus, in analogy with equation (4.6), under a rotation R:

$$RY_{\ell}^{m} = \sum_{m'} D^{(\ell)}_{m'm} Y_{\ell}^{m'}$$

The characters of the representations can be obtained by the following argument. Consider a rotation α about z, denoted by $R_{\alpha z}$, in analogy with equation (4.9):

$$R_{\alpha z} Y_{\ell}^{m}(\theta,\phi) = e^{im\phi} Y_{\ell}^{m}(\theta,\phi)$$

The representation of such a rotation is the diagonal matrix $D^{\ell}(\alpha)$, where

$$D^{\ell}(\alpha) = \begin{pmatrix} e^{i\ell} & & 0 \\ & \ddots & \\ 0 & & e^{-i\ell} \end{pmatrix}$$

and has the character $\chi^{\ell}(\alpha) = \text{Trace } D^{\ell}(\alpha) = e^{-i\ell\alpha} \sum_{k=0}^{2\ell} (e^{i\alpha})^k$

hence $\chi^{\ell}(\alpha) = \dfrac{\sin(\ell + \frac{1}{2})\alpha}{\sin \frac{1}{2}\alpha}$ 4.12

It has been noted previously that all rotations by α are in the same class, regardless of axis, hence they must all have the character calculated above for a

simple case.

The direct product of two representations of the full rotation group may be decomposed into it's irreducible components in a manner similar to equations (4.4), (4.5), this yields:

$$D^{(\ell_1)} \times D^{(\ell_2)} = \sum_{|\ell_1 - \ell_2|}^{\ell_1+\ell_2} D^{(\ell)} \qquad 4.13$$

which is nothing more than the familiar vector model for the addition of angular momenta. Using group theoretical techniques it is possible to obtain the partners in the irreducible representations contained in the product representations as a linear combination of products of the original functions. If $\psi^{m_1}_{\ell_1}$ transforms as a basis for $D^{(\ell_1)}$, and $\psi^{m_2}_{\ell_2}$ for $D^{(\ell_2)}$, then the space of products $\psi^{m_1}_{\ell_1} \psi^{m_2}_{\ell_2}$ is invariant under $D^{(\ell_1)} \times D^{(\ell_2)}$. The irreducible representations $D^{(\ell)}$, $\ell = \ell_1+\ell_2, \ldots |\ell_1 - \ell_2|$, of the products have, as partners, the functions:

$$\psi^{m}_{\ell} = \text{Normalising Factor} \sum_{m_1 m_2} (\ell_1 \ell_2 m_1 m_2 \mid \ell m)\, \psi^{m_1}_{\ell_1} \psi^{m_2}_{\ell_2}$$

4.14

where the set of coefficients $(j_1 j_2 m_1 m_2 | jm)$ are called Clebsch-Gordon coefficients, and are uniquely determined by the properties of the rotation group. They vanish unless $m_1 + m_2 = m$.

Thus far, the development of representations (1) of the full rotation group has been indicated. The manner of this development implies that the representations are odd dimensional since they correspond to integral angular momentum. Wigner[56] has shown how ordinary group theory techniques may be extended to account for spin. Briefly, the results of this extension indicate that systems having spherically symmetric Hamiltonians and total angular momentum j possess state functions which can be classified, with respect to behaviour under rotation, by representations $D^{(j)}$ of the full rotation group. The odd dimensional representations are those which are associated with integral j and correspond to the (2j + 1) degenerate states of the total angular momentum, while the even dimensional representations are associated with half integral j. When j is integral, the spherical harmonics Y_j^m are the basis functions for $D^{(j)}$, when j is half integral $D^{(j)}$ is not determined

as to sign. In either case the expression for the character, equation (4.12), remains unchanged. This means that since

$$\chi^j(\alpha + 2\pi) = (-1)^{2j}\,\chi^j(\alpha) \qquad 4.15$$

then for half integral j the character is double valued, i.e. a rotation of 2π should leave everything unchanged, whereas above:

$$\chi^j(\alpha + 2\pi) = -\chi^j(\alpha).$$

However, even for half integral j:

$$\chi^j(\alpha + 4\pi) = \chi^j(\alpha)$$

Thus these representations act as if a rotation through 4π should be considered the identity operation. In addition:

$$\chi^j(\pi + 2\pi) = \chi^j(\pi) = 0.$$

showing that the character of a two fold rotation is single valued. This situation is dealt with in practise by introducing the 'fiction' that the system is taken into itself, not under a rotation of 2π, but one of 4π. Consequently a new group element $\bar{E}$ is introduced which represents a rotation of 2π, and has the property $\bar{E} \neq E$, $\bar{E}^2 = E$. The resulting group contains twice as many elements as the original one, and is called the crystal double group. This double group

contains more classes than the original one, but not necessarily twice as many since $\chi^j(\bar{E}C_2) = \chi^j(C_2) = 0$, making it possible that $\bar{E}C_2$ and C_2 are in the same class. Double groups will be referred to later.

4. Point groups

A group of rotations (both proper and improper) and reflections which leave a point invariant is termed a point group. Since all rotations and reflections associated with a point group are contained in the group of three dimensional rotations and reflections, the point group is a subgroup of the full rotation group.

Consider a point group G containing improper rotations, this may be decomposed into the direct product of a point group H, containing only proper rotations, and the group C_i which consists of the identity E and inversion J. This implies that for every class C in H, there will be two classes, C and JC, in G. In particular the inversion EJ = J will be in a class by itself. If $\Gamma_\alpha(A)$ denotes an irreducible representation of H, A being a typical element, then those of G can be generated simply by allowing A to assume the values A or JA, then since the number of classes in G is twice that in H, all the irreducible representations of G have been generated.

Denoting those representations which are even under inversion by Γ^E, i.e. :

$$\Gamma^E_\alpha(A) = \Gamma^E_\alpha(JA) = \Gamma_\alpha(A)$$

and those which are odd by Γ^o, such that :

$$\Gamma^o_\alpha(A) = - \Gamma^o_\alpha(JA) = \Gamma_\alpha(A)$$

then the entire character table for G can be written:

G	H	JH
E	(χ)	(χ)
^{o}	(χ)	$(-\chi)$

4.16

where (χ) is the entire character table for H.

Crystal fields

When an ion is located, not in free space, but in a crystal, it is subject to various inhomogeneous electric fields which do not possess full rotational symmetry. Thus the symmetry group of the ion is reduced from that of the three dimensional rotation group (plus inversion) to some finite group of rotations and reflections. This reduced group allows the originally irreducible representations of the full rotation group (and hence of the ion in free space) to be reduced with respect to the subgroup characterising the crystalline electric field. This reduction in dimensionality of the irreducible representations causes the degeneracy associated with complete rotational symmetry to be lifted. Hence the free ion energy levels are split by the crystalline field. The degree of residual degeneracy is determined, as Bethe[57] originally pointed out, from symmetry by group theory, with ultimate accuracy since no perturbative approximation is involved.

In treating the effects of the crystal fields it is first necessary to decide how its strength compares with the various terms in the ionic Hamiltonian. Three distinct cases are normally distinguished[58]:

1. Strong fields

In this situation, theory seems to indicate that interactions between the electrons and their surroundings is large compared with the Coloumb interaction between electrons ($_i\Sigma_j$ e^2/rij), but less than the interaction of the electrons with the nucleus. The iron group cyanides typify this situation.

2. Intermediate fields

This case is characterised by a crystalline field which is large compared with spin-orbit coupling, but small compared with the Coloumb interaction. This situation is believed to occur in salts of the iron group and is treated by first characterising the system by its total orbital angular momentum L, which is then 'coupled' to the crystal field. Finally the effects of spin are considered.

3. Weak fields

Here the crystal field is less than the strength of spin orbit coupling. This occurs in salts of the

rare earths. In this case the 'finished' atom, described by quantum number J is studied.

In the system of interest in this thesis, rare earth impurities in noble metals, the effects of the crystal field of the matrix on the impurity is sought. Translational symmetry of the lattice is, thus, unimportant. The symmetry of the field experienced by the impurity is assumed to be characterised by the point group of the host lattice. Following the previous discussion the first question to be considered is what irreducible representations of this point group are contained in the (now reducible) representations $D^{(J)}$ of the full rotation group associated with angular momentum J.

a. Integral J

The point group for the f.c.c. lattice of Ag and Au is, in Schoenflies notation, Oh. This is the full symmetry group of a cube or octahedron, including improper rotations and reflections. It is the direct product of O and Ci, where O is the group of proper rotations of a cube, and Ci is defined previously.

The decomposition of the various (2J+1) dimensional representations, $D^{(J)}$, is accomplished by using equations

(4.5) and (4.12). In addition, the result of equation (4.16) implies that in conjunction with these equations, all splitting can be worked out simply by considering the group of proper rotations, in this case O, which has 24 elements (g) and five irreducible representations. The character table for O is reproduced in Appendix 1, together with the associated character table for the $D^{(J)}$'s, and the decomposition of the latter into irreducible representations of the former.

b. Half integral J

As mentioned previously, the difficulties encountered in this case can be overcome by introducing the artifact that the identity operation consists of a rotation of 4π . Consequently it is necessary to introduce another group element $\bar{E}$ corresponding to a rotation of 2π . For the case discussed here, the double group O' is obtained by combining the 24 elements in O with 24 new elements obtained by combining each element with $\bar{E}$. Again, as previously mentioned, the number of classes in O' need not be twice that in O, in fact, Opechowski[63] has shown that C_2 and $\bar{E}C_2$ are in the same class since there is another twofold axis

perpendicular to the one in question. Thus, in addition to the five classes of O, three new classes are introduced, $\bar{E}$, $\bar{E}C_3$ and $\bar{E}C_5$ (notation as in Appendix 1). Hence 24 elements and three classes have been added, and may be consistently accounted for by keeping the five ordinary representations of O, and, to satisfy equation (4.2), adding three new ones, Γ_6, Γ_7 and Γ_8, of dimensionality 2, 2 and 4.

Within the framework of the double group method, the half integral J's can be handled by the same procedure as used in (a). The results are summarised in Appendix 1.

Having obtained the residual degeneracies, the problem remains of finding the energy separation between the various crystal field split levels. In the classical electrostatic approximation the electric field is assumed to be produced by some charge distribution located outside the ion, and the potential is expanded in spherical harmonics, thus:

$$V_{cystal} = \sum_{\ell\, m} a_\ell^m r^\ell y_\ell^m(\theta,\phi) \qquad 4.17$$

the a_ℓ^m being coefficients which, in this context, are regarded as adjustable parameters. The crystal

potential must transform according to it's own identity representation, in this case that of O_h. Hence the expansion of the potential in the above terms need only contain those Y_ℓ^m for which $D^{(\ell)}$ contains the identity representation of O_h. From Appendix 1, is contained in $D^{(\ell)}$ for $\ell = 0,4,6$ and 8, hence only these terms in equation (4.17) need be retained. The $\ell=0$ term in the potential has full spherical symmetry and to first order produces a uniform shift of all levels. It is consequently disregarded.

According to equation (4.13), the product of two 'f' functions transforms like:

$$D^{(3)} \times D^{(3)} = \sum_{0}^{6} D^{(\ell)} = D^{6} + \ldots\ldots\ldots D^{0} \qquad 4.18$$

This implies, when used in conjunction with equation (4.7), that matrix elements of terms in the potential for which $\ell > 6$ do not give any contribution. Thus the expansion of the potential reduces to:

$$V_{crystal} = r^4 \sum_{m=-4}^{4} \left\{ a_4^m Y_4^m \right\} + r^6 \sum_{m=-6}^{6} \left\{ a_6^m Y_6^m \right\} \qquad 4.19$$

As shown in Appendix 2, a consideration of the symmetry operations of O_h further reduces this expansion to:

$$V_{crystal} = r^4(a_4^0 y_4^0 + a_4^4(y_4^4 + y_4^{-4}) + r^6(a_6^0 y_6^0 + a_6^4(y_6^4 + y_6^{-4}) \qquad 4.20$$

The problem of finding the splitting between the various levels has thus been reduced to evaluating matrix elements of the potential, given in equation (4.20) between states, in representations in which these states are eigenstates of the total angular momentum J. This process can be somewhat simplified by making use of the Wigner-Eckart theorem[60] which implies that matrix elements diagonal in J are proportional to matrix elements in which $\underline{J}$ is used as a replacement operator for other operators. As Steven's[62] points out, within a manifold of constant J, matrix elements of the potential operators are proportional to those of a suitably choosen combination of angular momentum operators. However, for such an equivalence to hold, the equivalent must transform in exactly the same way as the potential operator. Hence it becomes necessary to determine an angular momentum expression which has this property, due allowance being made for the non-commutation of Jx, Jy and Jz.

Once these equivalents have been determined, the evaluation of their matrix elements within some constant J manifold is quite straightforward. The manner in which the operator equivalents of the potential described by equation (4.20) are derived is illustrated in Appendix 2. In the notation used there, equation (4.20) becomes:

$$V_{crystal} = B_4(O_4^0 + 5O_4^4) + B_6(O_6^0 - 21O_6^4) \qquad 4.21$$

The coefficients B_4 and B_6 depend, in part, on the proportionality factor between the matrix element of the operator equivalent and that of the potential operator. It can be evaluated by calculating some suitable matrix element in either scheme, an example is provided in Appendix 2. One of the points to note about the above form of the crystal potential is that it couples states with m_J differing by four. Using equation (4.21) in conjunction with the expanded form ofthe operator equivalents given in Appendix 2 enables all matrix elements within a given manifold to be written down in terms of B_4 and B_6. When the values of these coefficients are specified, the crystal field Hamiltonian formed by the array of such

elements can be written down explicitly. The eigen vectors and eigen values - and hence the energy separations can be obtained by diagonalising the array.

CHAPTER 5

A REVIEW OF THE PREVIOUS WORK ON RARE EARTH IMPURITIES IN SILVER AND GOLD

The low temperature electric and magnetic properties of dilute alloys of transition metals in non magnetic host metals have received a great deal of experimental and theoretical investigation. The behaviour of such alloys in the low temperature region has frequently been interpreted in terms of indirect interaction between localised moments associated with solute atoms, via the polarisation induced by such moments in the conduction band. The situation is, however, often complicated by the extended nature of the magnetic state of the solute atom, which arises from the interaction of the energy levels of the latter with the conduction band states. In this connection, the situation in dilute alloys of the rare earths in non magnetic hosts should be clearer, since they can be described either by narrow virtual states or by real bound states below the bottom of the conduction band. Such alloys had received practically no investigation until the recent results of Rider[64] showed that the

solubility of the rare earths in non magnetic hosts such as gold and silver was, in fact, not negligible.

Measurements by Sugawara[65] et al on the temperature dependence of the electrical resistivity of AgGd alloys indicated a resistance minimum, followed by a maximum at lower temperatures. The temperatures at which these maxima occurred scaled almost linearly with temperature (roughly $7^{\circ}K$ per atomic % Gd). These authors attributed such maxima to the onset of magnetic ordering, since the magnetic susceptibility of the same alloys exhibited a marked change in slope at the temperature of the maxima. In contrast with these results, a rather more careful investigation by Bijvoet et al[66], in which the electrical resistivity in the range 1 to $4.2^{\circ}K$ was measured, revealed no maxima for similar alloys. Within the temperature range of their experiments, these authors find that the electrical resistivity of a Ag-0.1At% Gd alloy decreases slowly with decreasing temperature. A similar behaviour is observed in a Ag-0.3At% Gd alloy, with the slight modification of a gradually increasing slope of the resistivity curve as the temperature is decreased. This effect becomes more pronounced as the Gd

concentration is increased, and is a marked effect in a Ag-0.8At% Gd alloy at 1.5°K.

For the rare earth impurity Ho, the same authors find an almost linear decrease in resistivity with decreasing temperature for alloys of Ag containing 1.4 and 1.2At% Ho. However, for Ag containing 0.4 0.3 and 0.15At.% Ho, a minimum in the resistivity temperature curve was found (there was, however, no maximum observed in these alloys above 1°K). The temperature at which these minima occurred increased with decreasing concentration, but as the measurements extend up to 4.2°K only, the temperature of the minima in the two more dilute alloys was not determined. From similar measurements, supplemented by magneto-resistance investigations, Bijvoet concluded that Nd in Ag acts as a non-magnetic impurity,while from the observed resistivity and solubility of Yb in the same solvent it was concluded that the valence state of this rare earth in Ag was two.

Arajs and Dunmyre[67] have measured the electrical resistivity of Au containing 0.05, 0.23, 0.60, 0.88, 1.17, 1.88 and 2.35 At.% Er. Their measurements

covered the temperature range 1 to 20°K, and no anomalous behaviour was observed. Over the whole range of alloy compositions investigated it was found that $(\rho_{alloy}-\rho_{Au})$ at 4.2°K was linear in Er concentration, and had the value 6.7μΩ ,cms./at.% Er. This is quite close to the value of 6.1μΩ ,cms/at.% Er quoted by Bijvoet for Er in Ag.

Recent measurements in this laboratory[68] on the electrical resistivity of AgGd, AgEr and AgHo alloys essentially confirm Bijvoet's results. They also emphasize the need to avoid any transition metal contamination. These measurements extend to a much higher temperature than those of Bijvoet, and preliminary analysis indicates that $(\rho_{alloy}-\rho_{Ag})$ has a very marked temperature dependence.

Bijvoet[69] has also examined the magneto-resistance at 4.2 and 1.2°K, of AgGd and AgHo alloys on which the electrical resistivity measurements were made. The results are reproduced in figure (5.1).

The specific heat, C, of dilute alloys of Ag with the rare earths Nd, Gd, Tb, Dy, Ho and Er, has been measured below 4.2°K by Zimmerman et al[70]. The

FIG(5:1)

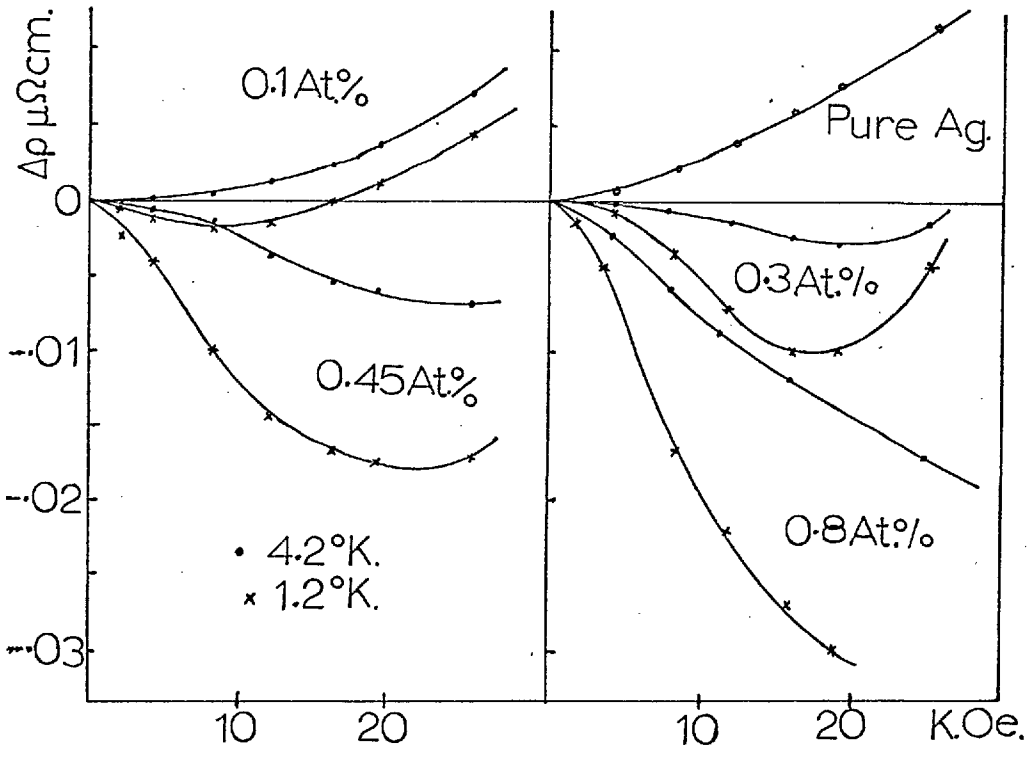

Ag-Gd alloys: Magnetoresistance vs. transverse magnetic field.

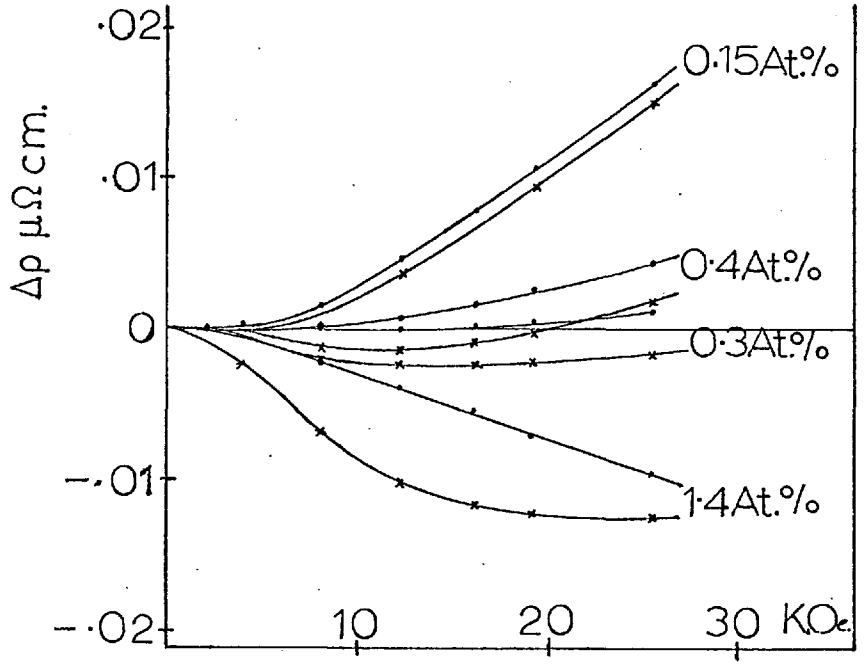

Ag–Ho alloys: Magnetoresistance vs. transverse magnetic field.

results on alloys containing Gd received the most detailed analysis. The alloys containing 0.3 and 0.5At.% Gd showed a rapid increase of C/T below $2^{o}K$, while the 0.1 At.% alloy exhibited a similar increase below $1^{o}K$. The experimental data on this last sample could be fitted reasonably well from $4.2^{o}K$ to $0.2^{o}K$ by

$$C = 0.91T + 0.17T^{3} + 1.55T^{-1} \qquad 5.1$$

Estimating the magnetic entropy from this equation suggests that about a half of the impurity spins are ordered at $0.2^{o}K$. It is, perhaps, significant to note, in the light of estimates of rare earth solubilities in Ag made by Bijvoet, that these authors find, on fitting their results for the Ag-1At.% Gd alloy, that the coefficient of the lattice term (T^{3}) in this alloy differs significantly from that in the less concentrated alloys and in pure Ag.

The results obtained by the same authors on a Ag-0.5At.% Ho alloy indicated, after subtracting the appreciable nuclear contribution[71], that (C/T vs.T) plot had the same general nature as the AgGd alloys increasing rapidly below $3^{o}K$.

The observed behaviour of the remaining alloys was rather different from the above systems. Measurements were made on Ag-0.1, 0.19 and 0.57 At.% Dy, in each case C/T decreased smoothly with temperature and finally became flat below 2°K. The 0.19At.% Dy alloy was also examined between 0.2 and 0.8°K and clearly showed the effects of the hyperfine term; the curves in the two temperature regions investigated (0.2 to 0.8, 1.5 to 4.2°K) do not, however, seem to join on to one another smoothly. Alloys of Ag containing 0.13At.% Nd, 0.5At.% Er and 0.57At.% Tb, were also measured between 1.5 and 4.2°K. The (C/T vs.T) plot for the former decreased smoothly with temperature; the Er alloy turned up quite sharply below 2°K and also exhibited a slight bump around 3.2°K which, along with a more pronounced bump around 2.2°K in the Tb alloy, the authors attribute to an oxide.

Measurements of the specific heat of Ag containing 0.41 and 0.69At.% Gd have been carried out by Pickett[72] The general form ofthe (C/T vs T) plots given by this author agree with those of Zimmerman, but show the opposite dependence on concentration.

The thermopower, S, of Ag and Au containing about 0.5At.% of rare earths has been measured at 5.5°K by Gainon et al[73]. They find that the value of this parameter is displaced towards positive values on passing from Au to Ag (except in Yb). Apart from this, the variation across the whole rare earth series is similar in both hosts. The general tendency in S is negative for the light rare earths and positive for the heavier ones, with 'giant' values occurring in Eu and Ce. The authors have suggested that this overall trend may reflect the change in sign of (g-1) on crossing the rare earth series since, as Kondo[74] has pointed out, the sign of S is given by the sign of (g-1)JV, where J is the exchange integral and V the static perturbing potential.

The same authors have also measured the magnetic susceptibility, between 4.2 and 300°K, of both Au and Ag containing Eu and Yb. Their results, in agreement with the data included in this thesis which was obtained prior to their publication, confirm the conclusions of Bijvoet that Yb is divalent in Ag (but trivalent in Au), and also indicate that Eu is divalent in both

hosts. The reciprocal susceptibility versus temperature for AuYb, AgEu and AuEu showed deviations from Curi Weiss behaviour around 40°K, while the extrapolated high temperature line in the last two alloyshad a positive intercept on the temperature axis. The authors claimed that a more careful examination indicated a ferromagnetic Curie temperature of around 7°K for these alloys, and measurements of S above these Curie temperatures revealed no significant decrease in this quantity. This, the authors claim, implies that theories which rely on the existence of polarisation of the impurity spins in order to explain giant thermopowers[75] cannot be retained.

Recent measurements[76], at 4.2°K, of the thermopowers of Ag containing the heavier rare earths as impurities are in general agreement with those of Gainon.

As originally indicated, alloys of the above type have been subjected to a relatively small amount of investigation. However, even at this stage, the experimental results seem to possess many inconsistencies, indeed in several cases where different authors have investigated the same properties, the

results are in total disagreement. As will be demonstrated in Chapter 8, much confusion can, and has, arisen from inferior alloy preperation. This chapter also contains a more detailed discussion of the results presented above.

CHAPTER 6

EXPERIMENTAL DETAILS, INCLUDING THE SERVO MECHANISM

1. General

The force (in the z direction) exerted on a magnetically isotropic sample placed in an inhomogeneous magnetic field can, under certain approximations (Appendix 3) be written:-

$$F_z = M_x \cdot \partial H_x / \partial z \quad \ldots\ldots\ldots \qquad 6.1$$

and holds whatever dependence the magnetisation M might have on the applied field H. When the magnetisation is proportional to the applied field then equation (6.1) becomes, in the usual notation:-

$$F_z = m\chi \cdot H_x \cdot \partial H_x / \partial z \quad \ldots\ldots\ldots \qquad 6.2$$

These equations form the basis for the measurements carried out in the present investigation, since they imply that the susceptibility per unit mass can be evaluated by measuring the force on a sample of known mass, when the latter is placed in a magnetic field of known $\frac{\partial}{\partial z}\left(\frac{H^2}{2}\right)$

2. The magnetic balance

Although this has been described in some detail elsewhere[77], it is worth while, in view of later discussion, to describe briefly its mode of operation.

The balance consists of a helical elinvar spring suspended from it's upper end, as indicated in figure (6.1). The loaded arms, indicated in this figure, at the bottom of the spiral, serve to increase its rotational period so that it becomes very different from its vertical vibrational period. Consequently the system acts as a mechanical noise integrator. A small scale pan is attached beneath these arms, and a small coil hangs from the underside of the pan. This coil is situated in the radial field of a loudspeaker magnet. As figure (6.1) indicates, a long quartz rod hangs beneath this coil, the specimen being attached to the lower end of this rod by means of the arrangement shown in figure (6.2).

The application of an inhomogeneous magnetic field to the sample produces a (time) steady force, which extends or compresses the spring, depending on the magnetic nature of the sample. Such a time steady extension causes the bottom of the spiral to rotate,

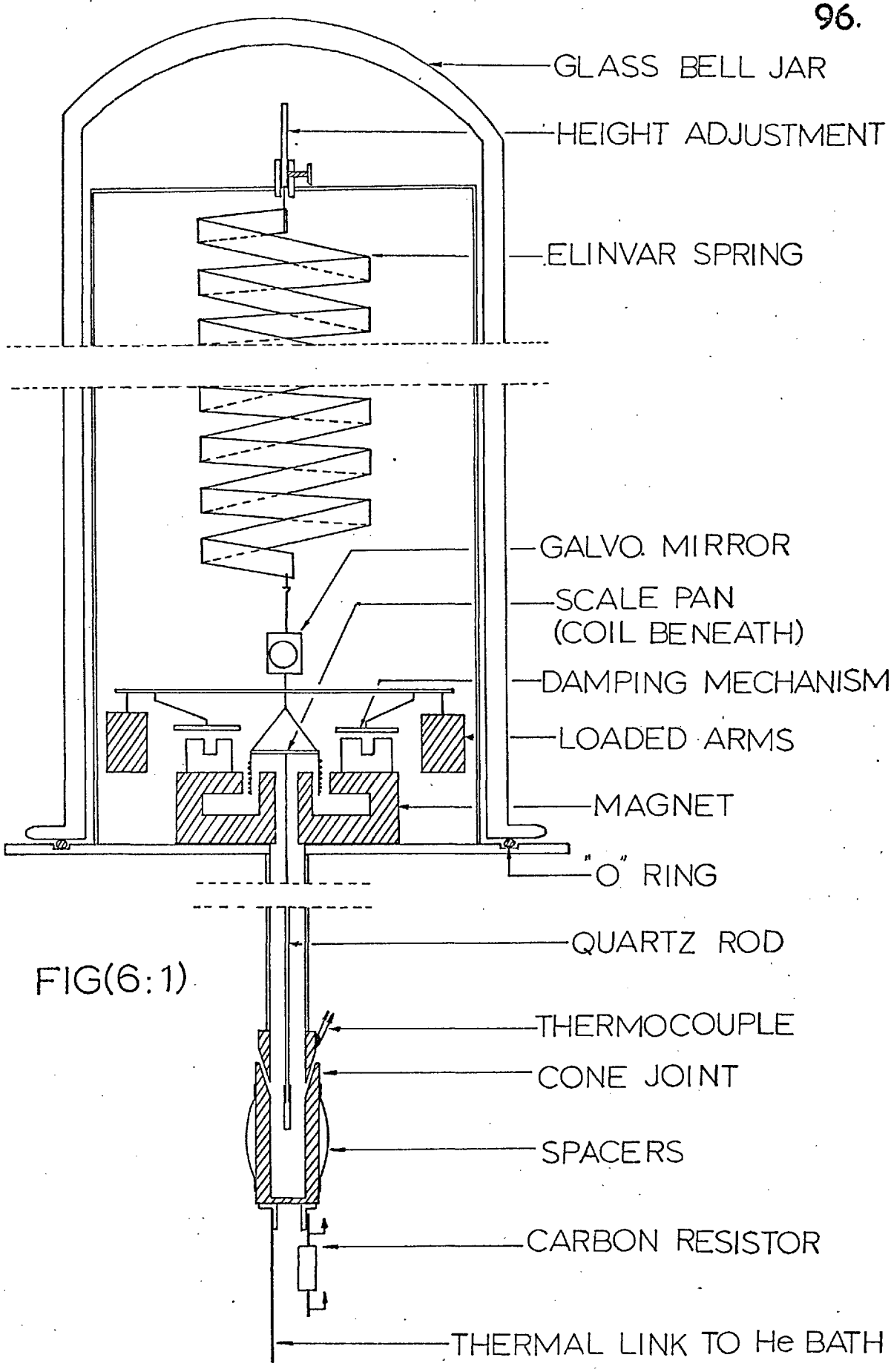
GLASS BELL JAR
HEIGHT ADJUSTMENT
ELINVAR SPRING
GALVO. MIRROR
SCALE PAN
(COIL BENEATH)
DAMPING MECHANISM
LOADED ARMS
MAGNET
"O" RING
QUARTZ ROD
THERMOCOUPLE
CONE JOINT
SPACERS
CARBON RESISTOR
THERMAL LINK TO He BATH

FIG(6:1)

FIG(6:2)

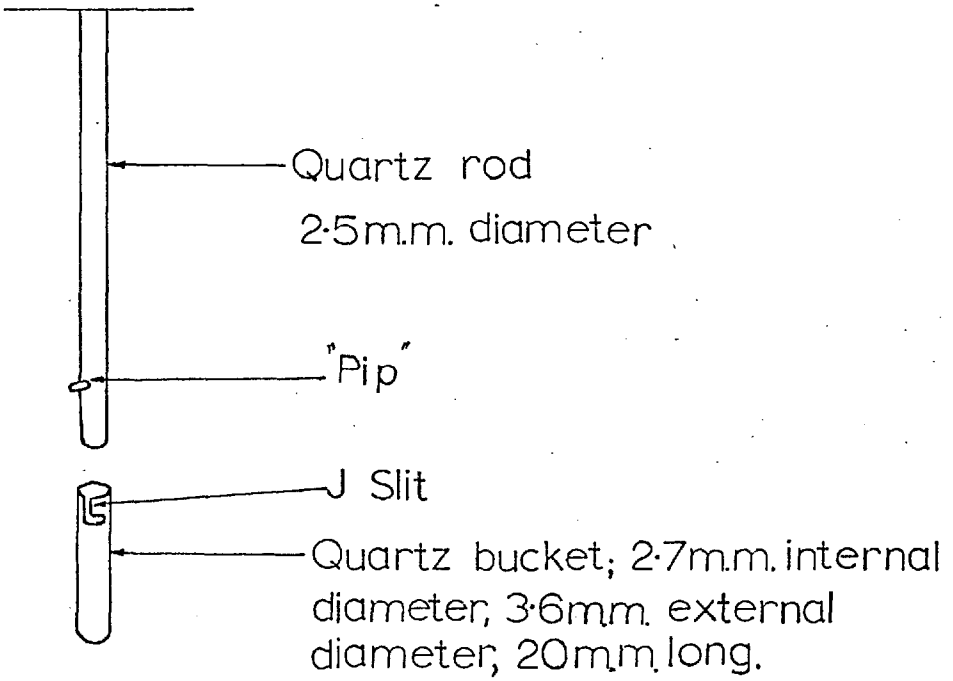

FIG(6:4)

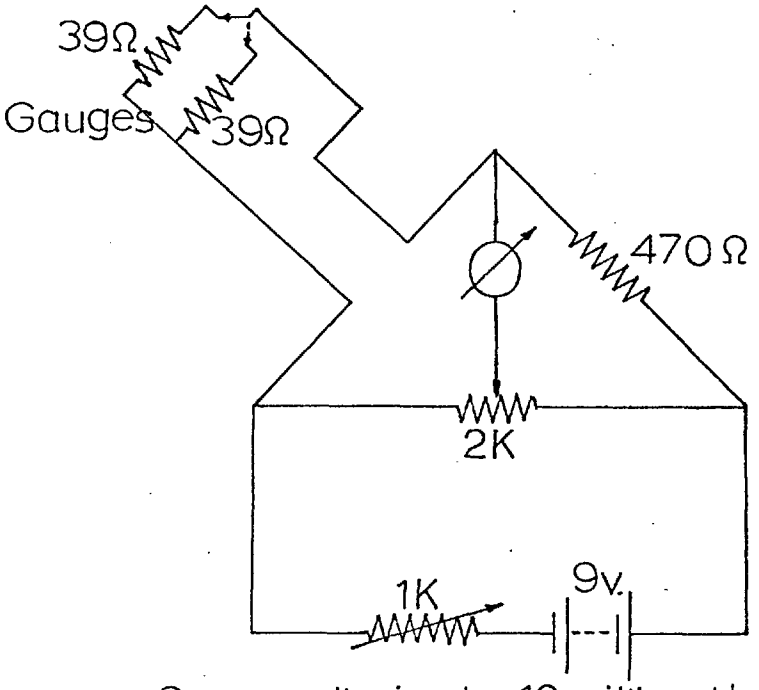

Gauges dissipate 12 milliwatts at 4·2°K

and a light beam incident on a galvanometer mirror located at the bottom of the spiral, to be deflected. This deflection is detected by observing the changing output from a differential selenium photocell, on which the light beam shines. The system is null detecting since the specimen can be restored to its initial position by passing a current through the restoring coil until the photocell output returns to its original value. The magnitude of this restoring current gives a measure of the extra force exerted on the sample by the applied field. The system is calibrated by using a known load (a Pt. rider of 105.48 mgms.).

The loudspeaker magnet, which surrounds the restoring coil, rests on a brass plate, the link to the quartz rod passing through a hole in the centre of this plate. The upper section of the system is housed in a glass bell jar which rests on a 'O' ring seated in a groove in the brass plate, while the lower part of the system is surrounded by a German silver tube attached to the underside of the plate and ending in the copper cone arrangement indicated in figure (6.1). This provides access to the lower end of the quartz rod and specimen. The cone joint is sealed with Edward's high vacuum grease,

and remains leak tight below the λ-point of helium. Such an arrangement enables the whole system to be evacuated and provides reasonably quick access to the specimen. It is accomplished in a very compact manner, an important consideration since the region surrounding the specimen must pass into a magnet pole gap of 31 mms.

3. Temperature measurement

With the type of experimental arrangement described above, it is not possible to measure the specimen temperature directly since this would involve attaching sensors directly to the suspension, drastically reducing its sensitivity. Instead, the temperature of the copper cap is measured, thespecimen being maintained in thermal contact with this by admitting a m.m. of helium exchange gas into the region surrounding the specimen.

In the range 1.9 to 30^{o}K the temperature of the cap is measured by a 39 ohm (nominal) Allen-Bradley resistor. From 20^{o}K to room temperature a Ag normal versus Au-2% Co thermocouple is used, the 10^{o} overlap providing a valuable check on the calibration of both sensors. The arrangement of thermocouple and carbon resistor relative to the sample is indicated in figure (6.1).

Two 40 gauge insulated copper wires are soldered across the resistor, one of these and one lead of the resistor are soldered directly to the base ofthe copper cap. The two 40 gauge wires were wrapped a few times around the cap and bound to it with G.E. varnish. They were then loosely coiled around the German silver tube (to reduce temperature gradients) and emerge from the cryostat via an Araldite seal. The varying resistance of this sensor is observed using the circuit indicated in figure (6.3).

The two thermocouple leads were joined in a small mound of solder on the lip of the cone joint. They were then wrapped several times around the base of the German silver tube, being electrically insulated from it and from each other by thin layers of condenser paper bound in G.E. varnish. The wires then passed into systoflex tubes loosely wrapped around the down tube, leaving the top of the cryostat via the Araldite seal. This seal also carried 40 gauge insulated copper leads to two depth gauges which monitored the helium level, this being concealed within a brass nitrogen dewar and a silvered glass helium dewar. These gauges were soldered directly to the German silver tube at suitable intervals, the

FIG(6:3)

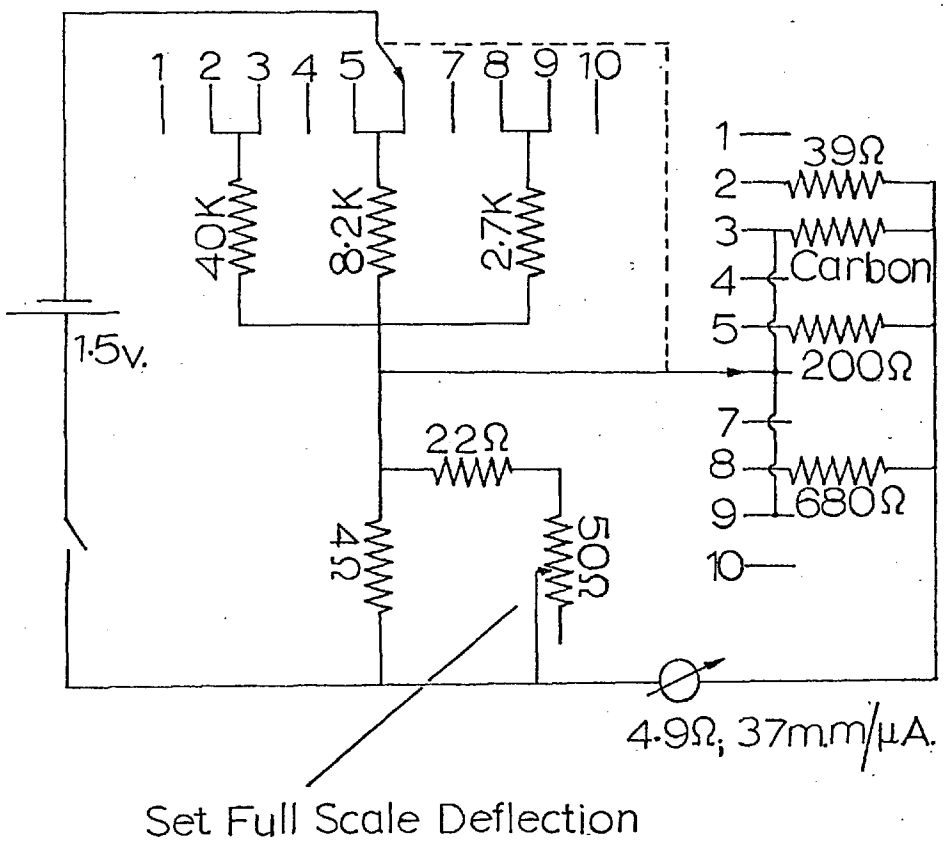
1 2 3 4 5 7 8 9 10
40K
8·2K
2·7K
1·5v.
22Ω
45
50Ω
1
2
3
4
5
7
8
9
10
39Ω
Carbon
200Ω
680Ω
4·9Ω; 37mm/μA.
Set Full Scale Deflection

tube being used as a return path for both. Ordinary 39 ohm (nominal) carbon resistors were used as gauges. They were wrapped in cotton wool held around them with masking tape, this arrangement resulted in a relatively large change in the observed resistance as the gauges passed below the helium level. The changing resistance was observed using the simple wheatstone bridge arrangement drawn in figure (6.4).

4. Calibrations

(a) Magnet

The required inhomogeneous magnetic field was produced by a Newport Type A magnet fitted with conical pole tips, having a 31 m.m. pole gap. The energizing current for the magnet was produced by a Wareham 1 K.W. power supply, controlled externally with the circuit indicated in Appendix 4. This current was read on a Crompton-Parkinson moving coil meter which was examined for reproducibility at regular intervals.

Equations (6.1) and (6.2) imply that the quantities $\partial H_x/\partial z$ and $H_x \partial H_x/\partial z$ must be known so that the magnetisation and susceptibility can be calculated from the force acting on the sample. These quantities can be evaluated by measuring H_x and $H_x \partial H_x/\partial z$.

The variation of the magnetic field perpendicular to the plane of the pole faces, H_x, along the vertical (z) direction, was investigated using a flip coil and flux meter. A correction was employed for the finite size of the flip coil (Appendix 5). These measurements indicated that this variation followed an almost universal curve for all values of the energizing current up to the maximum used, 6.5 amps. Rather than calibrate the flux meter so that the absolute field value could be determined, the central field was measured, as a function of magnet current, with a Hall probe of small cross sectional area (6m.m. square). The variation in field across the probe being about 0.3%. Combining these two sets of results enabled $H_x(z)$ to be tabulated as a function of magnet current.

A rough estimate of $H_x \partial H_x/\partial_z$ could be made from the above results. However, a more careful study of this quantity, in the region of the estimated maximum, was made using a Pd sample of known susceptibility (5.23×10^{-6} e.m.u./gm at 295^oK[78]). The results indicated that the position of this maximum did not alter on changing the magnet current. The calibration of $H_x \partial H_x/\partial_z$ at the maximum, as a function of energizing current, was done

with both Pd and Ta ($\chi = 0.849 \times 10^{-6}$ e.m.u/gm at 295°K)[79], the two sets of results were in very good agreement.

(b) Temperature

The carbon resistor was calibrated by measuring its resistance as a function of helium vapour pressure below 4.2°K, the temperature was obtained using standard tables[80]. Thirty such points were taken between 1.9 and 4.2°K, and fitted by the method of least squares to the equation[81]:

$$\log R + K(\log R)^{-1} = BT^{-1} + A \qquad 6.3$$

Measurements of the resistance at 77 and 293°K were also included in the fit.

The thermocouple was normally used with one junction at ice point. It was calibrated simply by comparing the measured output at 4.2 and 77°K with those tabulated by Powell[82] and employing a linear interpolation on the difference. This procedure was sufficiently accurate in this context since the arrangement of temperature sensors relative to the sample made it meaningless to measure the temperature to better than 0.5°K during warm up above 4.2°K. Measurements taken during warm up indicated that carbon resistor and thermocouple agree to within 0.5° in the region of overlap (20 to 30°K).

This, coupled with the agreement obtained between the tabulated[83] and 'measured' melting point of isopentane (113°K), encouraged confidence in both calibrations.

5. Experimental procedure

The force exerted on the quartz rod and elinvar spiral by the magnetic field made it necessary to perform two sets of measurements to obtain the force on the sample, i.e. one set on the sample and system, the other with the sample removed.

Before each complete set, the end of the quartz rod and the bucket were cleaned in dilute HCl, washed in distilled water, immersed for a short time in CCl_4 and finally allowed to dry. The specimen, usually in the form of a cylinder of diameter 2.5 mms, and a few mms long, was placed in the bucket and attached to the quartz rod. Following this the position of the damping discs relative to the button magnets was adjusted for maximum damping. The magnet was then wheeled into position, and its height arranged, using adjustable screws under the magnet bed, so that the centre of the specimen lay at the position of maximum Hx Hx/ z. This position was checked with a travelling microscope,

which was also used to check that the specimen lay equidistant from either pole face. The cone joint was then sealed with Edward's high vacuum grease, and the system evacuated.

After several hours pumping 1mm of helium exchange gas was admitted. Following this, the response of the system to a small restoring force indicated whether it was swinging freely, while the cone joint could be leak tested by surrounding it with liquid nitrogen. Any leak significantly increased the noise level. Provided both tests were satisfactory, the dewars were fitted around the down tube in such a position that the balance remained unhampered and the dewar tail passed freely into the magnet pole gap. Some adjustment was initially required to satisfy both conditions, but once established, the dewar locating device described in reference 84 ensured that subsequent dewar fittings could be accomplished with minimum effort.

The inherent drift in a system of this type meant that zero photocell output usually necessitated a finite restoring current. The latter was measured by recording the voltage it produced across some suitable resistor using a two dial Tinsley potentiometer. The series of

observations, required to evaluate the force exerted by the field on the sample, followed the pattern:

(i) Measurement of zero field restoring voltage.

(ii) Measurement of some finite field restoring voltage.

(iii) Estimating the zero field drift by noting the 'final' photocell output.

The actual force was obtained by correcting (i) for (iii), provided (iii) was not too large, and subtracting the result from (ii). Calibration of the system was achieved in the manner indicated previously. In this way the force on the sample at room temperature was measured at nine field values. The inner space of the helium dewar was then filled with an atmosphere of exchange gas, and the interspace of the same dewar evacuated by an oil diffusion pump backed by a spring-mounted rotary pump, and connected to the dewar by some 15" of PVC tubing. This arrangement allowed continuous pumping, yet produced no significant increase in background noise. Liquid nitrogen was then poured into the outer dewar. The temperature of the specimen was lowered in 10^{o} intervals by monitoring the interspace vacuum using a valve at the head of the pump. At each

temperature the force on the sample at a suitable field was measured, the temperature being estimated from the thermocouple voltage measured on a portable Tinsley potentiometer. In this way the temperature was lowered to 77°K, when once again the specimen force was measured at nine field values.

Liquid helium was then transferred intothe inner dewar, and when this had settled the force, as a function of field, was measured. Temperatures below 4.2°K were produced by pumping on the helium bath. It was found that stable temperatures could be produced simply by controlling the pumping rate with a needle valve, while at each temperature the specimen force was measured at a suitable field value. In this manner temperatures down to 1.9°K could be attained. At the lowest temperature the force was once again measured as a function of field.

Temperatures in the range 4.2 to 77°K were obtained by allowing the system to warm up naturally. The force was measured at a single field value in this range. The rate of warm up in this region (1° per minute) was somewhat improved by continually pumping the helium dewar interspace (1° in 90 seconds).

Measurements on the empty system were carried out in an analogous manner. However, it was usually necessary, on removing the sample, to readjust the system so that the quartz rod remained in the same position in the applied field.

6. Errors in measurement

Under ideal conditions the balance can resolve 2×10^{-3} dynes, however background noise and zero field drift tend to reduce this figure. Above 77°K the experimental arrangement allows temperatures to be maintained at a reasonably constant value, consequently the zero field drifts are small. The sensitivity limitation is then the background noise which is typically 10^{-2} dynes. Below 77°K zero field drift tends to reduce this figure typically to about 5×10^{-2} dynes.

The errors arising from such sources can be reduced by using samples of such a size that theforce exerted on them by the field is several orders of magnitude larger than the figures quoted above. However in many cases the $(T)^{-1}$ dependence of the susceptibility meant that large specimen forces (50 to 100 dynes) in the liquid helium range were considerably reduced on

warming up to liquid nitrogen temperatures. Consequently where possible, samples used below 77°K were replaced by larger ones for higher temperature measurements.

As mentioned previously, the arrangement of carbon resistor and thermocouple make it meaningless to measure the temperature to better than 0.5°K during warm up. Below 4.2°K however, this is not the case. Provided sufficient time is allowed for the temperature to stabilise (typically 5 minutes), the accuracy of the temperature measurement is better than 0.02°K. One disadvantage of the present arrangement is that the balance does not distinguish between a 'direct pull' and a couple. Consequently errors in measuring the sample force could arise from sample misalignment. These, however, have been roughly estimated (Appendix 6) and are typically less than 0.5% of the vertical sample force.

7. A servo-mechanism for the balance

As indicated previously, the warm up rate between 4.2 and 77°K (1° in 90 seconds) is such, compared with the time taken to make a single measurement (45 seconds for the actual balancing, 2 minutes after all readings have been taken), that in this temperature range readings

can be taken at one field value only, and in addition must be taken continuously to obtain a reasonable number of experimental points.

An attempt has been made to improve on this situation by making the balance servo-restoring. At the outset it was realised that any automated arrangement could not simultaneously be null detecting system since, having initially set the photocell output and the restoring current to zero, the application of a magnetic field to the sample requires an additional restoring force for null detection. The initial conditions however, imply that an additional force requires an out of balance signal for its production. Such an out of balance signal can be made quite small provided sufficient amplification is used. Automation can be accomplished by feeding the restoring coil with a suitably amplified photocell output. This suggests a d.c. amplifying system, but in order to overcome the drift problems inherent in such an arrangement, it was decided to convert the photocell output from d.c. to a.c. before amplification, reversing the process before feeding the final signal into the restoring coil.

Several methods of conversion were tried, including mechanically chopping the light beam with a fan, but the most suitable system was found to be the electronic chopper-amplifier drawn in figure (6.6). Basically the circuit consists of a apir of transistors which consititute a balanced chopper. The chopping action is produced by driving these transistors alternatively on and off by applying square waves from a multivibrator to their bases; these square waves are 180° out of phase. In this way the input signal, fed into one of the transistors, is sampled at the chopping frequency (1.7 Kc/s). The chopper is condensor coupled to an amplifying section, from which the signal is synchronously detected, giving an output in phase with the input. The smoothing action of the resistor-capacitor arrangement in the detector ensures a reproduction of the now amplified input signal. The output from this system is adjusted to zero, for zero input, using the variable resistor in the chopper circuit, while thermally anchoring the chopper transistors helped maintain this condition by reducing zero drifts to typically 2μv/$^{\circ}$C. The output from the chopper-amplifier was fed into another amplifying section via a zero set circuit, and finally into

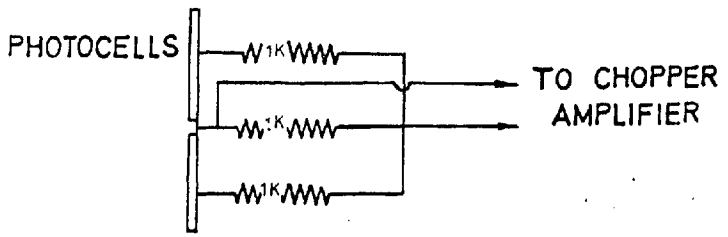

FIGURE [6:5]

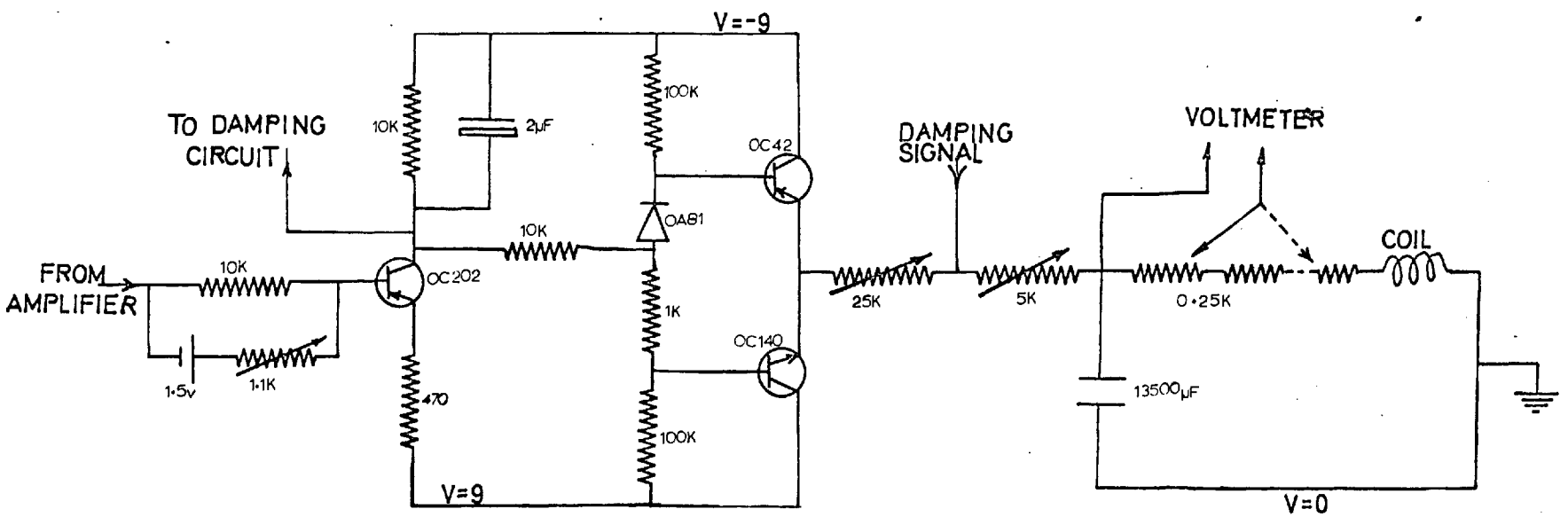

FIGURE [6:7]

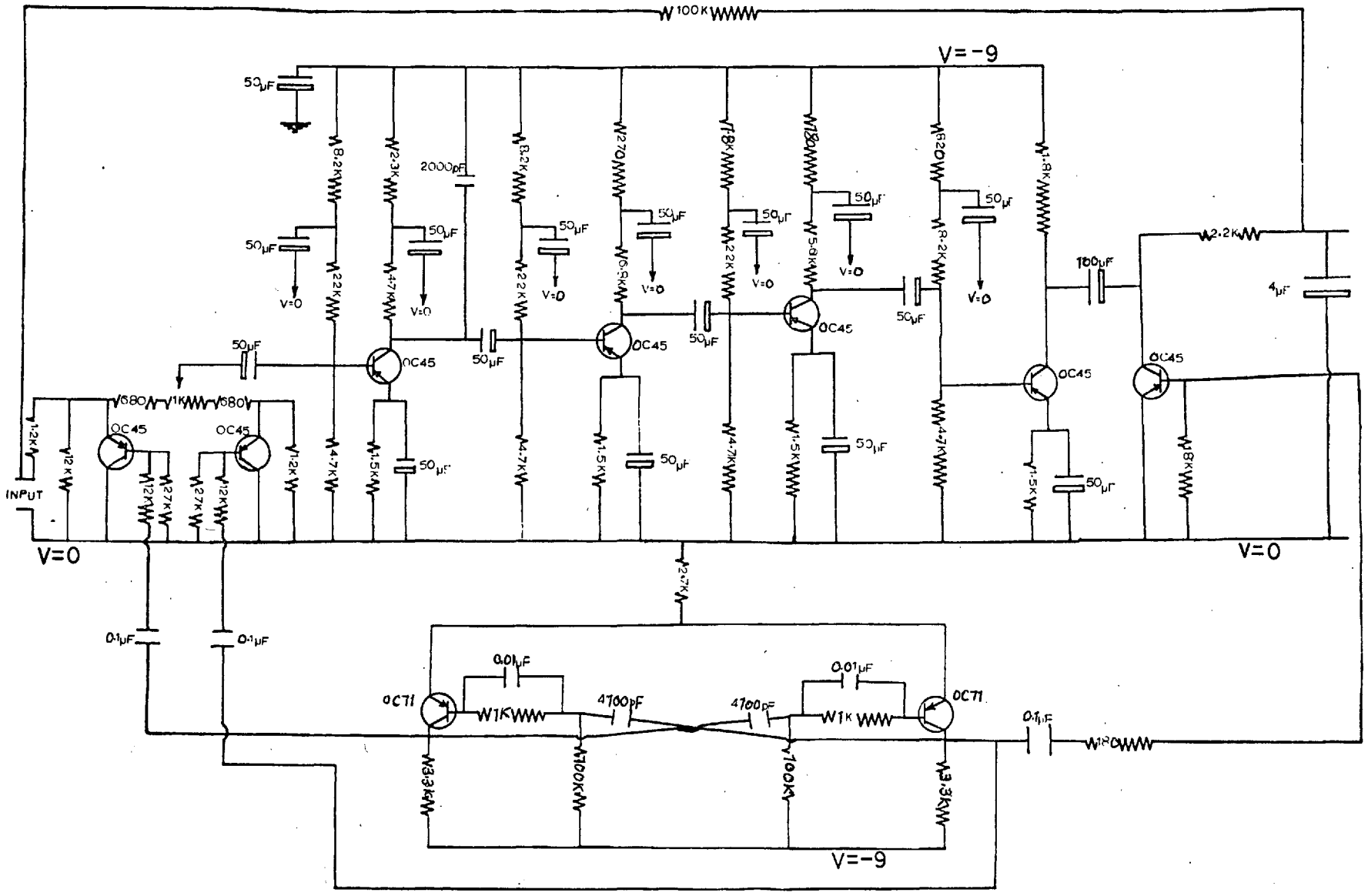
100K
V=-9
50μF
8.2K
2.3K
2000pF
8.2K
270
18K
18K
820
1.8K
2.2K
4μF
100μF
22K
4.7K
22K
5.6K
22K
5.6K
50μF
V=0
OC45
680
1K
680
1.2K
12K
27K
4.7K
1.5K
INPUT
V=0
0.1μF
2.7K
0.01μF
OC71
W1K
4700pF
3.3K
100K
V=-9

FIGURE [6.6]

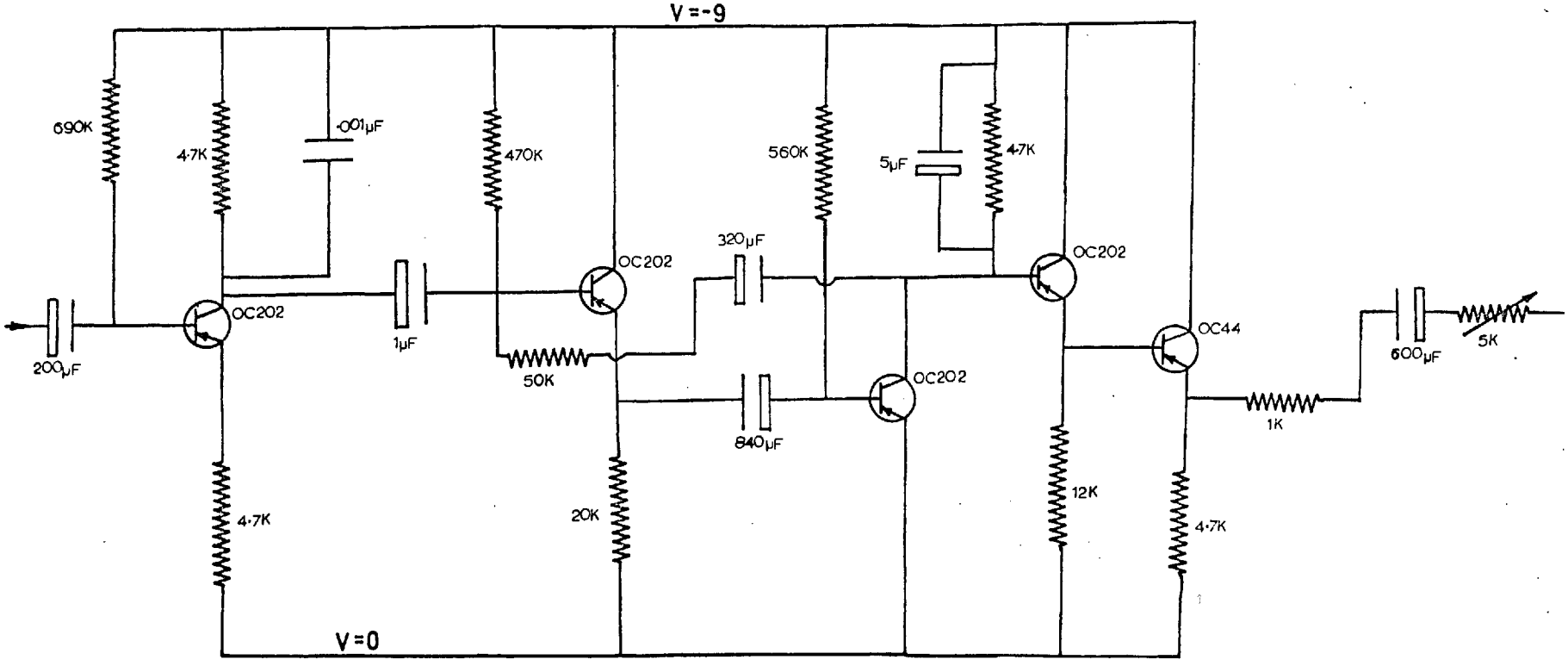
V=-9
690K
4·7K
·001μF
470K
560K
5μF
4·7K
320μF
OC202
OC202
OC202
OC44
200μF
1μF
50K
840μF
600μF
5K
1K
12K
4·7K
20K
4·7K
V=0

FIGURE [6:8]

a White follower-figure (6.7). The signal from this passes directly into the restoring coil via a variable protective resistor.

While the button magnets and copper discs introduce sufficient damping when using manual restoration, it has been found necessary to provide a greater degree of stabilisation for use with the servo mechanism. In the automated condition, relatively rapid damping can be obtained using a velocity damping technique in which the restoring coil is provided with a signal proportional to the rate of change of the actual servo-restoring signal. Paradoxically, some difficulty arose from that property of the balance which makes it so attractive for use in the present context, i.e. mechanical decoupling of the vibrational and rotational modes. Both specimen and restoring forces act in a vertical direction, but manifest themselves via a rotation in the torsional mode. Any velocity signal should be fed back into the system at the point at which it is appropriate, however, this was initially found to be rather difficult to accomplish owing to the attenuation that exists between the two operative modes. This difficulty has been partly overcome by using a differentiating circuit which

incorporates a transitional phase amplifier which was used to optimise the phase lead of the velocity signal in the appropriate frequency region. This circuit is drawn in figure (6.8). The signal from this circuit was fed into the coil via a series protecting resistor, the coil being shunted by a 13500μFd condenser which offered an easy ground path for relatively high frequency signals which would otherwise have set the balance into vertical vibration. The smoothing action of this condenser coupled with the coil series resistors enabled the feedback voltage to be read directly on a 'Digitec' voltmeter connected across these series resistors.

8. Servomechanism performance

During operation, it has been found that the servo-restoring current, for a given mechanical load, can be raised to some 92 or 93% of the restoring current necessary to maintain a null condition. Increasing the servo gain beyond this figure induces a strong tendency for the system to oscillate. The servo-system can be calibrated by comparing its output (i.e. the feedback voltage across a suitable resistor in series with the restoring coil) with that obtained using manual restoration.

These calibrations were carried out at nine different field values at various fixed temperatures (1.9, 4.2, 77 and 295^{o}K). A linear interpolation between differing fixed point calibrations was used, these differences being typically 1 to 2%. In addition to the normal zero field drift in the balance, which was reflected in the changing zero field servo-restoring output, there also existed a background noise of typically $\pm$ .05 dyne. This is due to imperfect stabilisation of the system and is a manifestation of the attenuation mentioned previously.

A comparison of the results obtained for a Pd sample using manual and servo-restoration is made in figure (6.9).

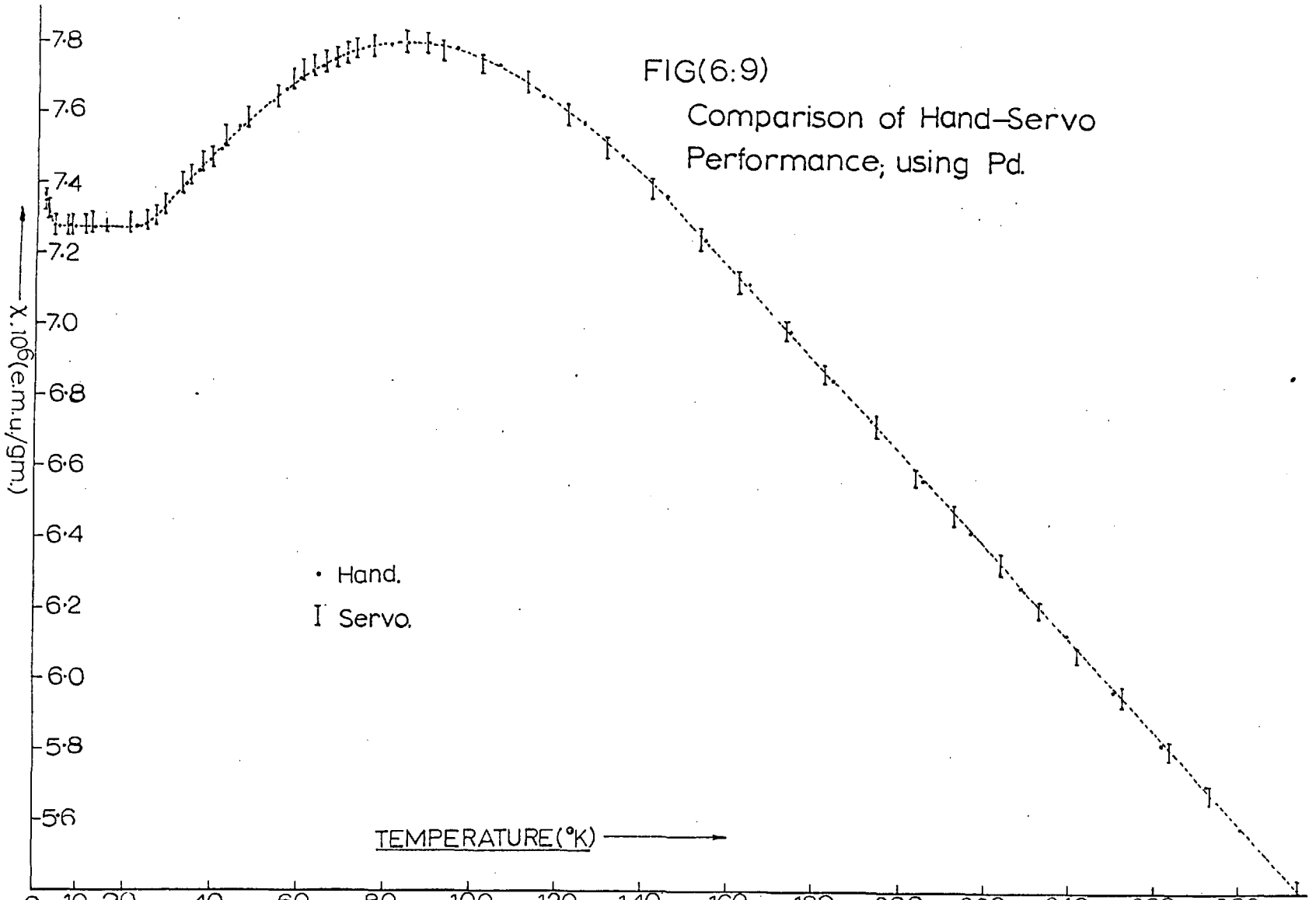

FIG(6:9)
Comparison of Hand–Servo Performance; using Pd.

CHAPTER 7

PRESENTATION OF EXPERIMENTAL RESULTS

The results for each specimen will be presented as Magnetisation versus Field plots at four fixed temperatures, together with a single field inverse susceptibility versus temperature plot. The history of the sample, and, where applicable, the metallographic analysis on the sample will be presented.

The alloy susceptibility was 'corrected' for that of the host using the data in Reference 86.

The source of each alloy is indicated.

General:

Many of the alloys were obtained in button form. These were machined into cylinders of diameter 2.5mm, from which a suitable length specimen was cut using a fine toothed hacksaw. Any burring of the edges of this specimen was removed with a small file. The specimens were etched for an hour in a solution of 1:2 $HCl:H_2O$ to remove any iron contamination of the surface, and finally washed in distilled water.

The microstructure of the dilute Ag rare earth alloys was examined by etching then in a solution of

approximately 2:2:5, H_2O:H_2O_2:NH_4OH. Photographs of this structure were taken with equipment loaned by the Department of Metallurgy.

Ag - 0.8At%Gd (Bijvoet, Amsterdam)

The alloy was cast forged and then annealed. Examination of its microstructure revealed a recrystallised, fairly fine grained f.c.c. solid solution, with some twinning and quite large amounts of second phase in the grain boundaries (and possibly in the body of the grains) - figure (7:1p).

Figures (7:1) to (7:4) summarise the experimental results.

Ag - 0.45At.%Gd (Bijvoet, Amsterdam)

This sample was cast, forged and then annealed. Metallographic analysis - figure (7:2p) - revealed a very similar microstructure to the more concentrated alloy, but with much less second phase. The experimental results appear in figures (7:5) to (7:8).

Ag - 0.1At.%Gd (Bijvoet, Amsterdam)

This alloy was cast, forged and then annealed at 650°C, and as figure (7.3p) indicates, formed a well crystallised single phase f.c.c. solid solution with much twinning.

The experimental data taken on this alloy is reproduced in figures (7.9) to 7.12). No measurements above 77°K were taken since the susceptibility difference between alloy and pure host decreases very rapidly with increasing temperature, reflecting the small concentration of rare-earth impurity.

Ag_3Gd(Harris, Birmingham)

A small lump, suitable for susceptibility measurements,,weighing about 5 milligms, was broken off a rather brittle original sample. This was etched for about 30 seconds in a 1:5 solution of $HCl:H_2O$, and then washed in distilled water.

Figures (7.13) to (7.15) summarise the experimental data.

Fig.(7:1p)

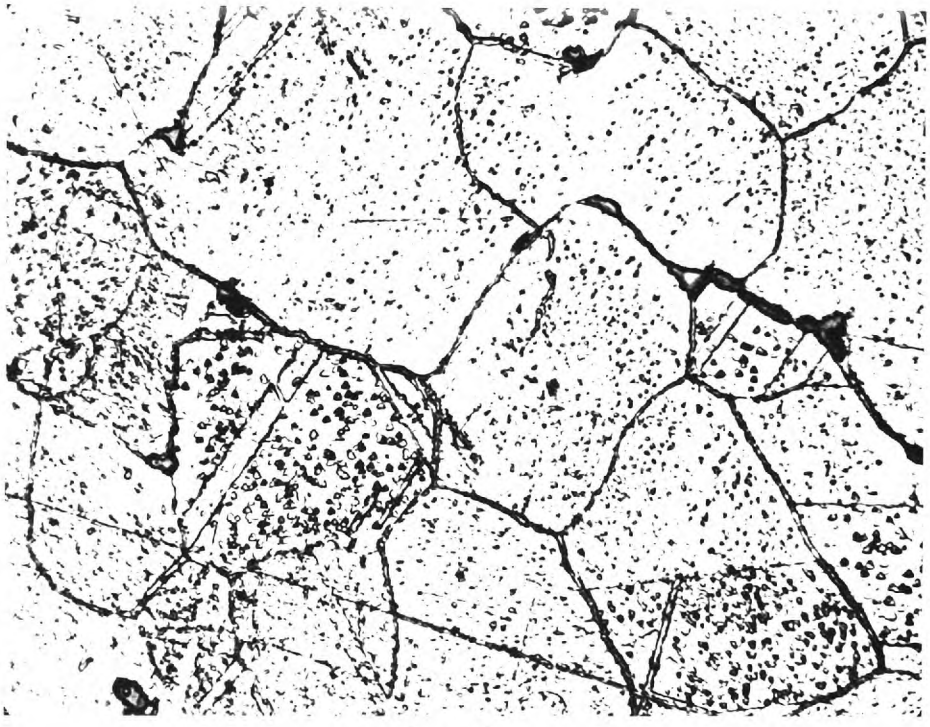

Fig.(7:2p)

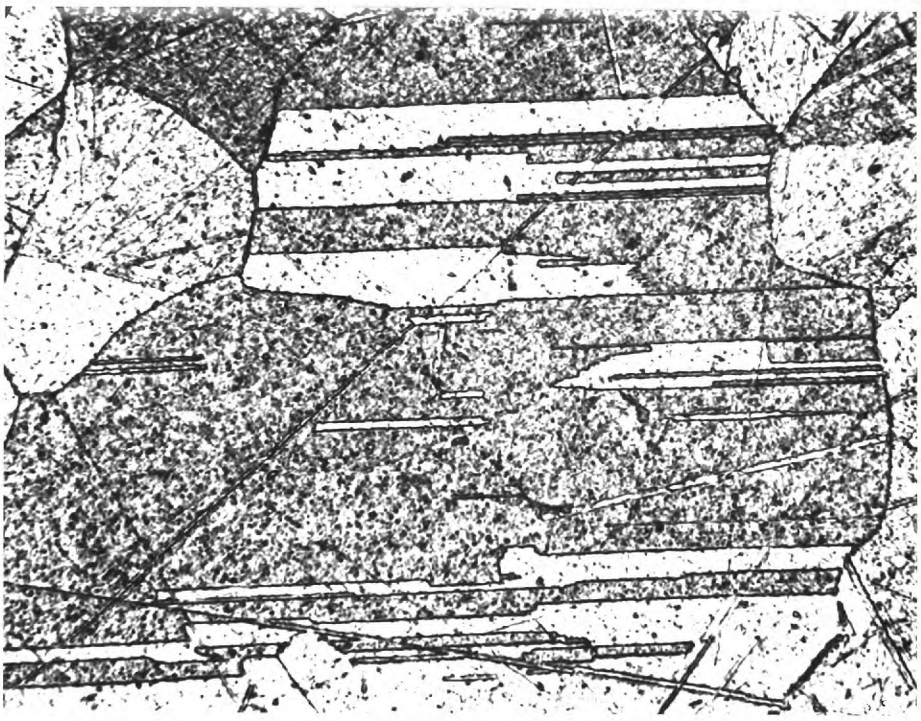

Fig. (7.3p)

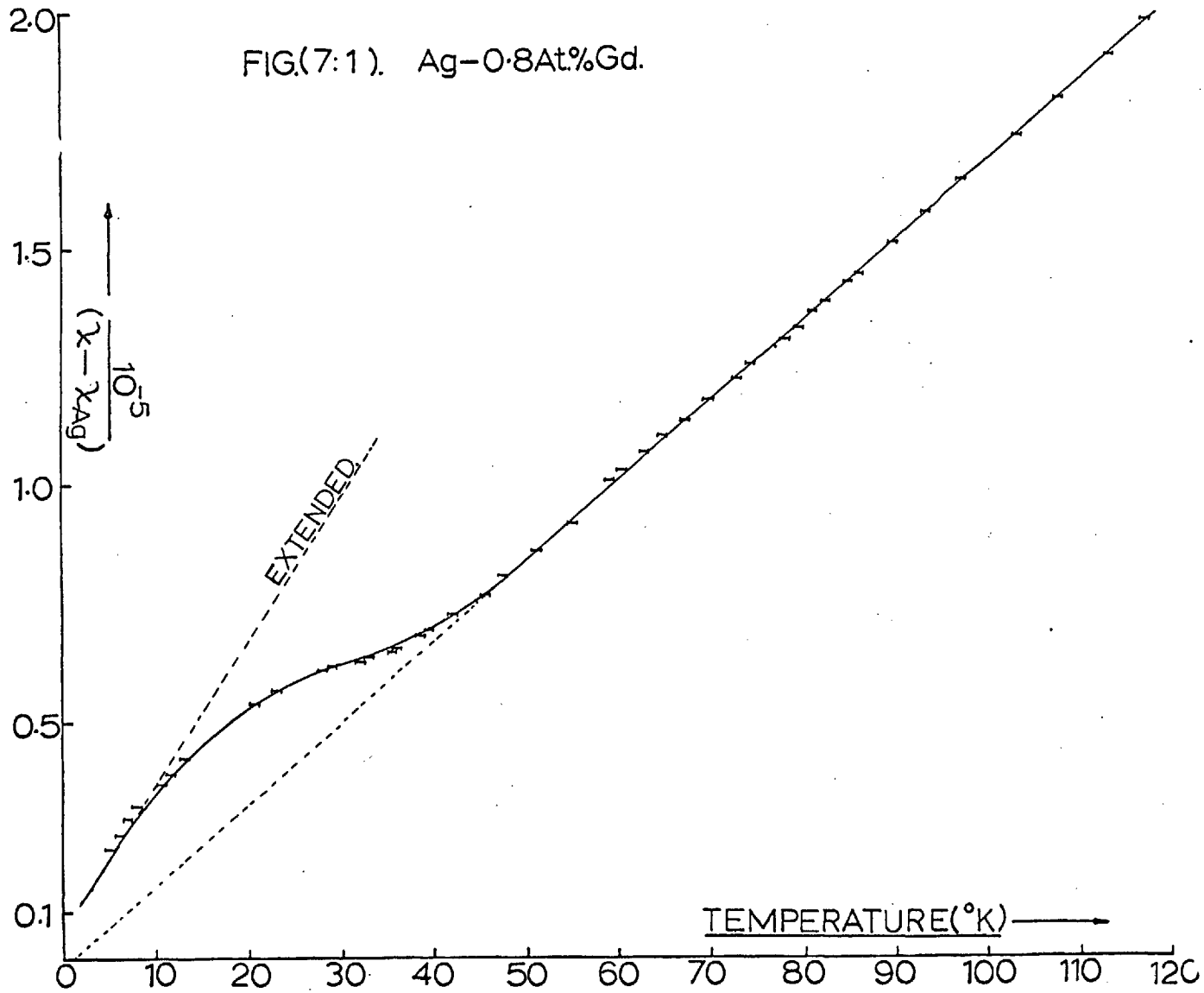

FIG.(7:1). Ag–0·8At.%Gd.

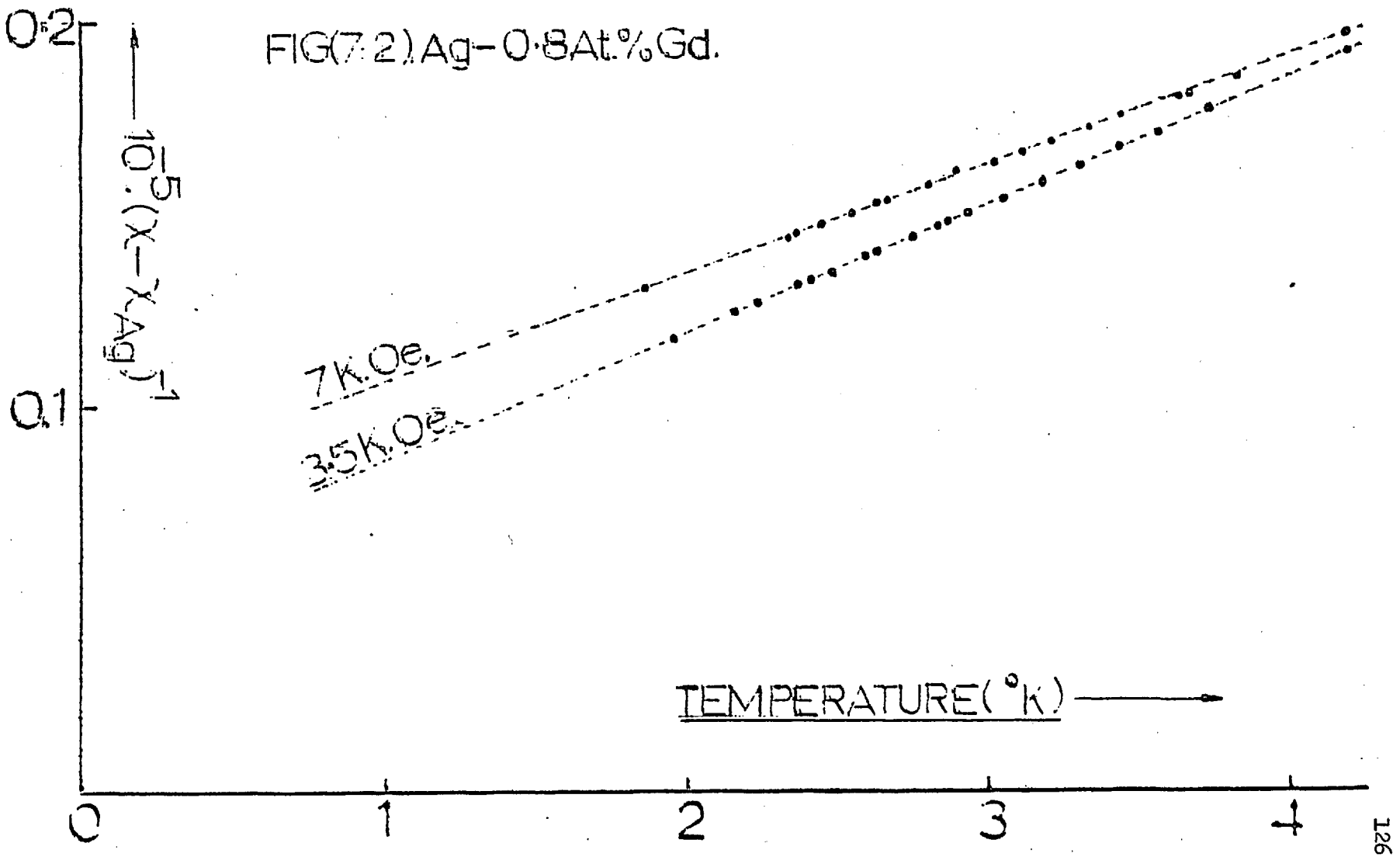

FIG(7·2) Ag–0·8At.%Gd.

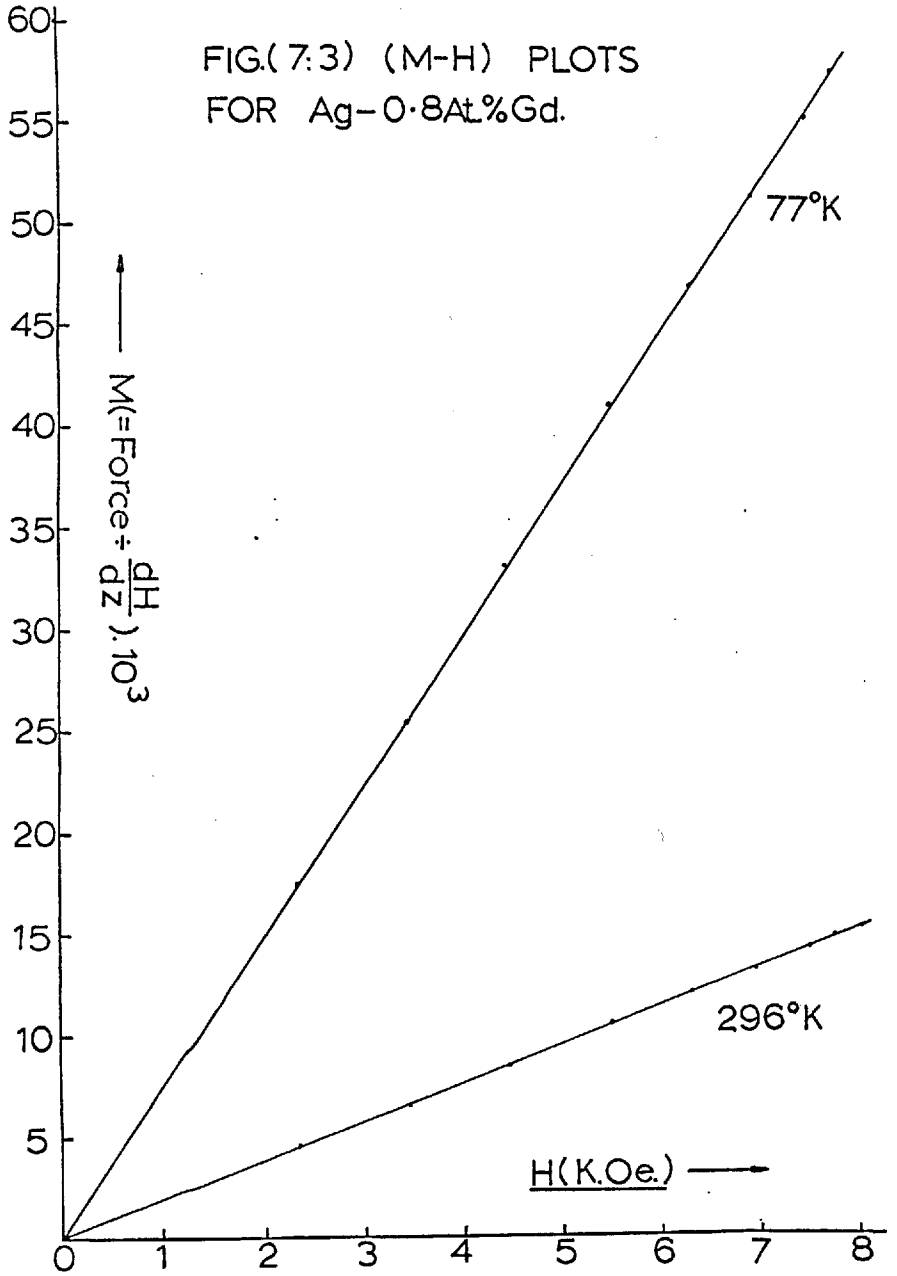

FIG.(7:3) (M-H) PLOTS FOR Ag-0·8At.%Gd.

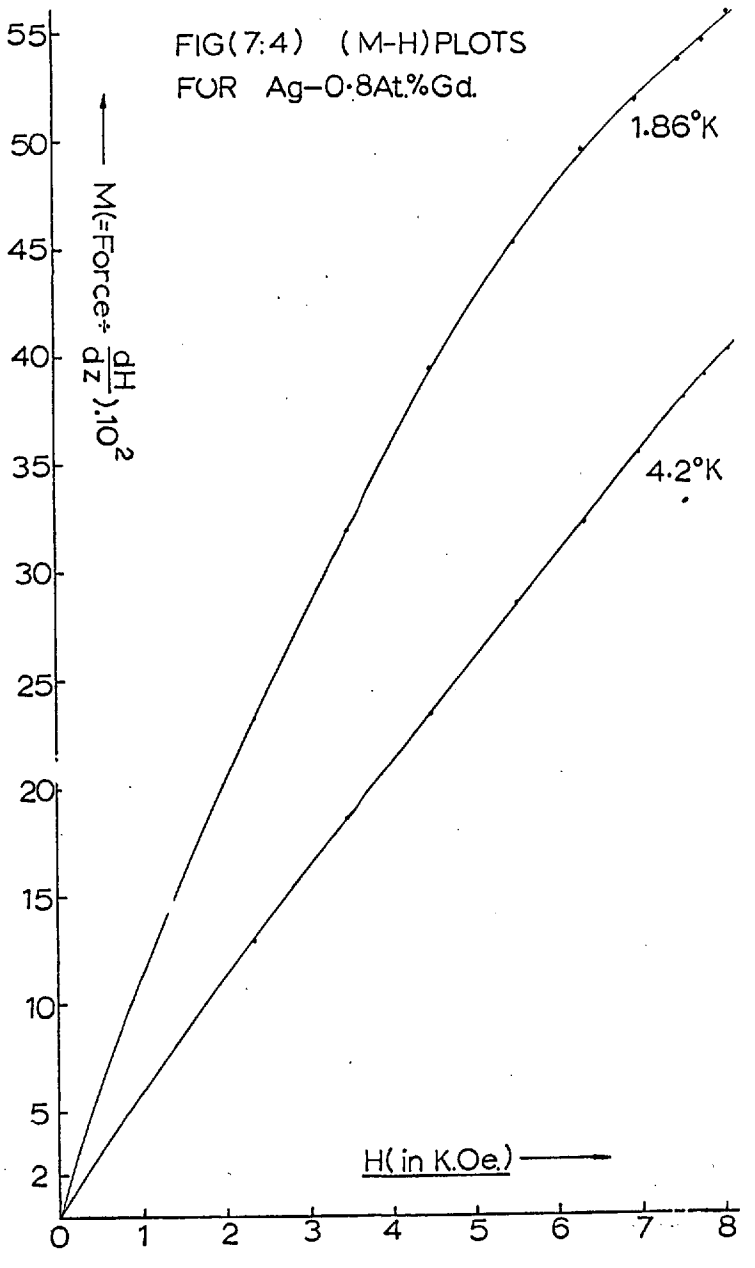

FIG(7:4) (M-H)PLOTS FOR Ag-0·8At.%Gd.

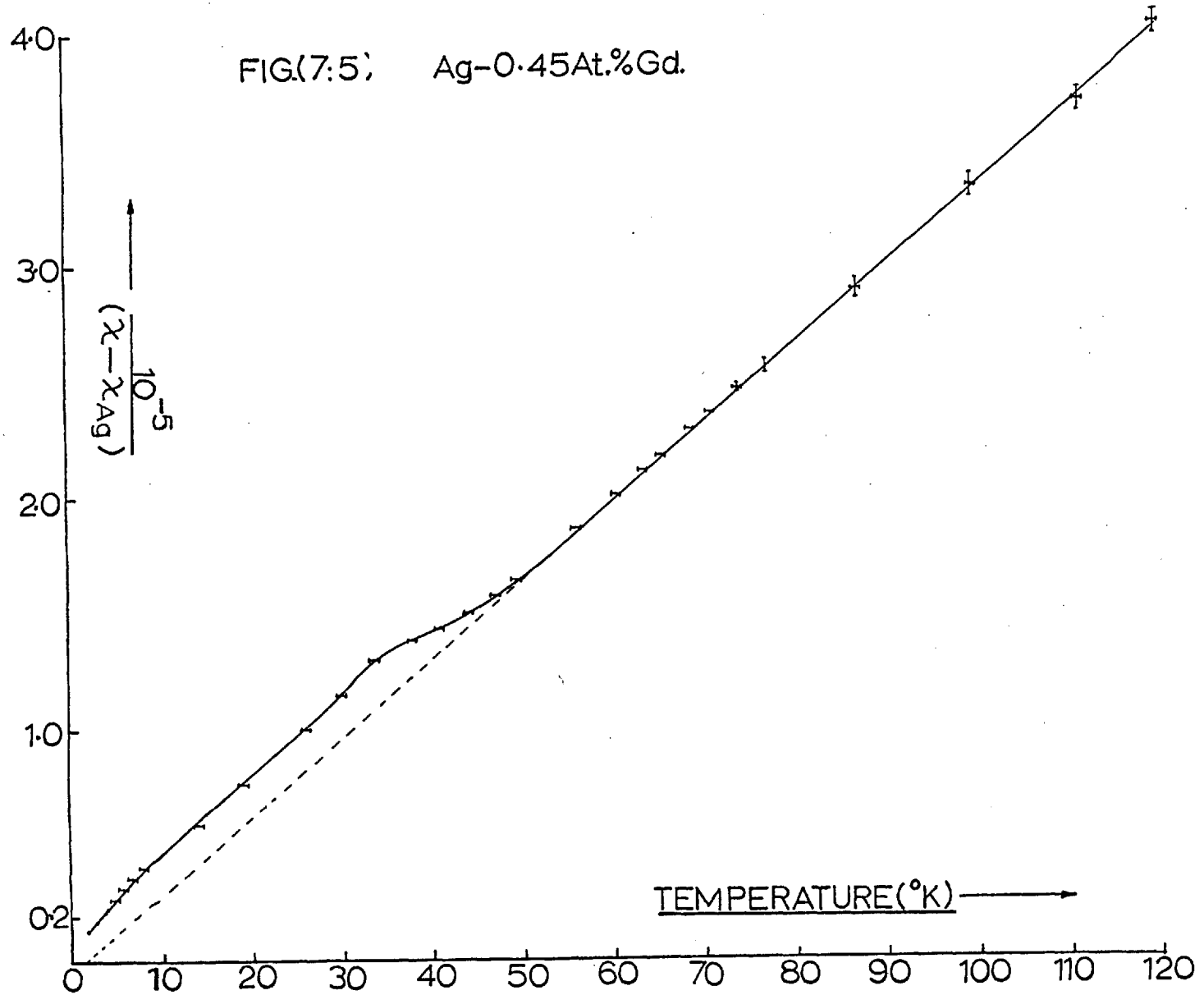
FIG.(7:5) Ag-0·45At.%Gd.
4·0
3·0
2·0
1·0
0·2
$\frac{10^{-5}}{(\chi - \chi_{Ag})}$
TEMPERATURE(°K)
0
10
20
30
40
50
60
70
80
90
100
110
120

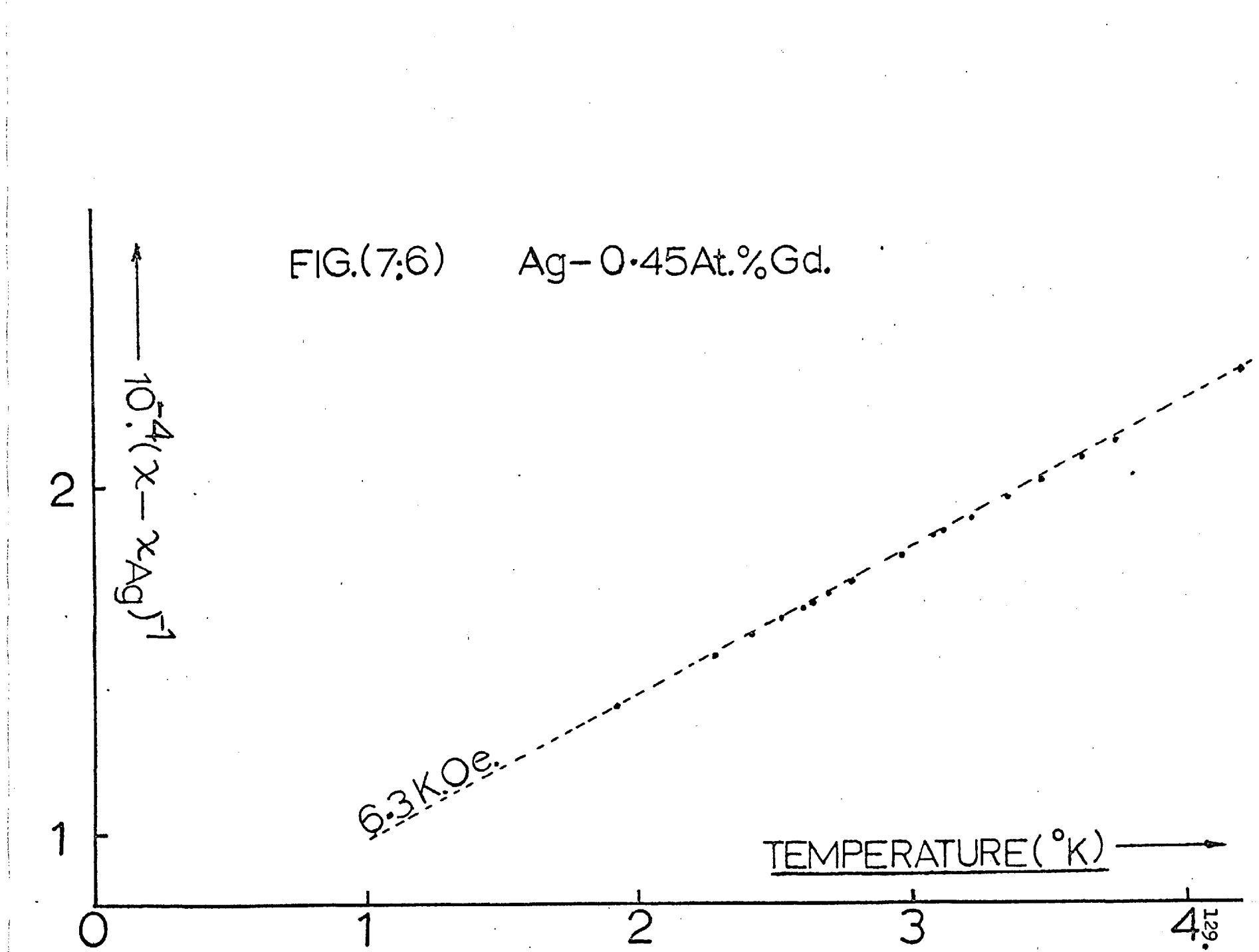
FIG.(7:6) Ag-0·45At.%Gd.
$10^{-4}(\chi - \chi_{Ag})^{-1}$
2
1
6·3 K.Oe.
TEMPERATURE(°K)
0
1
2
3
4

FIG.(7:7) (M-H) PLOTS
FOR Ag—0·45At.%Gd.

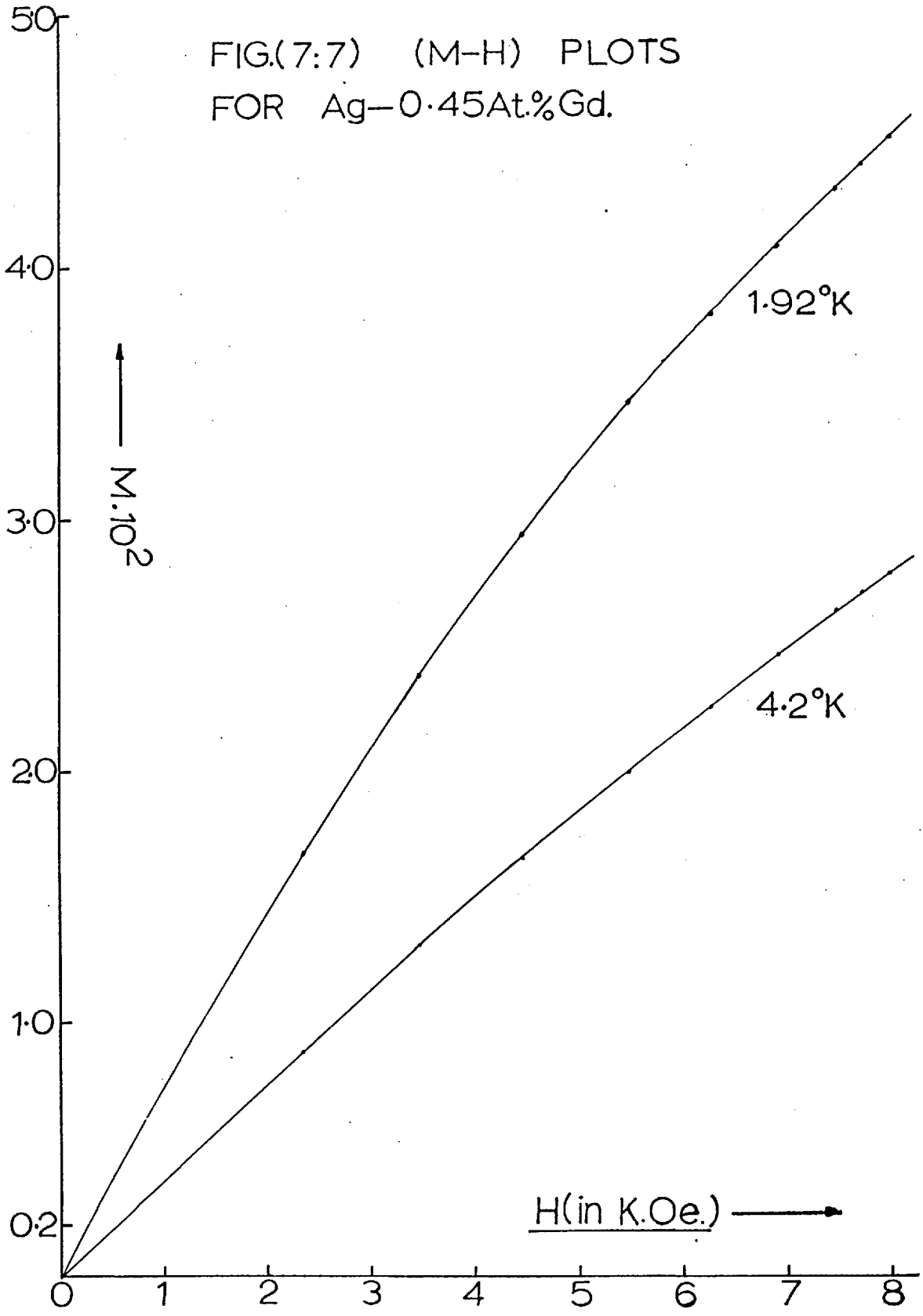

FIG.(7:8) (M-H) PLOTS FOR Ag–0·45At.%Gd.

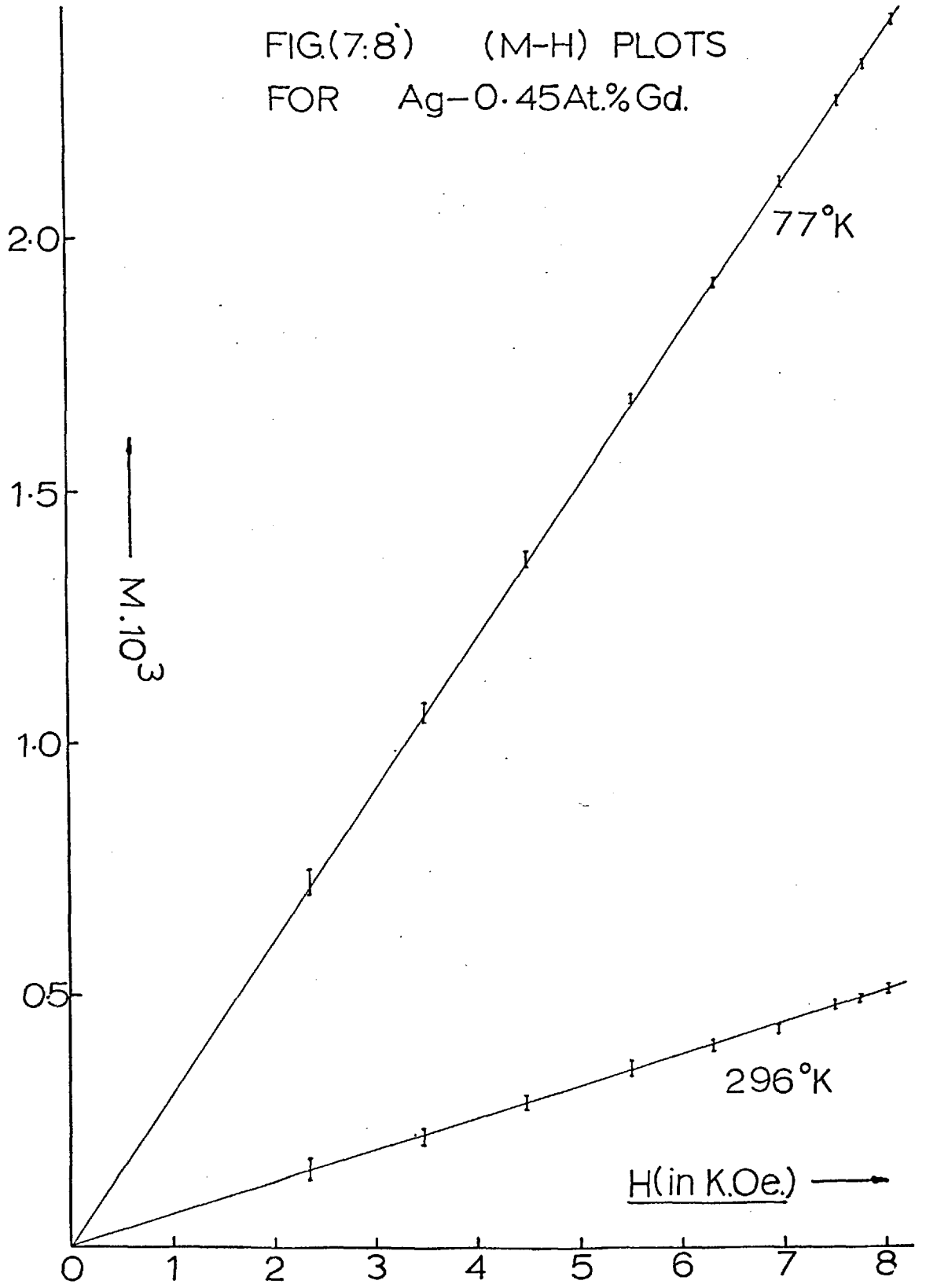

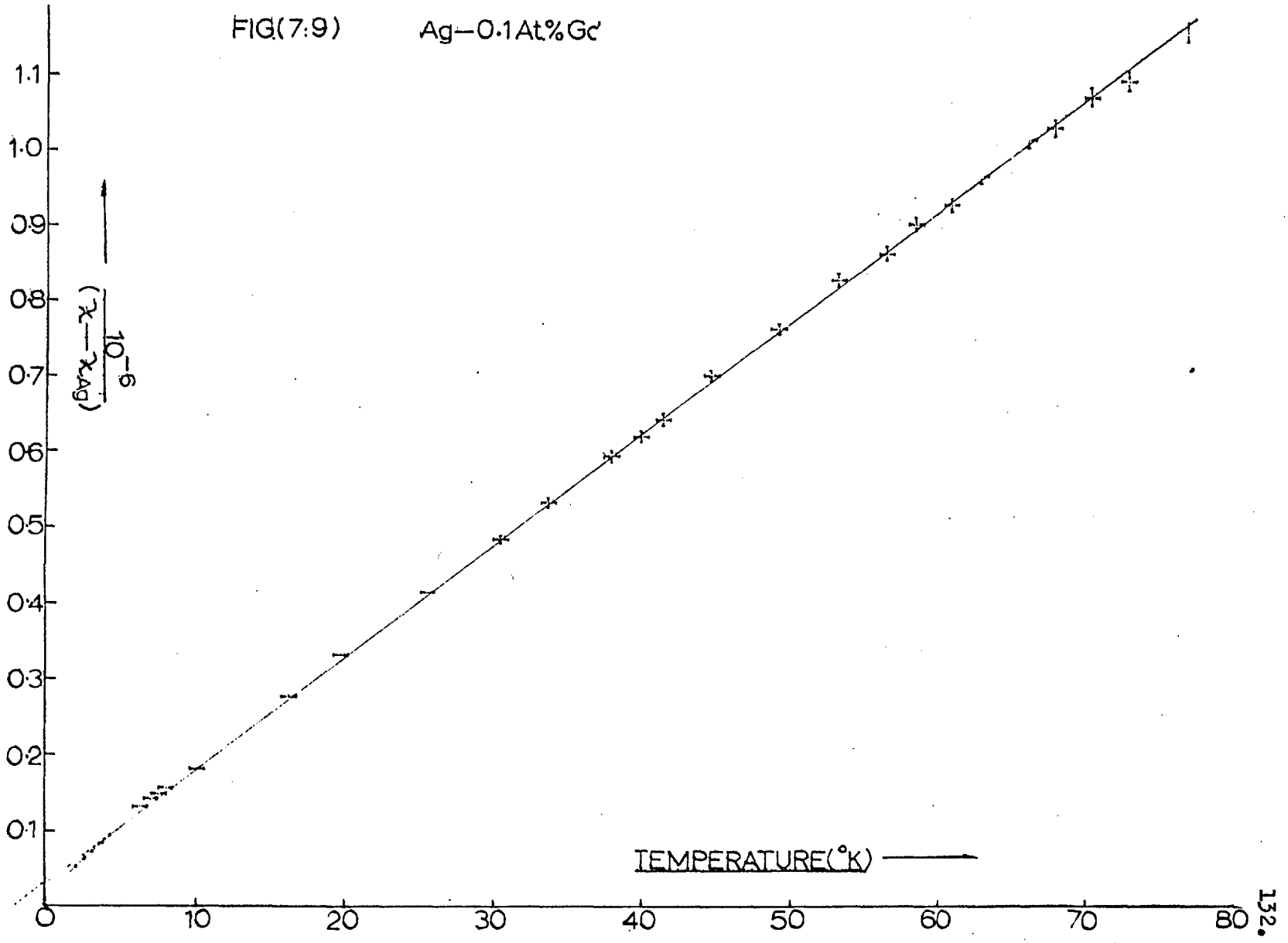
FIG(7:9) Ag—0.1At%Gd
1.1
1.0
0.9
0.8
0.7
0.6
0.5
0.4
0.3
0.2
0.1
$\frac{(\chi - \chi_{Ag})}{10^{-6}}$
TEMPERATURE(°K)
0
10
20
30
40
50
60
70
80

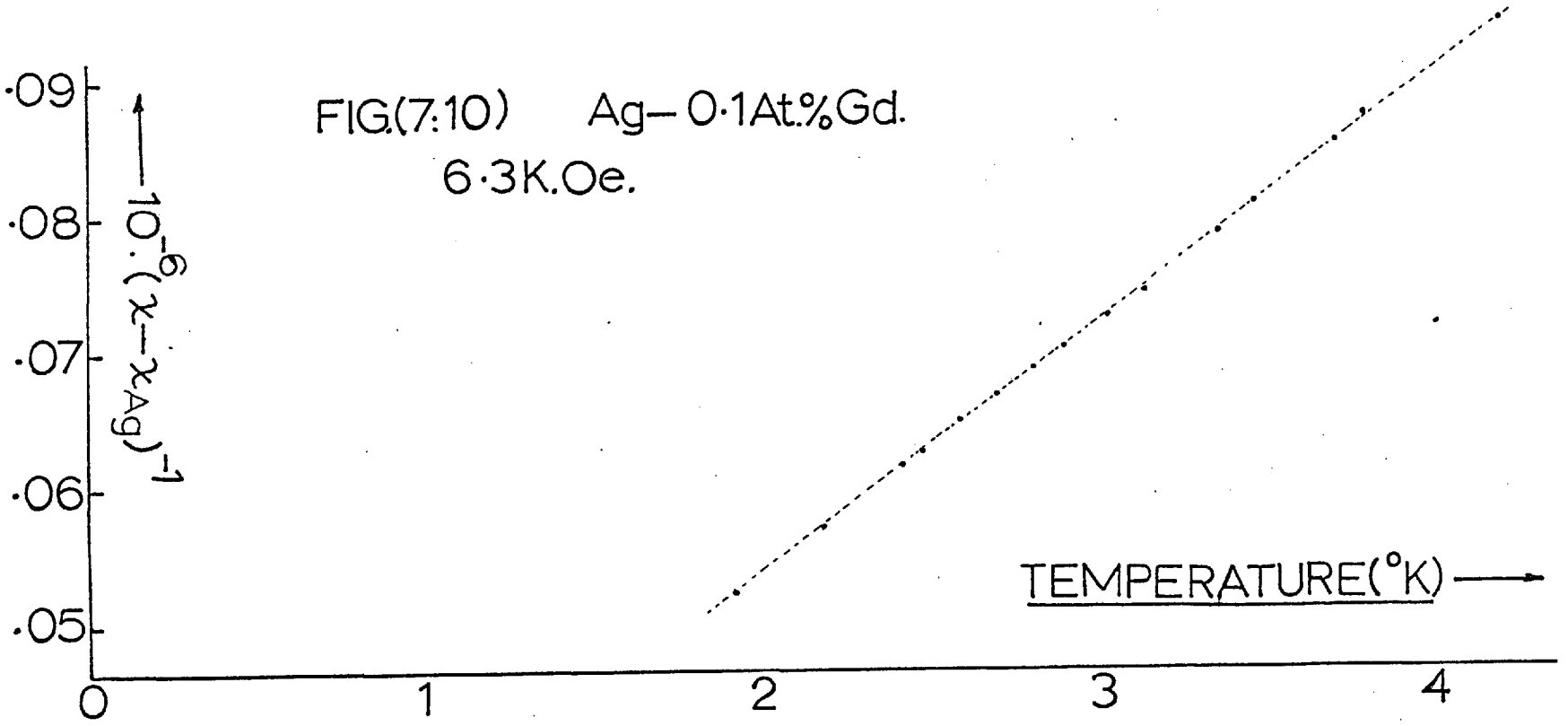
FIG.(7:10) Ag– 0·1At.%Gd.
6·3K.Oe.
·09
·08
·07
·06
·05
$10^{-6}(\chi-\chi_{Ag})^{-1}$
0
1
2
3
4
TEMPERATURE(°K)

FIG.(7:11) (M-H) PLOTS FOR Ag-0·1At.%Gd.

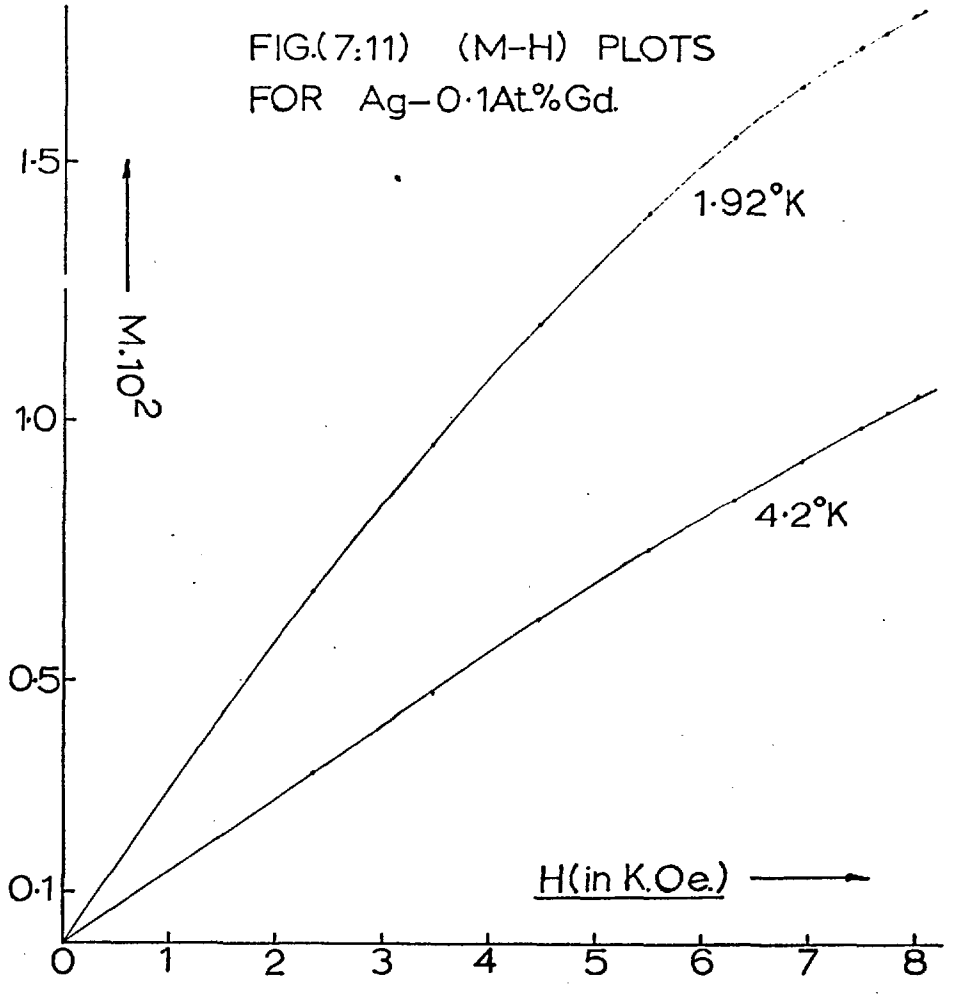

FIG(7:12) (M-H) PLOT AT 77°K FOR Ag-0·1At.%Gd.

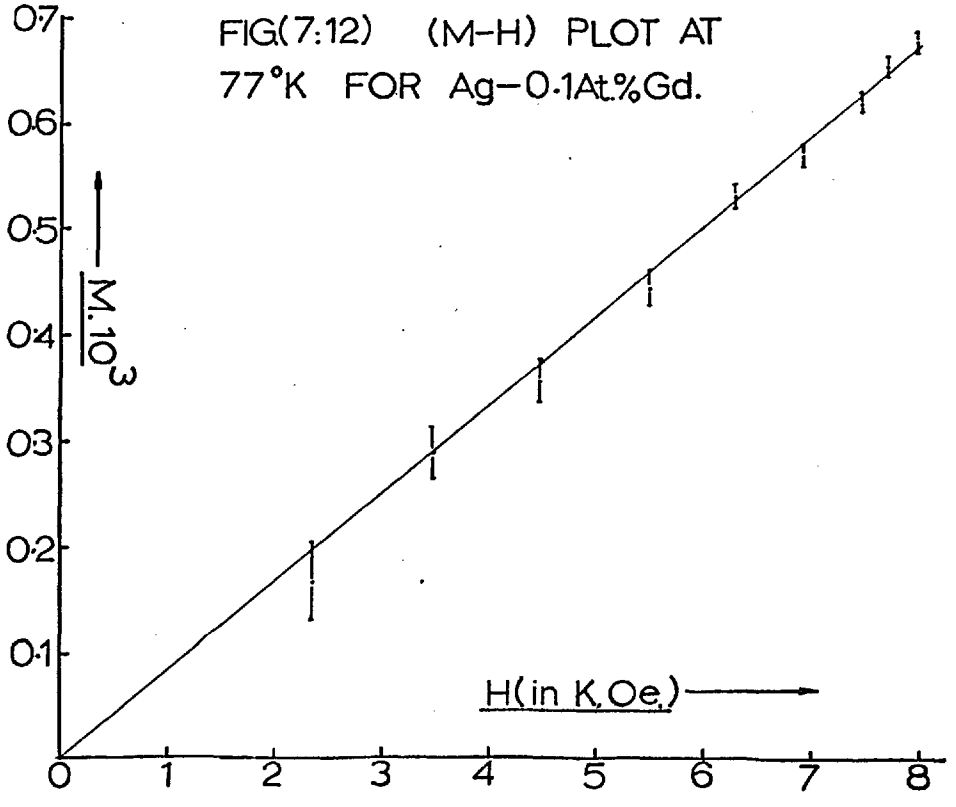

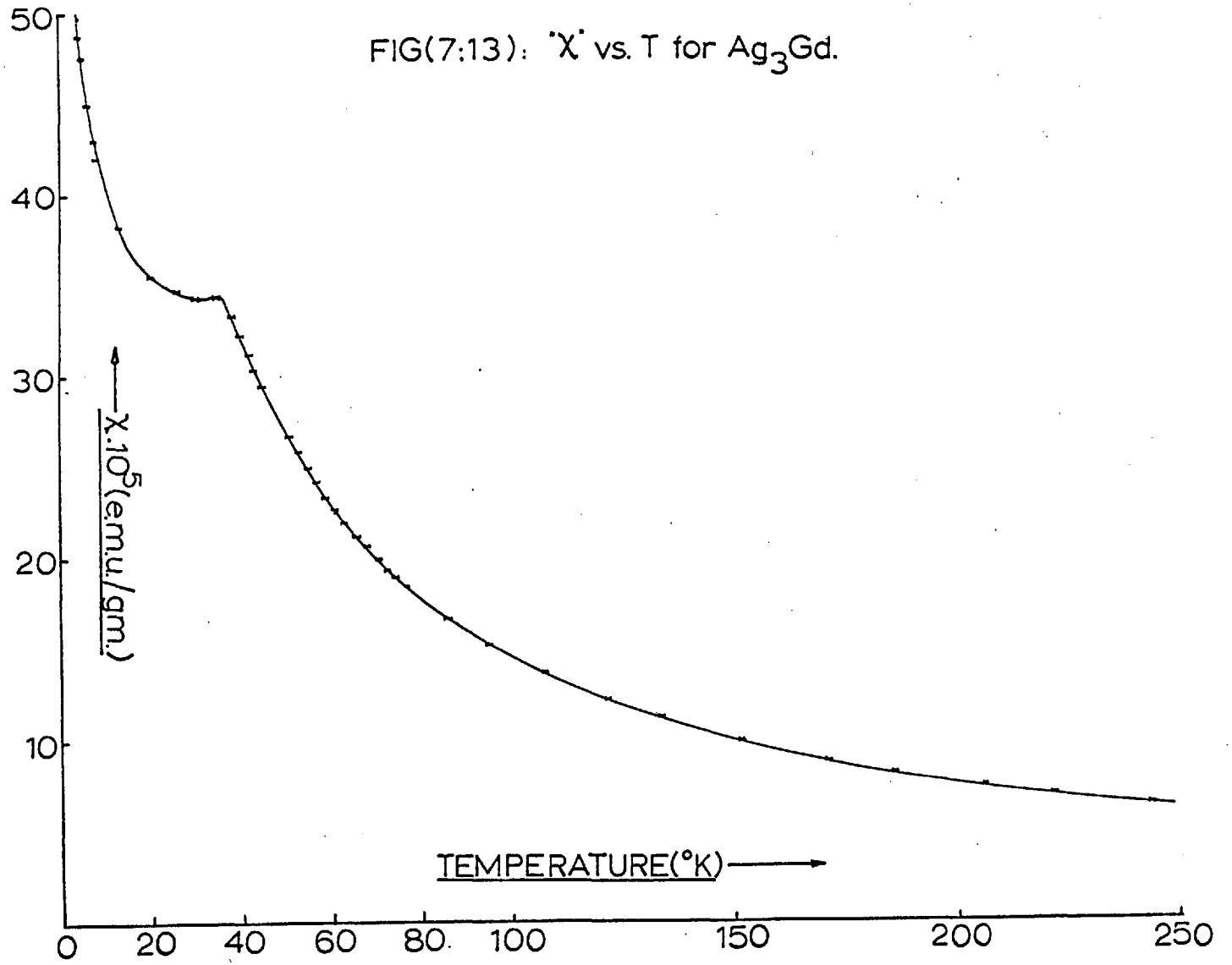

FIG(7:13): 'χ' vs. T for Ag_3Gd.

FIG(7:14). (M-H) PLOTS FOR Ag_3Gd.

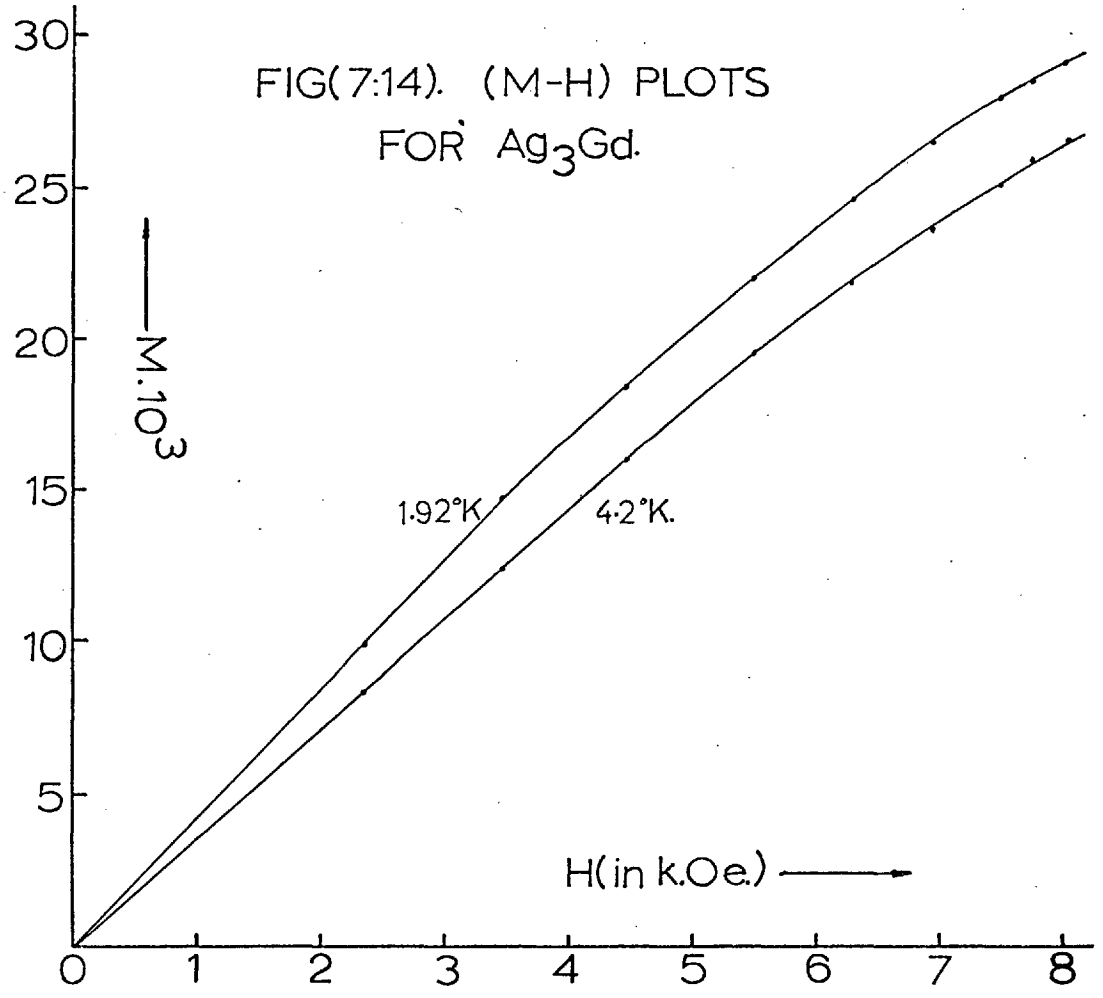

FIG(7:15) (M-H) PLOTS FOR Ag_3Gd.

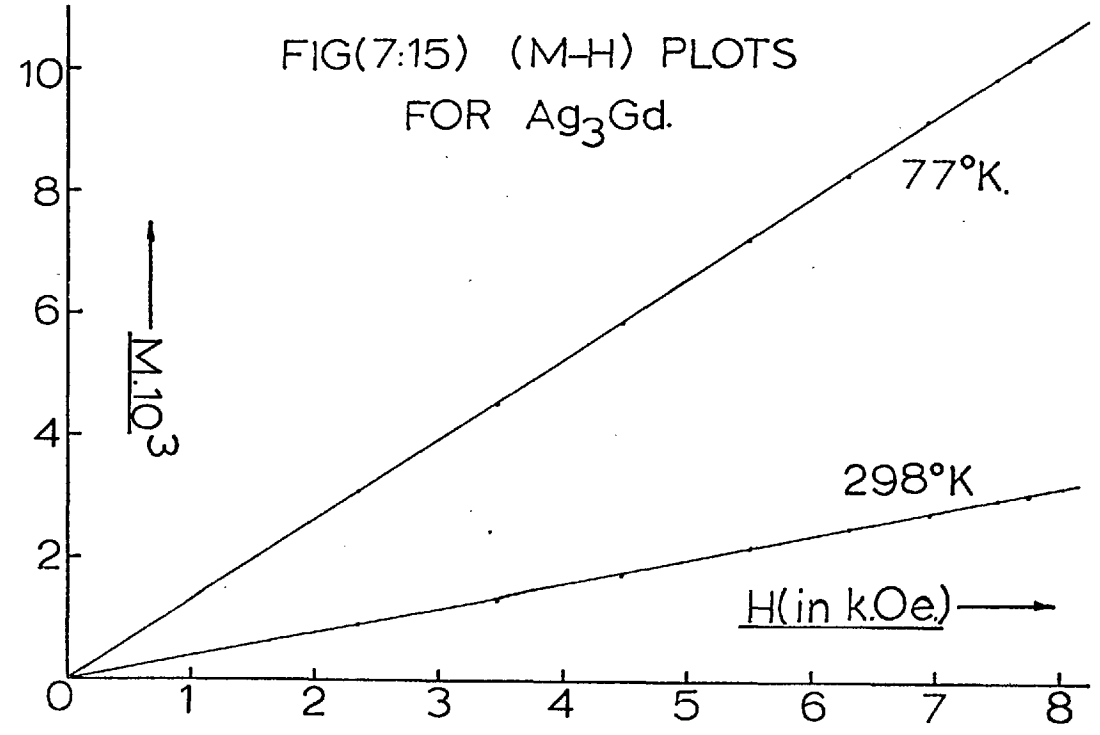

Ag - 0.55At.%Tb (Johnson Matthey & Co.)

This sample had originally been homogenised for 24 hours at 420°C. Metallographic analysis revealed dendritic structure with interdendritic second phase. The sample was reannealed for 5 hours at 700°C and quenched, this, however, produced little change in the microstructure. Consequently the sample was cold rolled prior to another reanneal, this time for 5 hours at 750°C, and again quenched. Metallographic analysis indicated, figure (7.4p), recrystallisation into a fine grained, single phase f.c.c. solid solution.

The experimental data appears in figures (7.16) to (7.19).

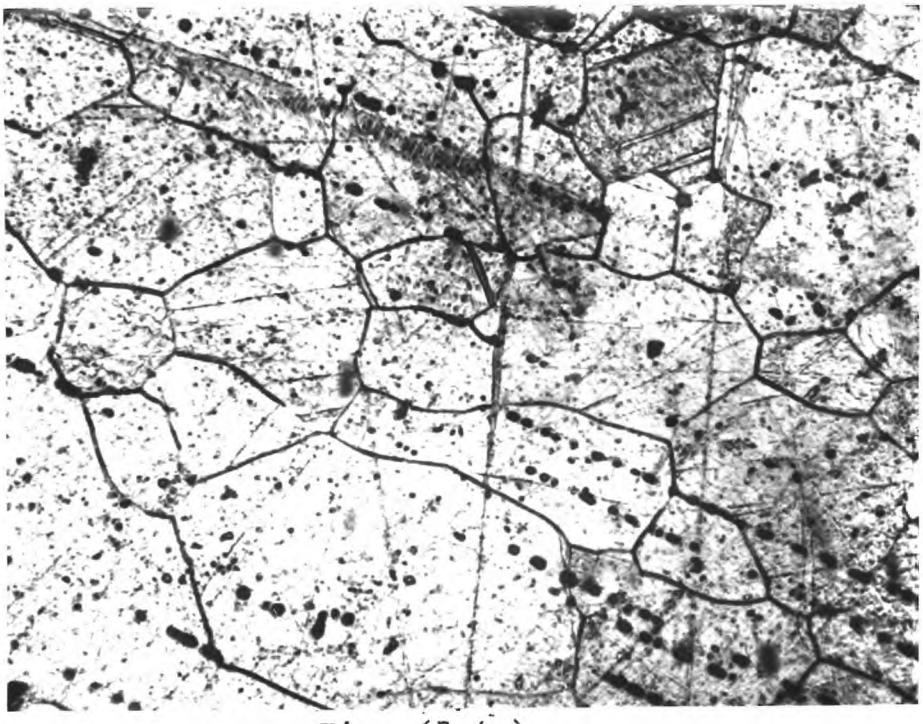

Fig. (7.4p)

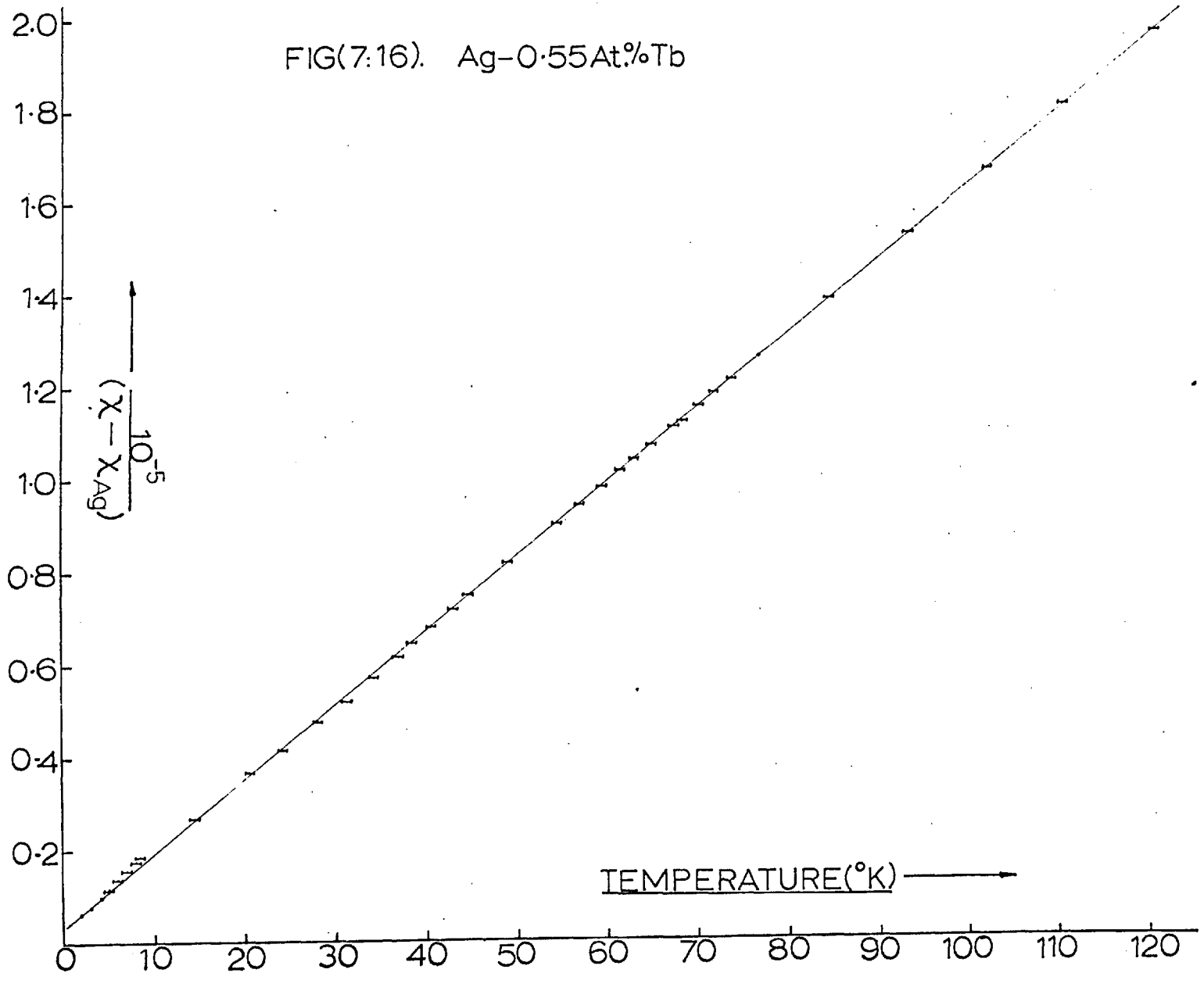

FIG(7:16). Ag-0·55At.%Tb

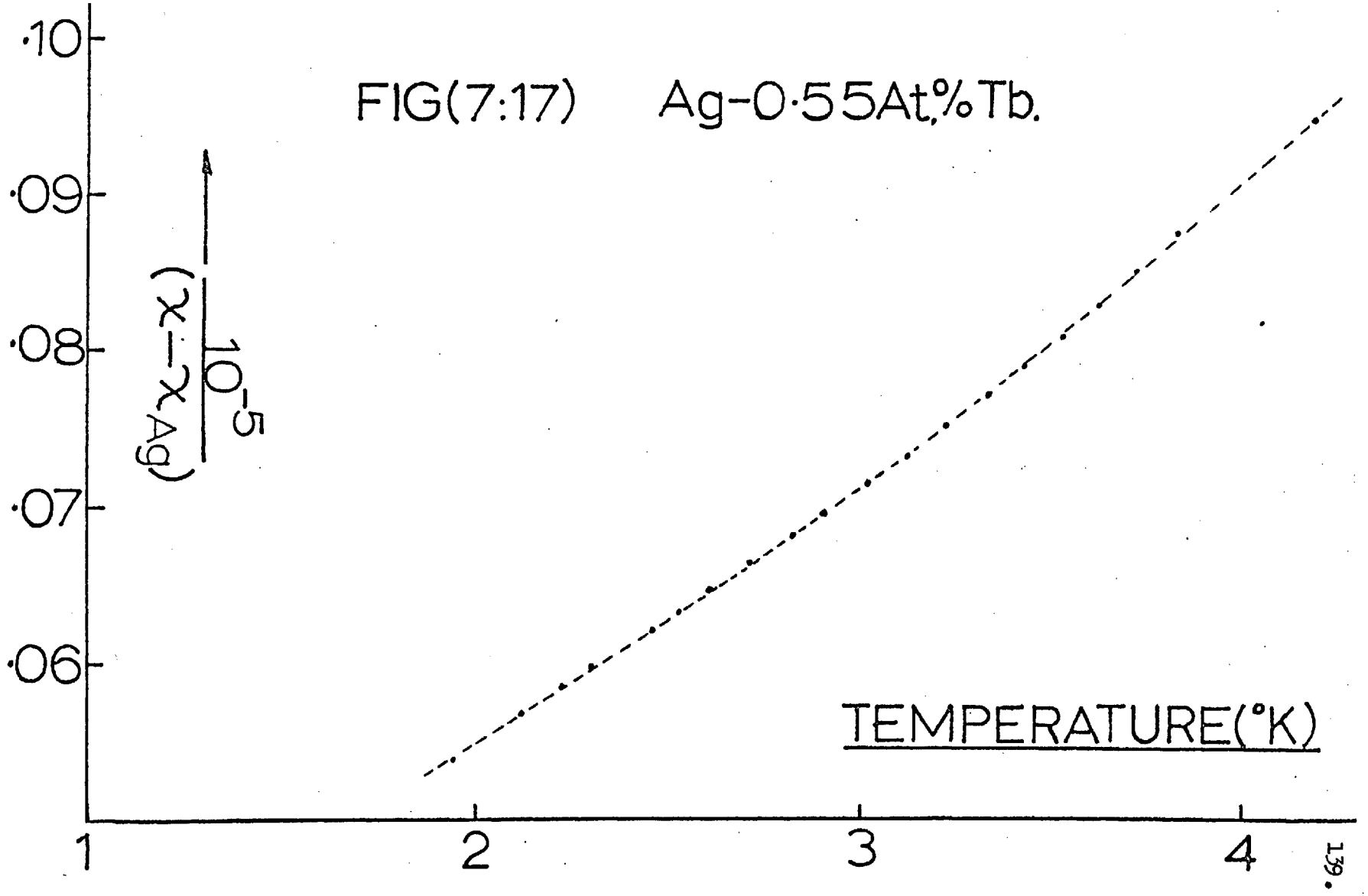
FIG(7:17) Ag-0·55At.% Tb.
·10
·09
·08
·07
·06
$(\chi - \chi_{Ag}) \frac{}{10^{-5}}$
TEMPERATURE(°K)
1
2
3
4

FIG(7:18) (M-H) PLOTS
FOR Ag-0·55At.%Tb.

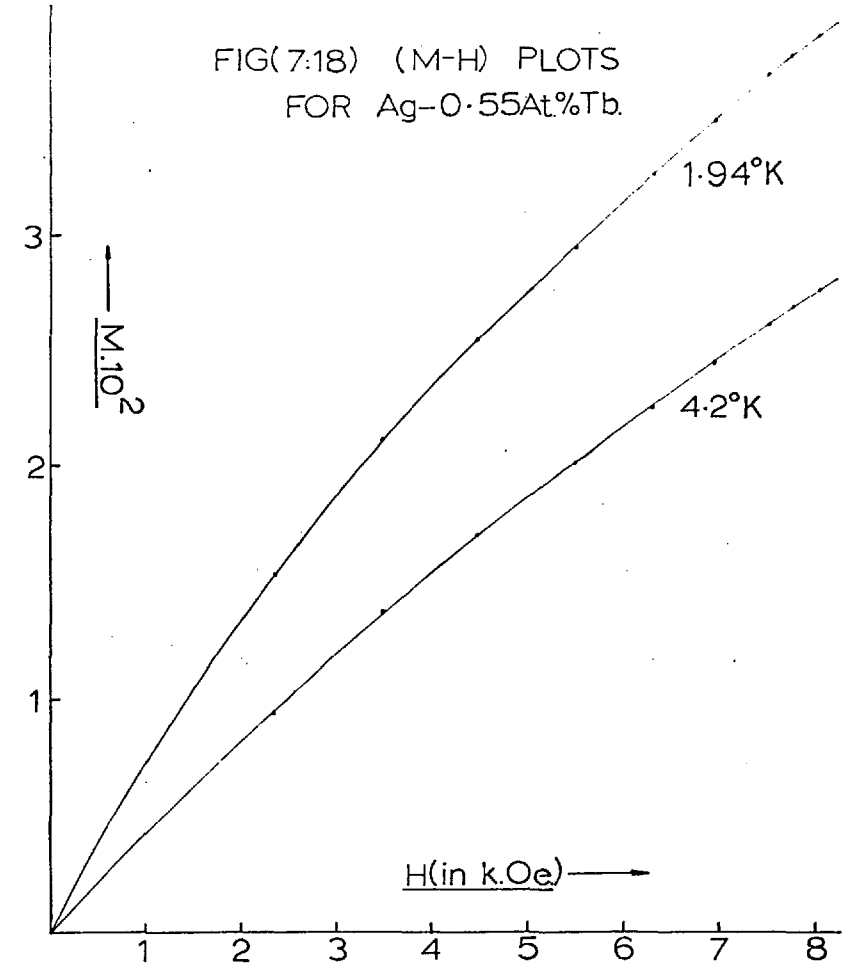

FIG(7:19). (M-H) PLOTS
FOR Ag-0·55At.%Tb.

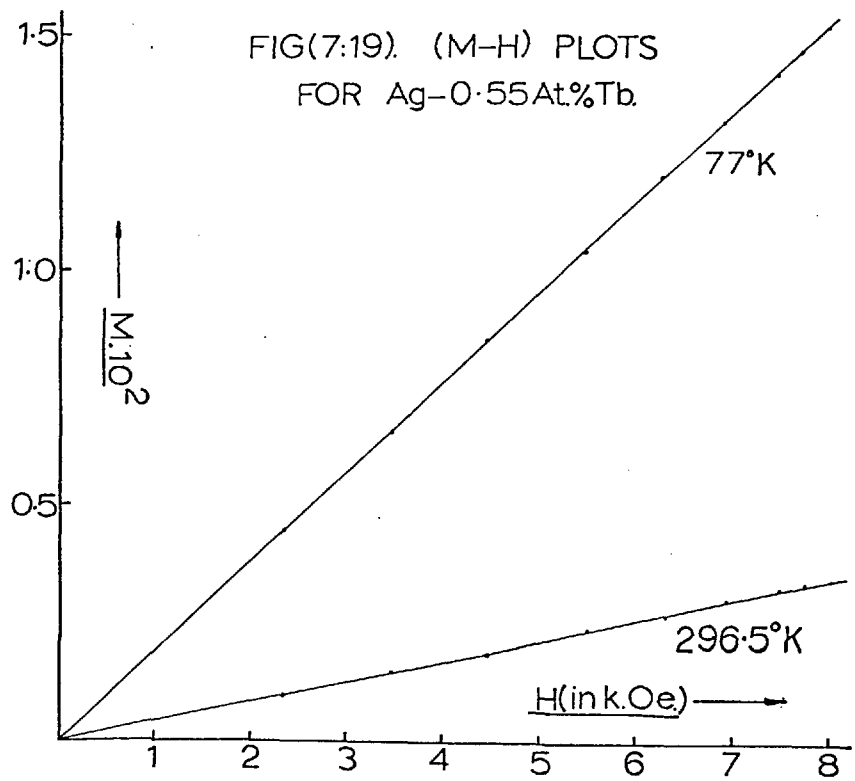

Ag - 0.86At.%Dy (Bijvoet, Amsterdam)

This sample was cast, forged and annealed, and constituted a single phase, recrystallised solid solution. The "crow's foot" structure at grain boundary intersections, figure (7.5p), indicates some incipient melting in these regions during annealing. Figures (7.20) to (7.23) summarise the measurements on this system.

Ag - 0.51At.%Dy (Bijvoet, Amsterdam)

This alloy had been subjected to the same treatment during manufacture as the more concentrated alloy from the same source. The button supplied was rather small and had to be cold worked into a suitably shaped susceptibility sample. Consequently the sample was given a strain releaving annealat 700°C for 15 minutes, from which it was quenched. The surface of this annealed specimen was cleaned in a 1:1 solution of H_2O:HNO_3 before etching in the usual manner.

Owing to the lack of material, this sample could not be microanalysed. However, similar conditions of manufacture, combined with the similarity between the results obtained for this alloy and the more concentrated sample, suggests that confidence can be placed in the results, summarised in figures (7.24)

(7.27).

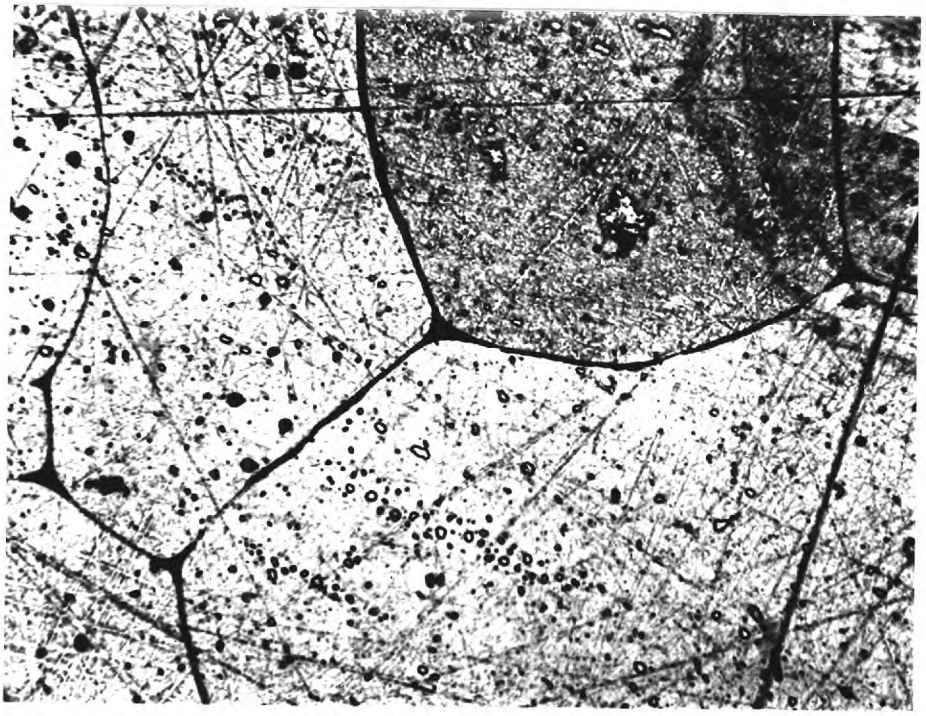

Fig. (7.5p)

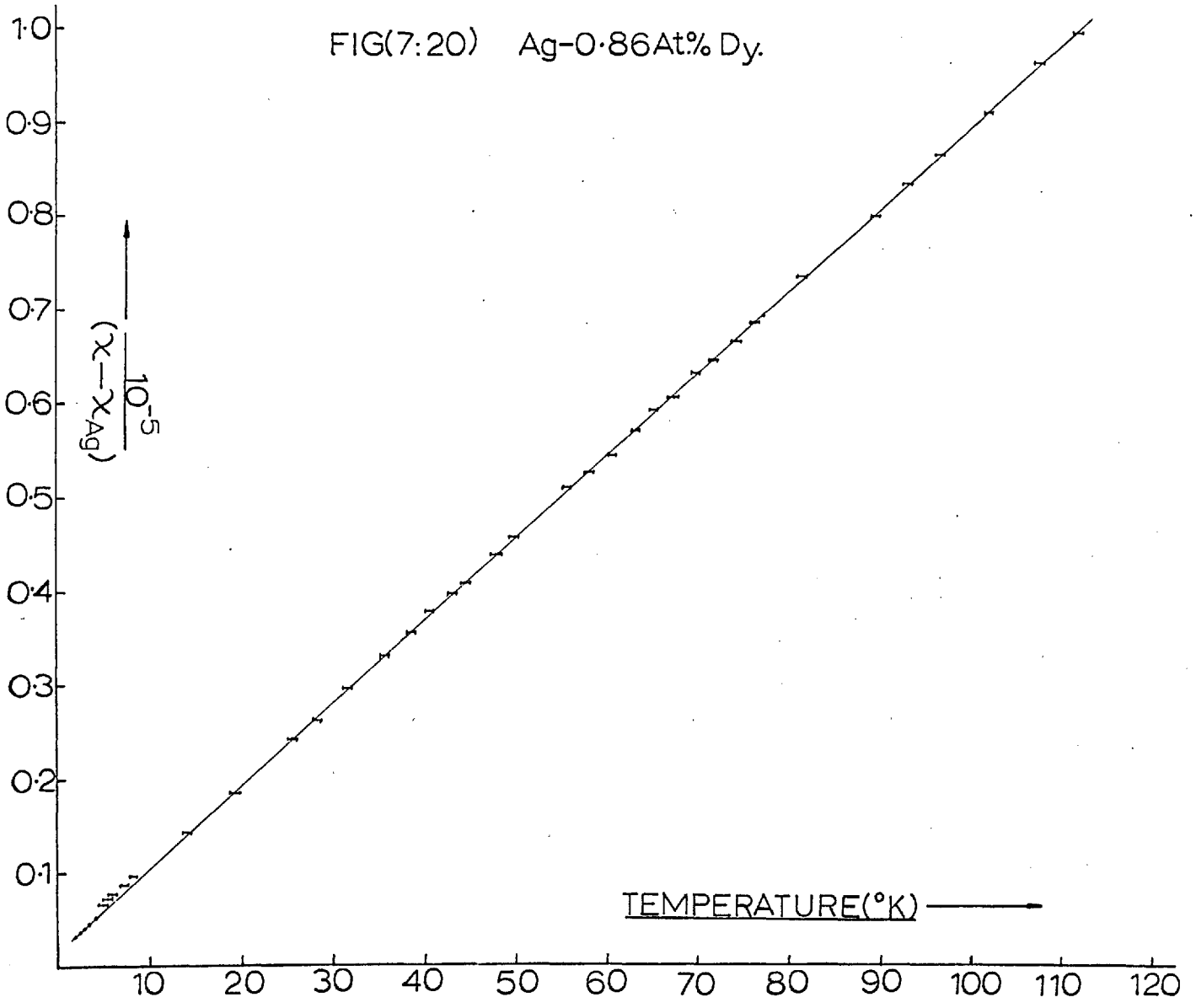
FIG(7:20) Ag-0·86At% Dy.
1·0
0·9
0·8
0·7
0·6
0·5
0·4
0·3
0·2
0·1
$\frac{(\chi - \chi_{Ag})}{10^{-5}}$
TEMPERATURE(°K)
10
20
30
40
50
60
70
80
90
100
110
120

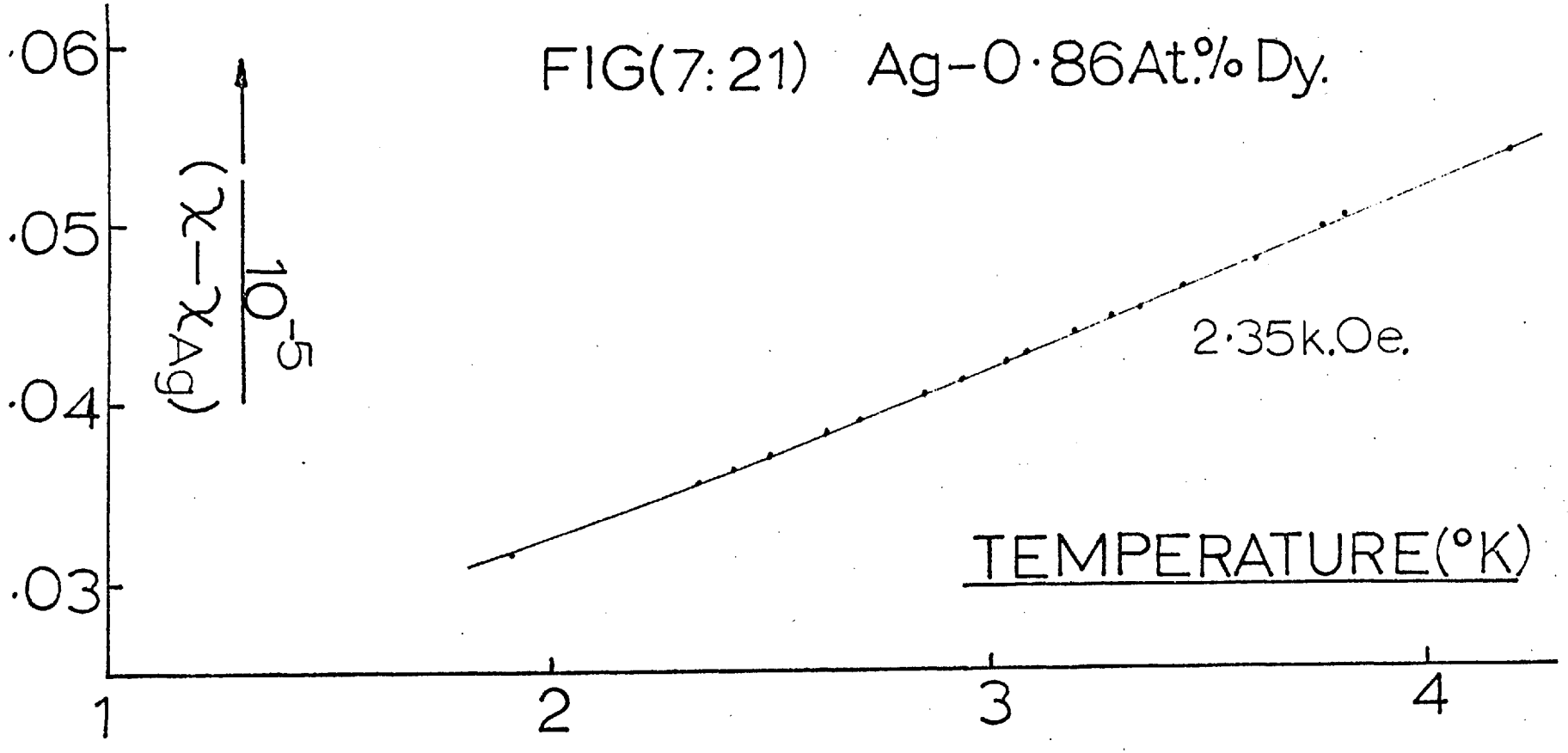
FIG(7:21) Ag-0·86At.% Dy.
·06
·05
·04
·03
$\frac{(\chi - \chi_{Ag})}{10^{-5}}$
2·35k.Oe.
TEMPERATURE(°K)
1
2
3
4

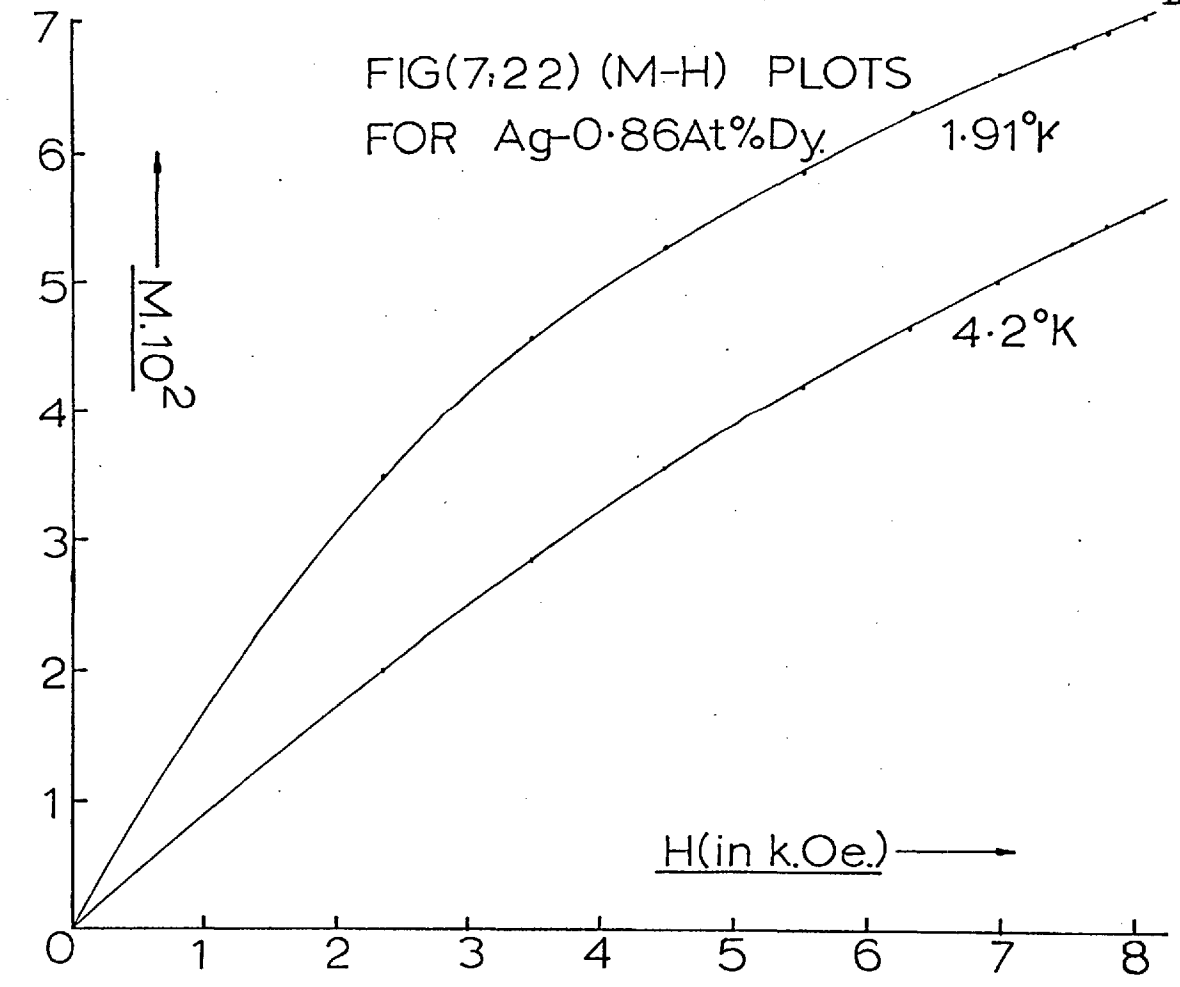
FIG(7:22) (M-H) PLOTS
FOR Ag-0·86At%Dy.
1·91°K
4·2°K
M.10²
H(in k.Oe.)
0
1
2
3
4
5
6
7
8

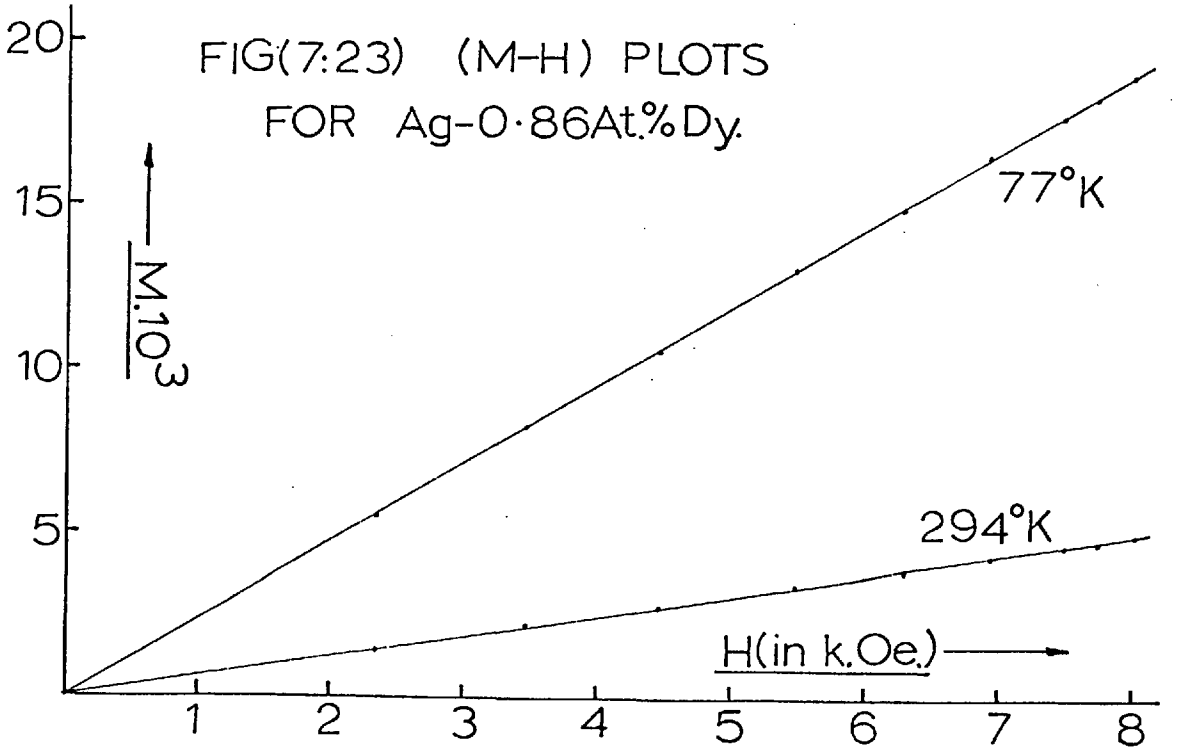
FIG(7:23) (M-H) PLOTS
FOR Ag-0·86At.%Dy.
77°K
294°K
M.10³
H(in k.Oe.)
5
10
15
20
1
2
3
4
5
6
7
8

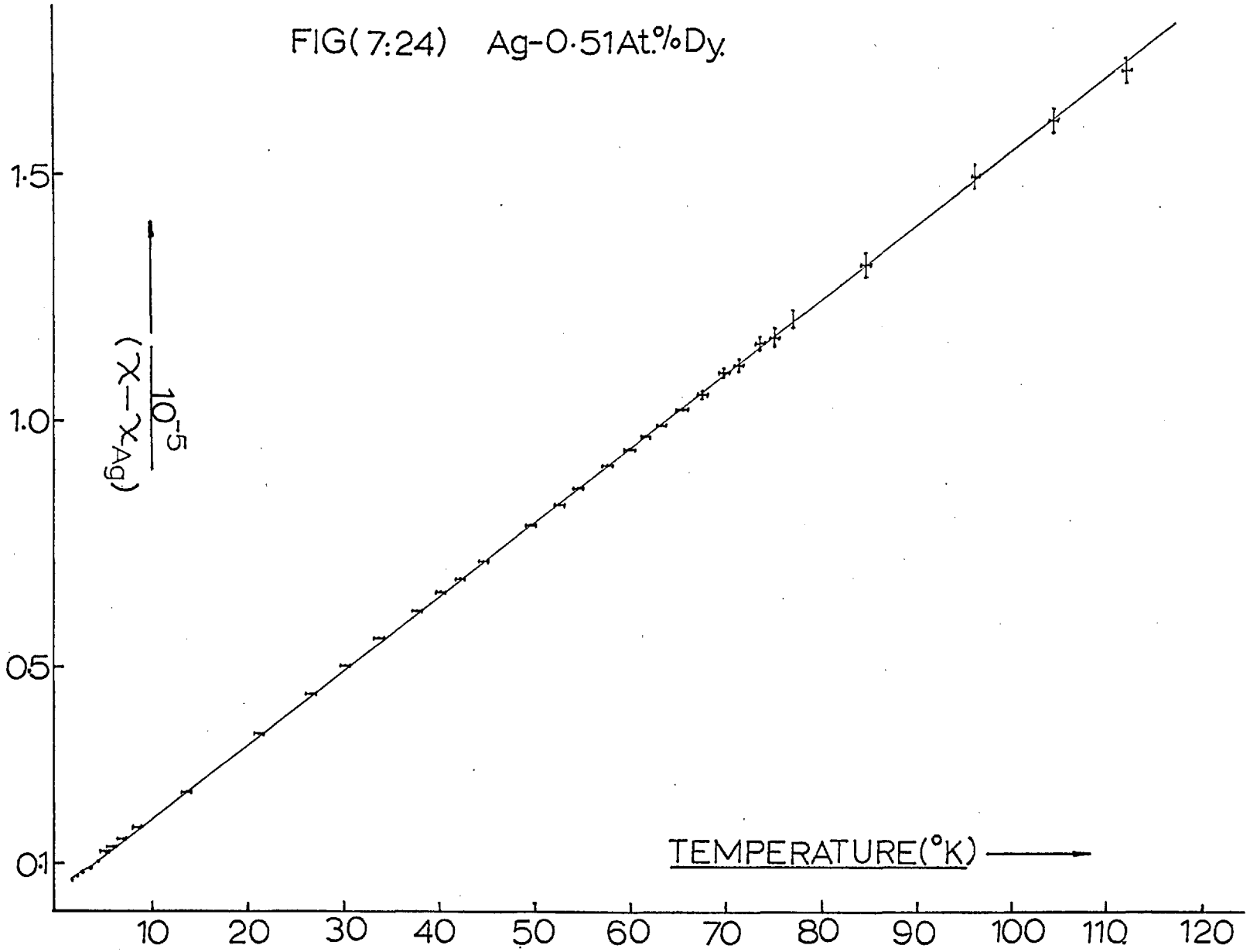
FIG(7:24) Ag-0·51At.%Dy.
1·5
1·0
0·5
0·1
$\frac{(\chi - \chi_{Ag})}{10^{-5}}$
TEMPERATURE(°K)
10
20
30
40
50
60
70
80
90
100
110
120

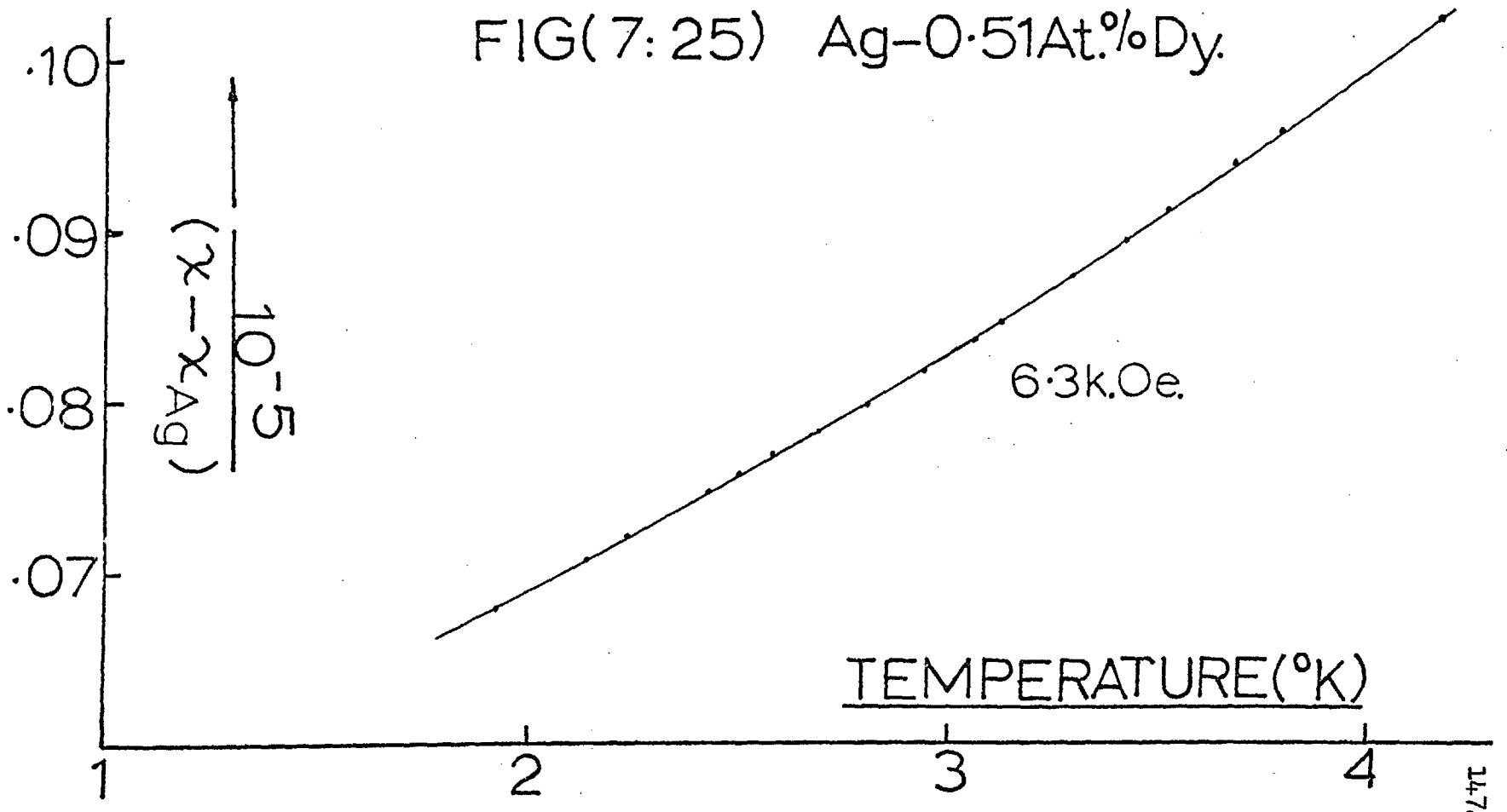
FIG(7:25) Ag-0·51At.%Dy.
·10
·09
·08
·07
$\frac{10^{-5}}{(\chi - \chi_{Ag})}$
6·3k.Oe.
TEMPERATURE(°K)
1
2
3
4
447.

FIG(7:26) (M-H) PLOTS
FOR Ag-0·51At.%Dy.

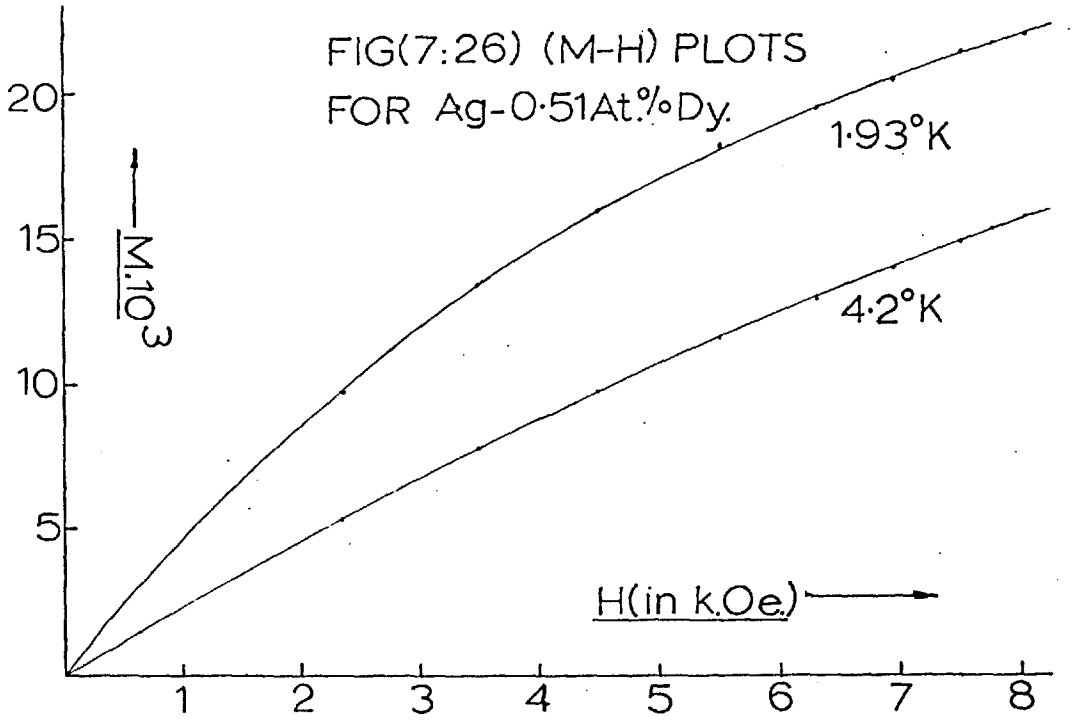

FIG(7:27) (M-H) PLOTS
FOR Ag-0·51At.% Dy.

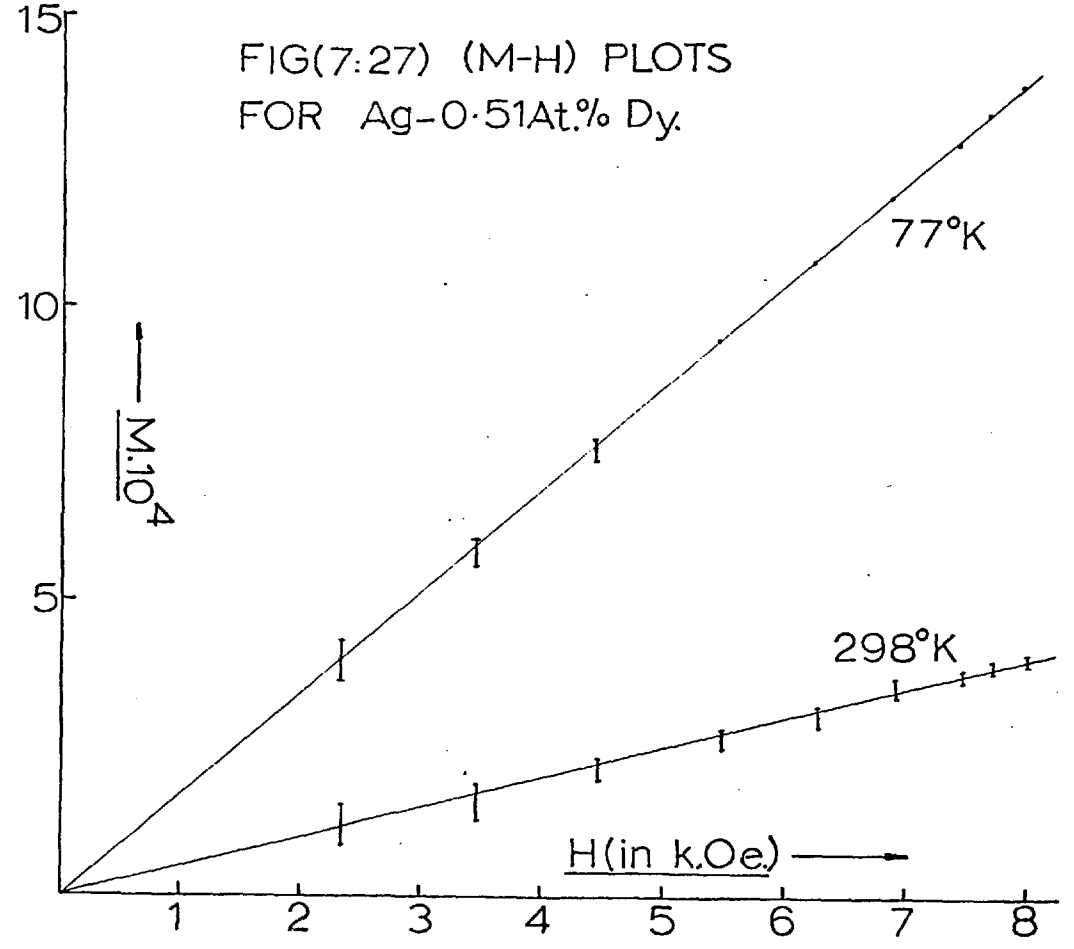

Ag - 0.35At.% Ho (Bijvoet, Amsterdam)

The original sample was rather small, and had to be cold worked into a suitably shaped specimen. The final specimen was given a 20 minute strain releaving anneal at 300°C.

Lack of material prevented microstructure analysis from being carried out, but the experimental results, figures (7.28) to (7.32) have the same general character as those reported for the less concentrated alloy.

Ag - 0.25At.% Ho (Johnson Matthey and Co.)

This alloy was provided in button form, having been homogenised at 550°C for 24 hours.

Examination of the microstructure - figure (7.6p) indicated a single phase, fairly large grained f.c.c. solid solution with some cored character, suggesting possible concentration gradients in the sample.

The experimental data is reproduced in figures (7.32) to (7.35).

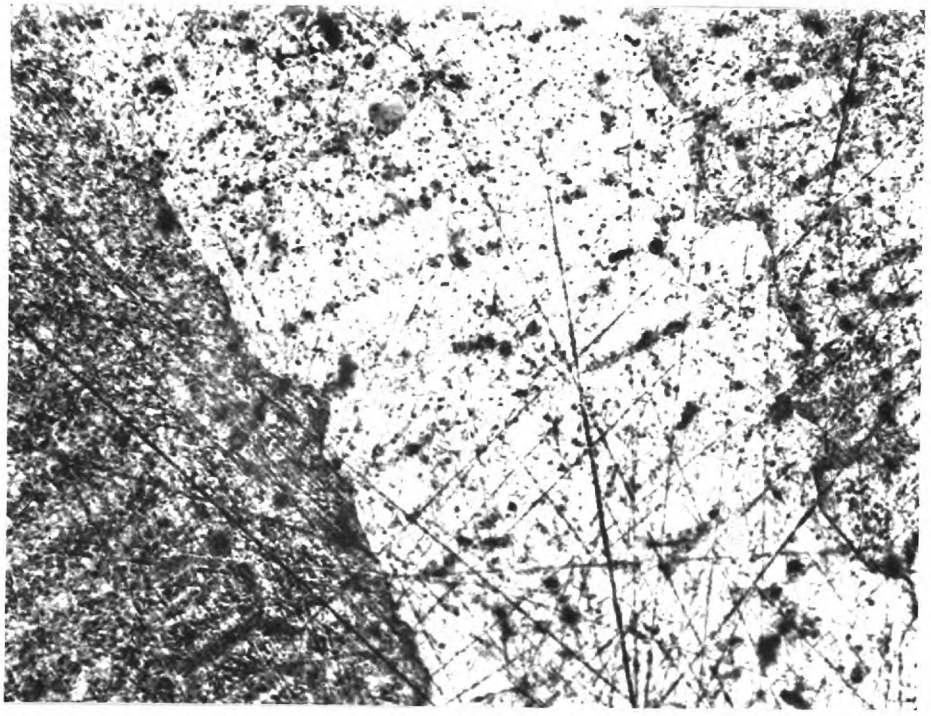

Fig. (7.6p)

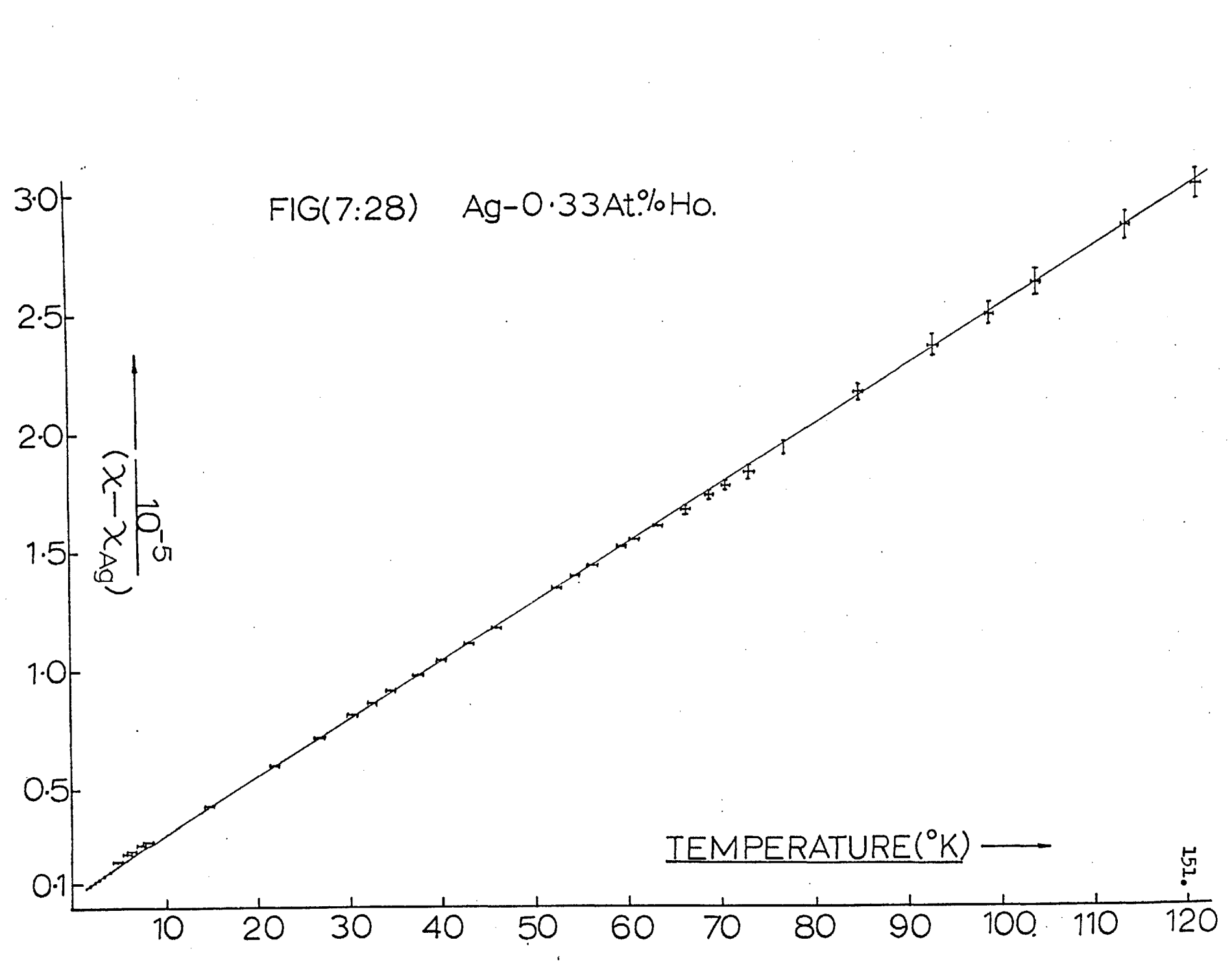
FIG(7:28) Ag-0·33At.% Ho.
3·0
2·5
2·0
1·5
1·0
0·5
0·1
$\frac{10^{-5}}{(\chi-\chi_{Ag})}$
TEMPERATURE(°K) ⟶
10
20
30
40
50
60
70
80
90
100
110
120
151.

FIG(7:29) Ag-0·33At.% Ho.

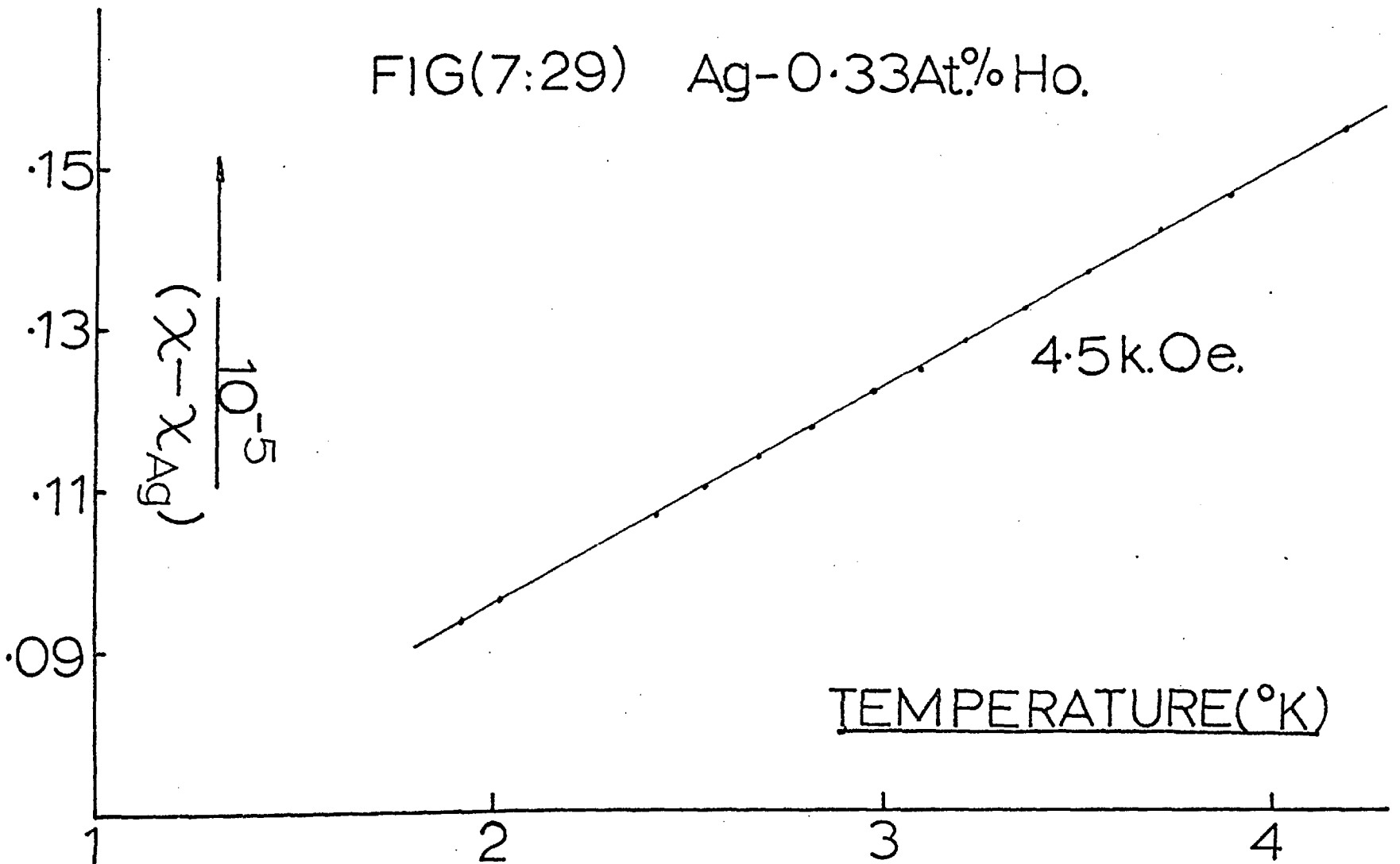

FIG(7:30) (M-H) PLOTS
FOR Ag-0·33At.% Ho.

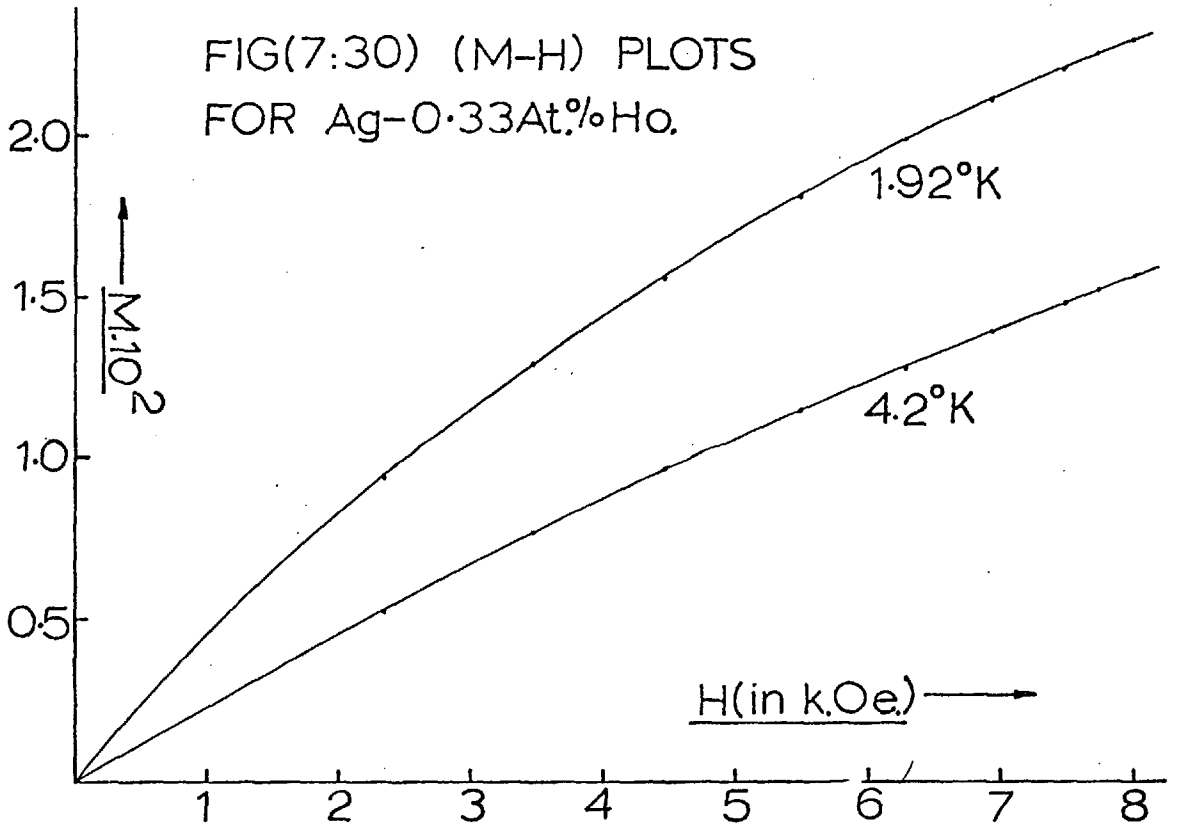

FIG(7:31) (M-H) PLOTS
FOR Ag-0·33At.% Ho.

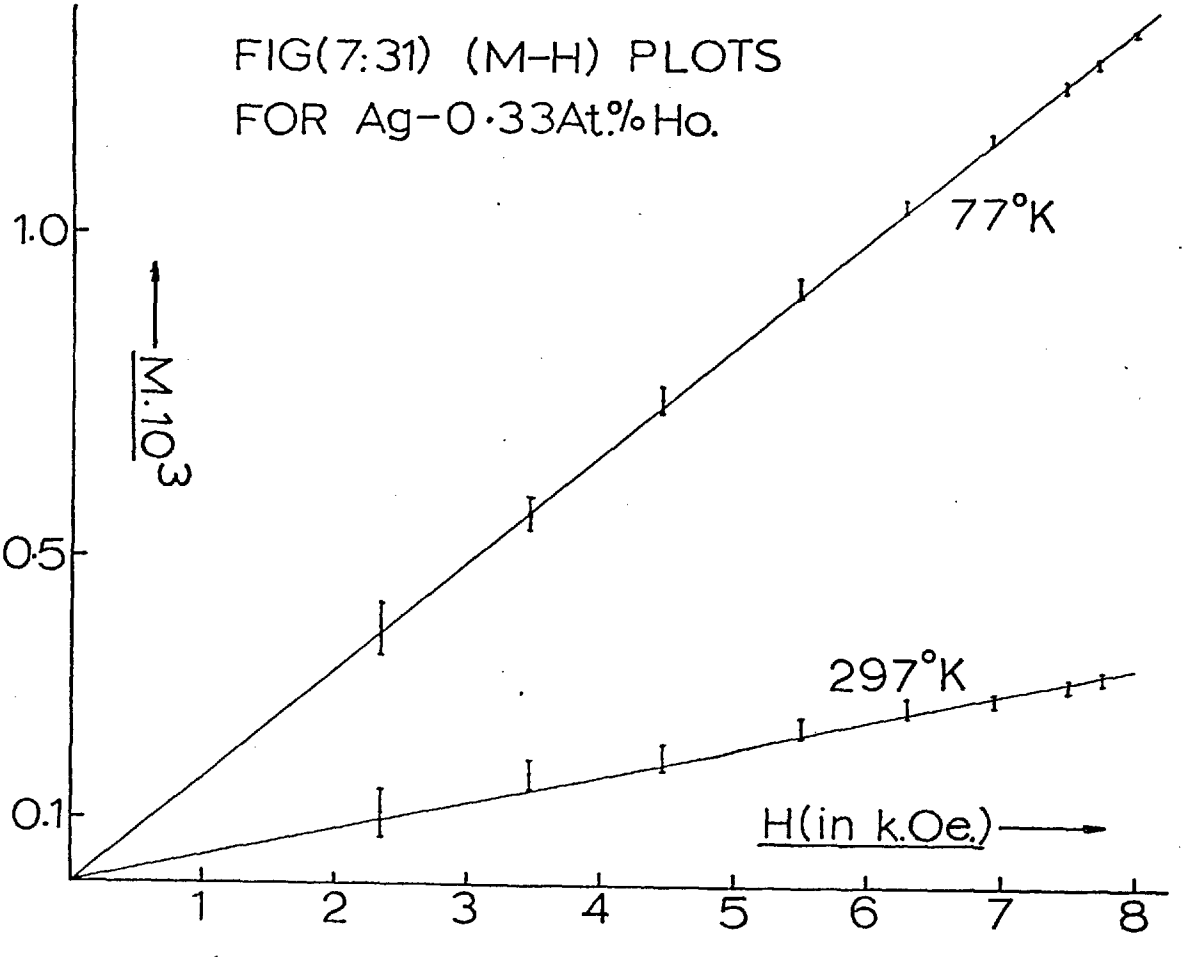

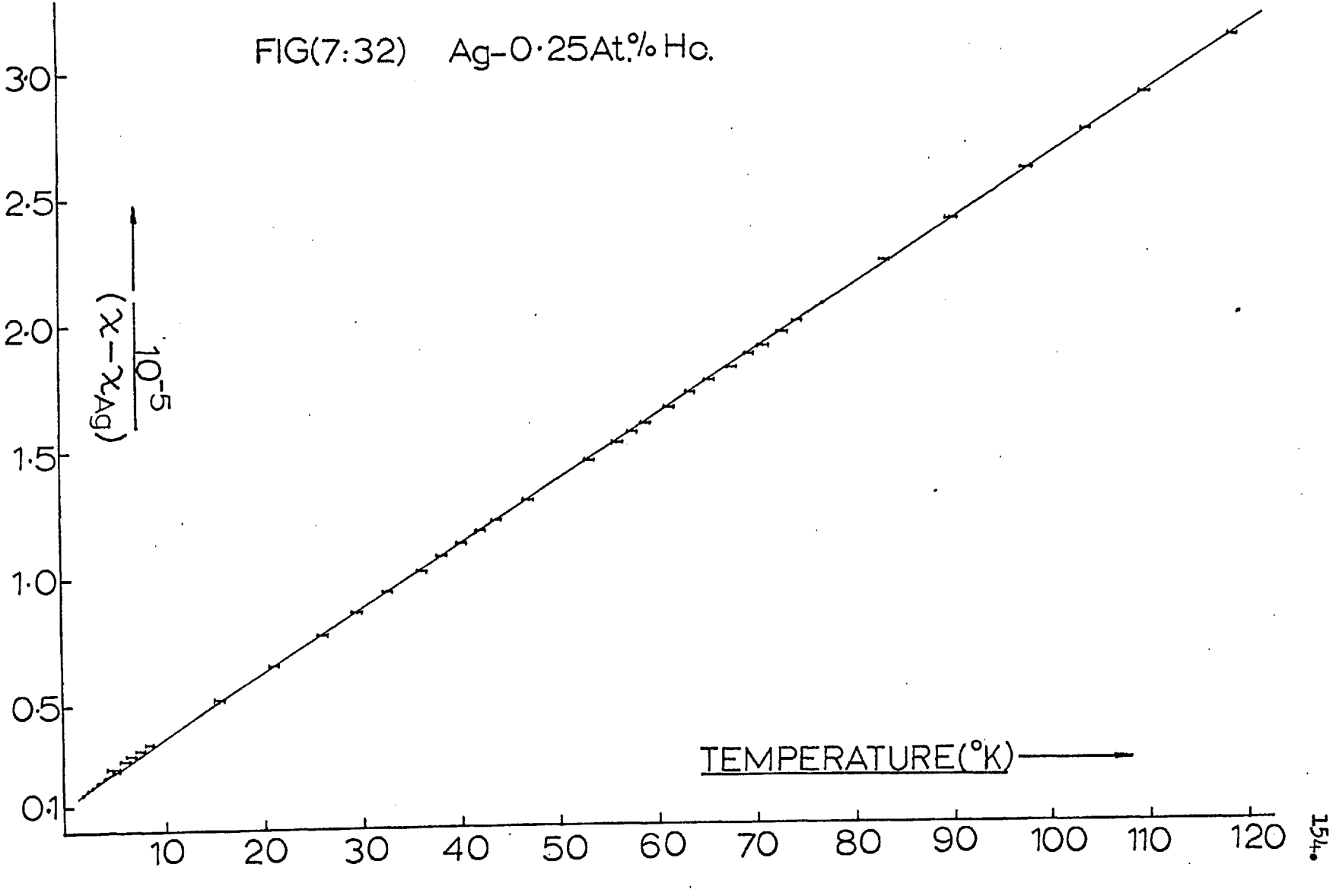
FIG(7:32) Ag-0·25At.% Ho.
3·0
2·5
2·0
1·5
1·0
0·5
0·1
$\frac{10^{-5}}{(\chi-\chi_{Ag})}$
TEMPERATURE(°K)
10
20
30
40
50
60
70
80
90
100
110
120

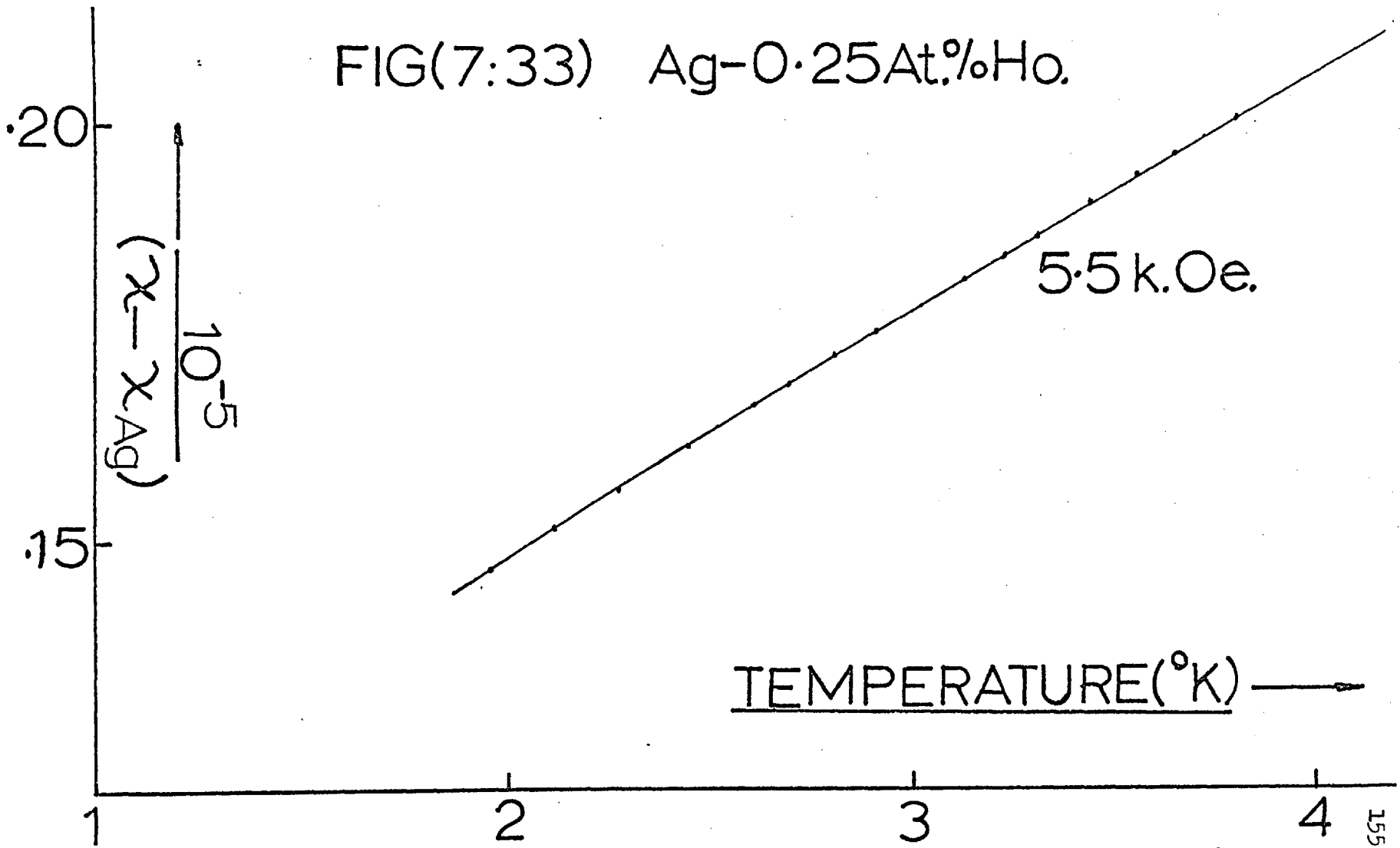
FIG(7:33) Ag-0·25At.%Ho.
·20
·15
$\frac{\chi - \chi_{Ag}}{10^{-5}}$
5·5 k.Oe.
TEMPERATURE(°K)
1
2
3
4

FIG(7:34) (M-H) PLOTS
FOR Ag-0·25At.% Ho.

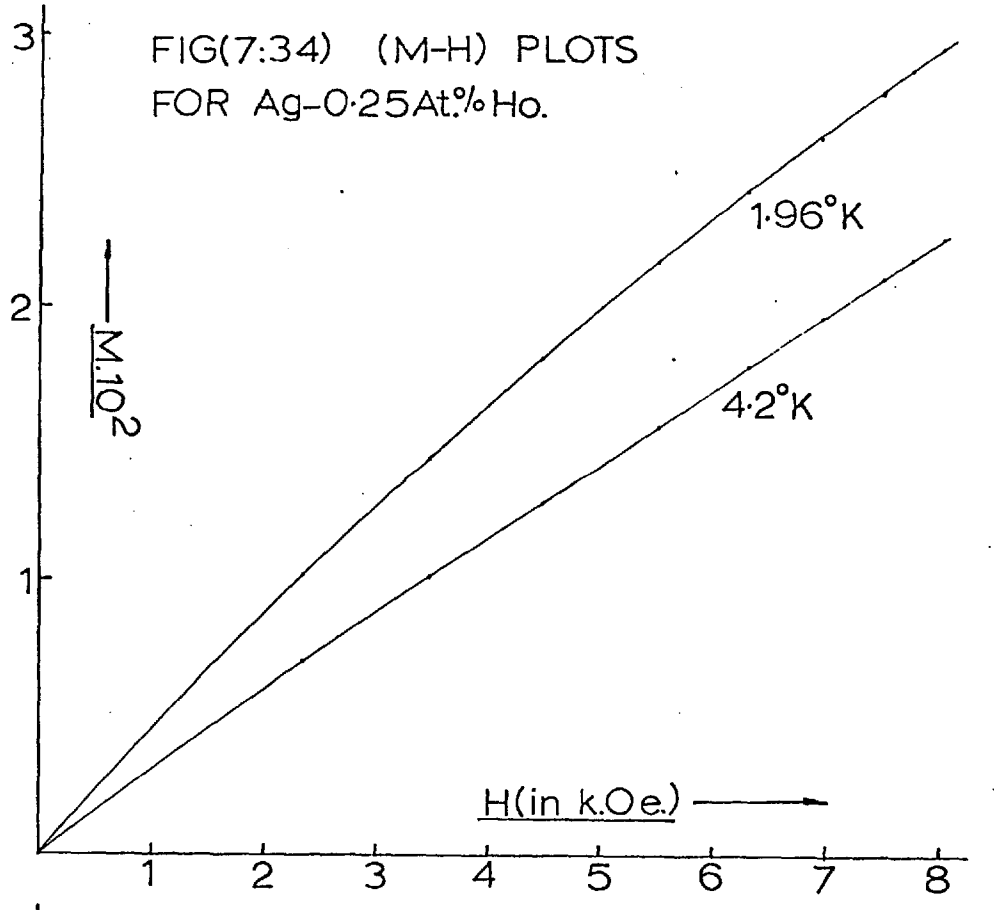

FIG(7:35) (M-H) PLOTS
FOR Ag-0·25At.% Ho.

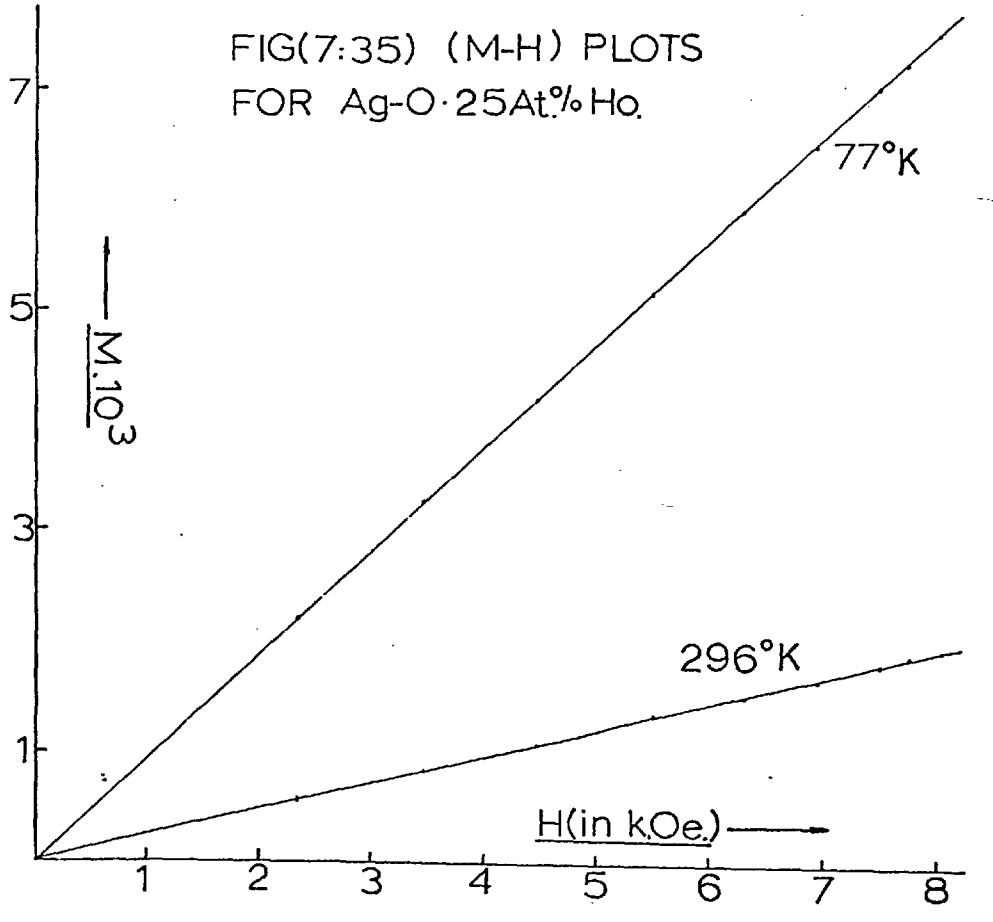

Ag - 0.28At.% Er (Johnson Matthey & Co.)

The susceptibility sample was obtained from an arc melted button which had been homogenised at 650°C. Metallographic analysis revealed large columnor crystals, with no evidence of recrystallisation or twinning, figure (7.7p). The experimental data appears in figures (7.36) to (7.39).

Ag - 1.0At.% Er (Johnson Matthey and Co.)

This alloy was manufactured in the same way as the more dilute sample, and as figure (7.8p) shows, had a similar microstructure.

As figures (7.40) to (7.43) indicate, the experimental results have the same general character as those for the more dilute sample.

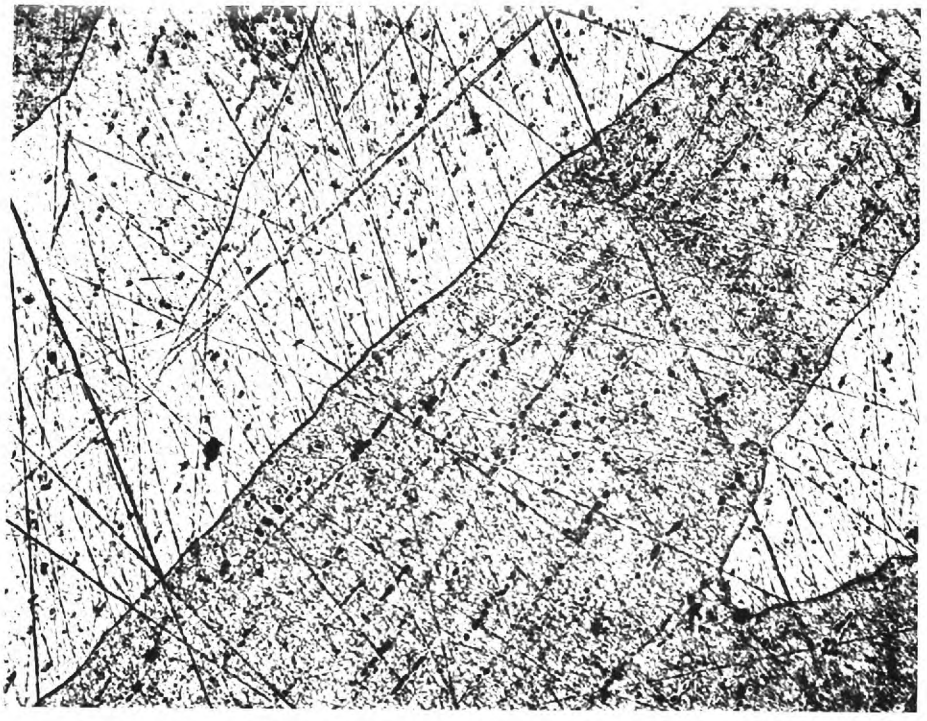

Fig. (7.7p)

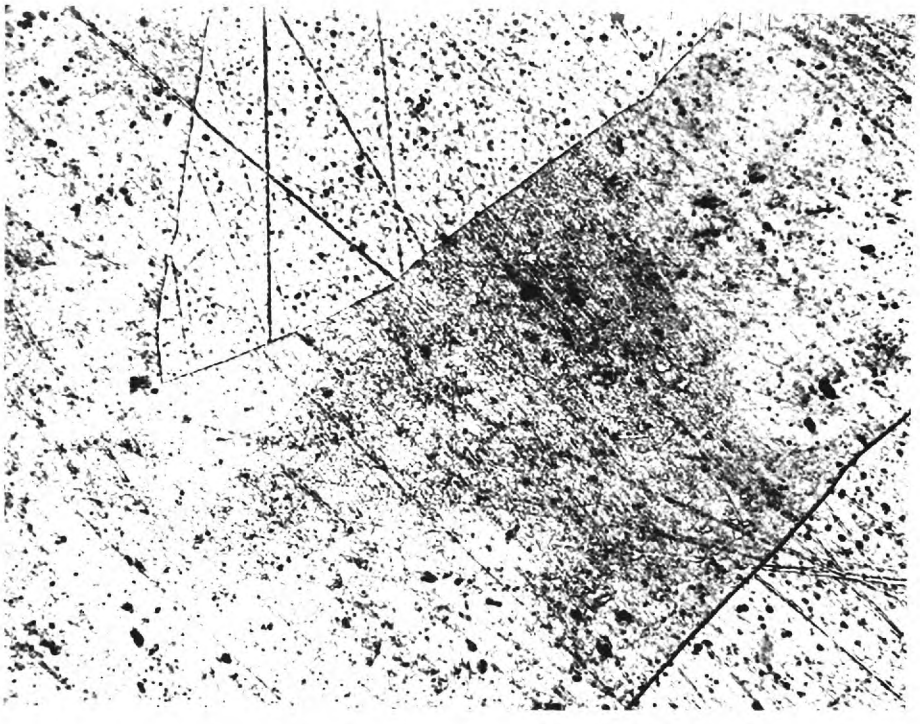

Fig. (7.8p)

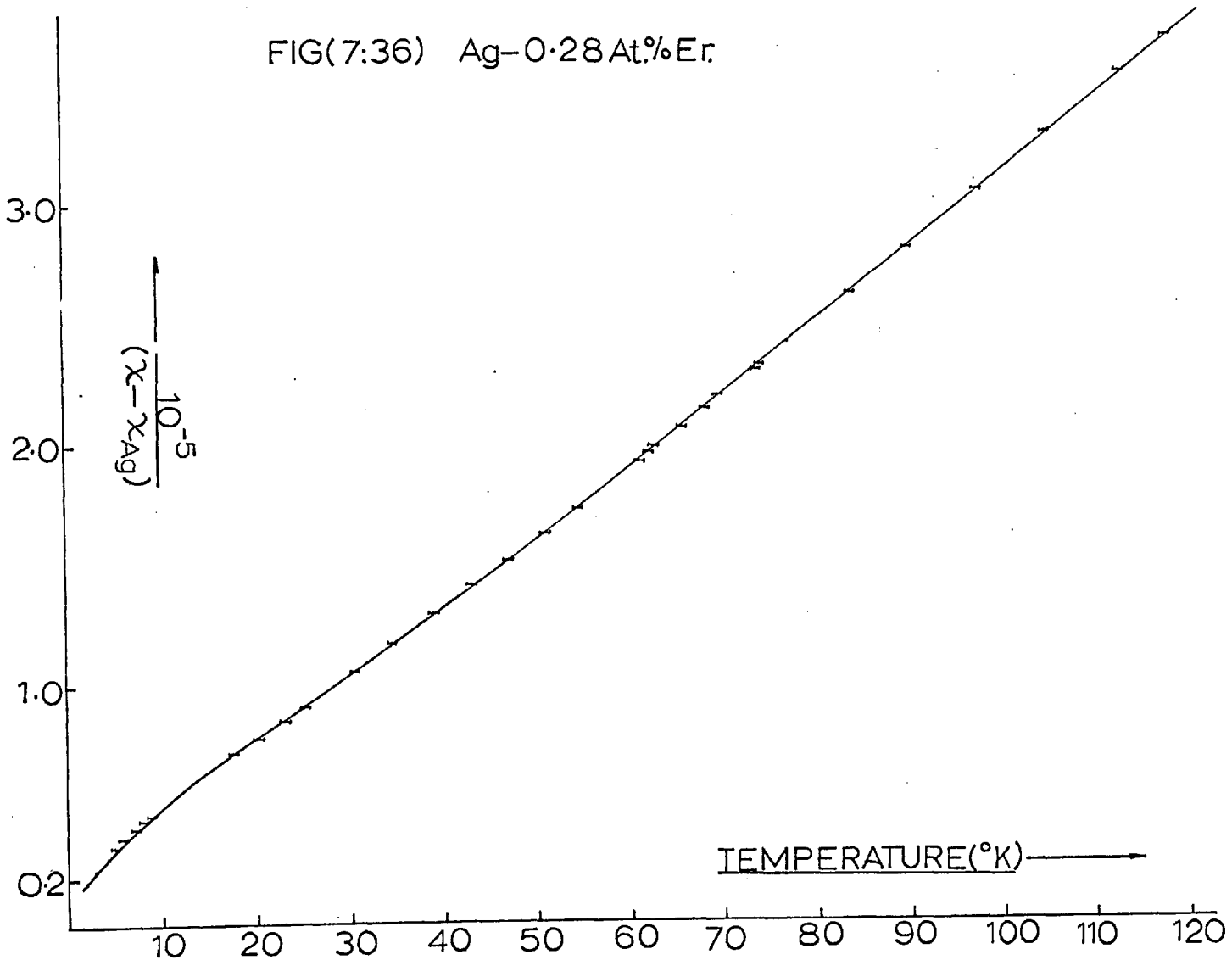

FIG(7:36) Ag–0·28 At.% Er.

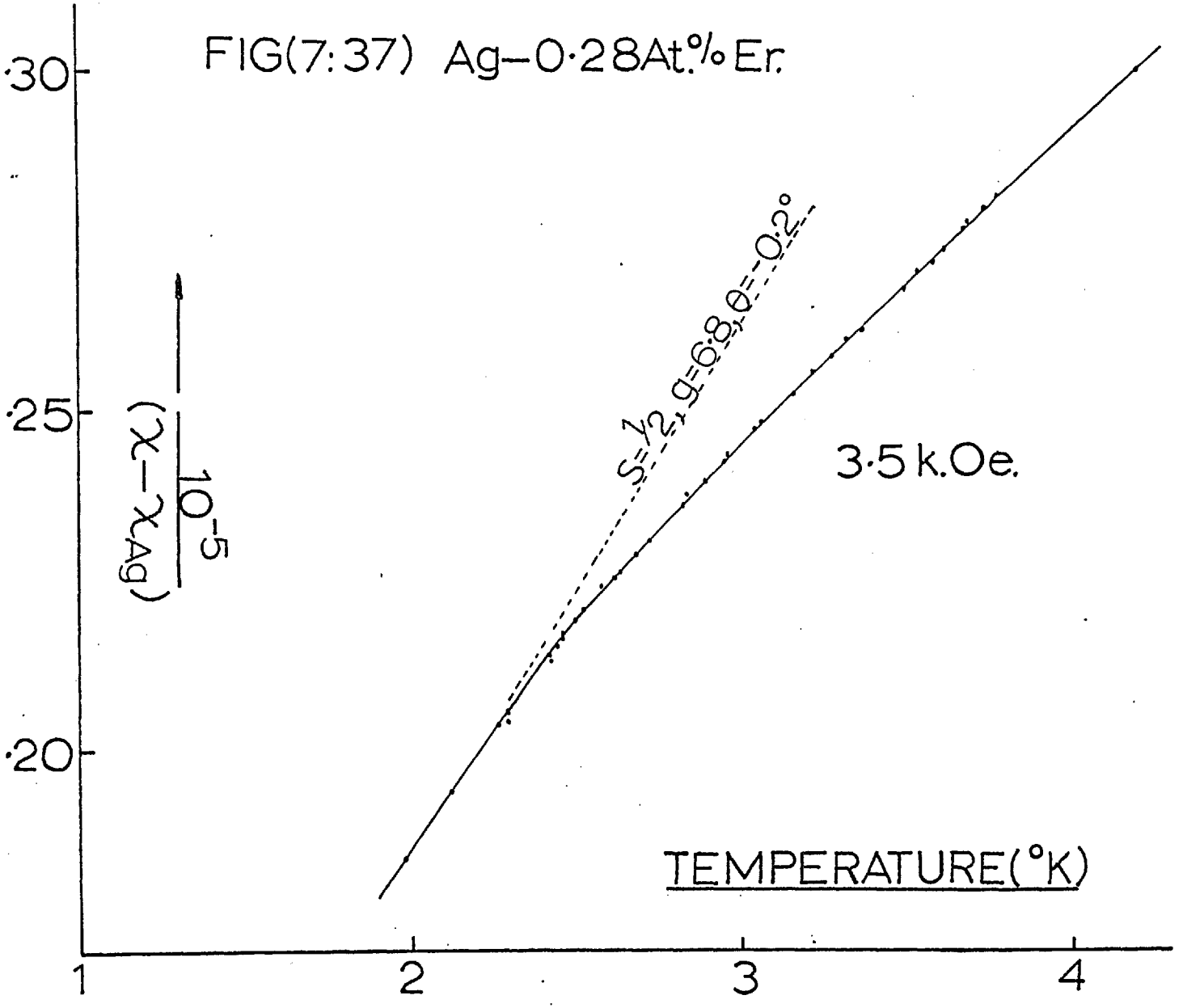
FIG(7:37) Ag–0·28At.% Er.
·30
·25
·20
$\frac{(\chi - \chi_{Ag})}{10^{-5}}$
$S=\frac{1}{2}, g=6·8, \theta=-0·2°$
3·5 k.Oe.
TEMPERATURE(°K)
1
2
3
4

FIG(7:38) (M–H) PLOTS
FOR Ag–0·28At.%Er.

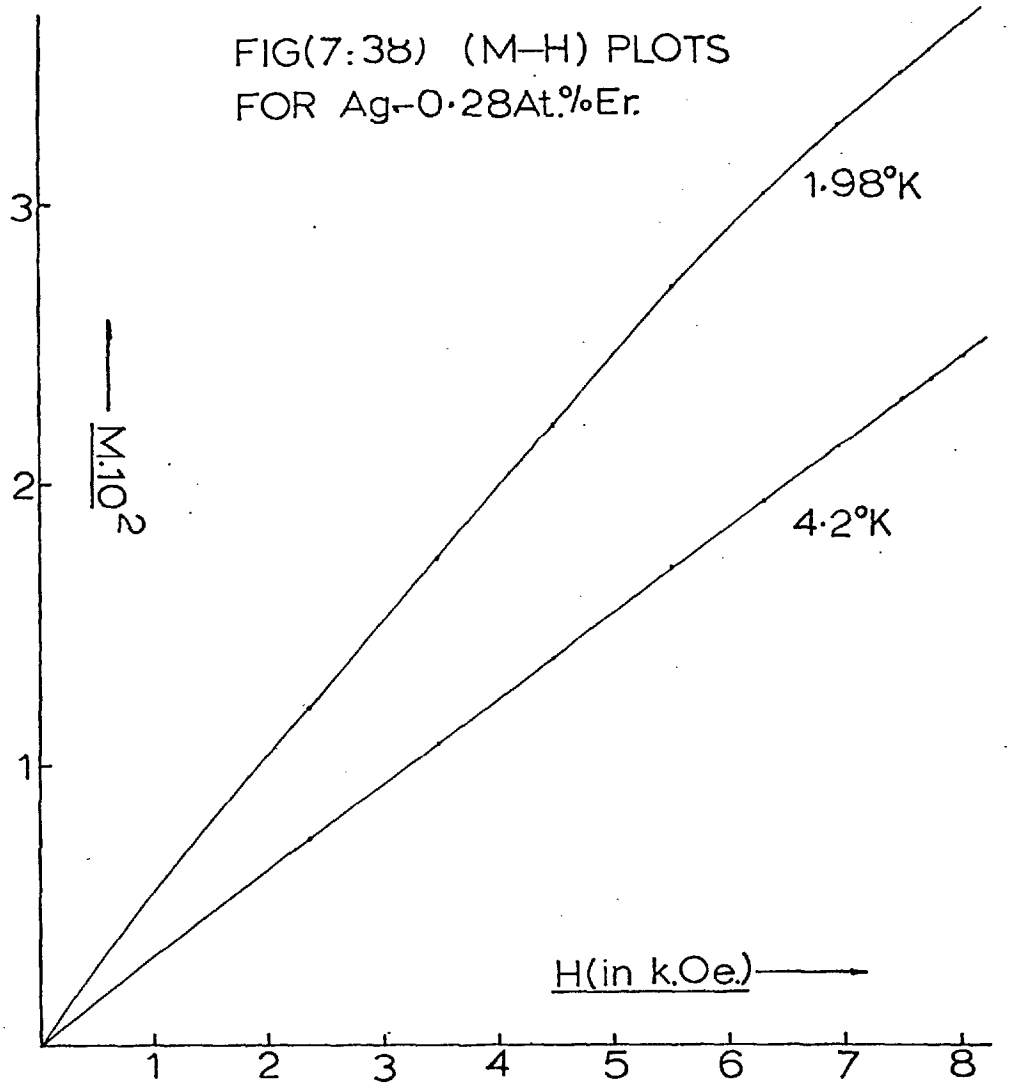

FIG(7:39) (M–H) PLOTS
FOR Ag–0·28 At.% Er.

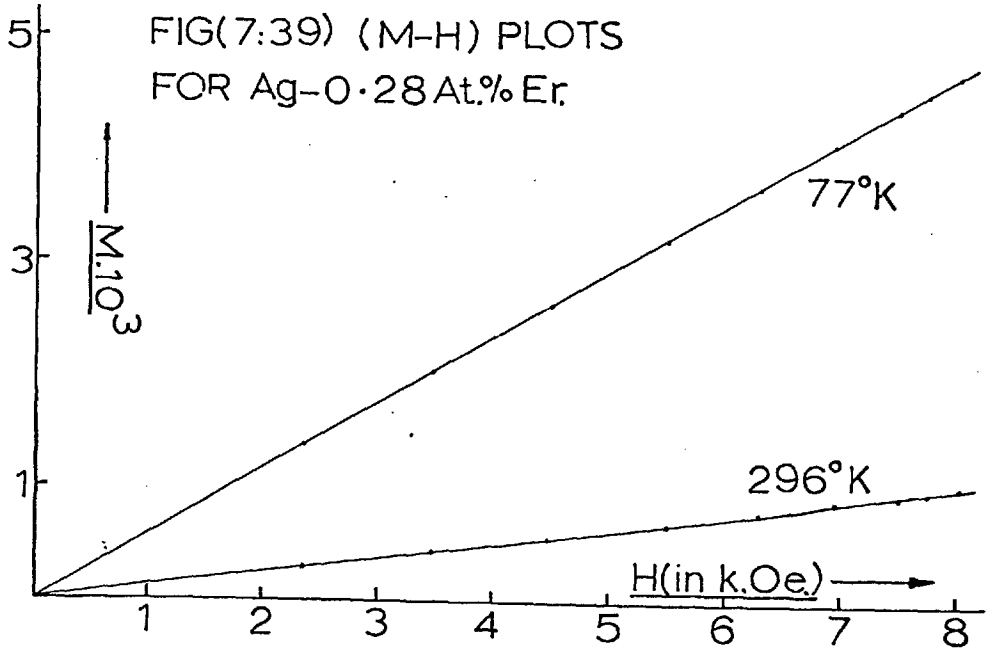

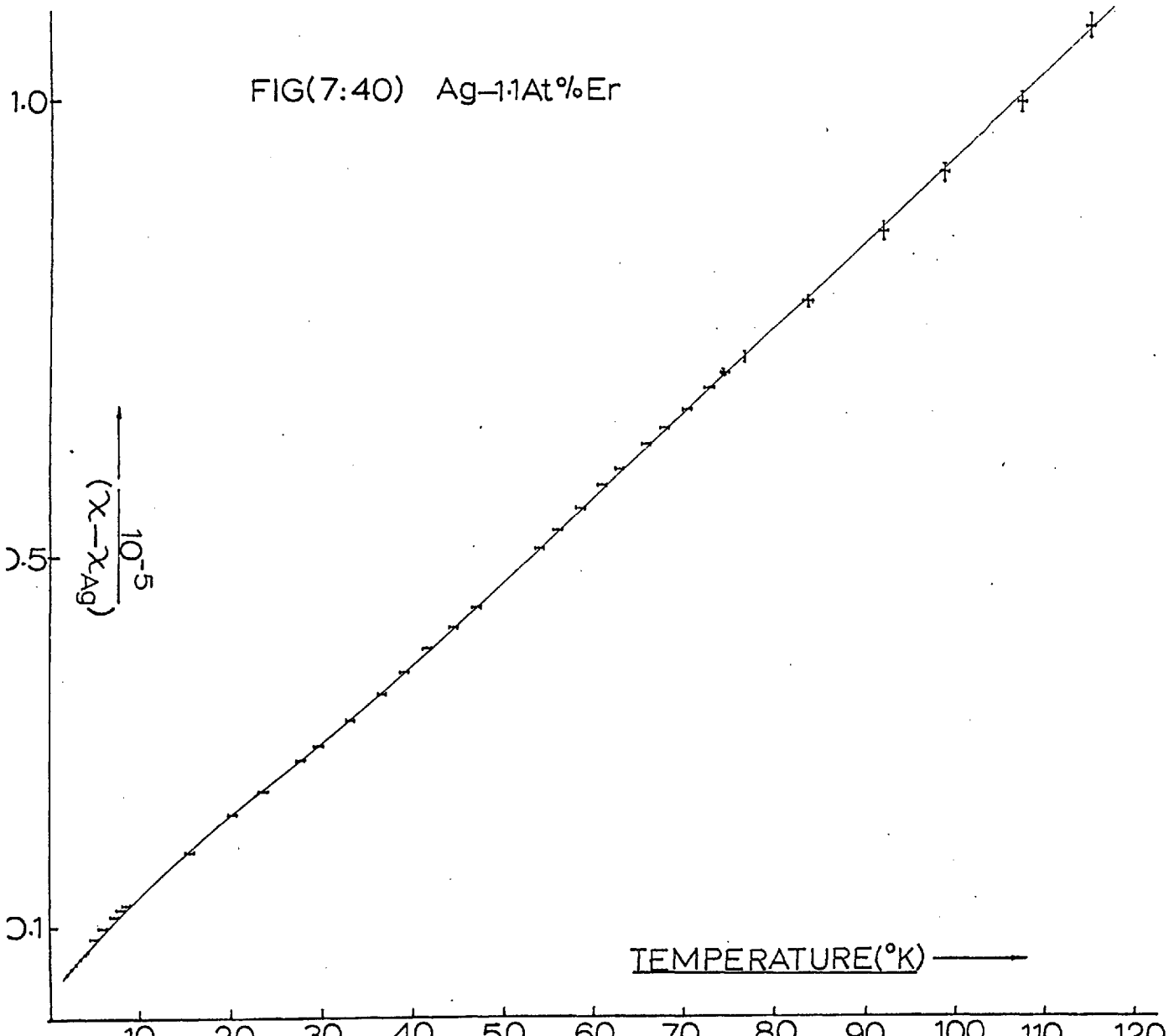
FIG(7:40) Ag–1·1At%Er
1.0
0.5
0.1
$\frac{(\chi-\chi_{Ag})}{10^{-5}}$
TEMPERATURE(°K)
10
20
30
40
50
60
70
80
90
100
110
120

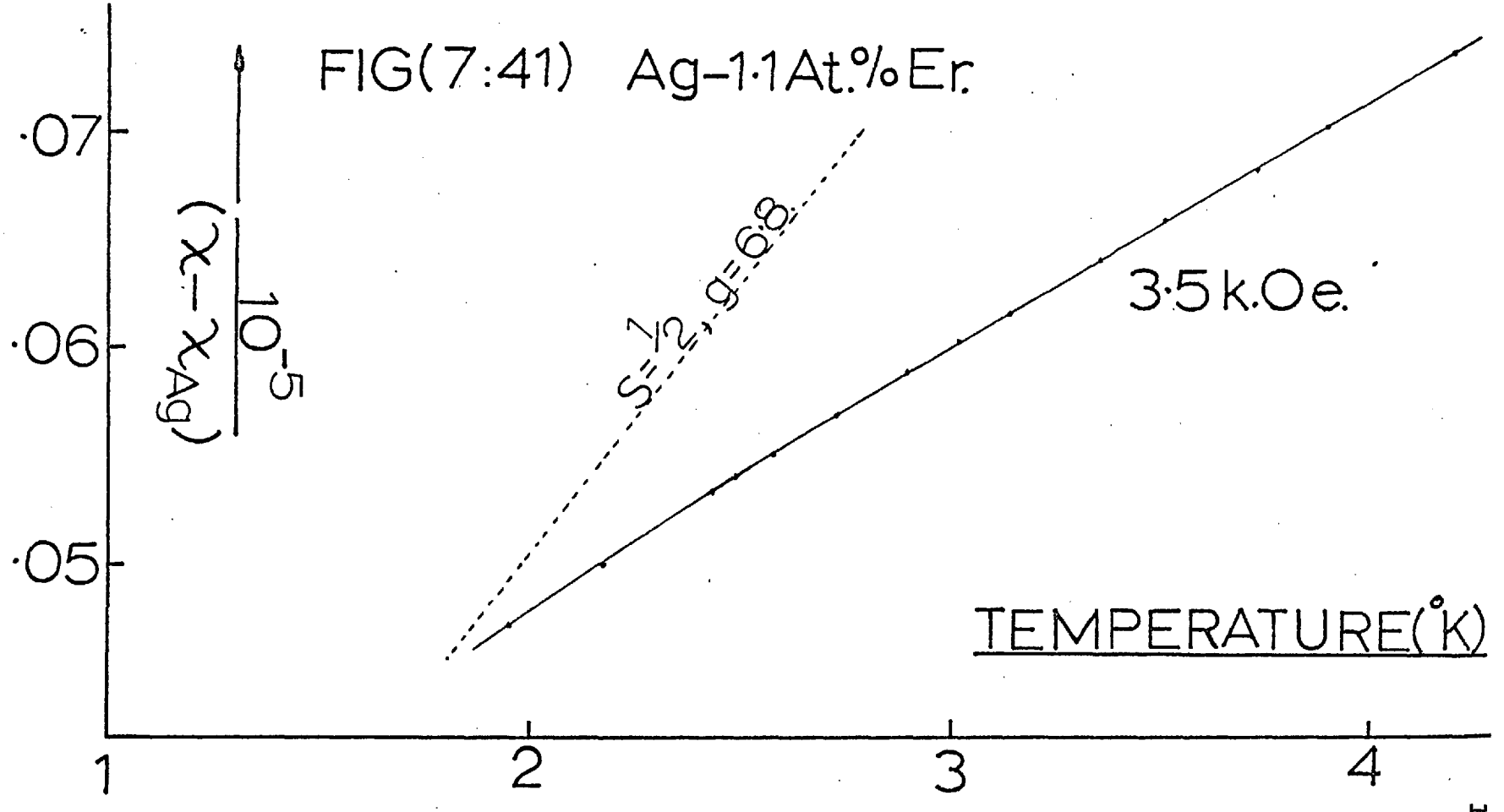
FIG(7:41) Ag-1·1At.%Er.
·07
·06
·05
$(\chi-\chi_{Ag})\ 10^{-5}$
$S=\frac{7}{2}$, g=6·8
3·5 k.Oe.
TEMPERATURE(°K)
1
2
3
4

FIG(7:42) (M-H) PLOTS
FOR Ag-1·1At.%Er.

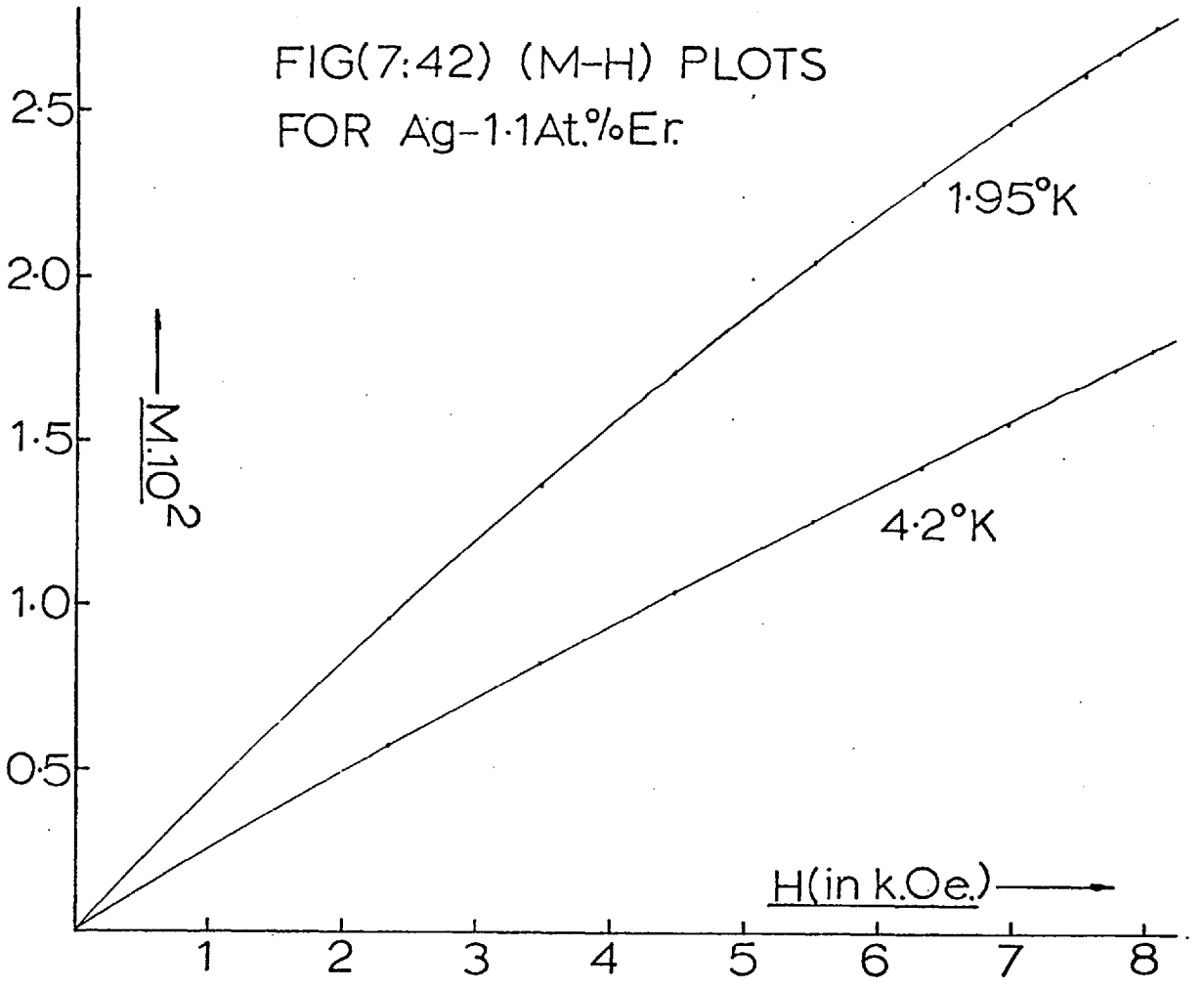

FIG(7:43) (M-H) PLOTS
FOR Ag-1·1At.%Er.

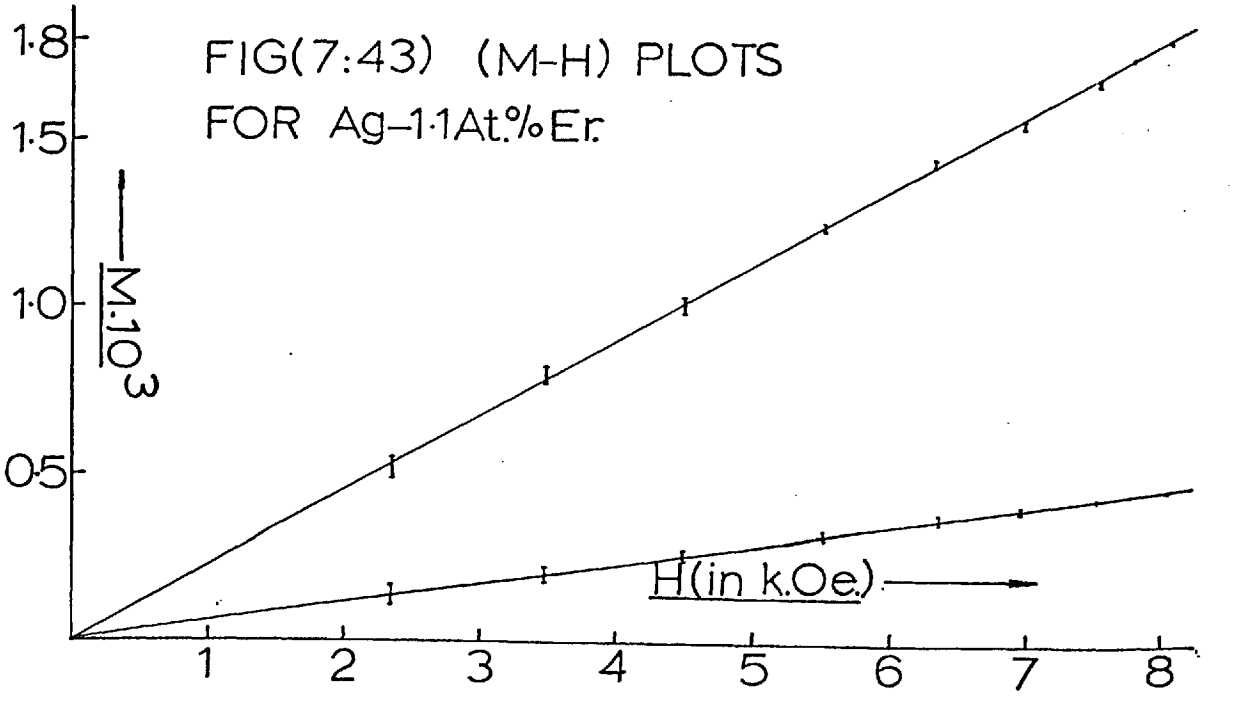

Ag - 0.5At.% Tm (Johnson Matthey and Co.)

The sample provided was in the form of an arc melted button which had been homogenised for 24 hours at 420°C. Metallographic analysis revealed a cored structure indicating possible concentration gradients. The sample was consequently cold rolled, reannealed for 5 hours at 650°C and finally quenched into iced water. As figure (7.9p) shows, this produced a recrystallised, fine grained, f.c.c. solid solution with much twinning.

The experimental data appears in figures (7.44) to (7.47).

Fig. (7.9p)

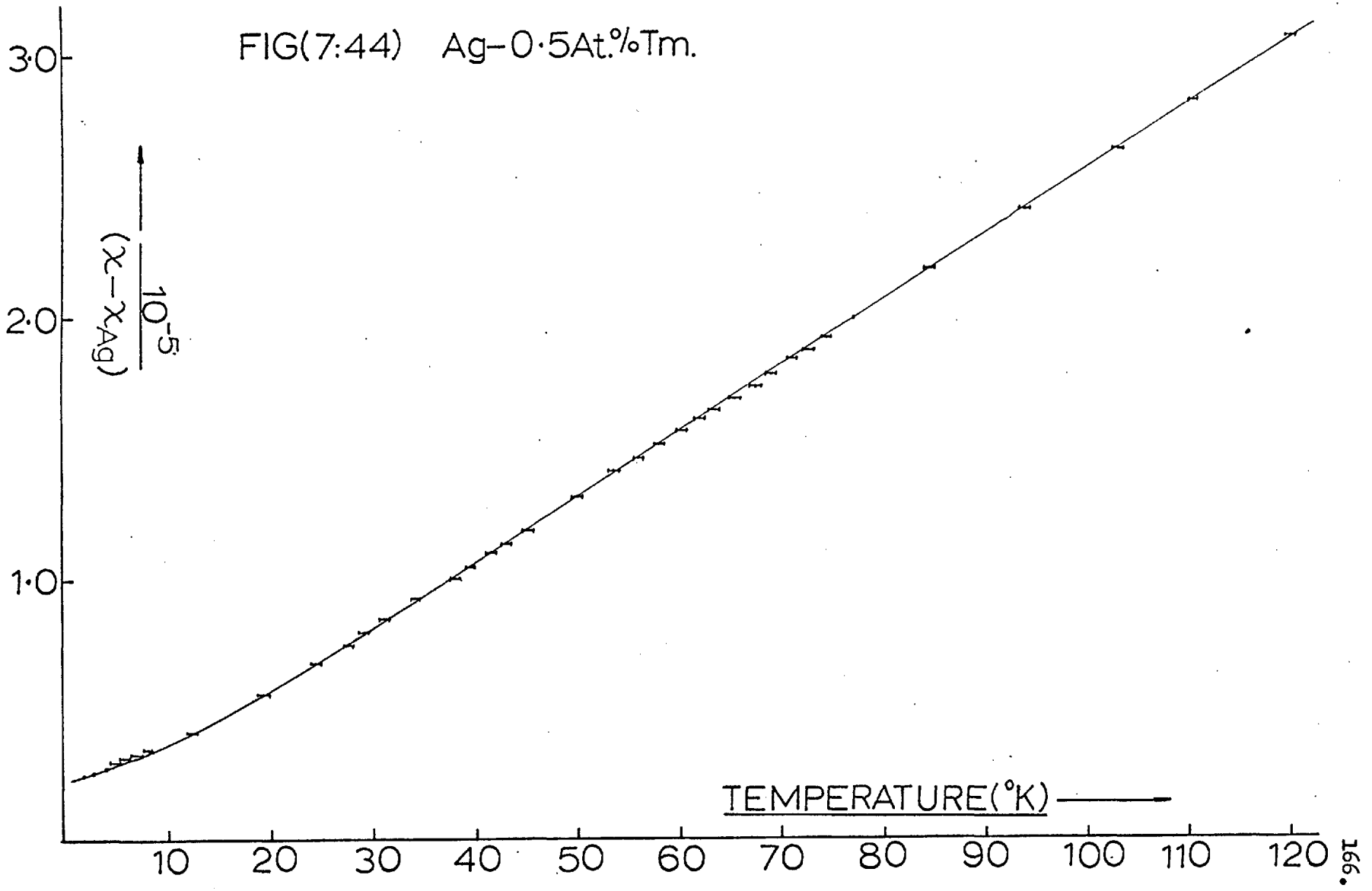
FIG(7:44) Ag–0·5At.%Tm.
3·0
2·0
1·0
$(\chi - \chi_{Ag})\ 10^{-5}$
TEMPERATURE(°K)
10
20
30
40
50
60
70
80
90
100
110
120

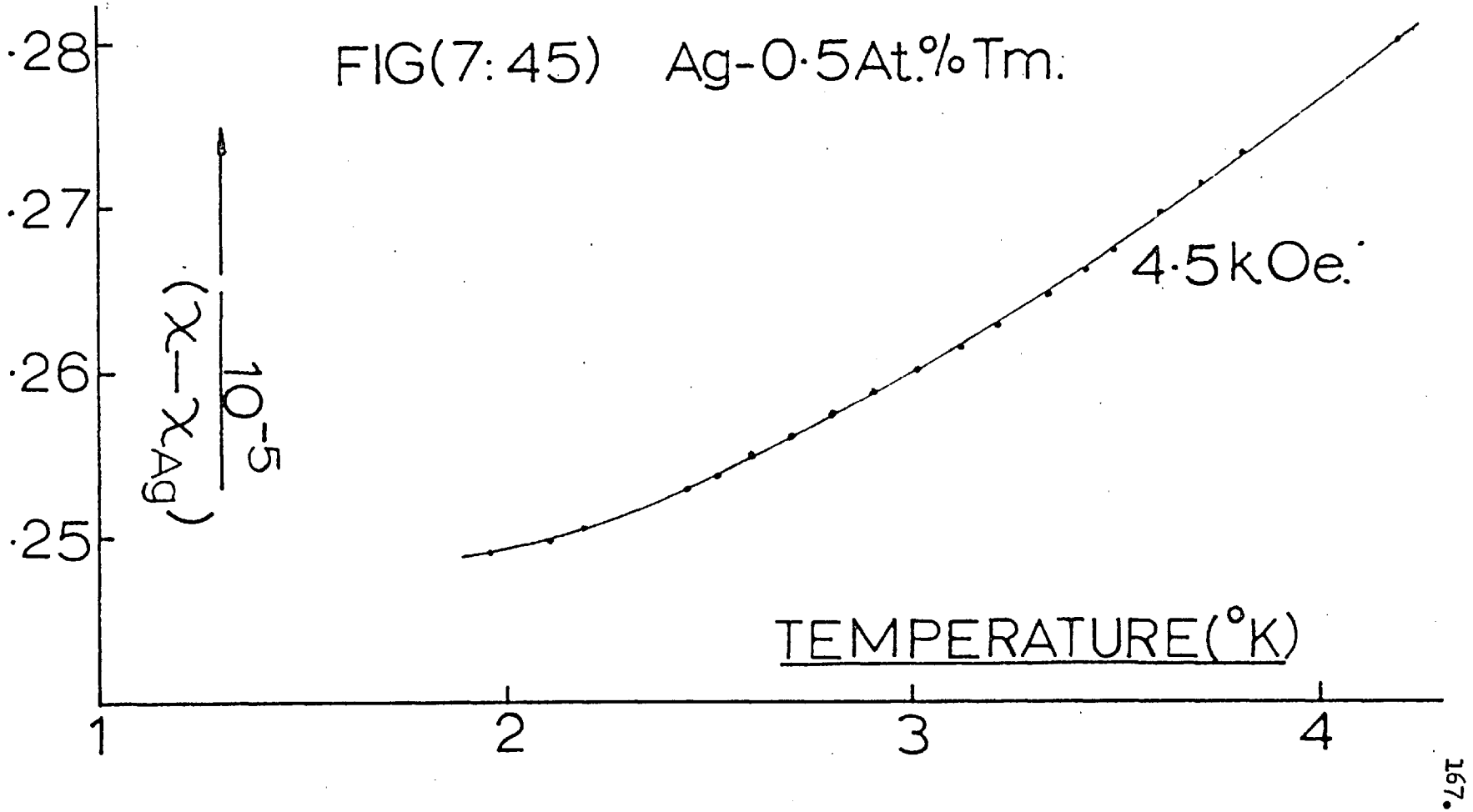
FIG(7:45) Ag-0·5At.%Tm.
·28
·27
·26
·25
$\frac{10^{-5}}{(\chi-\chi_{Ag})}$
4·5kOe.
TEMPERATURE(°K)
1
2
3
4

FIG(7:46) (M-H) PLOTS
FOR Ag-0·5At.% Tm.

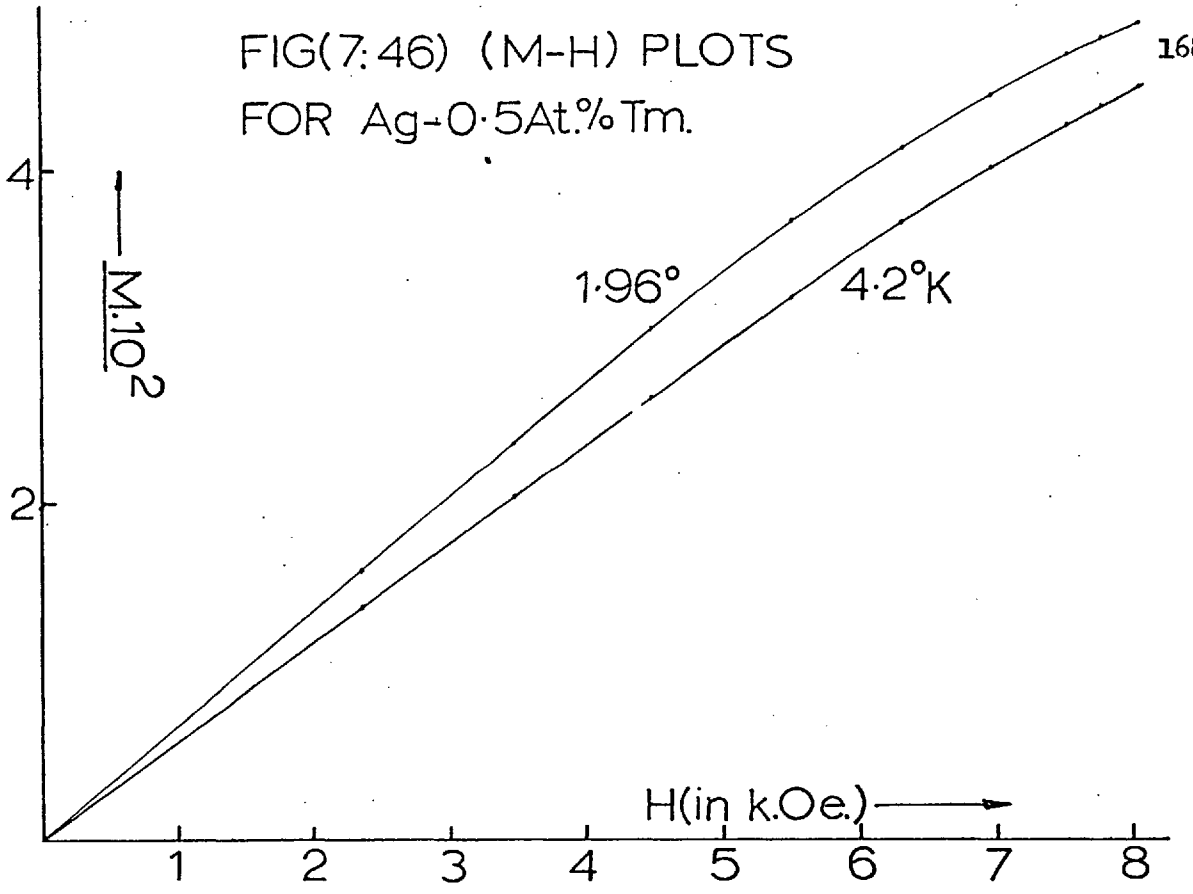

FIG(7:47) (M-H) PLOTS
FOR Ag-0·5At.% Tm.

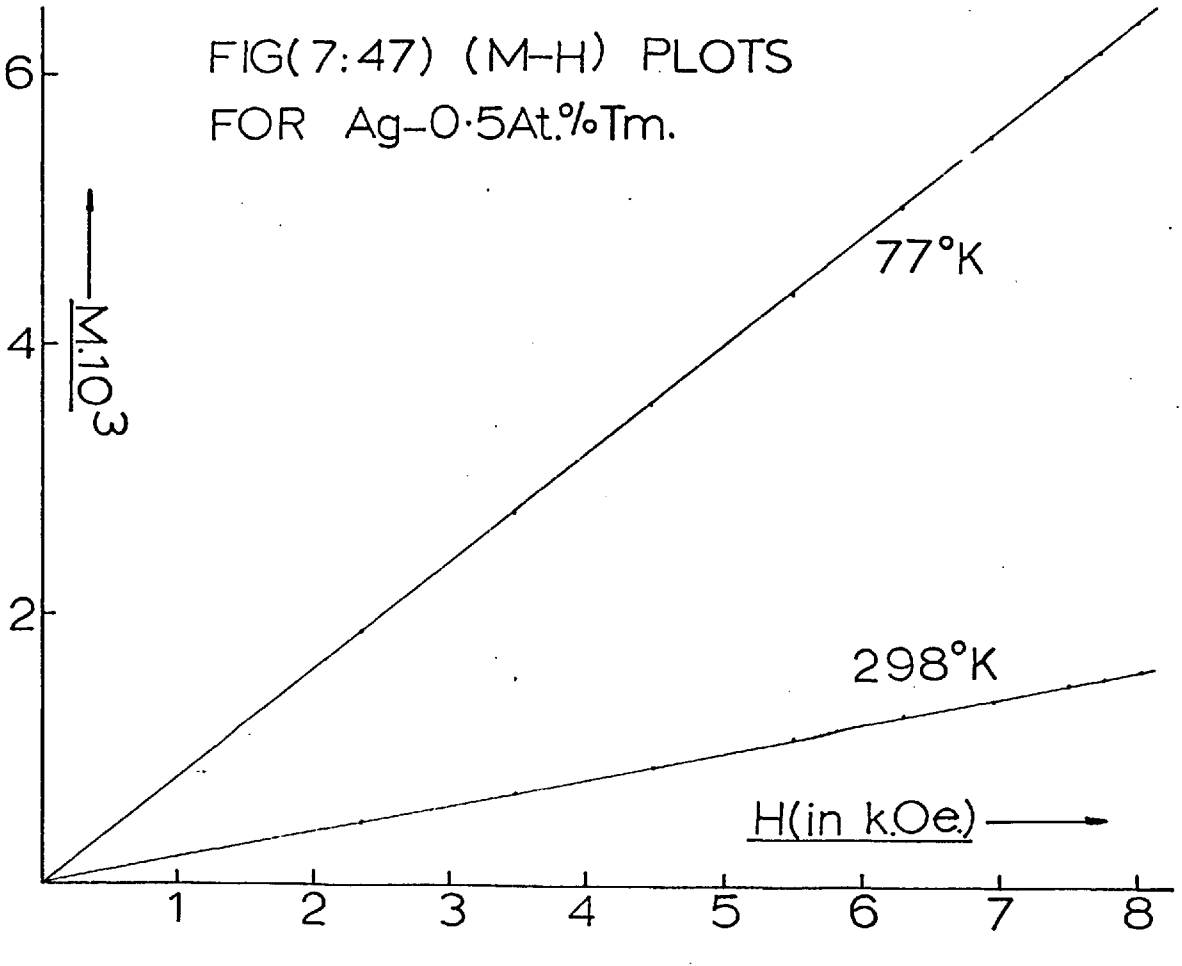

Ag - 0.5At.% Yb (Johnson Matthey and Co.)

The susceptibility sample was machined from an arc cast button which had been homogenised at 550°C for 2 days.

Examination of the microstructure showed large columnor or grains of dendritic character, with small amounts of interdendritic second phase, see figure (7.10p).

Figures (7.48) to (7.50) reproduce the experimental data.

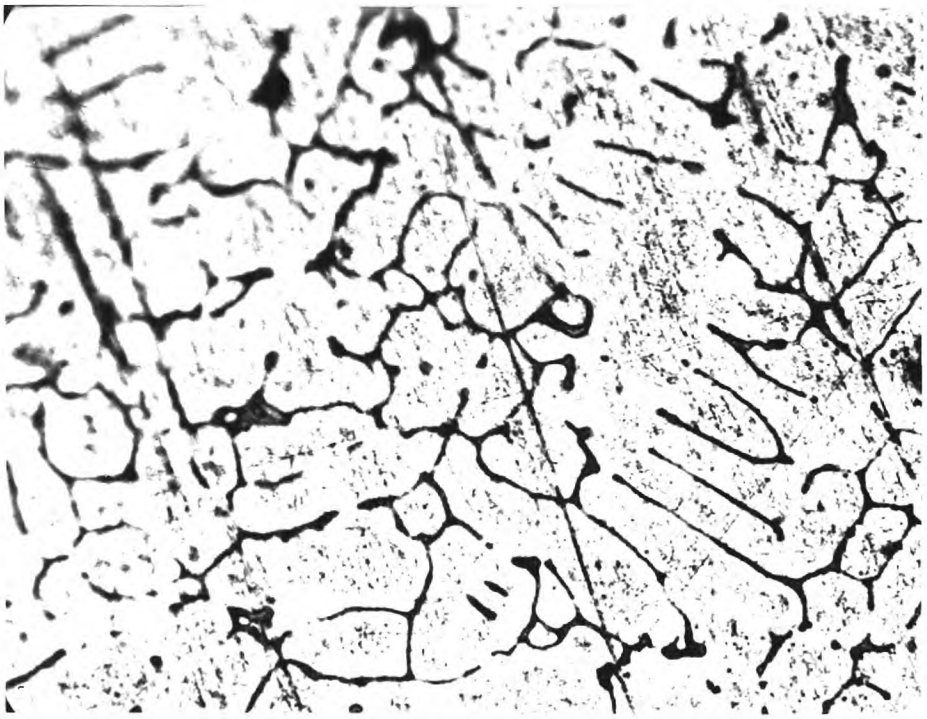

Fig. (7.10p)

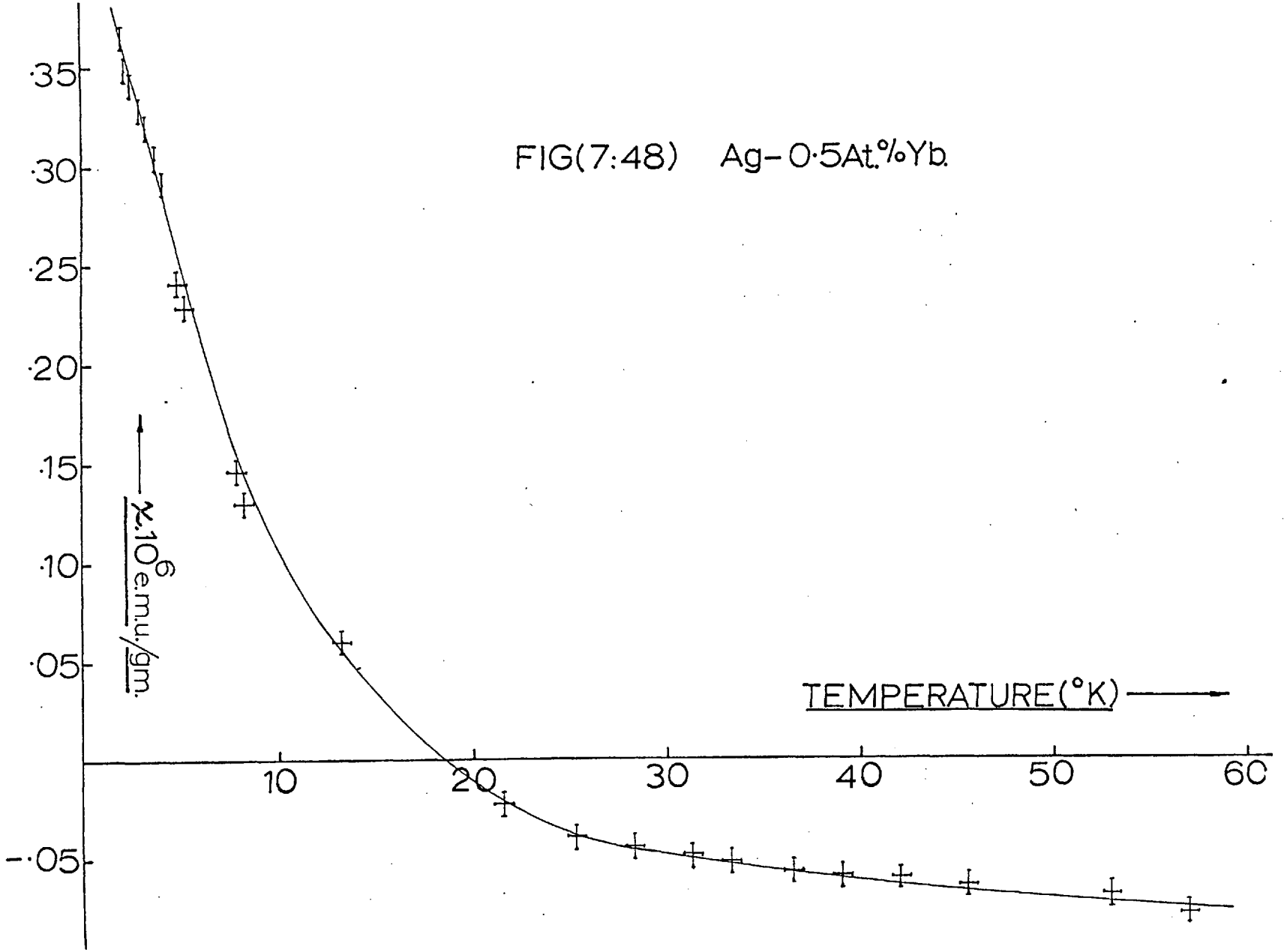
FIG(7:48) Ag-0·5At.%Yb.
·35
·30
·25
·20
·15
·10
·05
-·05
χ.10^6 e.m.u./gm.
TEMPERATURE(°K)
10
20
30
40
50
60

FIG(7:49) (M-H) PLOTS
FOR Ag-0·5At.%Yb.

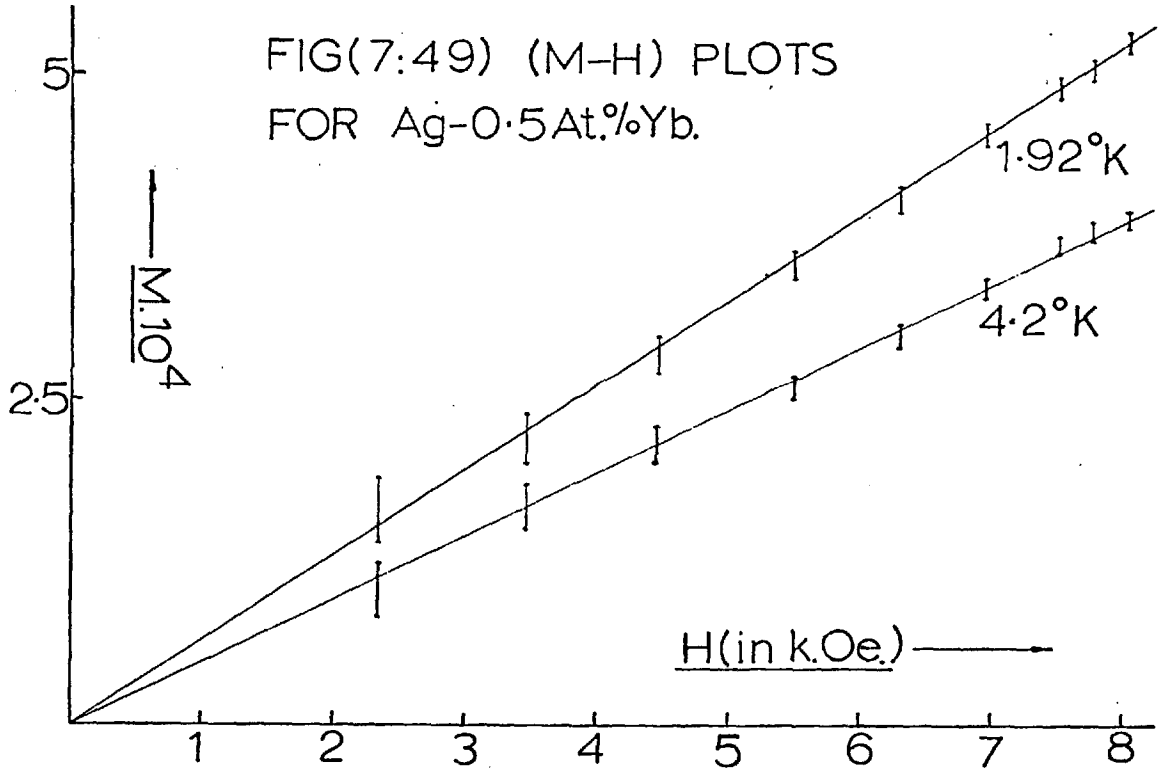

FIG(7:50) (M-H) PLOTS
FOR Ag-0·5At.%Yb.

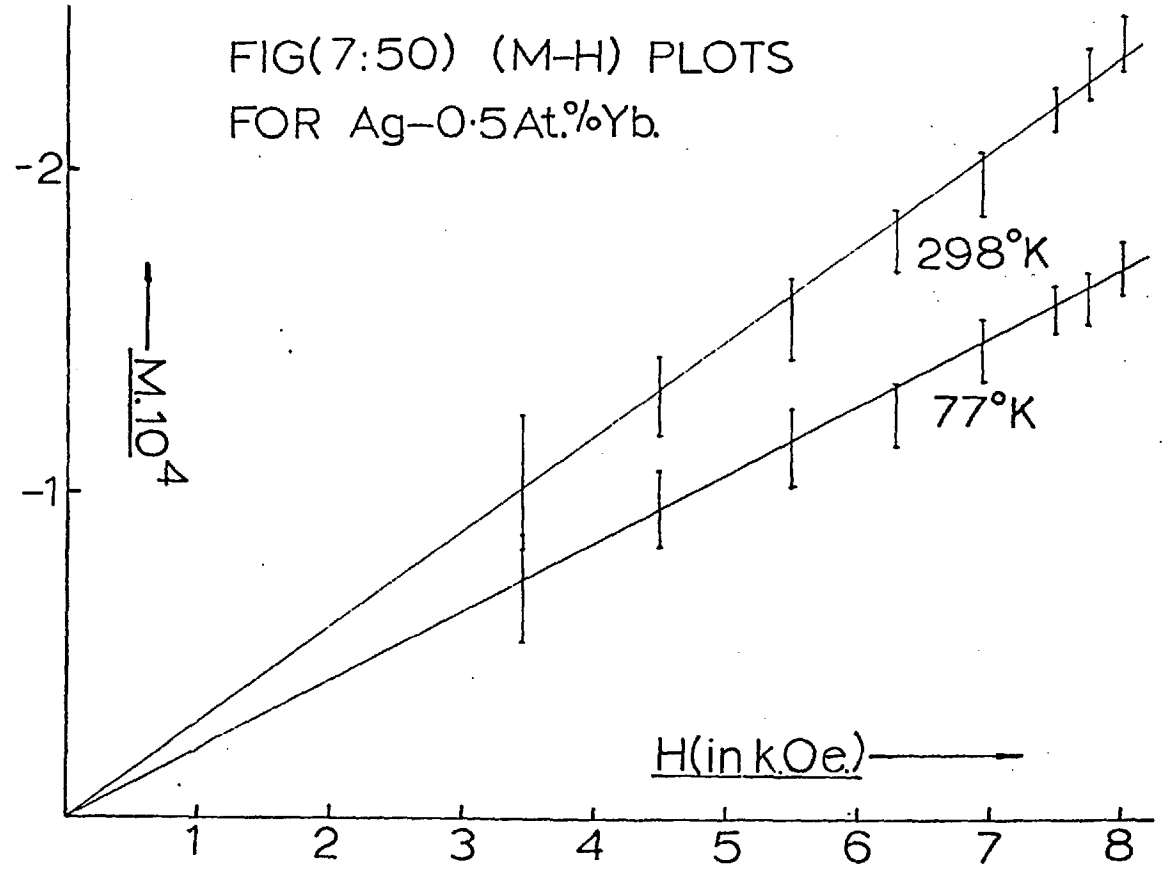

None of the dilute gold rare-earth alloys were subjected to metallographic analysis since the rare-earth solubilities in gold are almost double those for the corresponding silver alloys. (See, for example Rider[64].)

Au - 1.0At.% Er (Harris, Birmingham)

The susceptibility sample was machined from a button of this alloy which had been homogenised for one week at 900°C. The experimental data appears in figures (7.51) to (7.54).

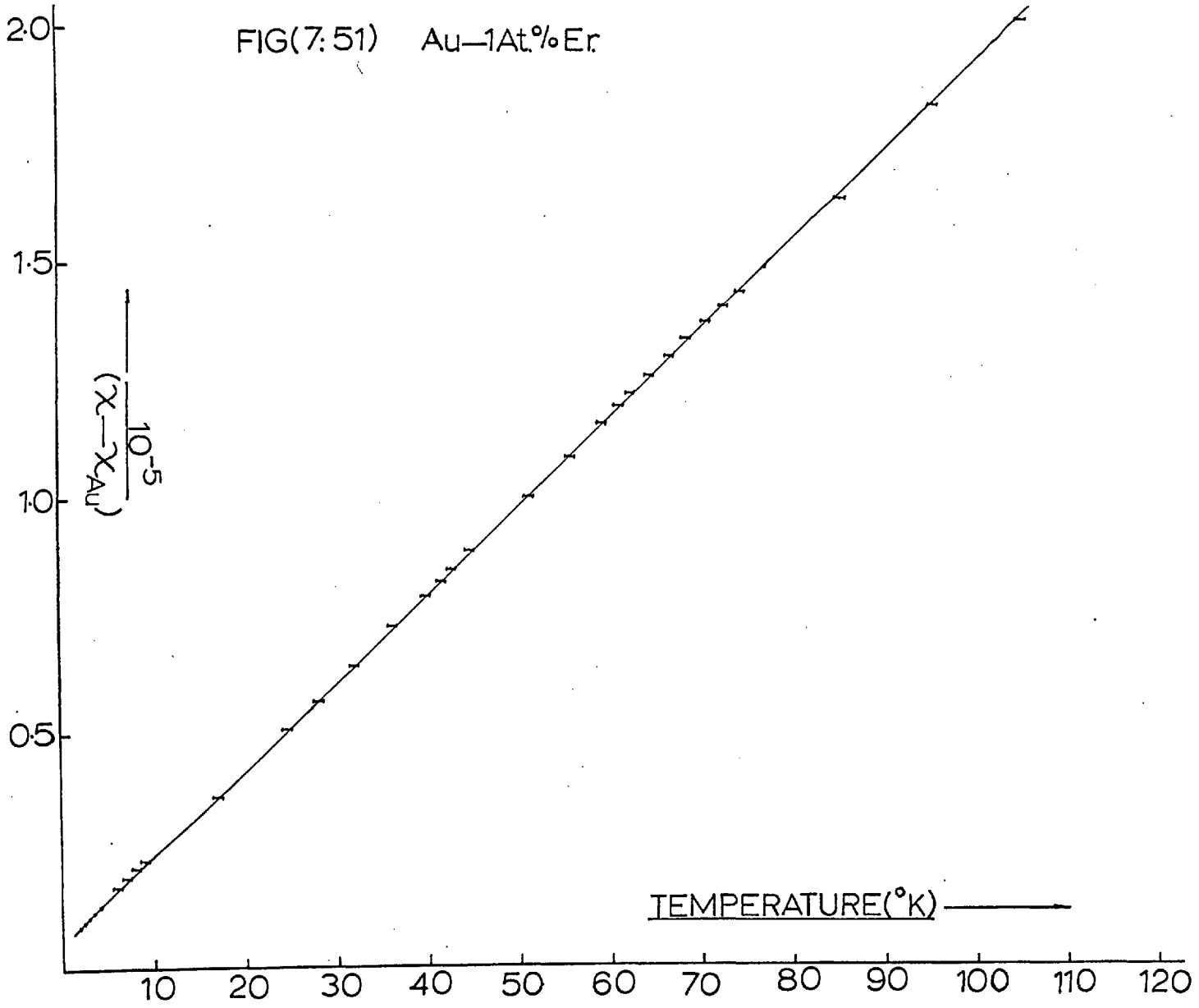
FIG(7:51) Au—1At.% Er
2·0
1·5
1·0
0·5
$\frac{10^{-5}}{(\chi - \chi_{Au})}$
TEMPERATURE(°K)
10
20
30
40
50
60
70
80
90
100
110
120

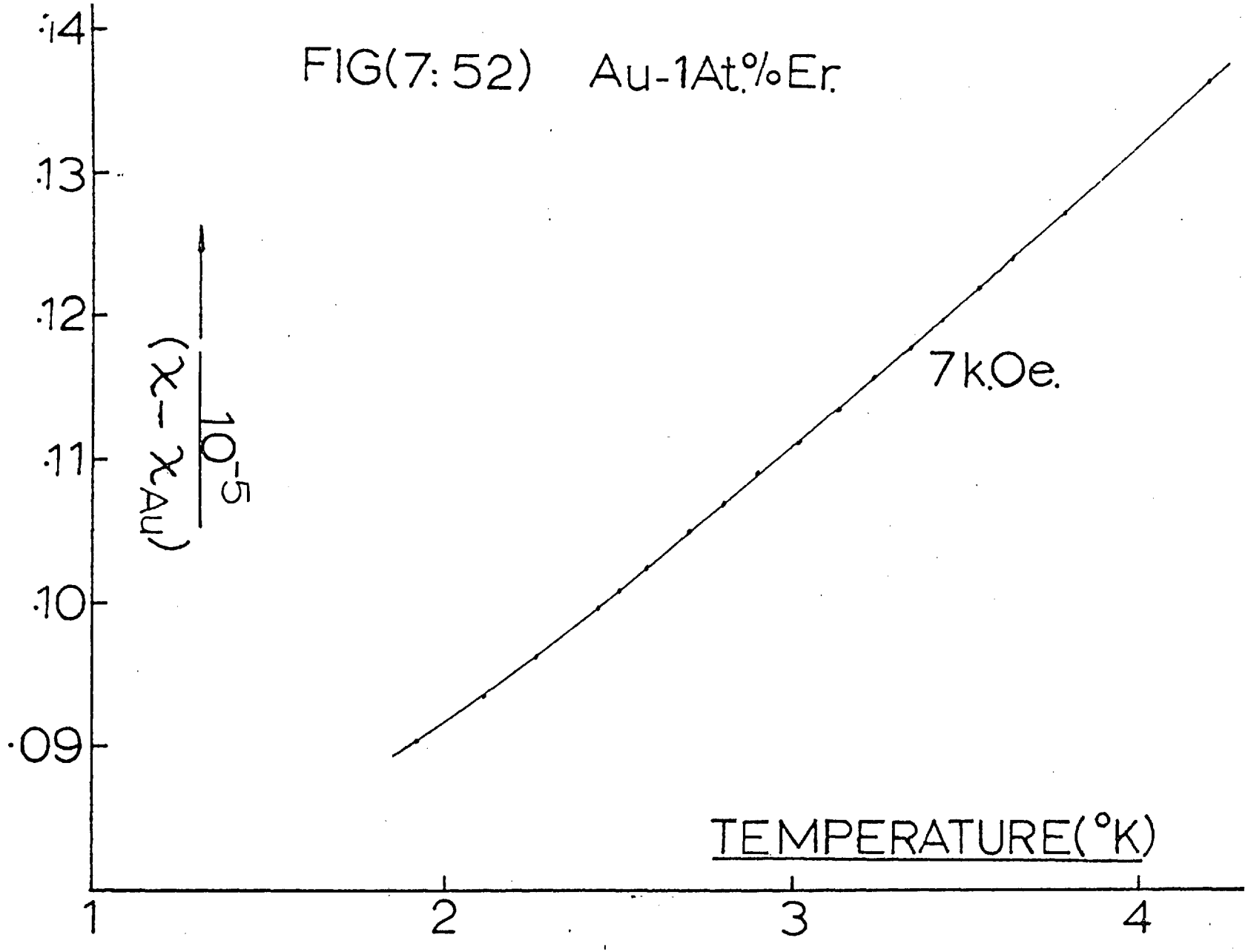
FIG(7:52) Au-1At.%Er.
·14
·13
·12
·11
·10
·09
$\frac{(\chi - \chi_{Au})}{10^{-5}}$
7k.Oe.
TEMPERATURE(°K)
1
2
3
4

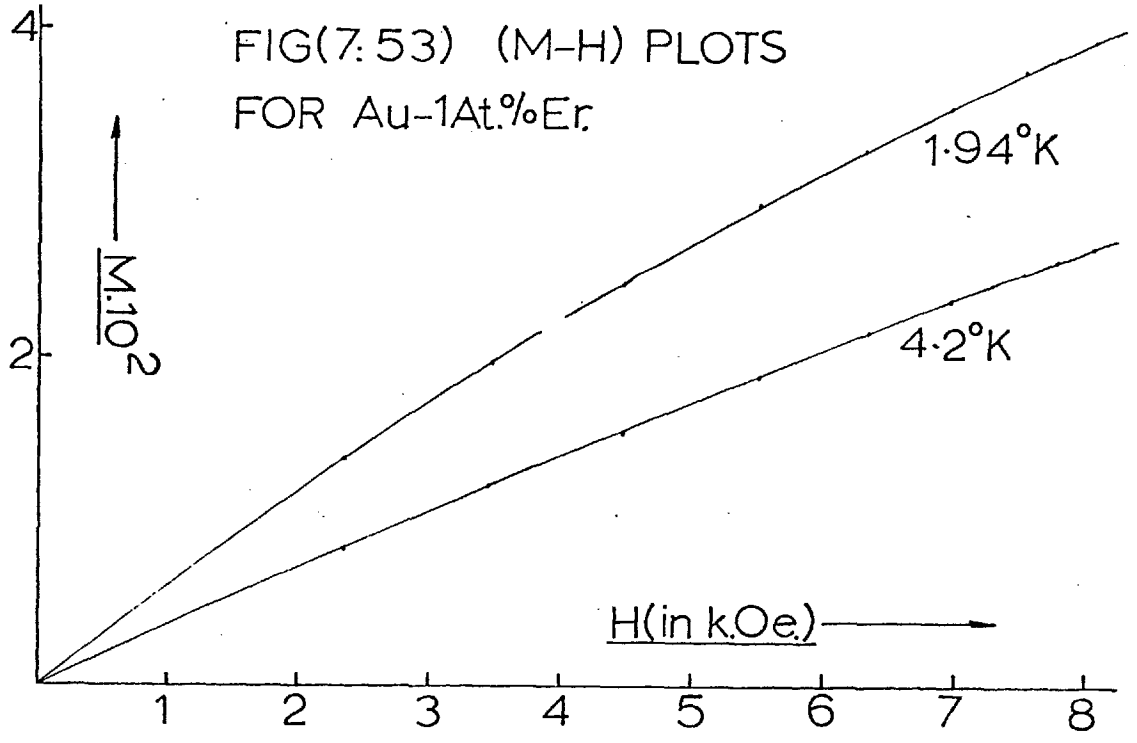

FIG(7:53) (M-H) PLOTS FOR Au-1At.%Er.

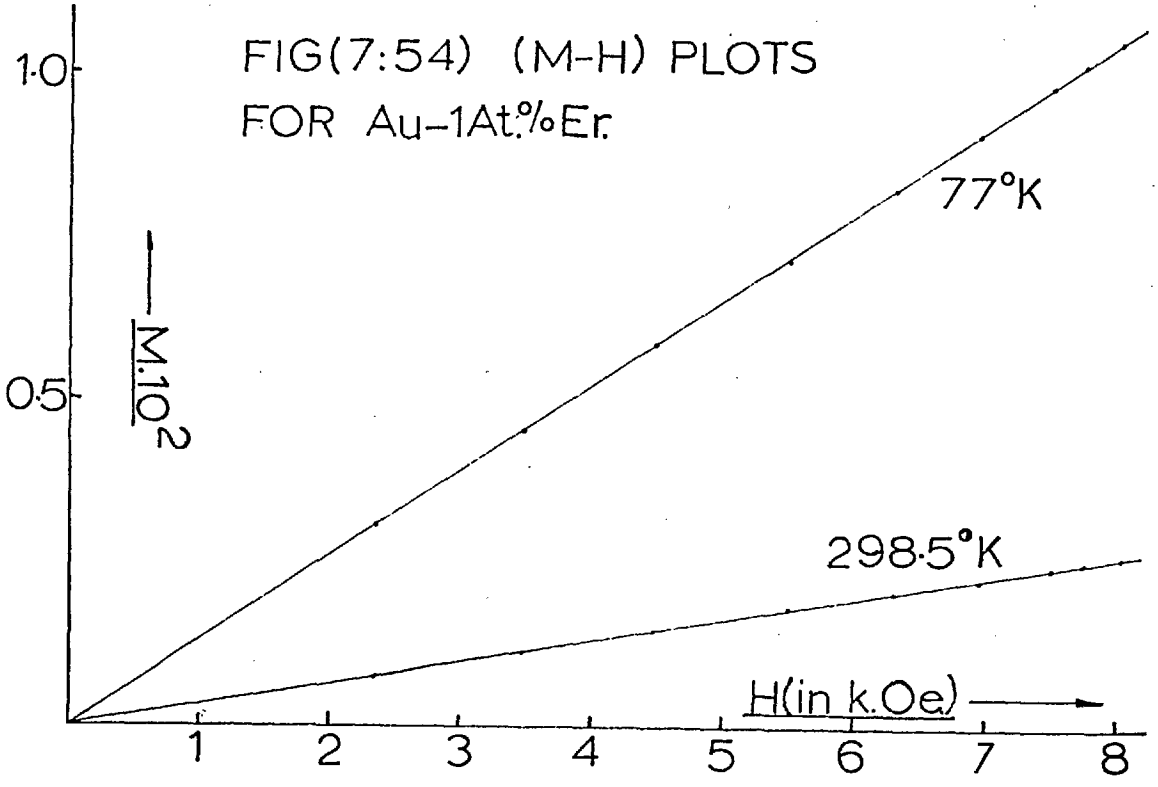

FIG(7:54) (M-H) PLOTS FOR Au-1At.%Er.

Au - 0.3At.% Tm (Harwell)

This alloy was supplied in the form of an arc melted button, which had not been homogenised. The button was cold colled before homogenising for 30 hours at 675°C, quenching the sample into iced water. A sample suitable for susceptibility measurements was made in the usual manner.

Figures (7.55) to (7.58) reproduced the experimental data.

FIG(7:55) Au-0·3At.% Tm.

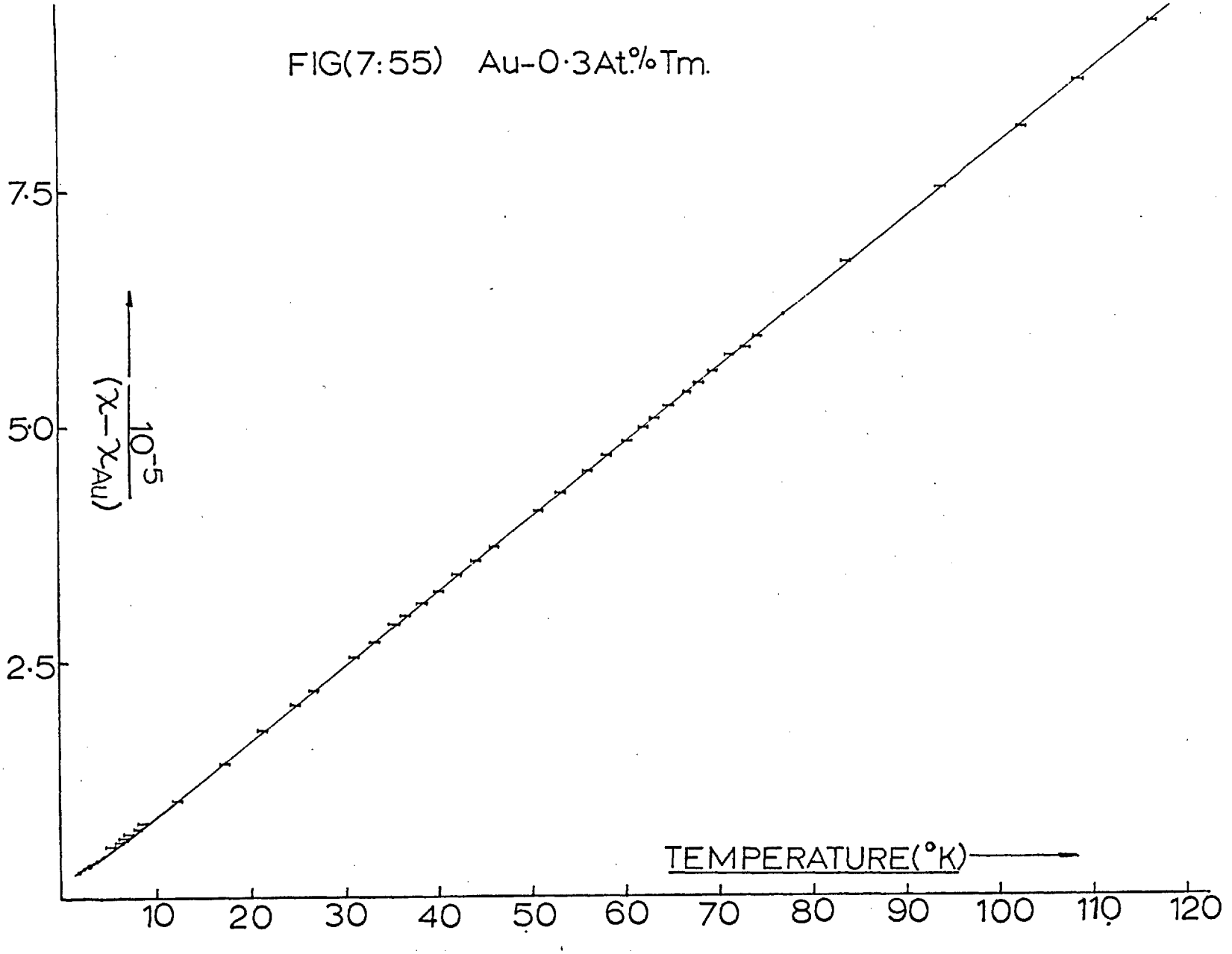

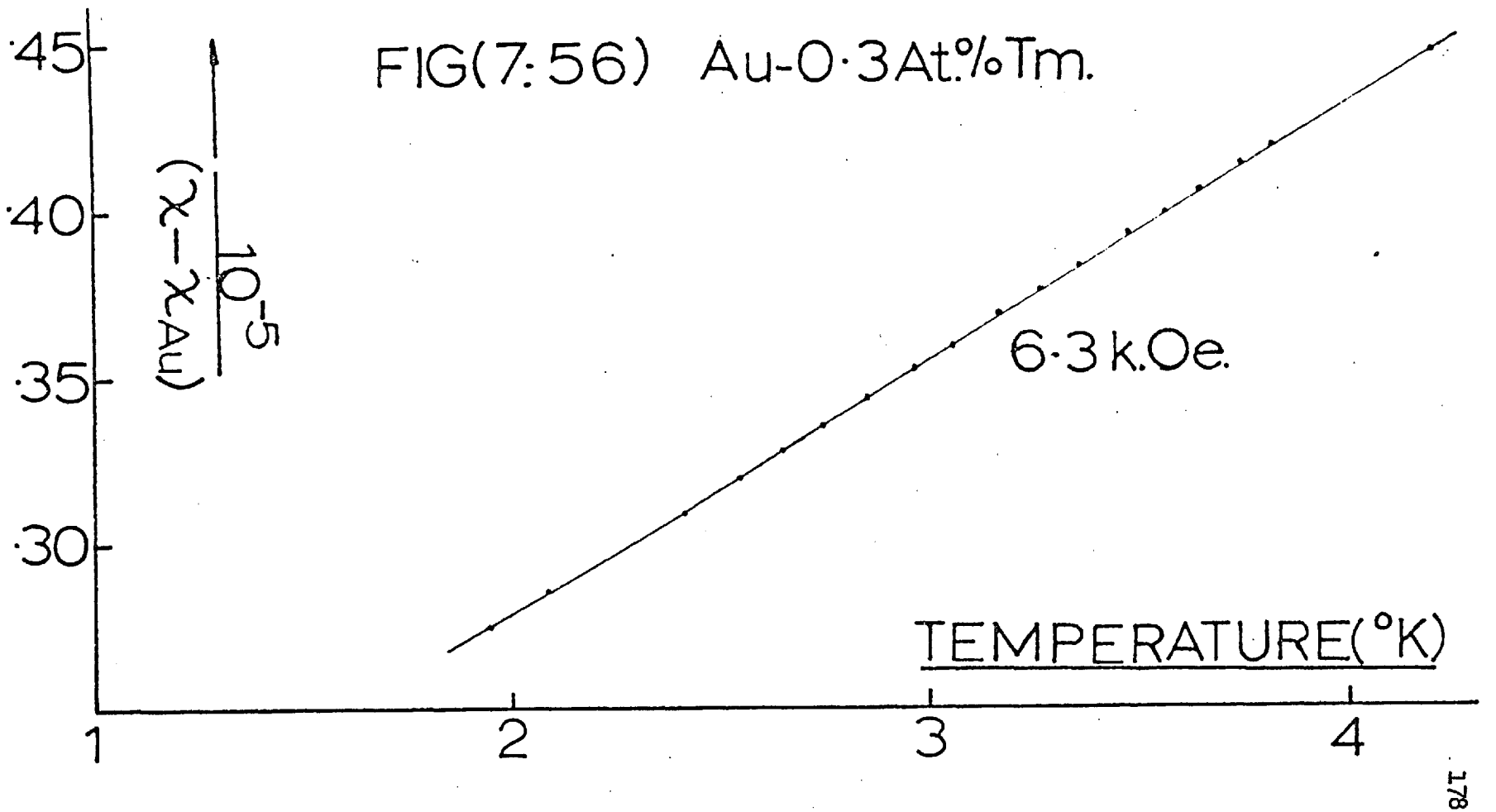
FIG(7:56) Au-0·3At.%Tm.
·45
·40
·35
·30
$(\chi-\chi_{Au})\ 10^{-5}$
6·3 k.Oe.
TEMPERATURE(°K)
1
2
3
4

FIG(7:57) (M–H) PLOTS
FOR Au–0·3At.% Tm.

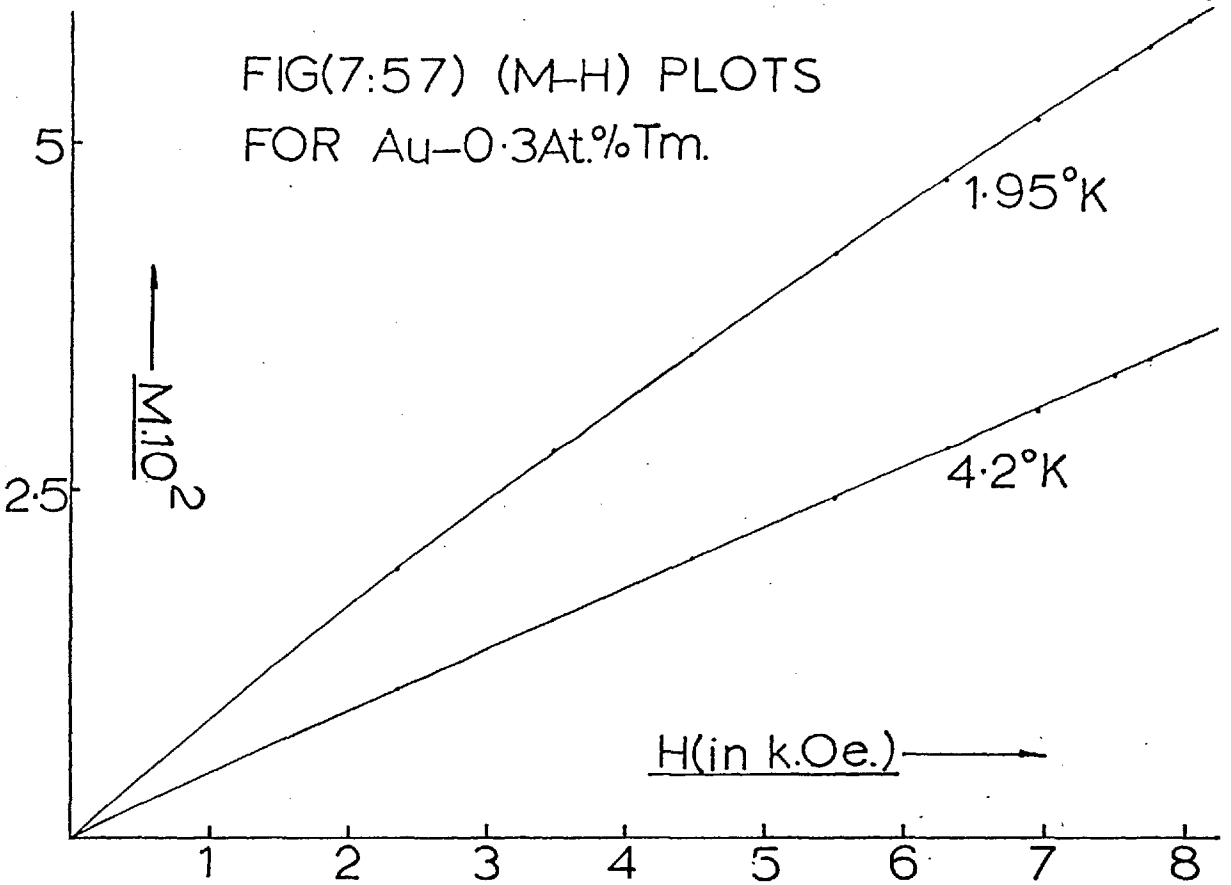

FIG(7:58) (M–H) PLOTS
FOR Au-0·3At.% Tm.

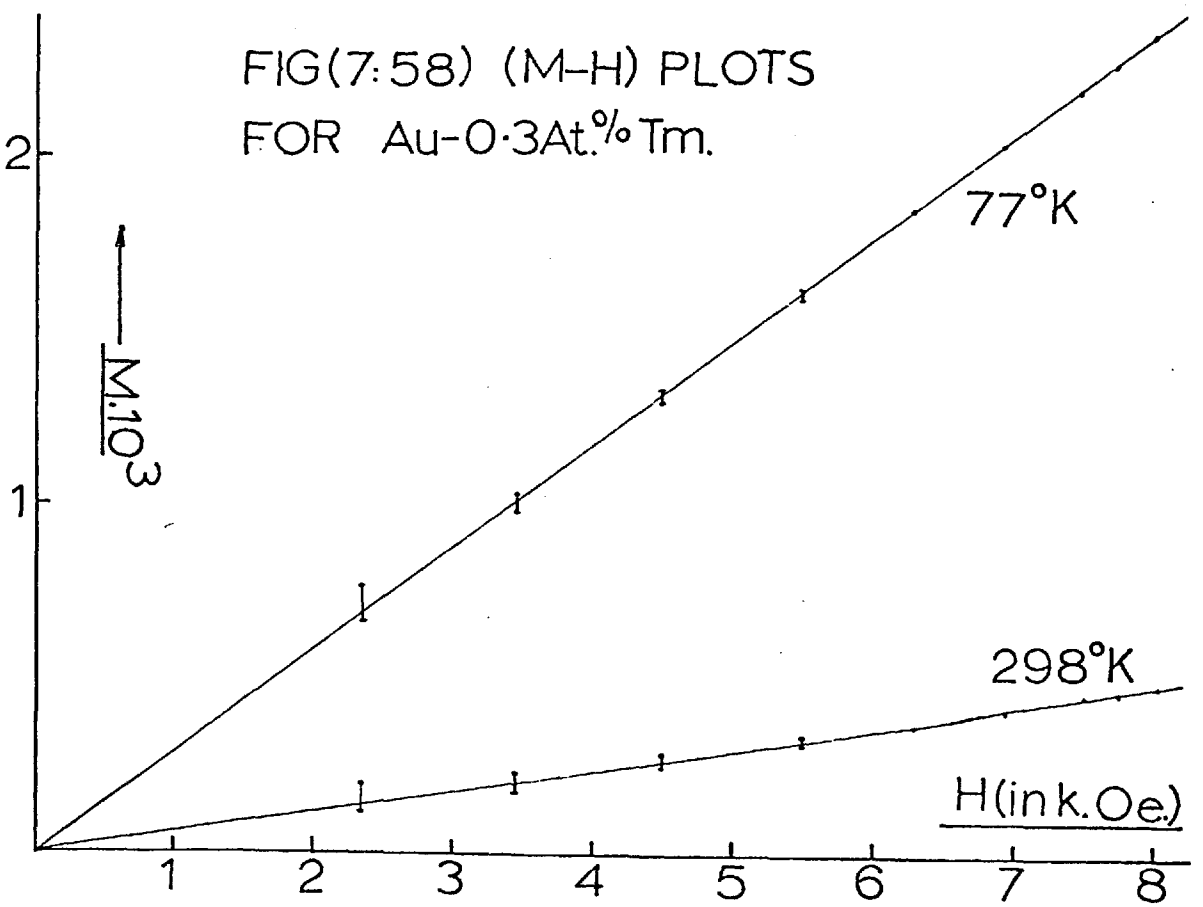

Au - 0.9At.% Yb

The specimen was obtained from an arc melted button which had been forged and then annealed at 800°C for several days. The specimen was given a strain releaving anneal at 450°C for 20 minutes.

Figures (7.59) to (7.62) summarise the experimental data.

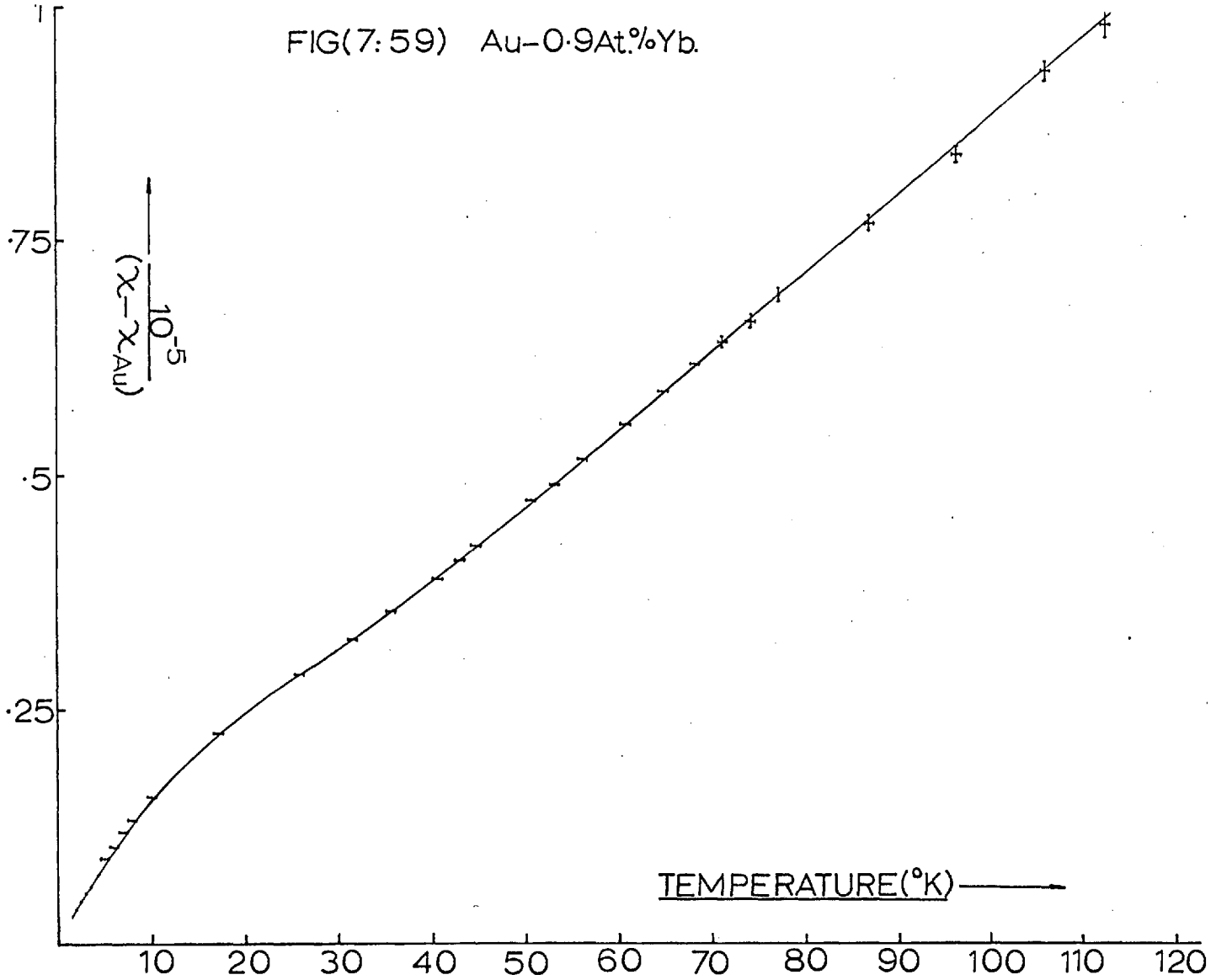

FIG(7:59) Au-0·9At.%Yb.

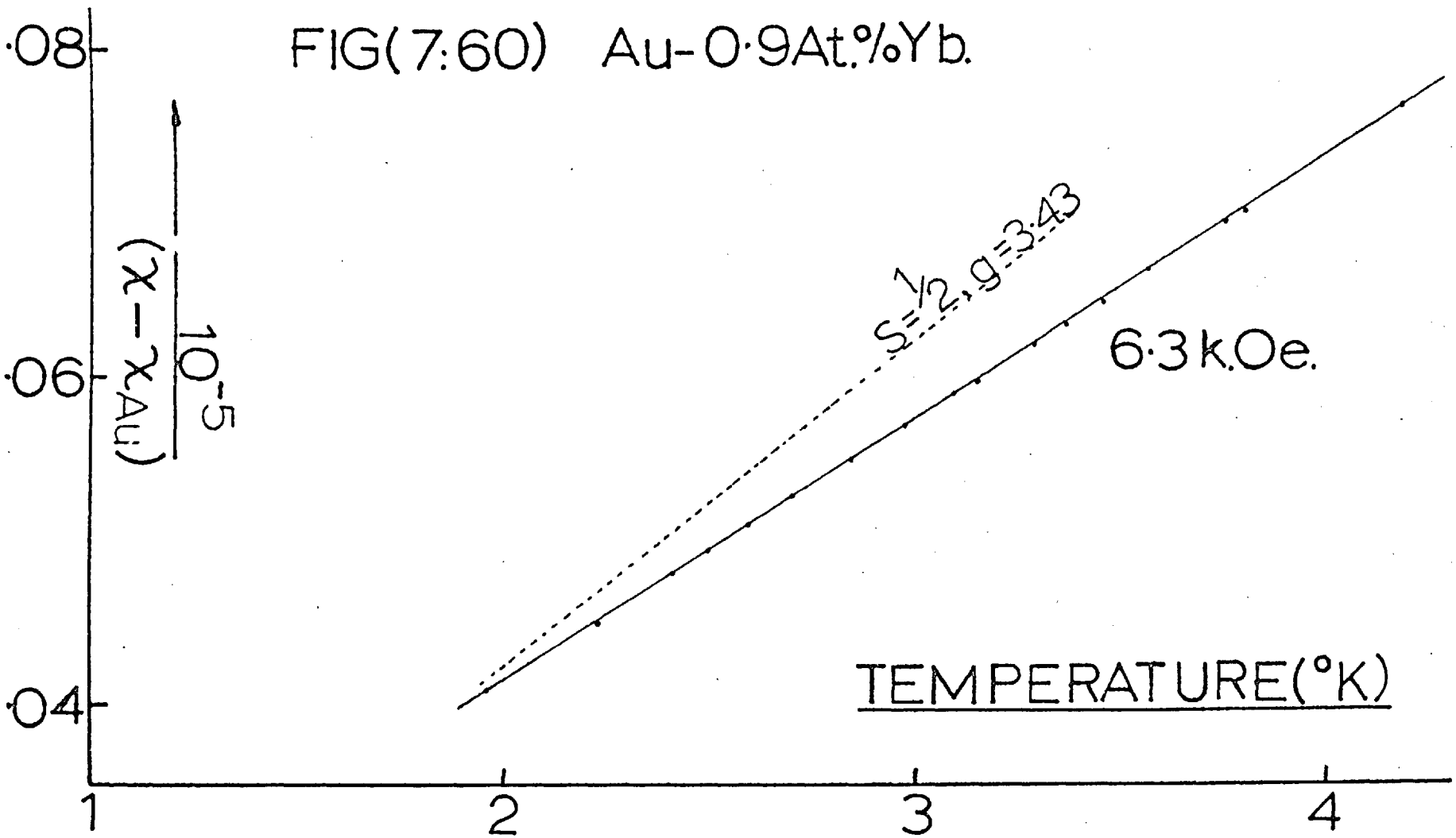
FIG(7:60) Au-0·9At.%Yb.
·08
·06
·04
$\frac{(\chi-\chi_{Au})}{10^{-5}}$
$S=\frac{1}{2}, g=3.43$
6·3 k.Oe.
TEMPERATURE(°K)
1
2
3
4

FIG(7:61) (M-H) PLOTS
FOR Au-0·9At.%Yb.

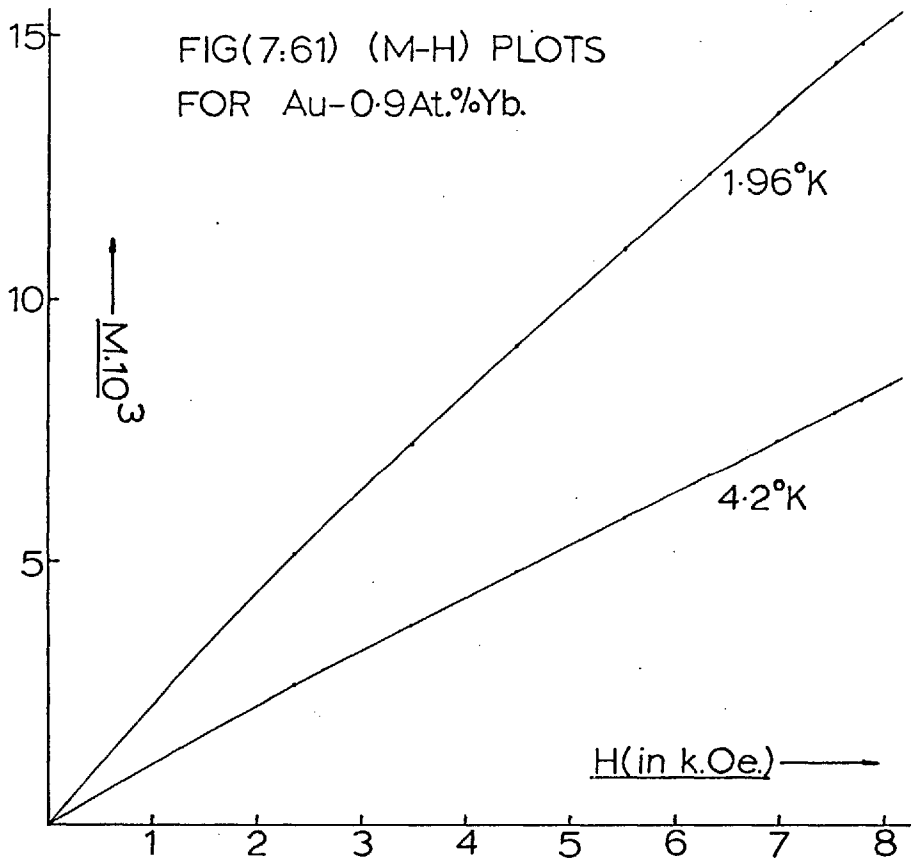

FIG(7:62) (M-H) PLOTS
FOR Au-0·9At.%Yb.

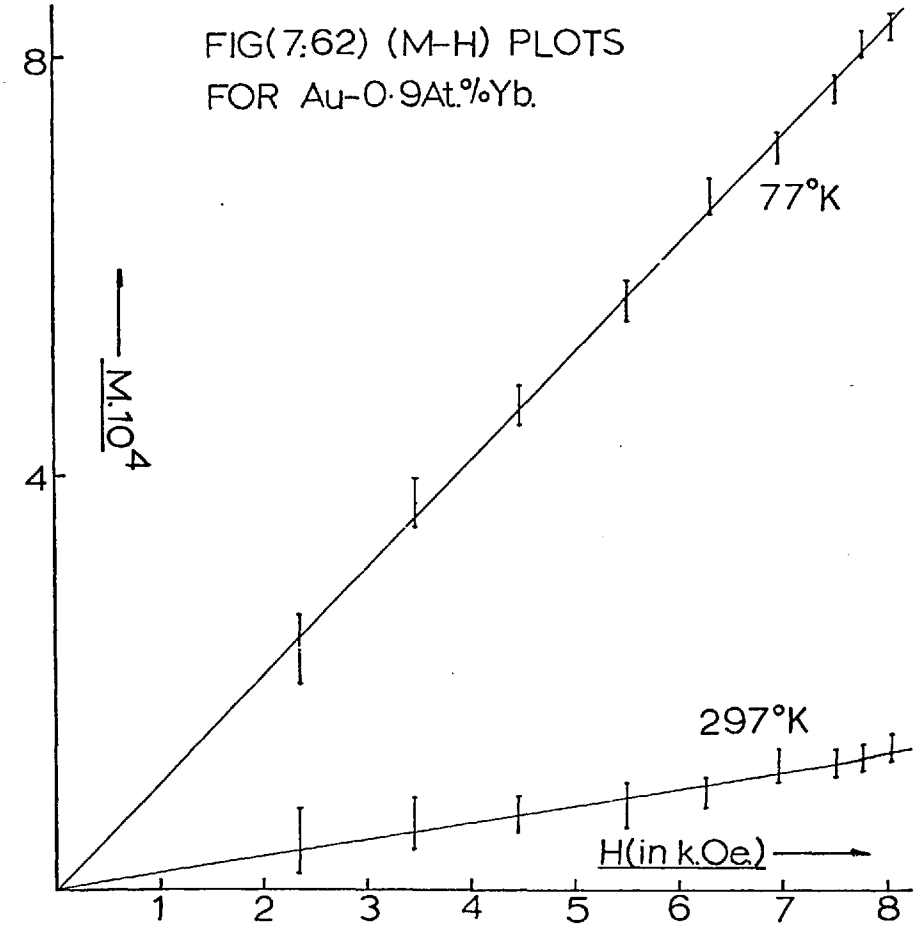

CHAPTER 8

DISCUSSION OF THE EXPERIMENTAL RESULTS

S-State impurities; The AgGd system

Typical theoretical estimates give the ground state splitting in Gd, due to configurational mixing, as $0.1^{o}K$,[87] a figure which has been shown to be of the right order of magnitude at least by the experimental data on gadolinium ethyl sulphate[88]. It would seem reasonable to assume that this figure is not significantly changed for Gd in a Ag host, but the experimental data already presented for the Ag-0.8 and 0.45At.% Gd alloys seems to refute this idea. The inverse susceptibility versus temperature curves for these alloys show deviations from Curie-Weiss behaviour at temperatures which are at least an order of magnitude larger than expected. Metallographic analysis reveals that this anomalous behaviour can be attributed to the effects of an intermetallic second phase compound in these alloys. For simplicity, if this compound is assumed not to contribute to the observed low temperature susceptibility of the alloy, then its susceptibility-temperature variation can easily be obtained - figure (8.1).

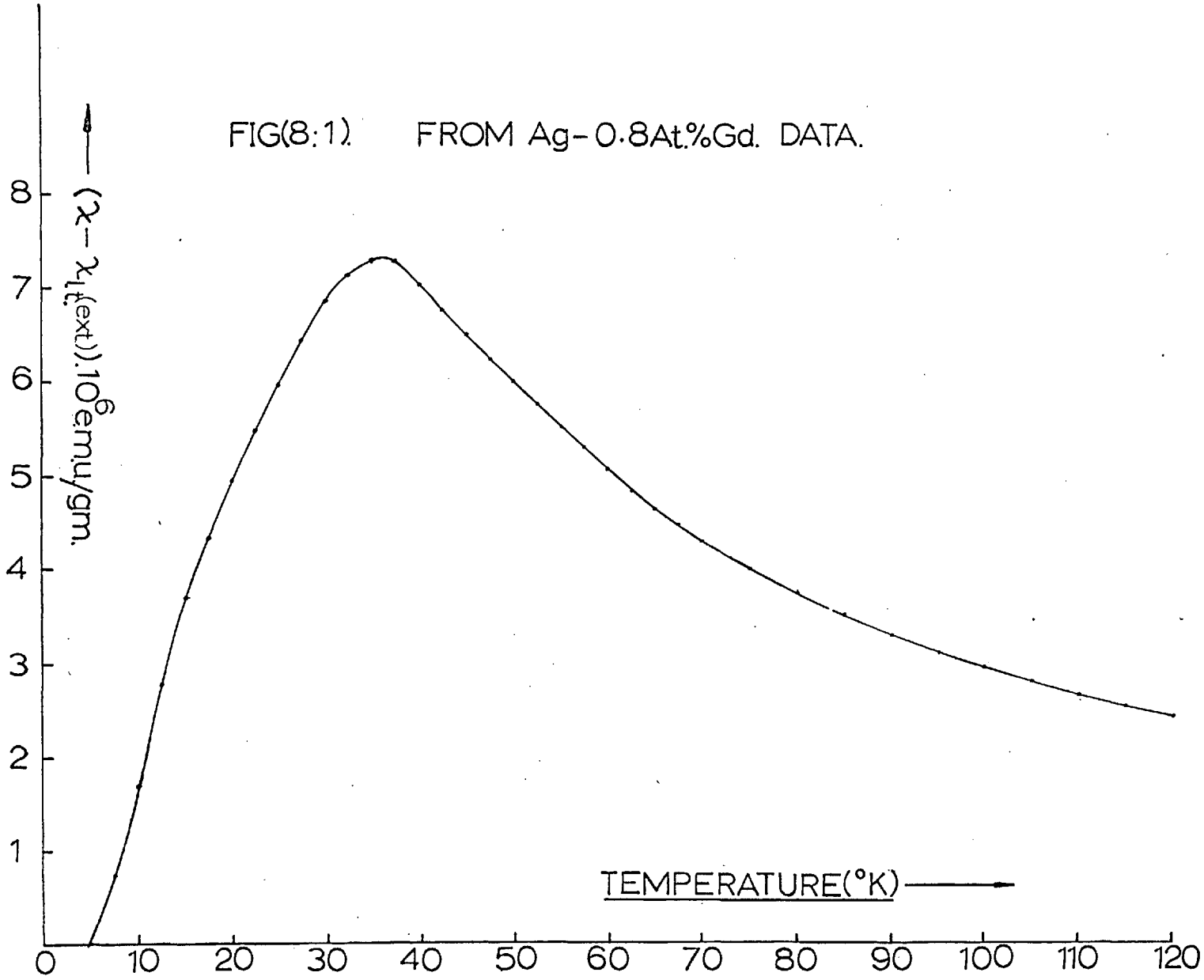
FIG(8:1). FROM Ag-0·8At.%Gd. DATA.
$(\chi - \chi_{t(ext)}).10^6$ emu/gm.
TEMPERATURE(°K)
0
10
20
30
40
50
60
70
80
90
100
110
120
1
2
3
4
5
6
7
8

From this the estimated transition temperature of the compound is 36°K.

An examination of the (Ag-Gd) phase diagram[89] suggests that this intermetallic compound is likely to be Ag_3Gd. Consequently the temperature variation of the susceptibility of this compound was measured and, as figure (7.13) indicates, it is a typical metallic antiferromagnet with a transition temperature of 36°K. This figure has been confirmed by e.p.r. measurements. The presence of a similar intermetallic compound could certainly explain the anomalous temperature dependence of the susceptibility of dilute AgEu and AuEu, in which the rare-earth impurity is divalent (S-state ion). The published ($\frac{1}{\chi}$ vs. T) plots of Gainon for these systems bear a close resemblence to those presented here for the Ag-0.8At.% Gd alloy, including an extrapolated high temperature line which has a positive intercept on the temperature axis. The effect of such a compound on (H/σ vs. σ^2) plots has not been investigated, but its presence would seem to throw doubt on the otherwise anomalously high Curie temperature observed by these authors, and from this point of view, would consequently modify some of their conclusions. In

addition to the work of Gainon, it would seem reasonable to explain the unusual concentration dependence of Pickett's specific heat data on metallurgical grounds.

Metallography carried out on the Ag-0.12At.% Gd alloy did not reveal any second phase. This alloy has a well behaved ($1/\chi$ vs.T) variation, except for the rather large 'θ' value ($-2 \pm 0.5^{\circ}K$), Of course, the relatively small susceptibility of this sample coupled with the accuracy of the temperature measurements, discussed previously, makes such an extrapolation rather inaccurate. Susceptibility measurements on the S-state ion Mn, in Cu[90], indicate that the intercept on the temperature axis of the extrapolated high temperature data is between +5 and + $10^{\circ}K$/At.% Mn. Specific heat measurements on the same system[91,92] indicate that ($\Delta C/T$ vs.T) curves have peaks occurring at about $10^{\circ}K$/At.% Mn, in good agreement with the susceptibility data. Using the appropriate expressions for the interaction energy (Chapter III) in the Ag Gd and Cu Mn systems, suggests that similar peaks in ($\Delta C/T$ vs.T) should occur in the former at about $1^{\circ}K$/At.% Gd. This figure is, of course, just an estimate since the equations used to obtain it represent a rather extreme approach, the figure

is however in good agreement with the published specific heat curves of Zimmerman et al for the Ag Gd system.

The general character of the (M-H) plots in AgGd is similar to that observed for CuMn[93]. The high field non-linearity is consistent with Brillouin function curvature, while the curved low field region indicates interaction effects, although a quantitative approach to these in such systems is still lacking.

Non S-state impurities

Introduction

As already mentioned in Chapter 5, the picture of a dilute alloy in which the impurity states closely resemble those of the free solute ion, is likely to be applicable to the case of rare-earth solutes in noble metal hosts. It is well known that spin-orbit coupling is strong in the rare-earths, consequently in the dilute, well isolated limit, the ground state of the solute will be characterised by a well defined total angular momentum ($J\hbar$). The (2J+1) fold degeneracy in zero magnetic field associated with the ground state will, however, be partially lifted by the cubic crystal field of the host. Indeed, the susceptibilities of these alloys, as previously presented, can, in some cases,

be understood directly in terms of the arrangement and residual degeneracies of these crystal field split levels. Typically in Au Yb, the well isolated Γ_7 ground state (already identified by e.p.r.[94]) clearly dominates the observed low temperature susceptibility while in Ag Tm the presence of a well isolated Γ_2 non-magnetic singlet ground state is seen to have a dramatic effect. In alloys containing most of the other heavier rare-earths however, the existence of Curie-Weiss behaviour does not facilitate a straightforward analysis in the above manner.

At the lowest temperature it is expected that the above picture will be complicated by inter-impurity effects arising from indirect spin-spin coupling via the conduction electrons. This idea is strongly supported by the low field non-linear character of the (M-H) plots presented in the previous chapter. Such effects are enhanced by increasing rare-earth concentration, which produces additional impurity - impurity effects via mutual distortion of the crystal field by neighbouring rare-earth impurities. As previously emphasized, quantitative estimates of the effects of the former are still lacking, in addition a precise

treatment of local distortions of the crystal field in a random alloy would be difficult. Qualitatively however, it seems reasonable to assume that both would tend to average out the effect of the crystal field.

Fitting the experimental data

Chapter 4 of this thesis concentrated on demonstrating the manner in which the Hamiltonian matrix for rare-earth ions in a cubic crystal field was obtained. In that chapter the approach was confined to a single manifold of constant J. This seems a reasonable assumption for the heavier rare-earths at least, in view of optical data[95] which indicates that different constant J manifolds are well separated (about 10,000°K).

When values of the coefficients (C_4,C_6) (see Appendix 2) have been specified, the Hamiltonian can be written down explicitly. The effect of an externally applied magnetic field can be taken into account simply by adding diagonal Zeeman elements to this matrix. A modified library sub-routine (for an I.B.M.7090 computer) has been used to diagonalise this Hamiltonian and find its eigenvalues and eigenvectors. Using the latter it is quite straightforward to evaluate the susceptibility at any temperature using equation (1.9).

For a crystalline field produced by an array of point charges located 'outside' the rare-earth ion, C_4 and C_6 would be proportional to $\langle r^4 \rangle$ and $\langle r^6 \rangle$, the mean fourth and sixth powers of the radii of the magnetic (4f) electrons[96]. These coefficients would thus depend on the detailed nature of the wave-function of the magnetic ion, and, to the extent that the 4f wave-functions are the same, would be the same for all the rare-earths as impurities. In a metal, however, the potential to which such electrons are subjected is almost certainly not purely electrostatic in origin, and on this basis the above conclusions would seem invalid, though to assume that the signs of C_4 and C_6 remain the same for all the rare-earths as impurities in a given host seems reasonable. If, in addition, the sign of these coefficients is assumed to be the same in both Ag and Au hosts, then the e.p.r. identification of the Γ_7 doublet ground state in Er and Yb requires that C_4 be positive and C_6 negative. These are, incidentally, the signs predicted by a simple point-charge model.

Initial computations sweeping over a wide range of the coefficients (C_4, C_6) have shown that the calculated susceptibilities in cubic symmetry are generally much

much more Curie-Weiss like than those calculated for a magnetic rare-earth ion in an environment of lower symmetry[97]. This means that for cubic symmetry the absence of strong deviations from Curie-Weiss behaviour does not necessarily indicate that the crystal field splitting is small. Of course, in such circumstances the calculated susceptibility is rather insensitive to changes in the overall splitting, consequently alloys which exhibit a Curie-Weiss temperature dependence of the susceptibility are not very useful for accurate determinations of (C_4, C_6).

With this in mind an attempt has been made to fit the experimental data for the dilute Ag-Rare earth alloy system starting with AgEr, since the temperature variation of the susceptibility of this alloy has rather more 'character'. E.P.R. has been observed at low temperatures in a powder sample of this alloy at $g = 6.73 \pm 0.1$[94], which corresponds to a g value of 6.80 expected for the Γ_7 eigenstate of Er^{+++} in a cubic crystal field. That this observation identifies the doublet as the ground state follows from the fact that the other possibility for the ground state, the Γ_6 eigenstate, has non-vanishing matrix elements of the

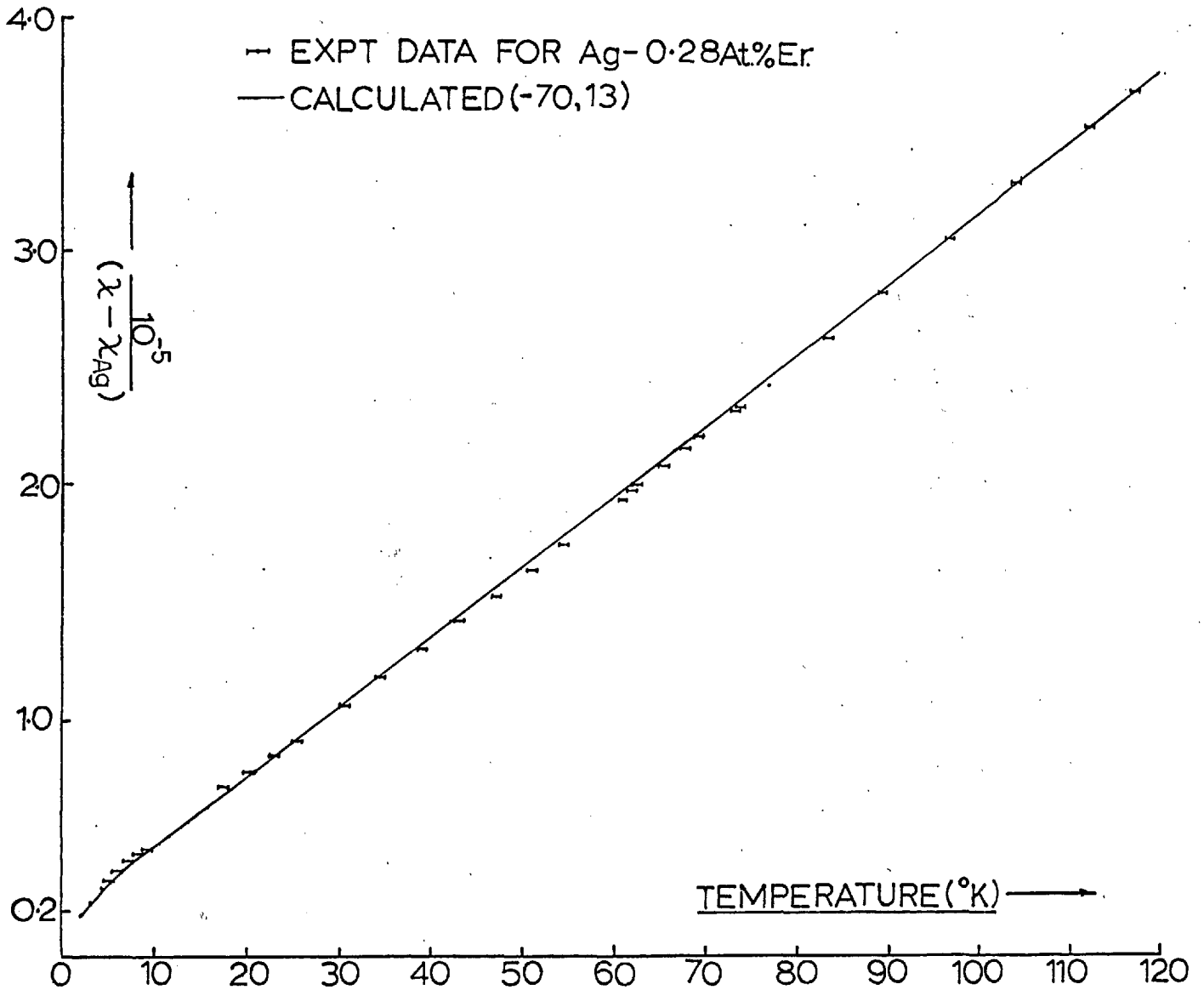
EXPT DATA FOR Ag-0·28At.%Er.
CALCULATED (-70,13)
$\frac{10^{-5}}{(\chi - \chi_{Ag})}$
TEMPERATURE (°K)
4·0
3·0
2·0
1·0
0·2
0
10
20
30
40
50
60
70
80
90
100
110
120

stepping operator $(J_x \pm iJ_y)$[98], and an expected g value, in cubic symmetry, of 6.00. Indeed the fact that only the Γ_7 resonance was observed up to 20°K (when the line became too broad for accurate observation) suggests that this state is well isolated, although with line widths of about 100 Oe it is perhaps unreasonable to assume that a resonance would be observed if the Γ_6 state were populated thermally. In any case this observation merely limits the C_4/C_6 ratio and does not assign a specific value to these parameters since the 'composition' (and hence g value) of this Γ_7 eigenstate is not affected by changing crystal fields. The best fit to the experimental susceptibility data has been obtained using crystal field coefficients(C_4, C_6) of (-70, 13)°K, figure (8.2). In fact these values give the calculated susceptibility the maximum deviation from Curie's law.

The effects of interactions in this alloy system can be seen by comparing the low temperature behaviour of the Ag-0.28 and 1.0 At.% Er alloys. In addition to increased low field curvature in the (M-H) plots, the influence of the Γ_7 ground state is much less apparent in the concentrated alloy, in agreement with

the previous qualitative suggestion.

The experimental data for the AgTb, AgDy and AgHo alloy systems, figures (7.16), (7.20) and (7.28), indicate that their susceptibilities do not deviate strongly from Curie-Weiss behaviour. The experimental curves can be fitted using several values of the coefficients (C_4, C_6), including the (-70,13)°K used to fit the AgEr data. Admittedly for this value the theoretical and experimental curves tend to separate below about 7°K, and an improved fit can be obtained by increasing the overall splitting, but as the (M-H) plots for these alloys indicate that interaction effects are operative, such a procedure is not without objection. In AgHo at least, specific heat measurements[70] have shown the importance of hyperfine effects, and it was felt that a breakdown of hyperfine coupling might be contributing to the observed low field (M-H) curvature. A consideration of such effects, in Appendix 8, in the very low temperature limit shows that this is certainly not the case.

Within the limits imposed by the accuracy of fitting, the data thus far presented are consistent with the supposition that, in a given host, (C_4,C_6) are the

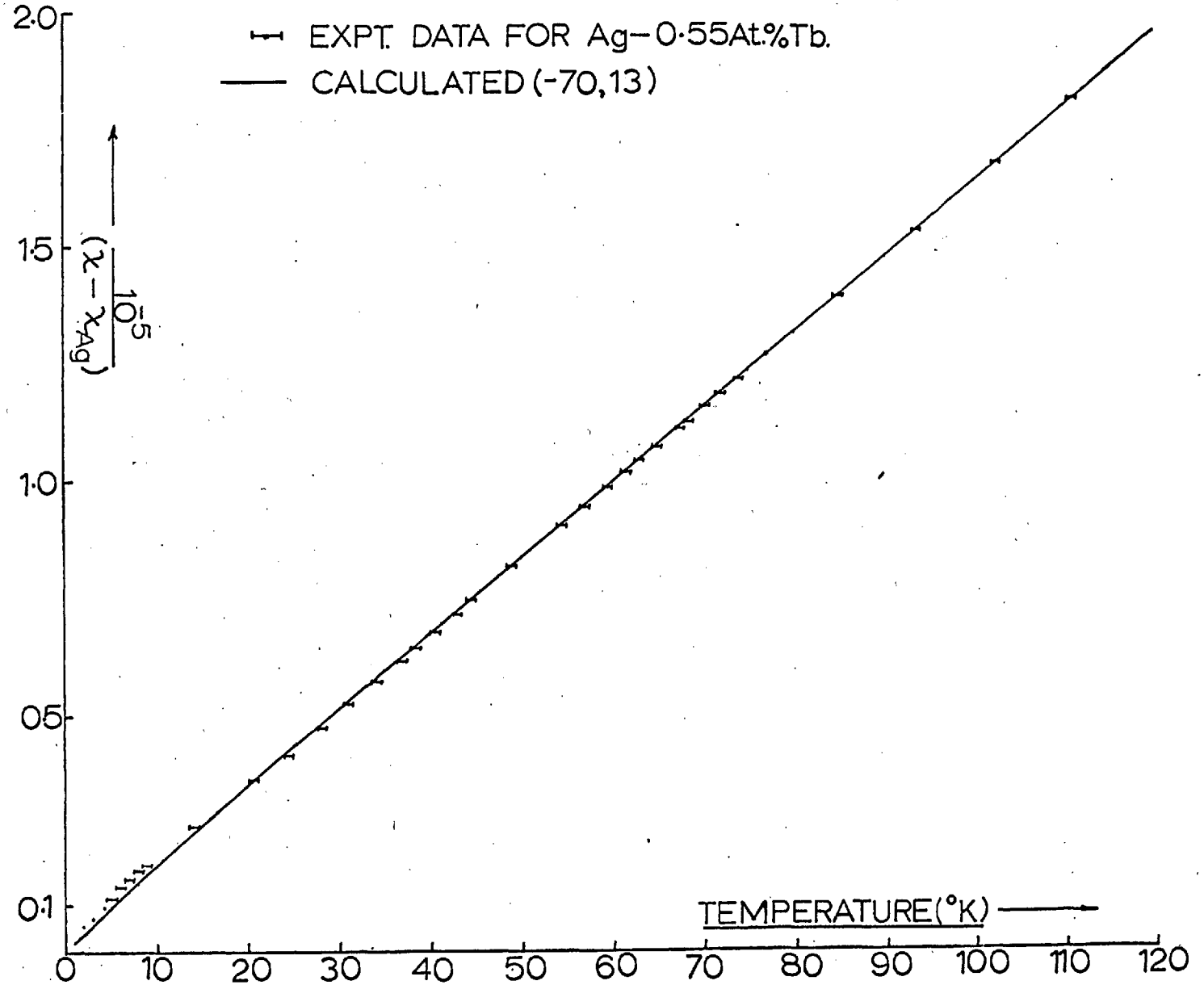
EXPT. DATA FOR Ag–0·55At.%Tb.
CALCULATED (-70,13)
$\frac{(\chi - \chi_{Ag})}{10^{-5}}$
2·0
1·5
1·0
0·5
0·1
TEMPERATURE (°K)
0
10
20
30
40
50
60
70
80
90
100
110
120

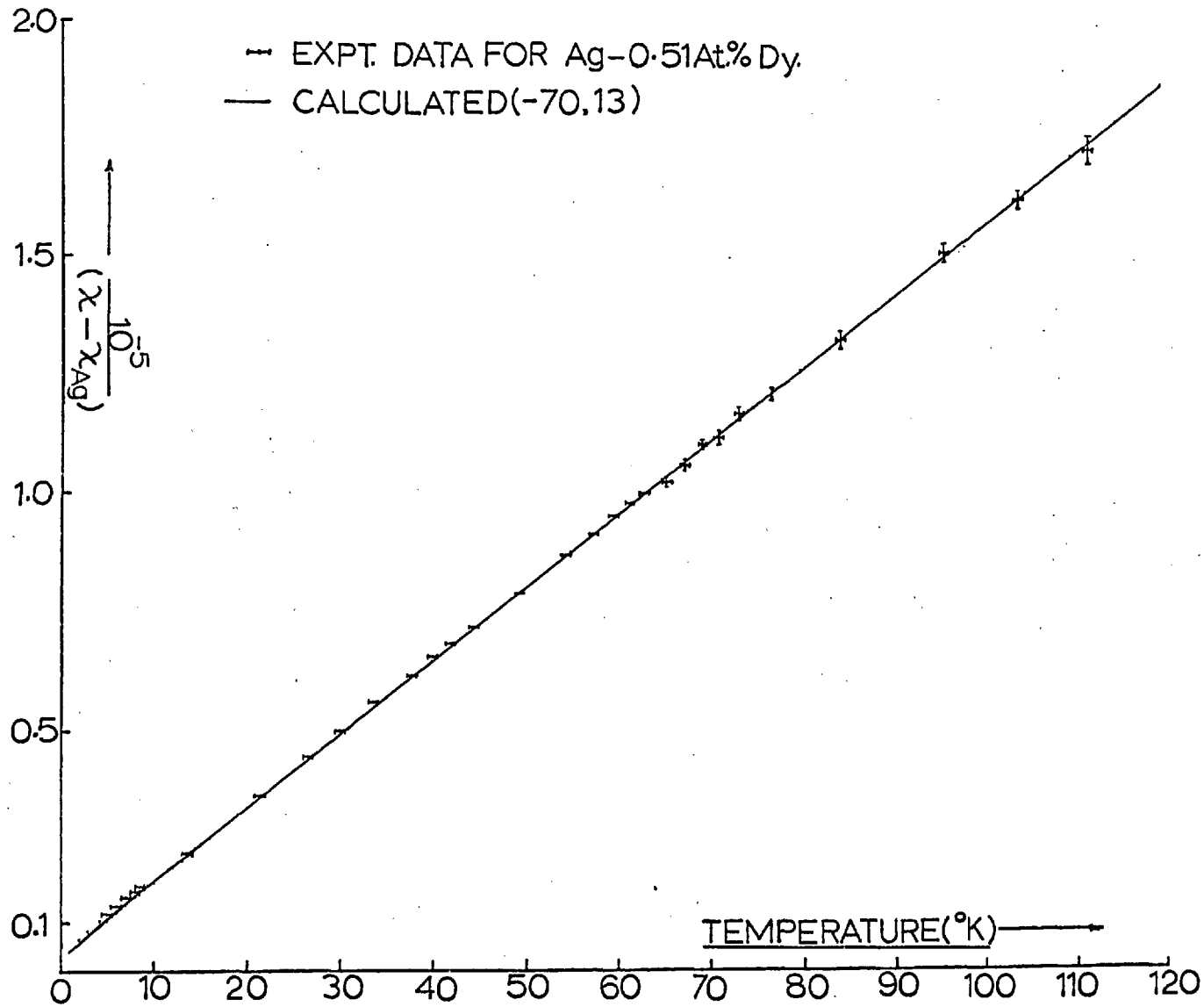
EXPT. DATA FOR Ag-0·51At.% Dy.
CALCULATED(-70.13)
$\frac{10^{-5}}{(\chi - \chi_{Ag})}$
2·0
1·5
1·0
0·5
0·1
TEMPERATURE(°K)
0
10
20
30
40
50
60
70
80
90
100
110
120

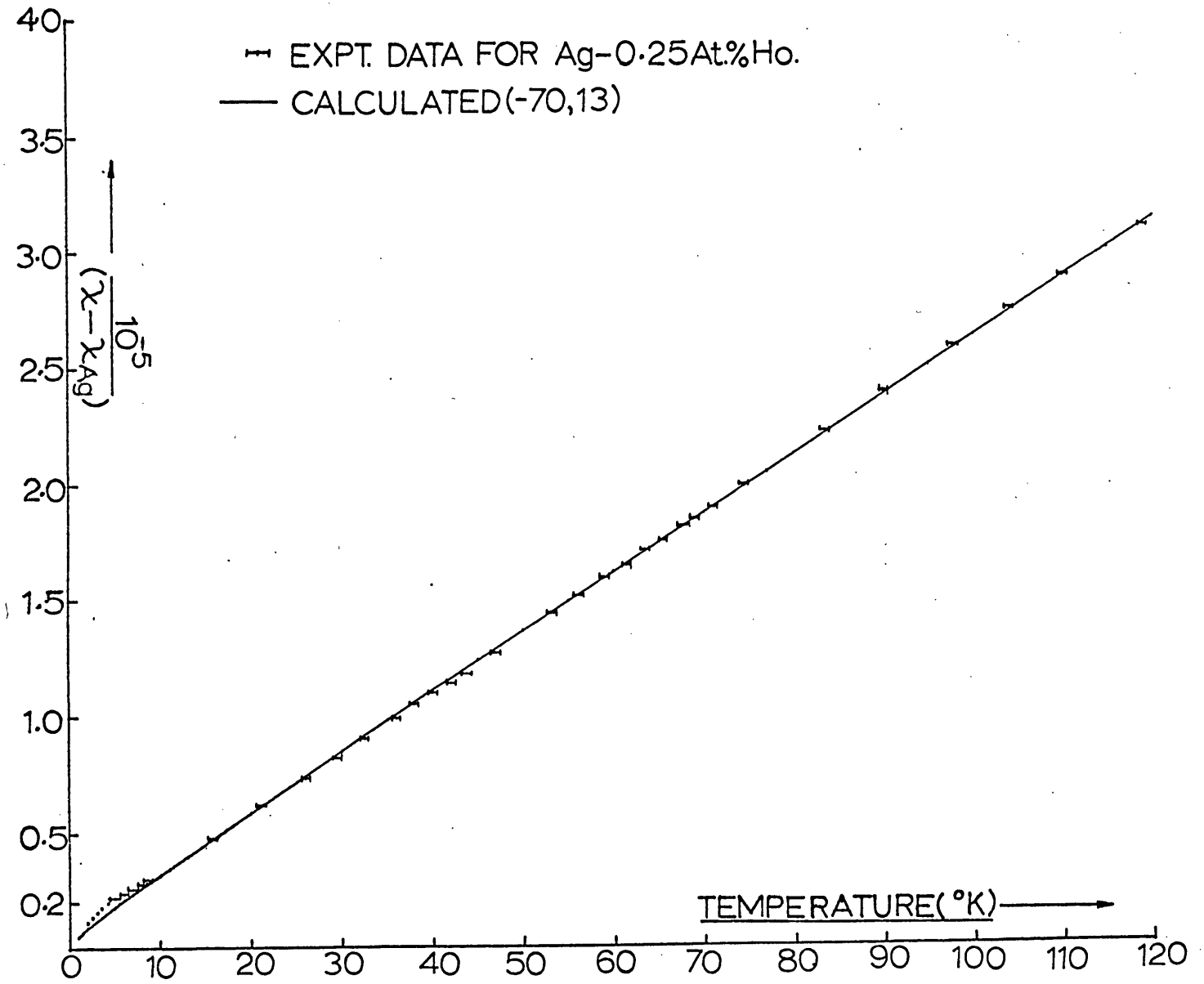
EXPT. DATA FOR Ag-0·25At.%Ho.
CALCULATED(-70,13)
$\frac{(\chi-\chi_{Ag})}{10^{-5}}$
TEMPERATURE(°K)
4·0
3·5
3·0
2·5
2·0
1·5
1·0
0·5
0·2
0
10
20
30
40
50
60
70
80
90
100
110
120

same for all the rare-earth solutes. In the case of AgTm however, the susceptibility computed with the (C_4, C_6) used to fit the AgEr data approaches a constant value at too high a temperature. This arises, in spite of the fact that these crystal field coefficients indicate a well isolated ground state singlet, Γ_2, which gives no 1/T term in the susceptibility, from the finite low temperature contribution of Van Vleck terms within the same constant J manifold, i.e. a mixing of higher crystal field eigenstates induced by the eternal magnetic field. If the previous supposition about the effect of interactions is correct, then they will tend to increase the low temperature slope by decreasing $(\frac{1}{\chi})$ However, it seems unreasonable to assume that in an 0.5 At.% alloy these effects will be of sufficient strength to account for the observed discrepancy. On this basis then, it must be concluded that the magnitudes of (C_4, C_6) are changing for the various rare-earth solutes, the values $(-30, 5.5)^{\circ}K$ giving a good fit to the AgTm data. Another interesting feature of this alloy system is provided by the linear, low field (M-H) variation at low temperature. If the low field curvature observed at low temperature in the (M-H)

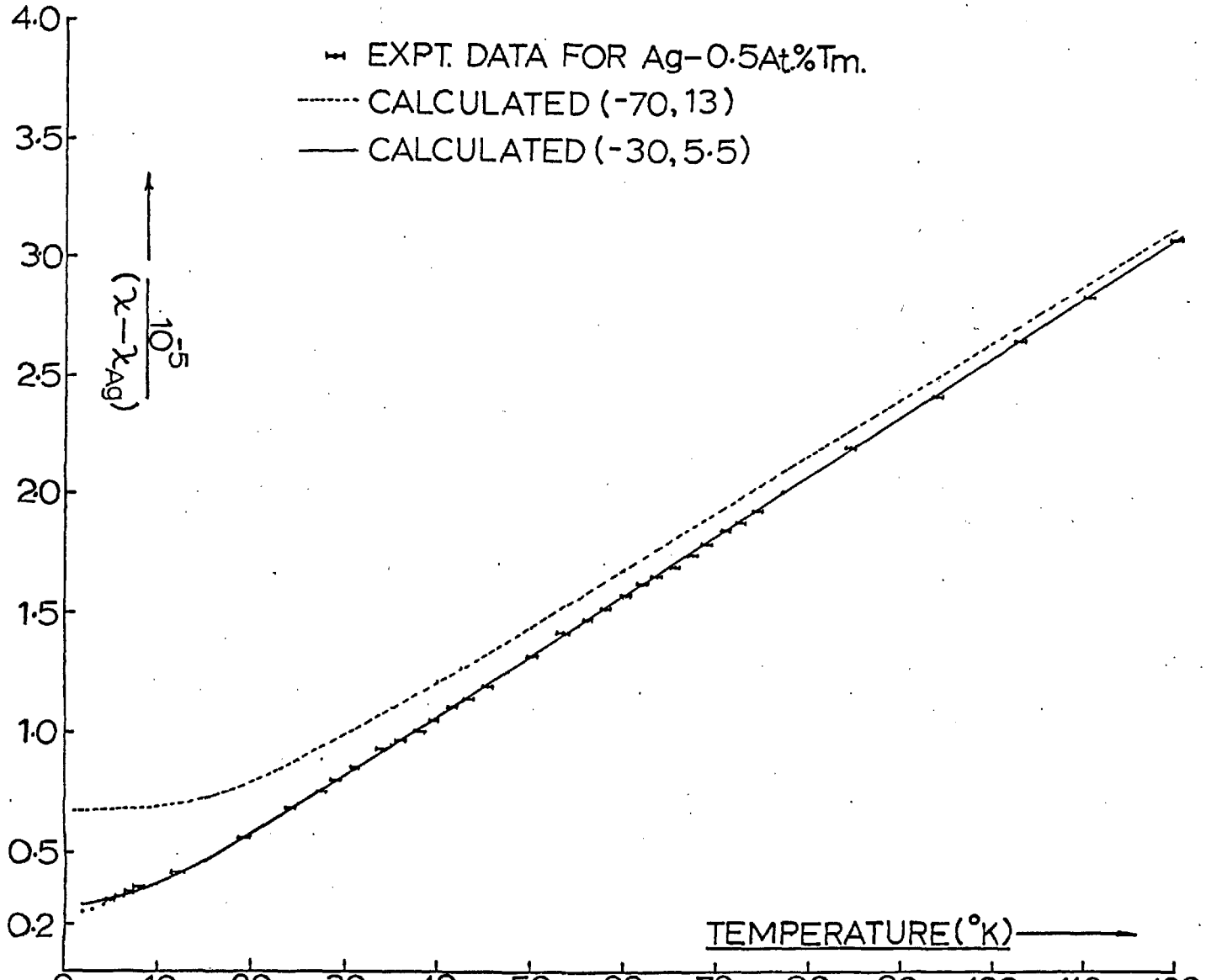
EXPT. DATA FOR Ag–0·5At.%Tm.
CALCULATED (-70, 13)
CALCULATED (-30, 5·5)
$(\chi - \chi_{Ag}) 10^5$
TEMPERATURE (°K)
4·0
3·5
3·0
2·5
2·0
1·5
1·0
0·5
0·2
0
10
20
30
40
50
60
70
80
90
100
110
120

plots for other alloys originates in indirect coupling of the impurity spins via the conduction electrons, then the well isolated singlet ground state in AgTm should experience no such coupling. This idea is clearly supported by the experimental data.

Following the concluded variation in magnitude of (C_4, C_6), it is particularly unfortunate that Yb is divalent in Ag. For trivalent Yb, both sets of values of (C_4, C_6) used to obtain the previous fits give a distinctive $(1/\chi$ vs.T) variation, consequently experiments on this system would provide useful data for ascertaining whether any systematic variation in these coefficients occurred. Indeed, from the point of view of theory this ion is one of the simplest to treat since all matrix elements occurring in equation (1.9) are independent of the crystal field coefficients, the susceptibility therefore depending only on the energy separation of the three eigenstate (Γ_6, Γ_7 and Γ_8) of Yb^{+++} in a cubic field. This situation occurs in AuYb. The low temperature e.p.r. observed at g = 3.30 ± 0.1[94] in powder samples of this alloy clearly identifies the Γ_7 eigenstate as the ground state (expected g value in cubic symmetry, 3.43), while a

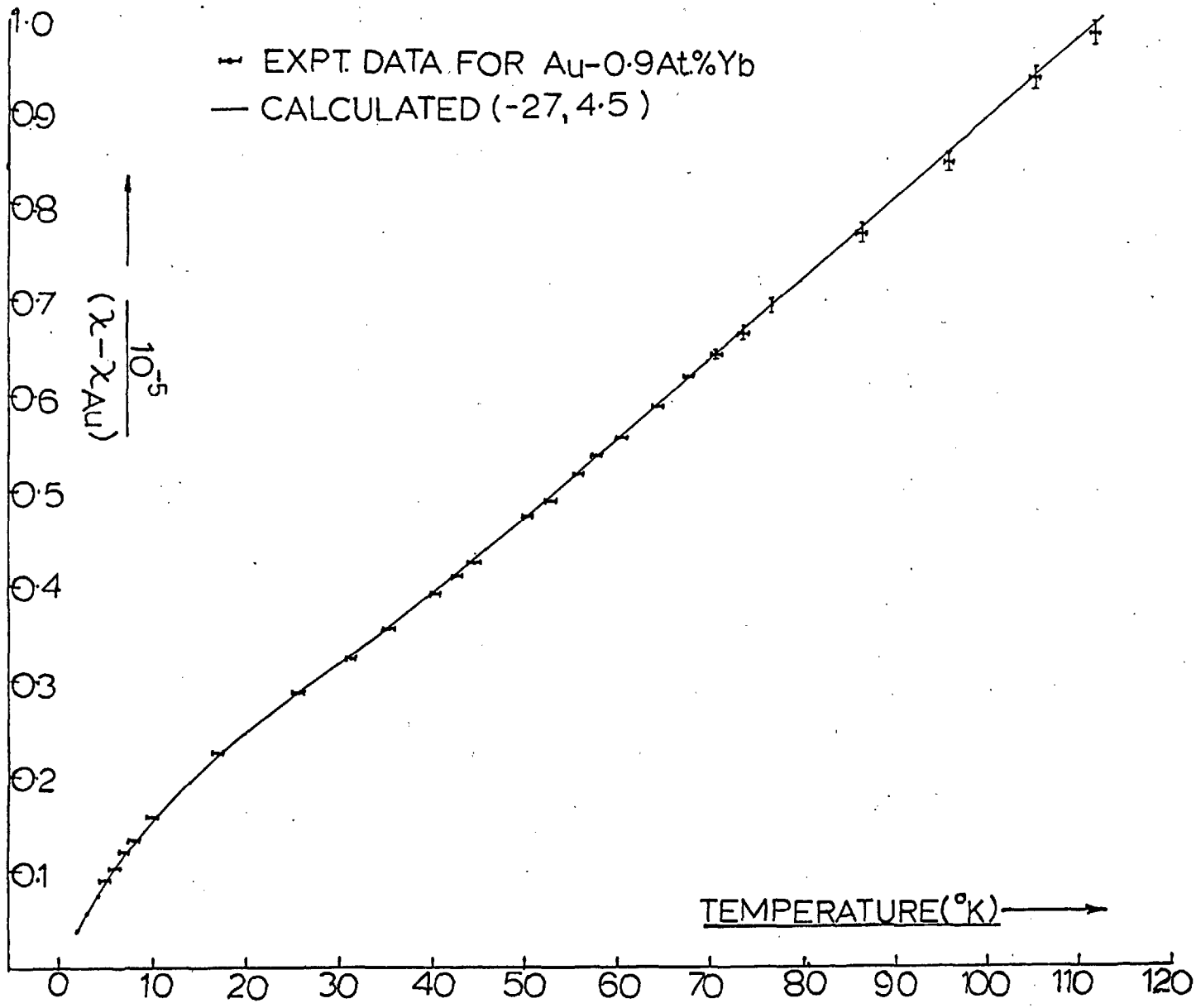
EXPT. DATA FOR Au-0·9At.%Yb
CALCULATED (-27, 4·5)
$\frac{10^{-5}}{(\chi-\chi_{Au})}$
1·0
0·9
0·8
0·7
0·6
0·5
0·4
0·3
0·2
0·1
TEMPERATURE(°K)
0
10
20
30
40
50
60
70
80
90
100
110
120

very good fit to the susceptibility data is obtained with $(-27, 4.5)^{\circ}K$. The susceptibility data on AuEr is rather less dramatic than that for AgEr, and in this respect is rather more difficult to fit uniquely, although e.p.r. again identifies Γ_7 as the ground state. It is clear however, that the (C_4, C_6) values of $(-30, 6.5)^{\circ}K$ give a considerably better fit than do the AuYb values of $(-27, 4.5)^{\circ}K$, thus supporting the view of changing crystal field parameters across the rare-earth series. As with AgTm, the AuTm data requires that (C_4, C_6), for a good fit, be considerably less than the values used to fit the experimental data on other rare-earth impurities in the same host. In this alloy the values $(-17, 2)^{\circ}K$ were required. These parameters indicate that the Γ_2 singlet eigenstate lies lowest, being separated by about $7^{\circ}K$ from the next eigenstate (Γ_5). Unlike AgTm, the (M-H) plots for this alloy, at both $4.2^{\circ}K$ and $1.95^{\circ}K$, exhibit some low field curvature, this is, however, consistent with a singlet ground state since its isolation is such that both the calculated and meaaured susceptibilities have not reached a constant value at $2^{\circ}K$.

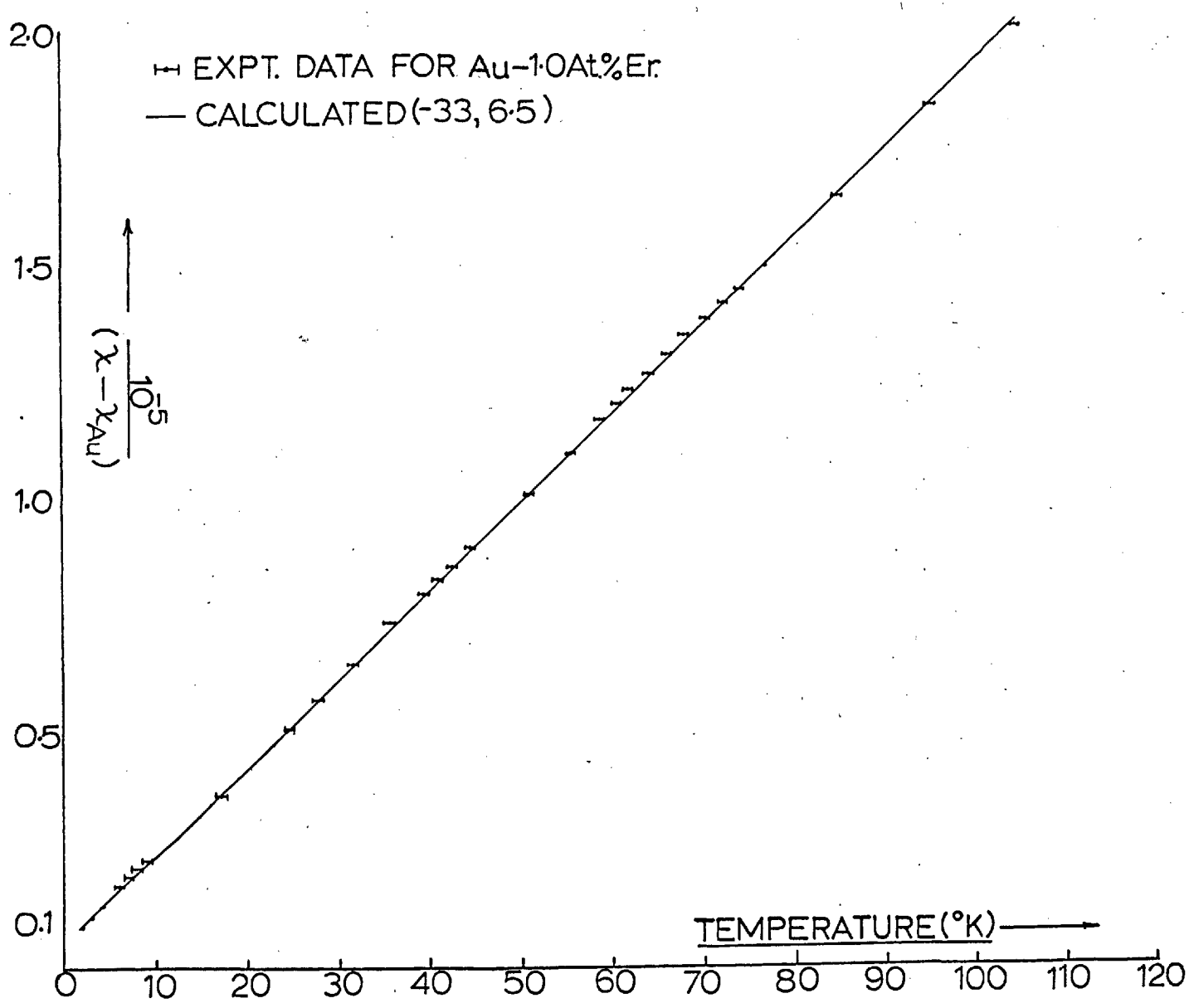
EXPT. DATA FOR Au-1·0At.%Er.
CALCULATED (-33, 6·5)
$\frac{(\chi - \chi_{Au})}{10^5}$
2·0
1·5
1·0
0·5
0·1
TEMPERATURE (°K)
0
10
20
30
40
50
60
70
80
90
100
110
120

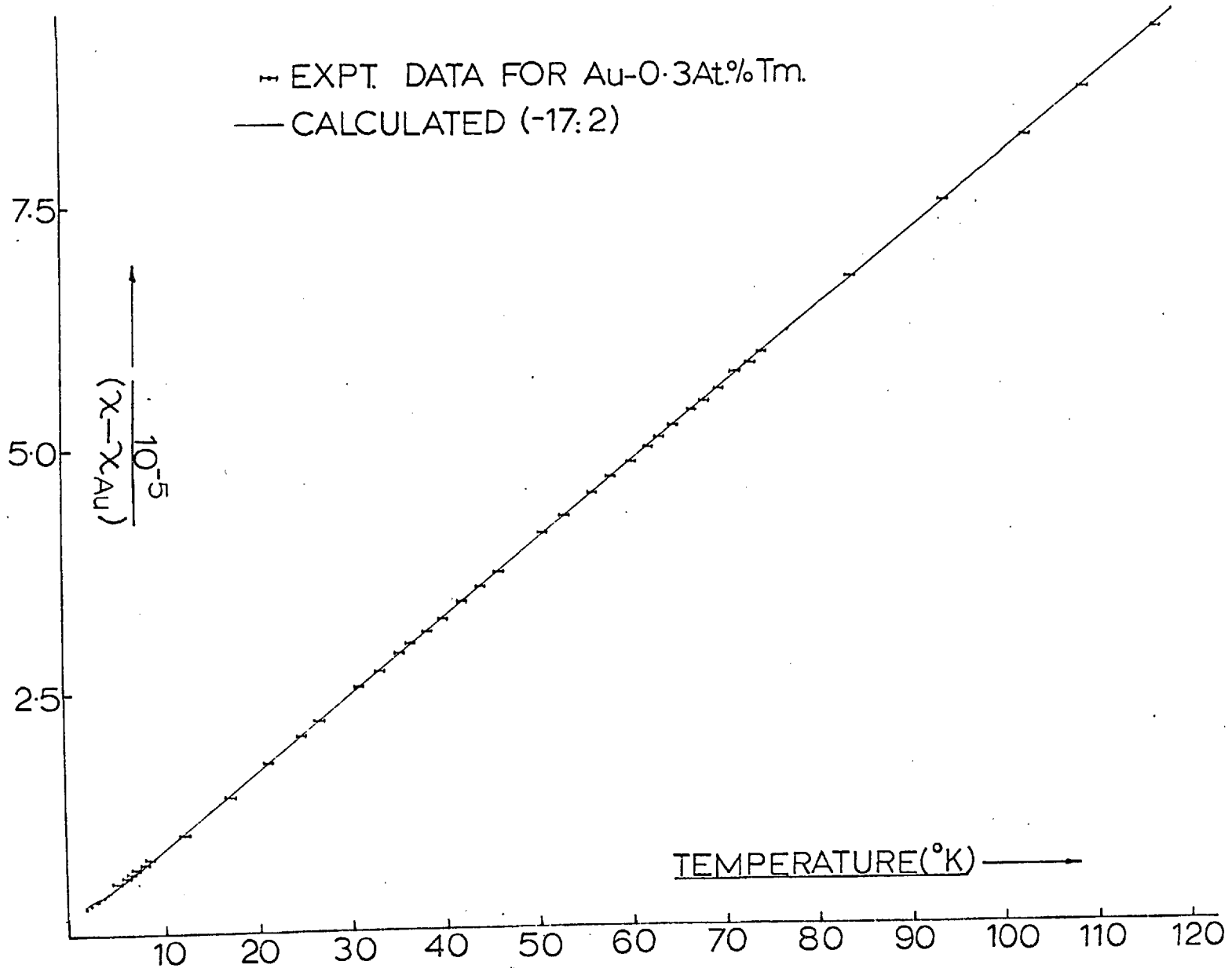
EXPT. DATA FOR Au-0·3At.% Tm.
CALCULATED (-17:2)
7·5
5·0
2·5
$\frac{(\chi-\chi_{Au})}{10^{-5}}$
TEMPERATURE(°K)
10
20
30
40
50
60
70
80
90
100
110
120

Table (8.1), below, summaries the data obtained from the fits described above:-

Alloy	C_4 (°K)	C_6 (°K)	Overall splitting (°K)	Ground state isolation
Ag Tb	-70	13	117	<1°K
Ag Dy	-70	13	157	1°K
Ag Ho	-70	13	182	<1°K
Ag Er	-70	13	207	35°K
Ag Tm	-30	5.5	95	21°K
Au Er	-33	6.5	105	19°K
Au Tm	-17	2	47	7°K
Au Yb	-27	4.5	83	79°K

The bulk of the experimental data presented seems to support the original supposition that, in alloys of this type, the localised impurity states closely resemble those of the free ion, in so far as a theoretical approach based on such an idea yield results which are in good agreement with experiment. In addition, in those alloys in which the rare-earth concentration was chemically analysed, the effective moment derived from the high temperature susceptibility was close to the free

ion moment (9.8 μ_B for the Ag-0.28 At.% Er alloy). An interesting general characteristic of this high temperature data, for most of the alloy systems examined, is that it extrapolates to give a negative intercept on the temperature axis. A power series expansion of the susceptibility at high temperatures, using equation (1.9), indicates (Appendix 7) that the thermal population of such a set of levels does not give rise to a $(1/T^2)$ term with which such an intercept would be associated, but examination of the computed susceptibility indicates that the high temperature susceptibility approaches on asymptotic Curie law variation - equation (1.10) - as (1/T). Unfortunately in the high temperature region the experimental data is not sufficiently accurate to distinguish between these two variations, consequently it seems to extrapolate in the above manner.

Concluding remarks

Following the discussion in the preceding sections, it seems that the experimental susceptibility data is well explained on the basis of a model in which the free ion-like localised rare-earth impurity states are subject to the cubic crystal field of the noble metal

host. The experimental data suggests that the coefficients (C_4, C_6) characterising this crystal field, change in magnitude forthe various rare-earth solutes, although they are assumed to retain the same signs. This variation seems quite plausible in view of the variation of such properties as the solubilities of the rare-earths in the various hosts. The assumption that (C_4, C_6) retain the same signs in Au and Ag is only seen to be plausible when the character of all the data presented is reviewed. Certainly the e.p.r. observations for the rare-earths in Au,provide definite evidence that C_4 is positive and C_6 negative, but the single observation on Er^{3+} in Ag only indicates that Γ_7 is the ground state and does not fix the signs of (C_4, C_6). Indeed, the susceptibility data on Ag Er and AgTm is not inconsistent with the signs of C_4 and C_6 being the same. The degeneracy scheme for the former is certainly not drastically changed, while the latter would still retain a reasonably well isolated singlet ground state (Γ_1 or Γ_2, depending on the C_4:C_6 ratio). The calculated susceptibilities for the AgTb and AgHo systems however, provided that the overall splittings remained at roughly the same magnitude, would

be rather different from those observed experimentally. Whatever $C_4:C_6$ ratio is choosen, the former would have a reasonably well isolated singlet ground state, which would cause the theoretical low temperature inverse-susceptibility to flatten, whereas that observed experimentally still decreases roughly as T at the lowest temperature, Similar effects should occur for AgHo, though for the same overall splitting they would be less pronounced. Thus, although the experimental data on AgTb, AgDy and AgHo is of little use for accurate determinations of (C_4,C_6), it does provide convincing evidence that the signs of (C_4,C_6) are the same in Ag and Au. In the latter, of course, the signs are established, and an extrapolation of the AuEr parameters to AuTb, AuDy and AuHo reveals that little is to be gained from susceptibility measurements on them.

The results presented in this thesis, rather than investigating in detail the properties of a single alloy, form a general survey of the properties of the heavier rare-earths in Ag and Au. They demonstrate that although general characteristics can be understood, detailed effects, particularly interactions, are still not well understood. In this respect a thorough

investigation of alloys of the noble metals containing initially about 0.1 at.% rare-earth seems desirable. These alloys should establish the behaviour in the dilute limit, and should provide a useful basis on which the effects of increasing impurity concentration could be studied. In addition, the effects of mutual distortions of the crystal field by near neighbour impurities could be studied using a fixed concentration of "magnetic" rare-earth (initially say, 0.1 At.%) and a variable concentration of Lu. In this way, initially, the complicating effects of indirect spin-spin coupling via the conduction electrons would be avoided. An attempt has been made along these lines using Ag-5 At.% Au alloys as hosts, however the metallurgical difficulties were rather serious.

By using the crystal field coefficients determined from the susceptibility data, a reasonable understanding of the e.p.r. data can be obtained. The non-Kramers ions Tb^{3+}, Ho^{3+} and Tm^{3+} have non-magnetic ground states (Γ_3, $\Gamma_3^{(2)}$ and Γ_2 respectively), although the (C_4, C_6) coefficients used in the AgEr fit indicate that the first two of these have triplet states ($\Gamma_5^{(2)}$ and $\Gamma_4^{(2)}$ respectively) energetically close to

the ground state. However, the rather large line-widths in this type of alloy seems to preclude e.p.r. observations in these triplets due to thermal population. If the parameters used to fit the Er^{3+} data can be extrapolated to the Kramers ion Dy^{3+}, then the situations predicted are rather interesting. For AuDy, the $(-33, 6.5)^{o}K$ values indicate that the Γ_7 eigenstate will be the ground state, which, in cubic symmetry, has an expected g value of 7.55. In AgDy however, the $(-70, 13)^{o}K$ values predict that the Γ_7 doublet and Γ_8 quartet lie roughly with one degree of each other. The latter, although of cubic symmetry, cannot be characterised by an isotropic g value[99]. In both alloys attempts are being made to observe resonances; for the latter, of course, a single crystal is being used, although the proximity of the two eigenstates will undoubtedly complicate matters.

For the susceptibility and e.p.r. then, this model of a free-ion like, localised, rare-earth impurity state acted on by the cubic crystal field of the noble metal host, yields a good description of the alloy in the dilute limit. It is interesting, therefore, to speculate about other properties of such alloys on the

basis of this model. The coupling of the different crystal firld eigenstates to the conduction electrons could result in a distinctive temperature variation of the electrical resistivity. This quantity has recently been measured in this laboratory, and the form of its temperature dependence suggested initially that it might indeed be explained by different scattering cross-sections for the various crystal field split levels. However, the observation of a similar behaviour in the AgGd alloy system indicated that deviations from Matthiessen's rule are important, and could account for some, or all, of the observed anomalies in the other alloy systems. In addition, a recent paper by Hirst[100] has shown that spin-flip scattering contributes a very small amount to the observed resistivities (roughly 0.02 $\mu\Omega$ cms /At.% rare-earths), an estimate which has been confirmed by preliminary analysis of the magneto-resistance data of Bijvoet et al. For this latter property, when the lowest cubic crystal field eigenstate is magnetic, the application of a magnetic field at low temperatures causes a "freezing out" of spin-flip scattering on angular momentum conservation grounds. However, when, in zero magnetic field, a singlet state

lies lowest, there is no spin-flip scattering. The effect of applying a small magnetic field is to perturb this ground state and, in general, mix into it some higher, magnetic states. This mixing is coherent, and the associated moment is consequently "frozen", and in this sense cannot give rise to spin-flip scattering, however since the induced moment is not well defined, normal conservation laws would not seem to apply to the situation. In either case, the practical effects would be very small.

The thermal population of such a set a crystal field split levels should, if one eigenstate is well isolated, give rise to a Schottky type anomaly in the specific heat. Preliminary calculations of this quantity have already been made, concentrating mainly on the region above $4^{\circ}K$ where the complications of hyperfine and interaction effects should be absent. More systematic calculations are being made, but those already available indicate that a Schottky anomaly should be observable even in an 0.5 At.% alloy against a background of the increasing lattice term (Ag should be much more favourable than Au in this respect, owing to the latters low Debye temperature). Typically,

in Ag Er, using the $(-70,13)^{o}K$ value, this anomaly is peaked around $10^{o}K$. In general the shape of the "bump" is changed by using different crystal field parameters, consequently specific heat data in this temperature region should be of some help in determining these coefficients. It is hoped that measurements of this property will be forthcoming in the near future.

The arrangement and residual degeneracy of the crystal field eigenstates should have an interesting effect on the properties of superconductors such as La_3 In containing rare-earth impurities. The interpretation of their effects is more readily accomplished in those alloys for which the lowest eigenstate is well isolated (compared with kTc). Under these conditions the depression of Tc, the superconducting transition temperature, in the alloy will depend on the character of this lowest eigenstate. When the latter is non-magnetic, the depression of Tc should be governed by the Markowitz-Kadanoff[101] relation, since, in these circumstances, the effect of the impurity is simply to reduce the electronic mean free path. For a magnetic ground state the appropriate expression for the depression of Tc would be that given by

Abrikosov and Gorkov[102]. In addition, the variation in the depression of Tc for, typically, different rare-earth impurities, as given by the de Gennes factor, $(g-1)^2 J(J+1)$, would be valid only in those alloys in which the overall crystal field splitting is less than kTc.

Finally, returning from general considerations to the more specific question of the e.p.r. linewidth in these alloys. For powder samples, the observed derivative e.p.r. lines had a Dysonian shape (the amplitude of the first to the second peak being about 2.5[103]). In the temperature range in which the non-s state resonances were observable (below about 20°K) the line width, ΔH, could be represented by:

$$\Delta H = A + BT \quad \ldots\ldots \qquad 8.1$$

For the dilute Ag Er, A had the value 59 oersteds, and B was 9.5 oersteds per degree; while for Au Yb, A was measured at 370 oersteds and B at 12 oersteds per degree. The T^{-1} dependence of ΔH could have its origin in Korringa[104] or direct phonon processes[105]. The description of the coupling between a magnetic ion of effective spin Seff, at site Rn, and the electronic spin density $\sigma(x)$, at x, by the phenomenologival exchange-

interaction density[106]:

$$\mathcal{H}_{ex} = -\sum_{n} \frac{(G_J-1)}{n_o} 2J_{ex} \cdot \left(\frac{g_{eff}}{g_J}\right) \underline{S}_{eff} \cdot \underline{\sigma}(\underline{x})\delta(\underline{Rn}-\underline{x}) \qquad 8.2$$

where no is the number of lattice sites per unit volume, J_{ex} a parameter with the dimension of an energy, and g_J the Lande factor, leads, in the case of a "free electron" solvent, to an ionic 'g shift', Δg_i, given by

$$\frac{\Delta g_i}{g_{eff}} = \frac{3Jn(g_J-1)}{2E_f g_J n_o} \qquad 8.3$$

where n is the number of conduction electrons per unit volume. This coupling affords a possible relaxation mechanism, with an associated relaxation rate given by[107]

$$\frac{1}{T_1} = \frac{9\pi n^2}{16\hbar n_o^2}\left[2J_{ex}(g_J-1)\left(\frac{g_{eff}}{g_J}\right)\right]^2 \frac{kT}{E_f^2} \text{ secs}^{-1} \qquad 8.4$$

Assuming that the corresponding (Korringa) broadening accounts for all of the observed temperature dependence of the line widths leads to the following conclusions:

For AgEr : $|J_{ex}| \simeq 0.145$ ev and $\Delta g_i/g_{eff} \simeq 7.10^{-3}$

For AuYb : $|J_{ex}| \simeq 0.315$ ev and $\Delta g_i/g_{eff} \simeq 10^{-2}$

An exact evaluation of the sum of the various matrix elements which occur in the expression for the relaxation

rate associated with direct phonon processes (see, for example, Reference 105) is a lengthy task. However, a rough estimate of the magnitude of this effect can be obtained from the measured relaxation rate of Yb^{3+} in cubic sites in CaF_2 (at X-band frequencies)[108]. For an order of magnitude calculation, the form of the dependence of this relaxation rate on the crystal field parameters suggests that changing hosts has no effect in this respect. Correcting for the appropriate density and mean phonon velocity yeilds a temperature dependence of the line width which is less that 10^{-2} oersted per degree in Ag.

Orbach and Raman processes[105] become increasingly important as the temperature is raised. As in the above case, rough estimates of their effects on the linewidths can be obtained from the experimental data on trivalent rare-earths in cubic sites in CaF_2[105]. For Raman processes, the relaxation rate should be roughly unchanged on changing hosts, except for the modified density and phonon velocity, and in this approximation yield appreciable line widths (≈ 40 oersteds) in Ag at about $35^{\circ}K$. The relaxation rate associated with Orbach processes in addition to the modifications

mentioned above, needs to scaled for different crystal field parameters. These parameters are roughly ten times bigger in CaF_2 than in Ag, and with these modifications, temperatures of about 100°K are needed for these processes to give rise to linewidths of the order of 50 oersteds.

The AgEr alloy system is, as yet, the only one in which e.p.r. measurements have been made for different rare-earth concentrations (0.28 and 1 at %). The effect of increased concentration manifests itself in a sharply differing temperature dependence of the e.p.r. amplitude in the two alloys below about 7°K.

CHAPTER 9

RESULTS AND DISCUSSION ON Pd AND Pd-BASED ALLOYS

General

The various samples examined were provided either in button form, from which susceptibility samples were machined, or in wire form out of which specimens were made in the manner indicated in figure (9.12) In either case the sample was left for an hour in a solution of 1:2 $HCl:H_2O$, washed in distilled water, then etched for a few minutes in a solution of concentrated nitric acid containing a few drops of hydrogen peroxide, and finally washed again in distilled water. After drying the samples were heated to $150^{o}C$ at a pressure of 10^{-6}mm Hg for about 24 hours to remove hydrogen contamination. (For this same reason Silicon 702 oil was used as a lubricant during machining.)

Dilute Pd-rare earth alloys

Tentative measurements have been carried out on these alloys to investigate any modifications introduced by using Pd as a host, in view of its partially filled 4d band.

Crangle and Layng [112] have examined the Pd-rare earth alloy system, but their investigations have been

concerned primarily with more concentrated alloys, containing more than 1 At.% r.e. This investigation has shown that it is desirable to work with rather more dilute alloys if the complication of a transition to the ferro-magnetic state in the low temperature region (about $2^{\circ}K$) is to be avoided. With this in mind measurements were made on Pd containing ½At.% (nominal) of the rare earths Gd and Er.

Pd-0.5At.% Gd (International Nickel)

The experimental results are summarised in figures (9.1) to (9.4).

Pd-0.5 At.% Er (Naval Research Labs., Washington)

Figures (9.5) to (9.8) reproduce the experimental results. Neither sample was subjected to metallographic analysis since the intended alloy compositions were well within the maximum solubilities[113].

It was hoped that by doing measurements on these two systems, any crystal field effects would result in a general difference in the character of the temperature variation of their respective susceptibilities provided, of course, that the rare earth ions are in their normal valence states.

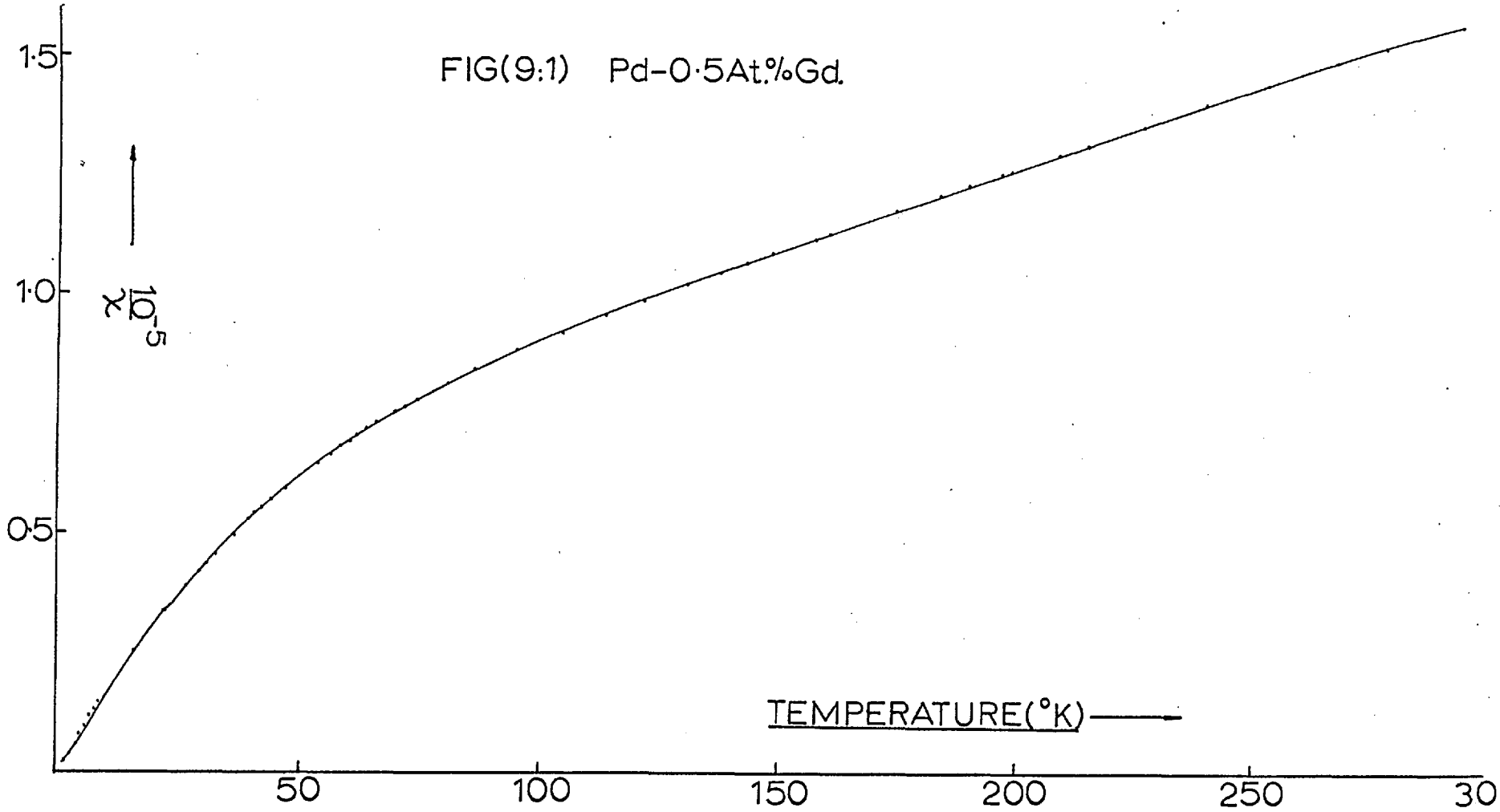

FIG(9:1) Pd-0·5At.%Gd.

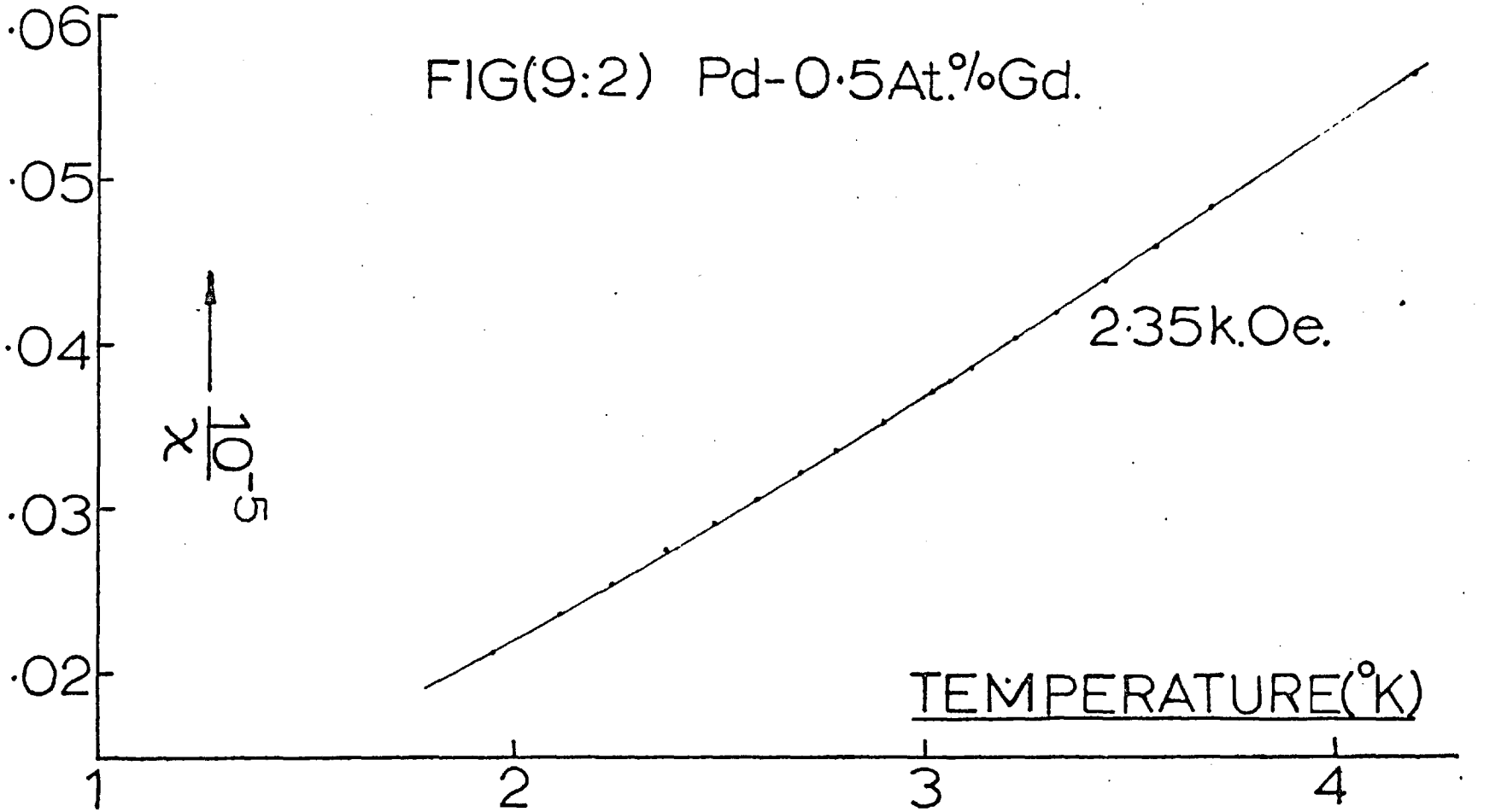

FIG(9:2) Pd-0·5At.%Gd.

FIG(9:3) (M-H) PLOTS
FOR Pd-0·5At.%Gd.

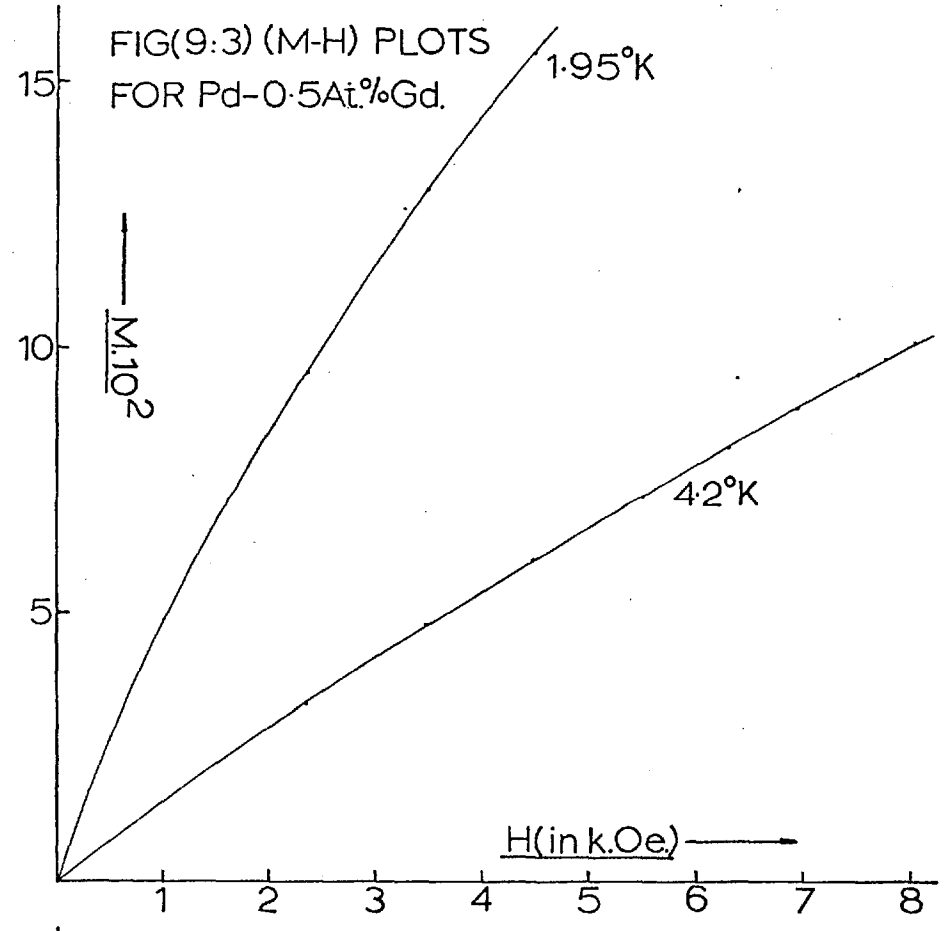

FIG(9:4) (M-H) PLOTS
FOR Pd-0·5At.%Gd.

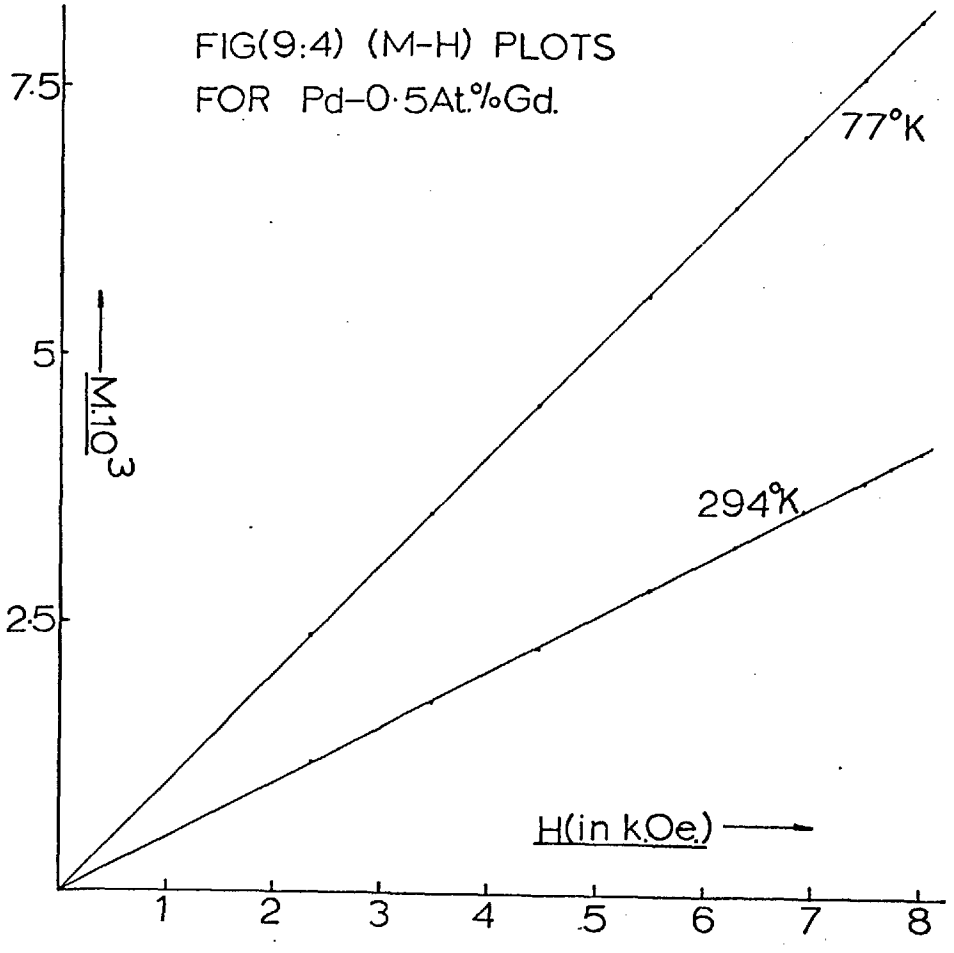

FIG(9:5) Pd-0·5At.% Er.

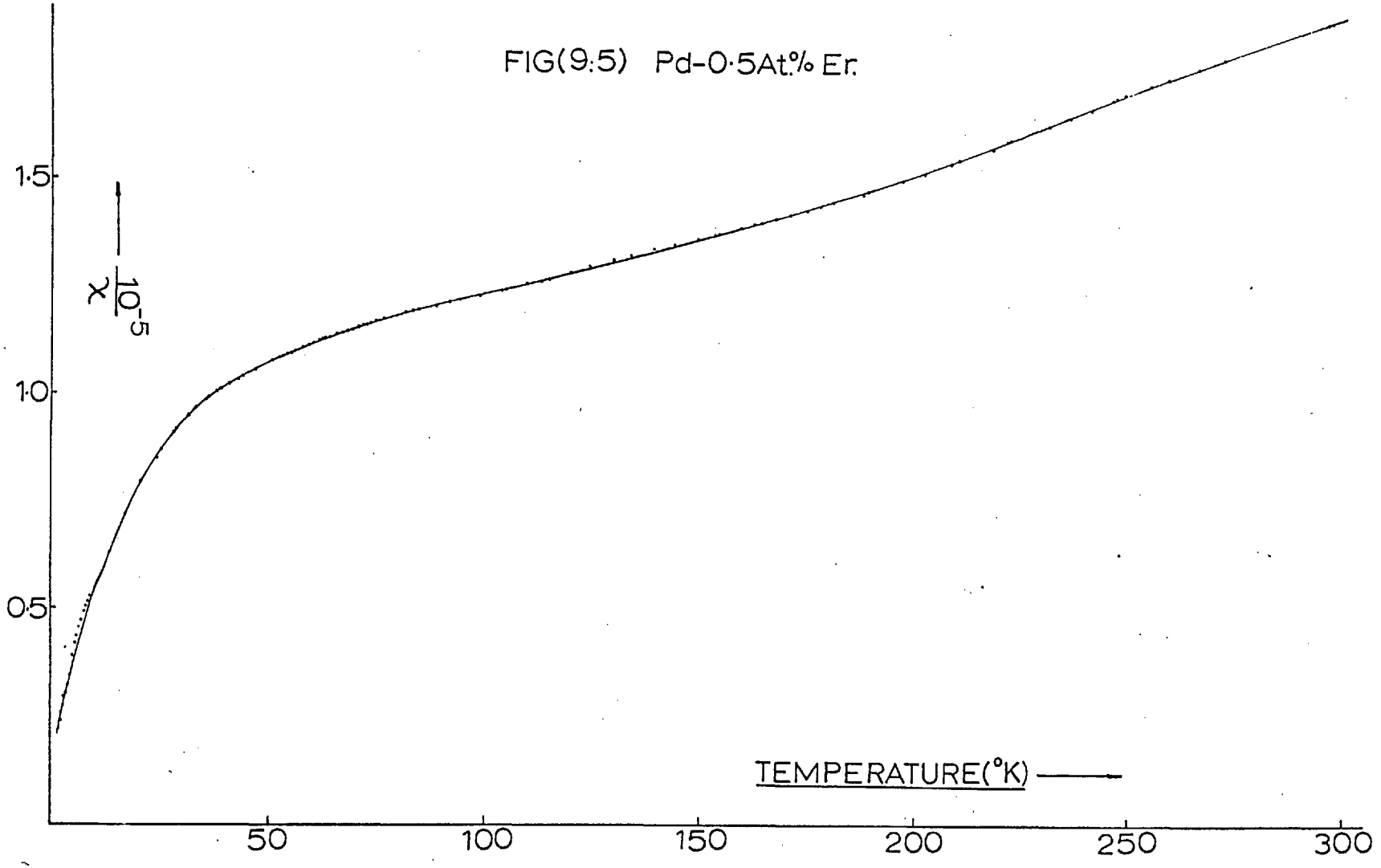

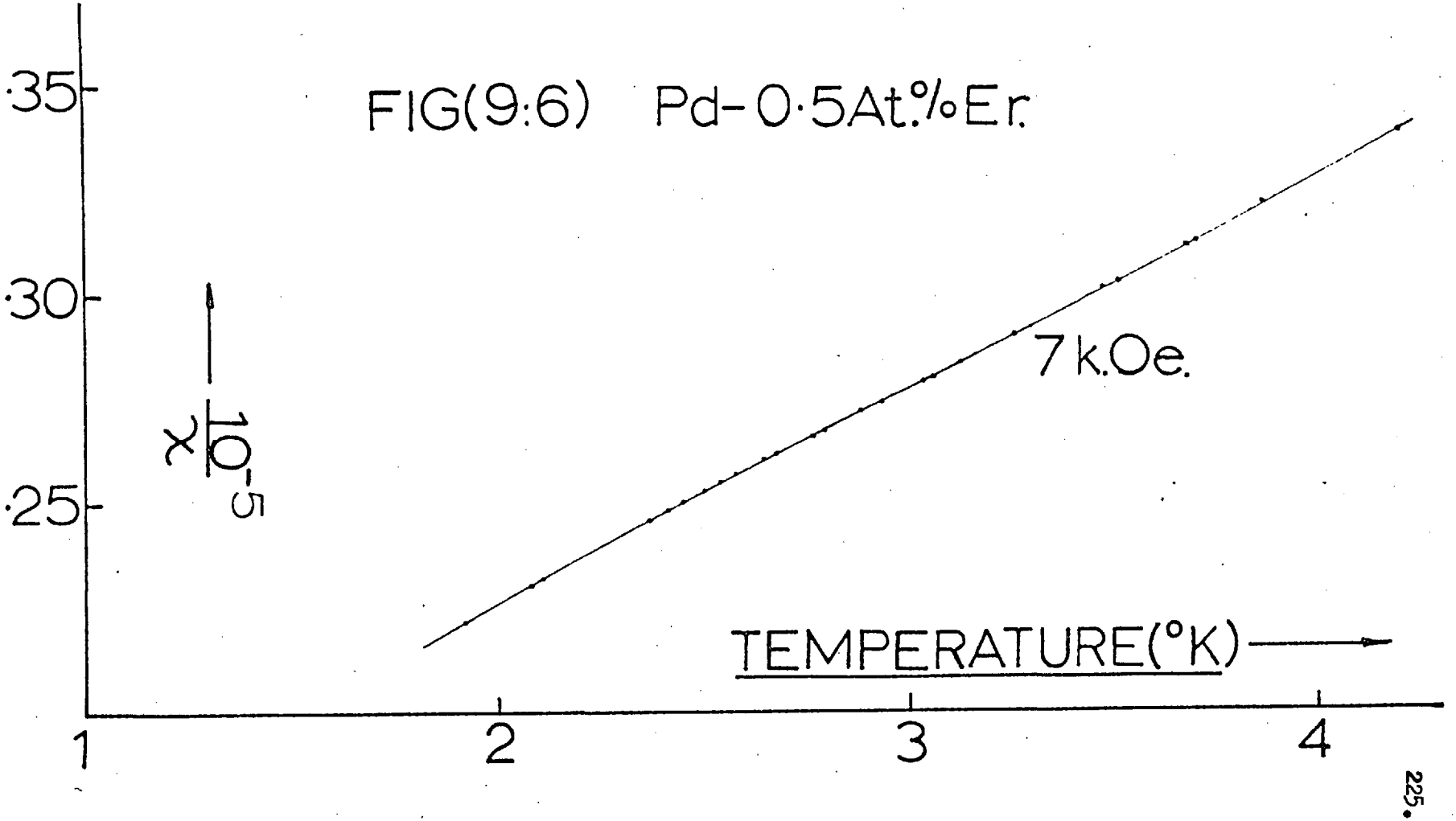
FIG(9:6) Pd-0·5At.%Er.
·35
·30
·25
χ 10⁻⁵
7 k.Oe.
TEMPERATURE(°K)
1
2
3
4

FIG(9:7) (M-H) PLOTS
FOR Pd-0·5At.%Er.

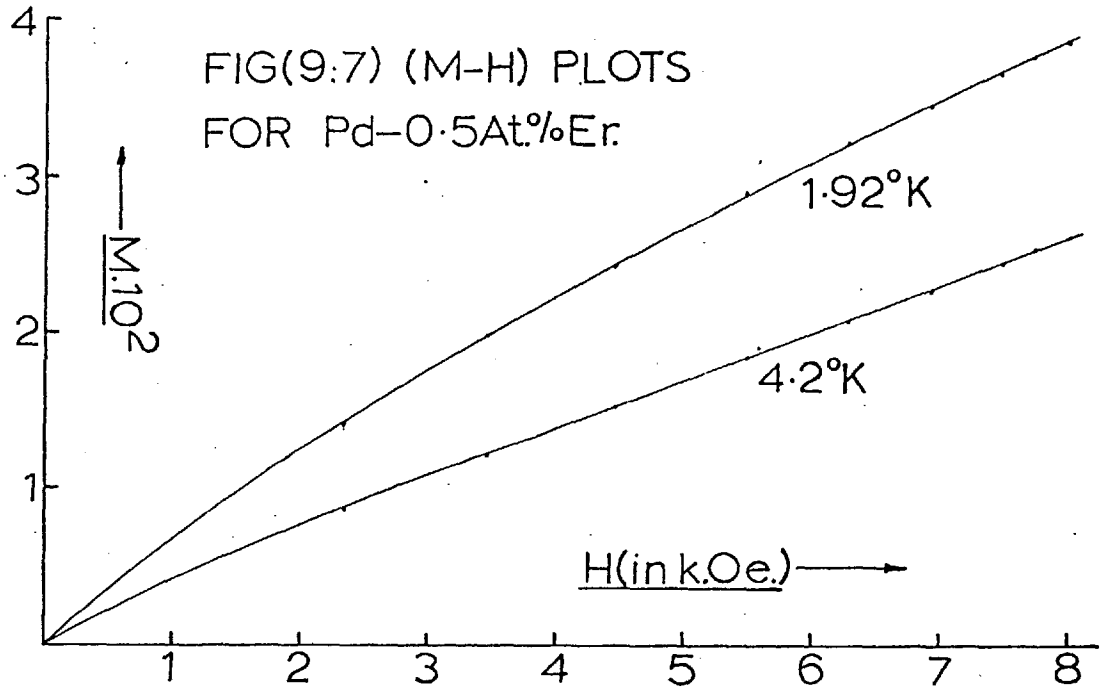

FIG(9:8) (M-H) PLOTS
FOR Pd-0·5At.%Er.

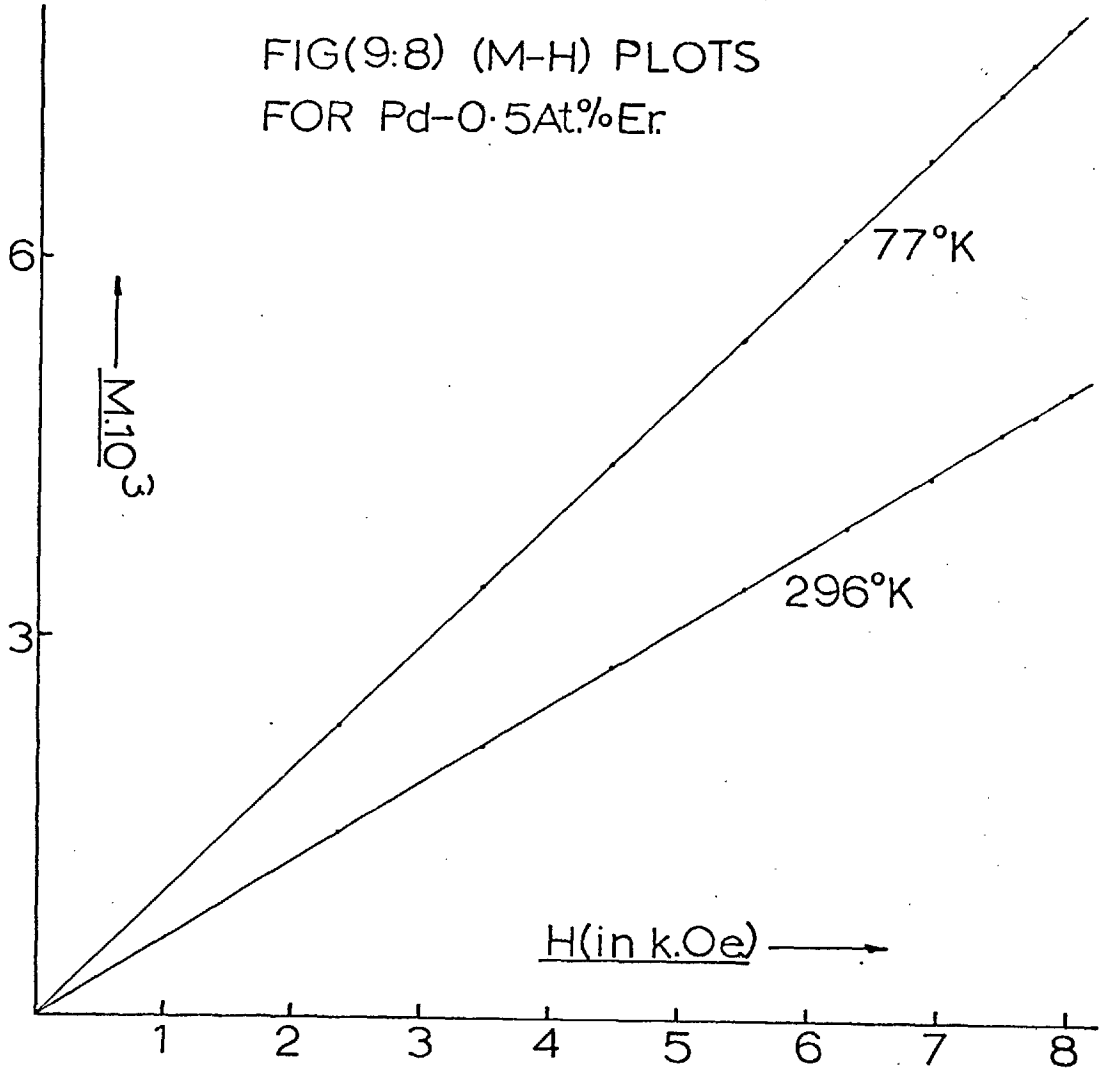

Precise comparison of the experimental results is hampered by ignorance of the exact composition of either system, and inability to proceed with measurements on suitable Pd Lu alloys (these would have provided information about the modifications of the host susceptibility by the valence electrons of the rare-earth impurities). An attempt has been made to extrapolate from the results of Shaltiel[114] for a Pd-4 At.% Lu alloy, but this procedure was found to be rather unreliable owing to the 'sensitivity' of the expression $(\chi_{alloy} - \chi_{Pd\ (corrected)})^{-1}$ at the compositions used. Examination of the experimental results show, as found by Crangle, that deviations from a Curie-Weiss behaviour in the higher temperature region become more pronounced as the rare earth concentration is reduced, and the role played by the susceptibility of the Pd host becomes more important. In very general terms, the character of the inverse susceptibility versus temperature variation is similar for both systems, though the (presumably) more concentrated Pd Gd alloy exhibits a more marked temperature dependence.

At the lowest temperature, the curvature of the magnetisation-field plots at high field values are

consistent with Brillouin function curvature, while departures from linearity in the low field region are indicative of interactions between the rare-earth ions. The more marked curvature in the case of the Pd Gd alloy can be attributed to a higher impurity concentration, to the high 'effective spin' on the impurity $[(g-1)/J(J+1)]$, or to both effects.

In principle, the question of crystalline field effects could have been resolved by e.p.r. data on the rare-earth, non S state ions. However, experiments carried out in this laboratory have failed to detect a resonance in Pd Er. Thisresult, however, is still not decisive, since it could merely reflect the difficulty of observing a resonance for some impurity which has a 'g' value different from that of the matrix in which it is dissolved, when the matrix is nearly ferromagnetic. In addition, the large polarizibility of the Pd matrix means that at any appreciable rare-earth concentration the internal fields to which the latter would be subjected could be sufficient to cause breakdown of any crystal field effects.

Pd and Pd-Ni alloy system

The measurements reported here form part of a more extensive examination of the properties of this system, and include electrical resistivity[115] and thermopower measurements.[116]

Interest in this system has been aroused by the recent theoretical investigations into the properties of nearly ferromagnetic transition metals[117]. Briefly, on the basis of a model in which the electronic transport processes are dominated by electrons in the s-band, Rice has examined the contribution to the electrical and thermal resistivities arising from s to s transitions induced by scattering from spin density fluctuations in the itinerant d band. This author finds that for temperatures $T << \Theta$, where Θ is a cut-off temperature and is regarded as a disposable parameter, the contribution ρ_s to the electrical resistivity from the above process has the form:

$$\rho_s = AT^2 - BT^5 \qquad 9.1$$

(while the contribution W_s to the thermal resistance has the form:

$$W_s \simeq aT - bT^2 + \text{terms } O(T^4) \qquad 9.2$$

Explicit expressions for the various coefficients have been given by Rice, however, for the present purpose it is sufficient to note that in the low temperature regime this author predicts that A should be proportional to the square of the observed enhancement of the Pauli susceptibility. The coefficient B should increase as the enhancement increases, while under the same conditions θ should decrease. Thus, as the ferromagnetic state is approached, the negative T^5 term from the ρ_s contribution to the total resistivity should eventually suppress the low temperature T^5 term arising from the electron-phonon scattering contribution, and the T^2 term should dominate. However, as the enhancement increases the low temperature coefficient of T^2 should increase, but θ is lowered in magnitude and so the range of the region in which this T^2 law is valid deminishes. The author draws similar conclusions about the range of validity of the linear T law found for the thermopower.

Some of the results predicted by Rice have been tested by investigating the properties of Pd and the Pd-Ni system, since the additions of small amounts of Ni to Pd may be considered to increase the magnitude of the exchange enhancement. The results are summarised below.

Pd (Naval Research Labs., Washington)

The susceptibility specimen was obtained by turning down a button which had been annealed for 24 hours at 1100°C under a purified argon atmosphere. The resistivity ratio of this sample was better than 1500.

Figures (9.9) to (9.11) summarise the experimental data.

Pd-Ni system (Naval Research Labs., Washington)

These alloys were prepared by induction melting 5N nickel and palladium in quartz lined, stabalised zirconia crucibles under a purified argon atmosphere. They were supplied in the form of 0.01" diameter wires which had been annealed for 20 hours at 1200°C. The susceptibility samples were made from these by winding a suitable length of the wire around a length of 20 gauge Cu wire to form a tight helix, with an external diameter of about 2.5 mm

Fig. (9.12)

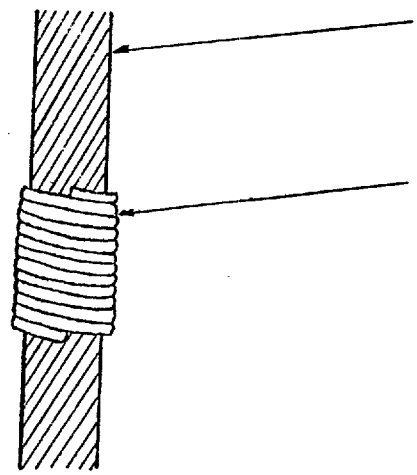

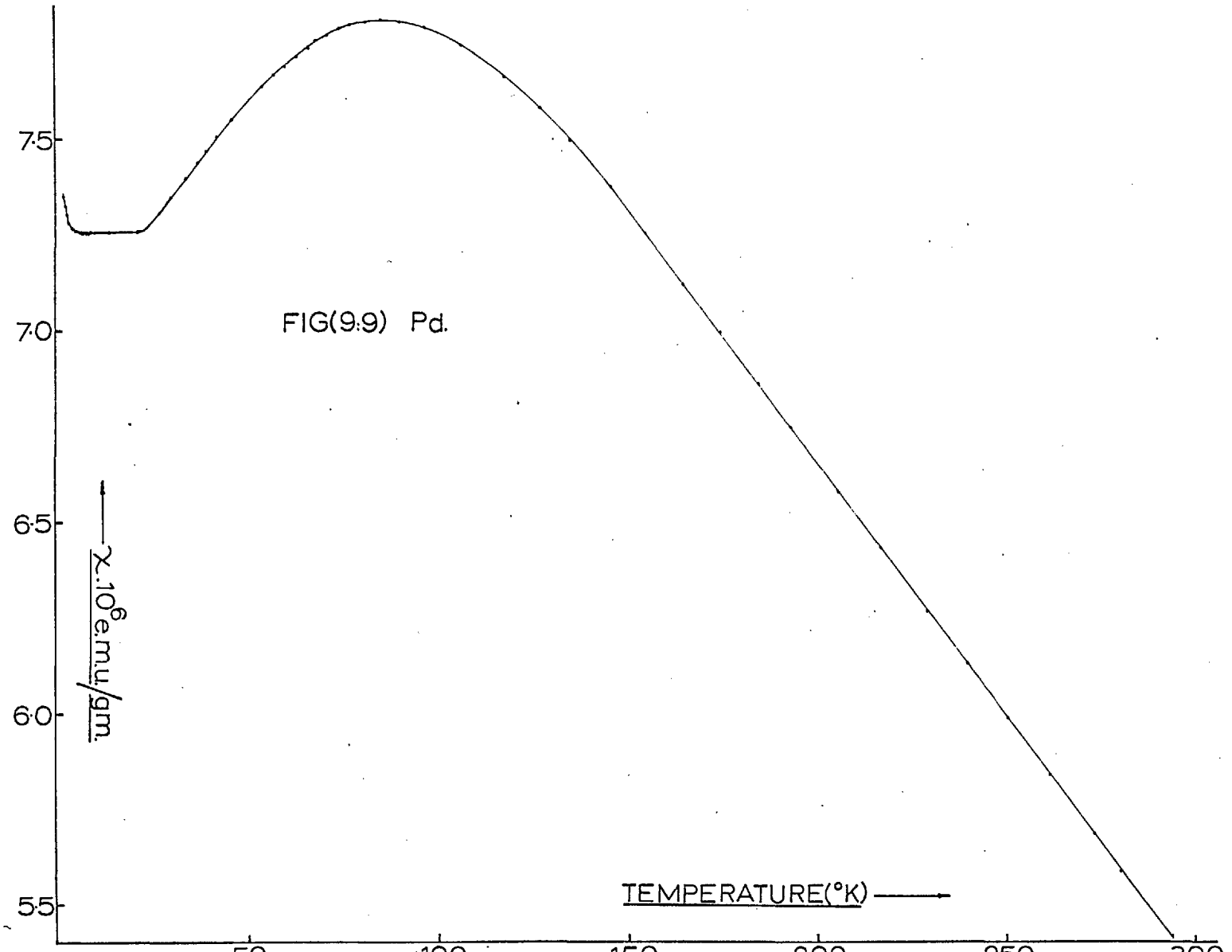

FIG(9.9) Pd.

FIG(9:11) (M–H) PLOTS FOR Pd.

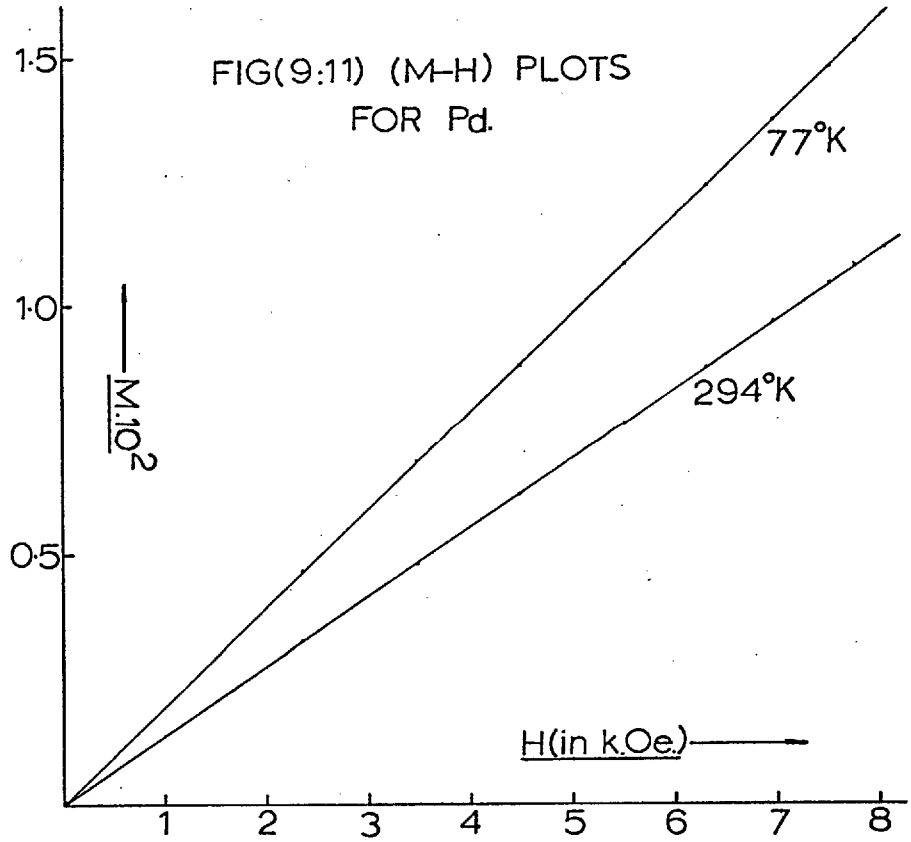

FIG(9:10) (M–H) PLOTS FOR Pd.

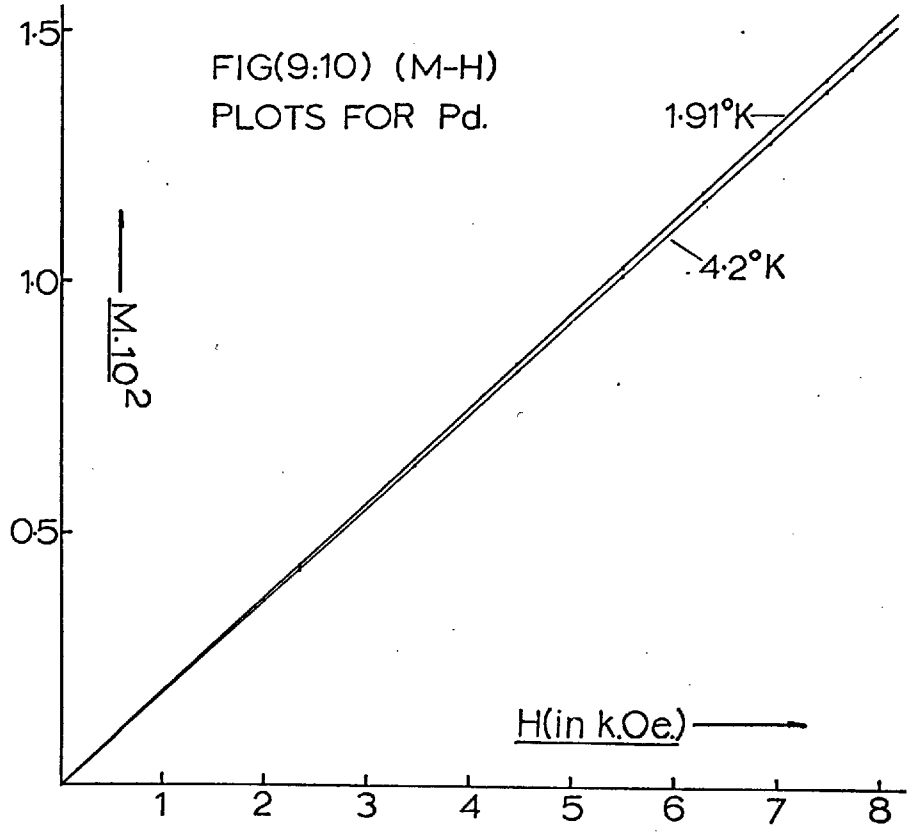

FIG(9:13) (M-H) PLOTS
FOR Pd-0·5At.%Ni.

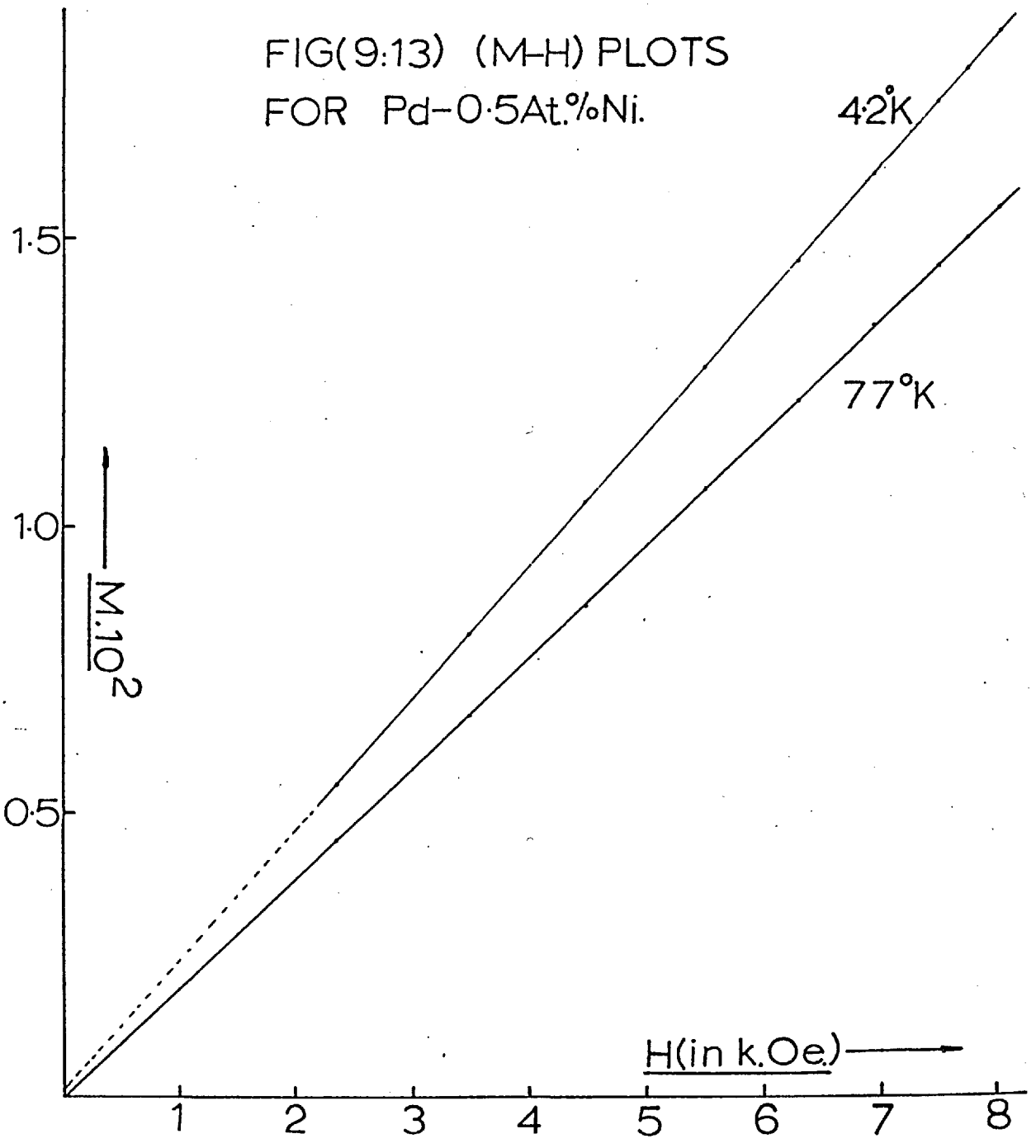

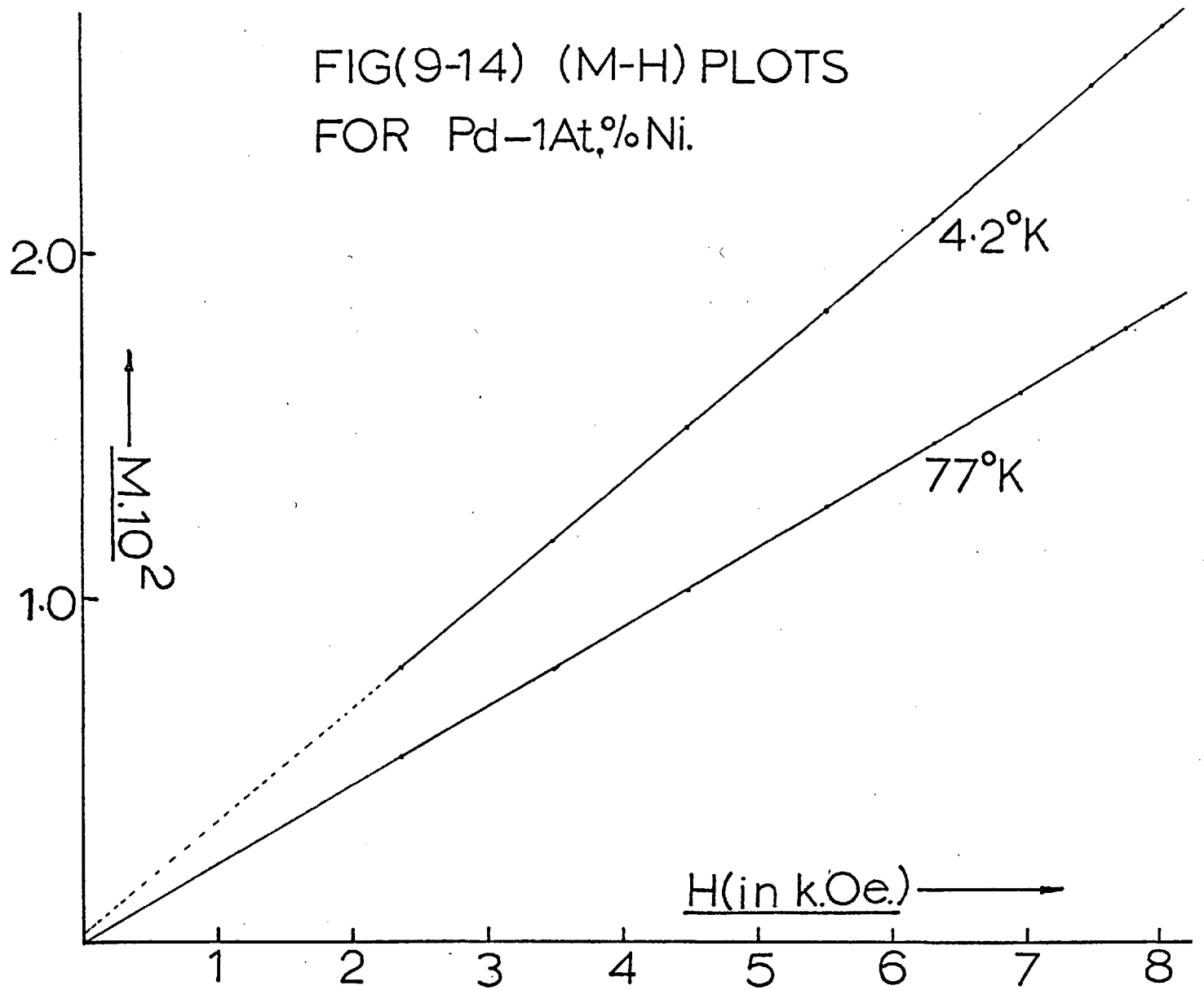
FIG(9-14) (M-H) PLOTS
FOR Pd–1At.% Ni.
4·2°K
77°K
2·0
1·0
M.10²
H(in k.Oe.)
1
2
3
4
5
6
7
8

FIG(9:15) (M-H) PLOTS FOR Pd-1·67At.%Ni.

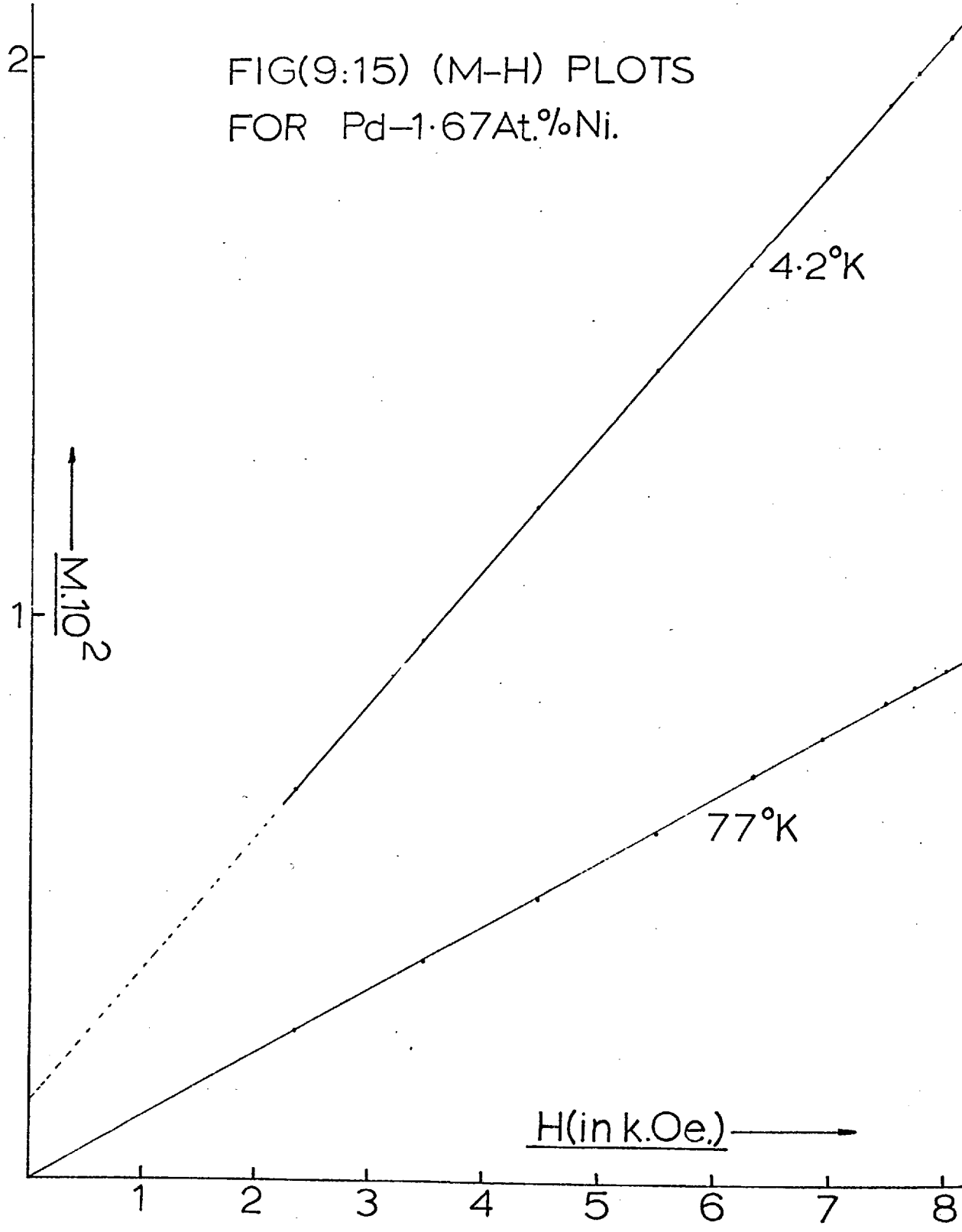

Measurements on the sample were carried out at 4.2 and 77°K, the former to obtain the low temperature enhanced susceptibility, the latter to check against any ferromagnetic inclusion. Figure (9.13) shows the data on Pd-0.5 At.% Ni, figure (9.14) that for Pd-1.0 At.% Ni and figure (9.15) for Pd.-1.67 At.% Ni.

The experimental results on the resistivity of these alloys are reproduced in figure (9.16) (Ref.115), and indicate that at the lowest temperature the resistivity is proportional to T^2 for all the samples, as predicted by equation (9.1). As the temperature is increased deviations from this T^2 behaviour are observed, which, the authors claim, reflects the T^5 contribution in equation (9.1) and from the electron-phonon interaction. Figure (9.16) also illustrates the predicted increasing importance of the T^5 term in equation (9.1) as the Ni concentration is increased, assuming, for pure Pd, that:

$$\rho_s = AT^2 \qquad 9.3$$

over the entire range investigated ($\theta_{Pd} \gg 30°K$), then the contribution from electron-phonon scattering to the total resistivity can be evaluated, and provided Matthiessen's rule is fairly well obeyed, then as a first approximation the authors suggest that this

FIG(9:16)

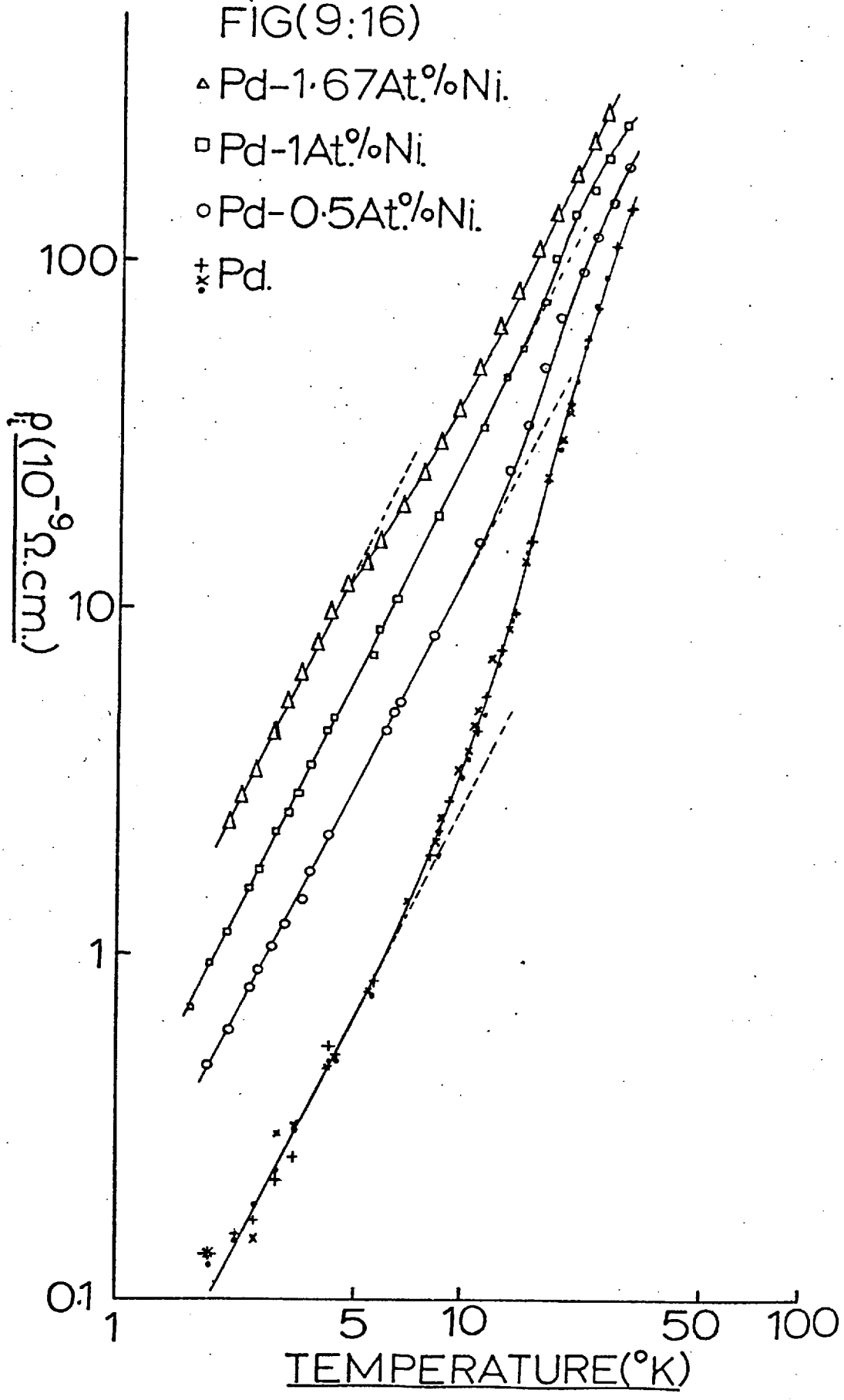
Pd-1·67At.%Ni.
Pd-1At.%Ni.
Pd-0·5At.%Ni.
Pd.
100
10
1
0·1
$\rho_i (10^{-9}\Omega.cm.)$
1
5
10
50
100
TEMPERATURE(°K)

contribution is the same in all the alloys measured. Figure (9.17) shows the temperature variation of the estimated spin density fluctuation contribution to the resistivity, and indicates that the temperature region for which equation (9.3) is valid extends to $14^{\circ}K$ in Pd-0.5 At.% Ni, to $10^{\circ}K$ for Pd-1.0 At.% Ni, and only to $3^{\circ}K$ for Pd-1.67 At.% Ni. This verifies the prediction that the range of validity of the previous equations decreases as the enhancement increases. The full lines in figure (9.17) are the calculated variation of $\rho_s(T)$ on the basis that $\rho_s \propto T^2$ for $10T \leq \theta$ i.e. so that θ can be estimated.

Figure (9.18) shows A, the coefficient of the T^2 term in equation (9.1) plotted against the measured value of the susceptibility χ, at $4.2^{\circ}K$. Small additions of Ni are regarded as not affecting the value of unenhanced Pauli susceptibility, consequently theory predicts that A should vary as χ^2. However, figure (9.18) shows that this is not so. Rice has suggested that this may reflect the rather restricted spectral density of spin density fluctuations employed in his calculation. Indeed, initial results available from a calculation employing a less approximate form for

FIG(9:17)

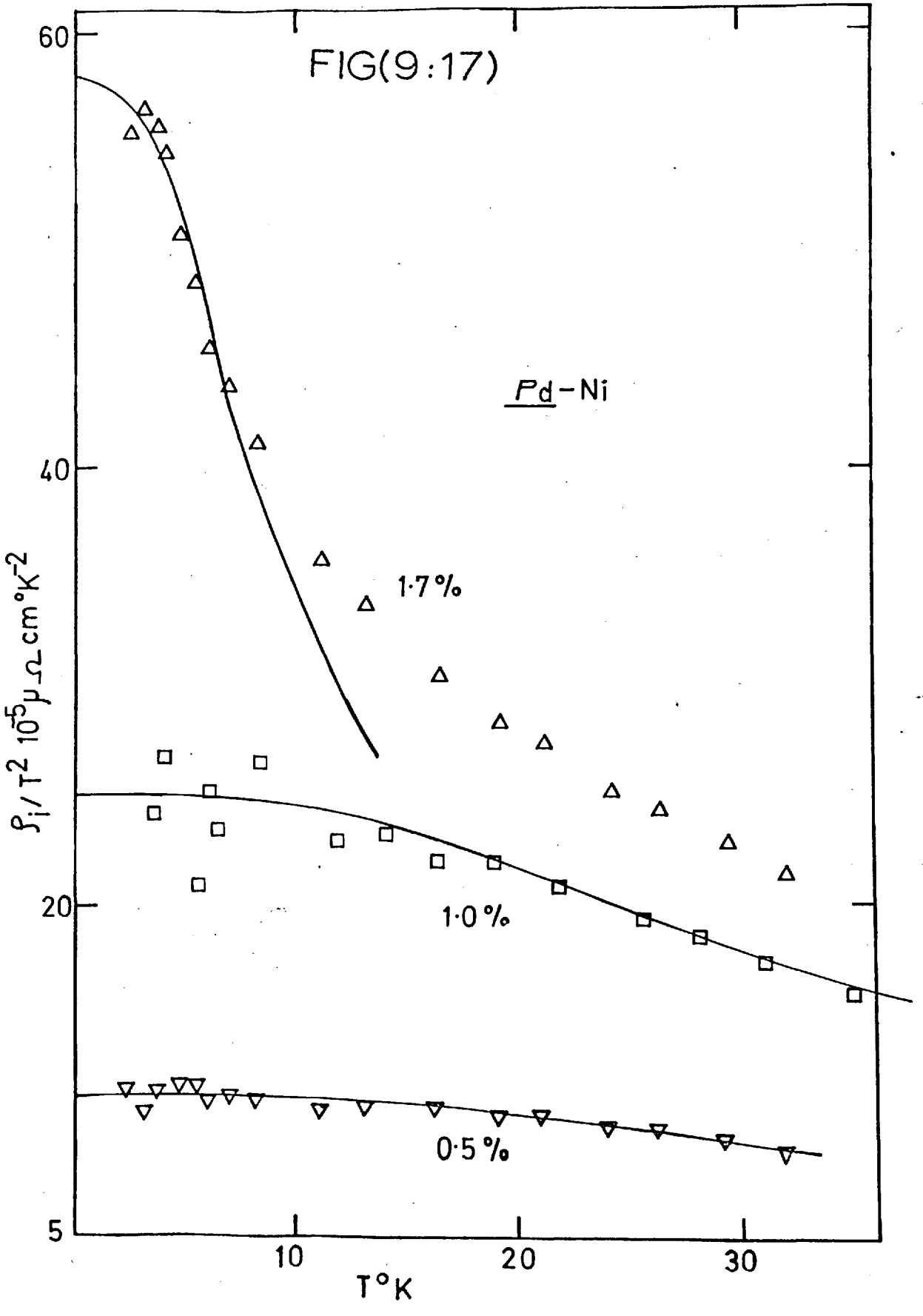

FIG(9:18)

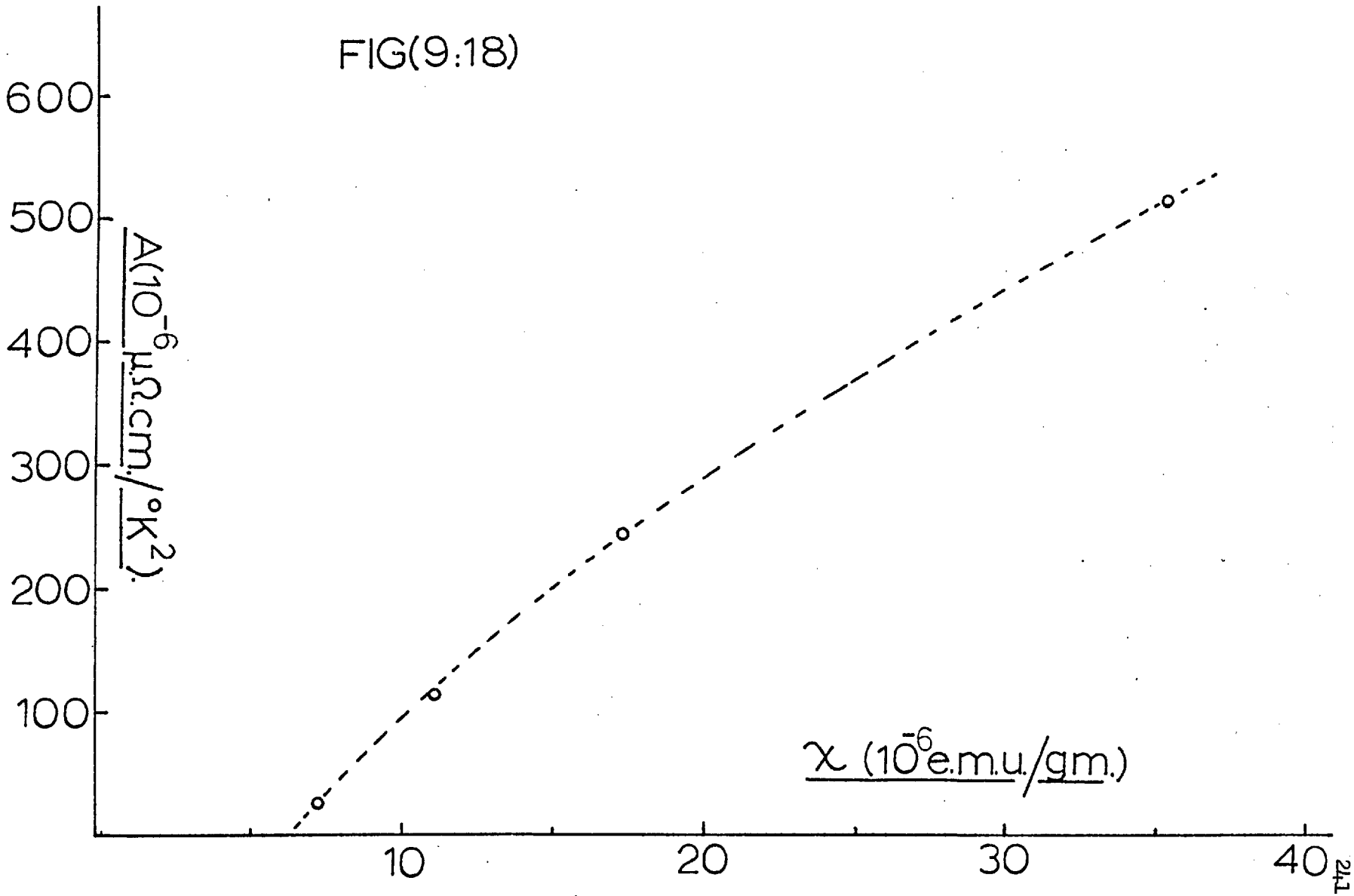

$A_q(w)$, the spectral density function, are in much better agreement with experiment.

Pd-1 At.% Pt (Naval Research Labs., Washington)

The alloy was prepared by induction melting Pt with Pd in a quartz lined crucible under an atmosphere of purified argon. It was then cold forged into a $\frac{1}{4}$" diameter cylinder, from which a susceptibility sample was machined. The final specimen was etched in the usual manner and then annealed at $600^{o}C$ for 5 hours at 10^{-5} mm Hg.

The experimental data appears in figures (9.19) to (9.21).

The susceptibility temperature variation for this alloy bears a close resemblence to that for pure Pd, although closer inspection reveals that the susceptibility variation in the alloy is rather smoother than that in the pure material. The room temperature depression of the susceptibility, on alloying, supplied conclusive evidence that these are band effects, i.e. on a simple model of alloying, a depression of about 0.03×10^{-6} e.m.u./gm/At.% Pt would be expected, while that observed is about 0.39×10^{-6} e.m.u./gm/At.% Pt. The latter is, incidentally, in quite good agreement with the early

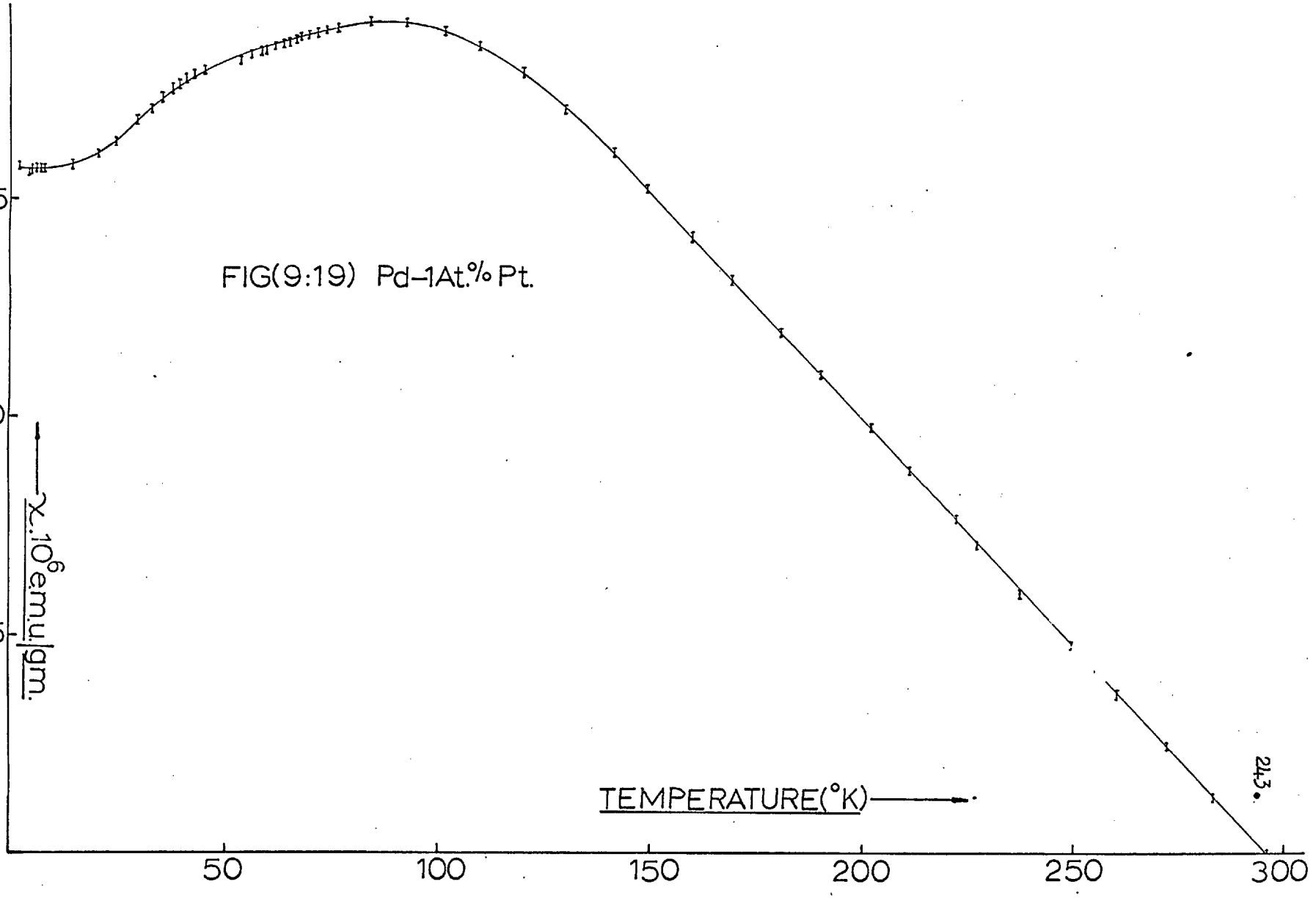

FIG(9:19) Pd–1At.% Pt.

FIG(9:20) (M-H) PLOTS
FOR Pd-1At.% Pt.

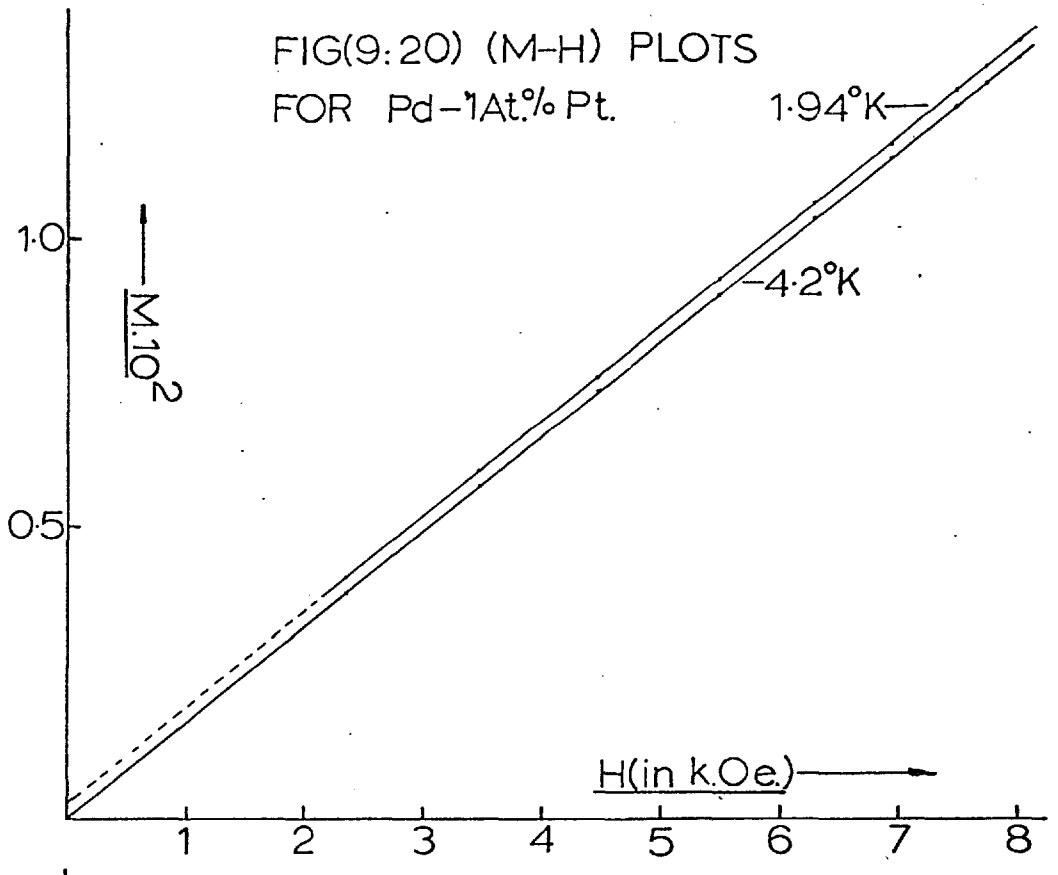

FIG(9:21) (M-H) PLOTS
FOR Pd-1At.% Pt.

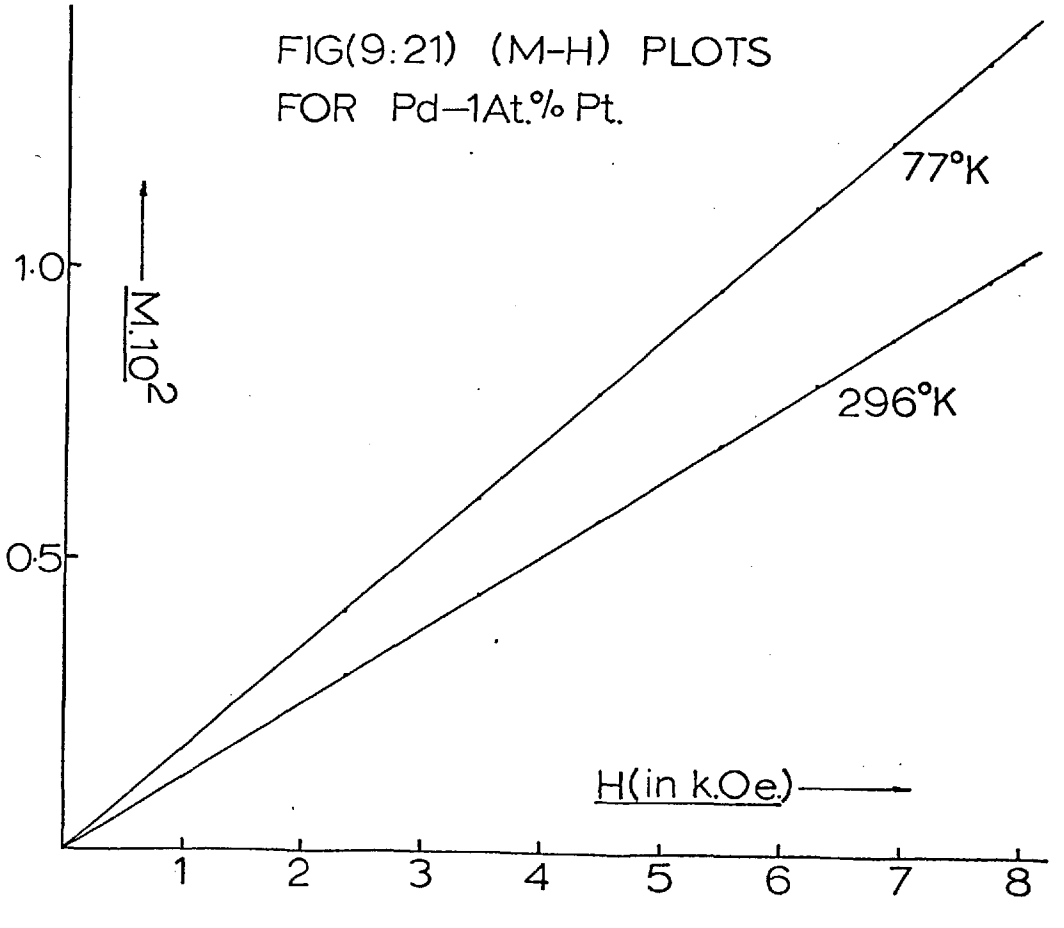

data of Vogt[118] for this system. Further, the difference in the temperature variation of the susceptibility of the alloy and pure material can be qualitatively understood in terms of a band model. In a disordered systed, the effect of alloying is to introduce a 'blurring' of the Fermi limit[119], which would tend to smooth the susceptibility-temperature variation. In addition to this, the introduction of Pt should, owing to its relatively large spin-orbit effects[120] with consequent distortion and shift of the bands[121], in itself give rise to a modified susceptibility temperature variation.

The low temperature experimental data on this alloy is immediately understandable in terms of the previous discussion on the Pd Ni system. As a small amount of Ni added to Pd was regarded as increasing the exchange enhancement of the susceptibility so a small amount of Pt can be regarded as supressing this quantity. This indeed, is observed. It would also seem desirable to have resistivity-temperature data on this system since it would provide another interesting test of Rice's theory. In addition it would be revealing to try and see how the resistivity-susceptibility relationship fits into this author's scheme.

APPENDIX 1

Character table for O (Bethe, 59)

CLASSES

O	E	$3C_2$	$6C_3$	$6C_4$	$8C_5$	
Γ_1	1	1	1	1	1	
Γ_2	1	1	-1	-1	1	
Γ_3	2	2	0	0	-1	
Γ_4	3	-1	1	-1	0	
Γ_5	3	-1	-1	1	0	
For $D^{(J)}$						Irreducible Reps. of O
J=0	1	1	1	1	1	Γ_1
1	3	-1	1	-1	0	Γ_4
2	5	1	-1	1	-1	$\Gamma_3+\Gamma_5$
3	7	-1	-1	-1	1	$\Gamma_2+\Gamma_4+\Gamma_5$
4	9	1	1	1	0	$\Gamma_1+\Gamma_3+\Gamma_4+\Gamma_5$
5	11	-1	1	-1	-1	$\Gamma_3+2\Gamma_4+\Gamma_5$
6	13	1	-1	1	1	$\Gamma_1+\Gamma_2+\Gamma_3+\Gamma_4+2\Gamma_5$
7	15	-1	-1	-1	0	$\Gamma_2+\Gamma_3+2\Gamma_4+2\Gamma_5$
8	17	1	1	1	-1	$\Gamma_1+2\Gamma_3+2\Gamma_4+2\Gamma_5$

C_2: the class of rotations of π about the 3 cubic 100 axes

C_3: " " " " " $\pm\pi/2$ " " " " " " "

C_4: " " " " " π " " 6 twofold axes 110

C_5: " " " " " $\pm 2\pi/3$ " " 4 threefold axes 111

Character table for O'

In setting up the table for O', the characters of all normal single valued representations $\Gamma_1 \ldots \Gamma_5$ are obtained simply by taking $\chi(\bar{E}R) = \chi(R)$ where R is any group element, which assues satisfaction of the requirement on orthonormality between the rows, while in the double valued representations $\chi(\bar{E}R) = -\chi(R)$ with $\chi(C_2,4) = \chi(\bar{E}C_2,4) = 0$, so that the $\bar{E}$ column is orthonormal to the E column. With these, and the various orthonormality relations, equations (4.3a and 4.3b), the character table of O' can be derived.

O'	E	$\bar{E}$	$3C_2:3\bar{E}C_2$	$6C_3$	$6\bar{E}C_3$	$6C_4:6\bar{E}C_4$	$8C_5$	$8\bar{E}C_5$
Γ_1	1	1	1	1	1	1	1	1
Γ_2	1	1	1	−1	−1	−1	1	1
Γ_3	2	2	2	0	0	0	−1	−1
Γ_4	3	3	−1	1	1	−1	0	0
Γ_5	3	3	−1	−1	−1	1	0	0
Γ_6	2	−2	0	$\sqrt{2}$	$-\sqrt{2}$	0	1	−1
Γ_7	2	−2	0	$-\sqrt{2}$	$\sqrt{2}$	0	−1	1
Γ_8	4	−4	0	0	0	0	1	−1

$D^{(J)}$	E	$\bar{E}$	$3C_2:3\bar{E}C_2$	$6C_3$	$6\bar{E}C_3$	$6C_4:6\bar{E}C_4$	$8C_5$	$8\bar{E}C_5$	Irreduc. Reps. O'
$J=\frac{1}{2}$	2	−2	0	$\sqrt{2}$	$-\sqrt{2}$	0	1	−1	Γ_6
$\frac{3}{2}$	4	−4	0	0	0	0	−1	1	Γ_8
$\frac{5}{2}$	6	−6	0	$-\sqrt{2}$	$\sqrt{2}$	0	0	0	$\Gamma_7+\Gamma_8$
$\frac{7}{2}$	8	−8	0	0	0	0	1	−1	$\Gamma_6+\Gamma_7+\Gamma_8$
$\frac{9}{2}$	10	−10	0	$\sqrt{2}$	$-\sqrt{2}$	0	−1	1	$\Gamma_6+2\Gamma_8$
$\frac{11}{2}$	12	−12	0	0	0	0	0	0	$\Gamma_6+\Gamma_7+2\Gamma_8$
$\frac{13}{2}$	14	−14	0	$-\sqrt{2}$	$\sqrt{2}$	0	1	−1	$\Gamma_6+2\Gamma_7+2\Gamma_8$
$\frac{15}{2}$	16	−16	0	0	0	0	−1	1	$\Gamma_6+\Gamma_7+3\Gamma_8$

This last table indicates that for all half integral J, the residual degeneracies are at least twofold; this result can be proved in general for half integral angular momentum (odd number of electrons) for an electric field of any symmetry since it is a consequence of time reversal symmetry[61]. It is known as Kramer's theorem.

APPENDIX 2

1. Reduction of the crystal field Hamiltonian under the symmetry operations of Oh

$$V_{crysral} = r^4 \sum_{m=-4}^{+4} a_4^m y_4^m + r^6 \sum_{m=-6}^{6} a_6^m y_6^m$$

A rotation of $\pi/2$ about the z axis shows that only Y_4^o, Y_4^{+4}; Y_6^o and Y_6^{+4} remain unchanged. Reflection in the xz plane leaves Y_4^o and Y_6^o unchanged and sends Y_4^4 into Y_4^{-4} and Y_6^4 into Y_6^{-4}, hence $a_4^{-4} = a_4^4$ and $a_6^{-4} = a_6^4$, and

$$V_{crystal} = r^4(a_4^o Y_4^o + a_4^4(Y_4^{+4} + Y_4^{-4})) + r^6(a_6^o Y_6^o + a_6^4(Y_6^{-4} + Y_6^4))$$

Finally a rotation of $2\pi/3$ about a threefold axis reveals that, on transforming to the cartesian form:

$$V_{crystal} = C_4(V_4^o + \frac{5}{2} V_4^4) + C_6(V_6^o - \frac{21}{2} V_6^4)$$

where $V_4^o = 35z^4 - 30z^2r^2 - 3r^4$

$V_4^4 = (x + iy)^4 + (x - iy)^4$

$V_6^o = 231z^6 - 315r^2z^4 + 105r^4z^2 - 5r^6$

and $V_6^4 = (11z^2 - r^2)\left[(x + iy)^4 + (x - iy)^4\right]$

C_4 and C_6 are numerical coefficients.

2. Operator equivalents for the above potential (Stevens, 52)

Take for example V_4^o, Stevens points out that in order to account for the non commutation of Jx, Jy and Jz, it is incorrect to replace X^2Z^2 (appearing in $r^2 z^2$) by Jx^2Jz^2, but an expression consisting of all possible different combinations of Jx, Jy, Jz and Jz should be used; i.e.

$$35z^4 \longrightarrow 35Jz^4$$

but $30x^2z^2$ becomes

$$30\,\frac{1}{6}(JxJxJzJz + JxJzJxJz + JxJzJzJx + JzJxJzJx + JzJxJxJz + JzJzJxJx) + \frac{1}{6}\ (x \text{ replaced by } y) + Jz^4$$

Using the usual commutation relations for Jx, Jy and Jz this reduces to:

$$JxJxJzJz + JyJyJzJz + Jz^4 = J(J+1)Jz^2$$

$$JxJzJxJz + JyJzJyJz + Jz^4 = J(J+1)Jz^2 - Jz^2$$

$$JzJxJzJx + JzJyJzJy + Jz^4 = J(J+1)Jz^2 - Jz^2$$

$$JzJxJxJz + JzJyJyJz + Jz^4 = J(J+1)Jz^2$$

$$JxJzJzJx + JyJzJzJy + Jz^4 = J(J+1)Jz^2 + J(J+1) - 3Jz^2$$

$$JzJzJxJx + JzJzJyJy + Jz^4 = J(J+1)Jz^2$$

thus $30r^2z^2 \longrightarrow (30J(J+1)-25)Jz^2 - 5J(J+1)$

In a similar manner: $3r^4 \longrightarrow J(J+1)(3J^2+J-1)$

Thus $V_4^o \longrightarrow 35Jz^4 - 30J(J+1)Jz^2 + 25Jz^2 - 6J(J+1) + 3J^2(J+1)^2$. Similarly (from Stevens)

$$V_4^4 \longrightarrow (J_+^4 + J_-^4)$$

$$V_6^o \longrightarrow 231J_z^6 - 105(3J(J+1)-7)Jz^4 + (105J^2(J+1)^2 - 525J(J+1) + 294)Jz^2 - 5J^3(J+1)^3 + 40J^2(J+1)^2 - 60J(J+1)$$

$$V_6^4 \longrightarrow \tfrac{1}{2}(11Jz^2 - J(J+1) - 38)(J_+^4 + J_-^4) + \tfrac{1}{2}(J_+^4 + J_-^4)(11Jz^2 - J(J+1) - 38)$$

Finally putting O_4^o equal to the angular momentum expression for V_4^o, O_4^4 equal to one half that of V_4^4, O_6^o equal to that of V_6^o and O_6^4 equal to one half that of V_6^4, then

$$V_{crystal} = B_4(O_4^o + 5O_4^4) + B_6(O_6^o - 21O_6^4)$$

The coefficients B_4 and B_6 are parameters which are usually determined experimentally, their relation to C_4 and C_6 is considered below, the term connecting the coefficients is, in fact, the proportionality constant between the matrix element of the potential operator and that of the operator equivalent. This factor is evaluated by making use of the spin independence of the potential functions, which implies that similar operator equivalent hold in manifolds of constant orbital angular momentum L. A convenient state in L, S, J, Jz quantization is choosen and the value of

the matrix element of some potentialfunction is written down using the operator equivalent of the function i.e. for the case of Er^{+++}, $^4I_{15/2}$ for which $\underline{L} = 6$, $\underline{S} = 3/2$, $\underline{J} = \frac{15}{2}$ and $Jz = 15/2$

$$\langle |V_4^o| \rangle = \alpha O_4^o (\text{for } J=\tfrac{15}{2};\ Jz = \tfrac{15}{2}) = 16380\alpha$$

This state is then expressed in $\underline{L}$, $\underline{S}$, L_z, S_z quantization thus:

$$|\underline{L},\underline{S},\underline{J},Jz\rangle = \sum_i a_i |\underline{L},\underline{S},L_z^i,S_z^i\rangle \text{ subject to } L_z^i+S_z^i = J_z$$

where the a_i's are Clebsch Gordon coefficients, for the example choosen

$$|\underline{L}=6,\ \underline{S}=\tfrac{3}{2},\ \underline{J}=J_z=\tfrac{15}{2}\rangle = a|\underline{L}=6,\underline{S}=\tfrac{3}{2},\ L_z=6,S_z=\tfrac{3}{2}\rangle$$

where a=1; the termination of the expansion after a single term is due to the parallel coupling of L_z and S_z which occurs in the second half of the rare earth series. Within a manifold of constant $\underline{L}$;

$$\langle |V_4^o| \rangle = \beta O_4^o \text{ (for } \underline{L} \text{, inside } \underline{L}=6,\ L_z=6)$$

$$= 5940\,\beta$$

The state is now expressed in $l_z s_z$ quantization thus:

$$|\underline{L}=6,\underline{S}=3/2,L_z=6,S_z=3/2\rangle = \left\{ \overset{+}{3},\overset{+}{2},\overset{+}{1},\overset{+}{0},\overset{+}{-1},\overset{+}{-2},\overset{+}{-3},\overset{-}{3},\overset{-}{2},\overset{-}{1},\overset{-}{0} \right\}$$

again the passage from one type of quantization to the other is straightforward since the rare earth ions adhere to Hund's rules. From this last expansion

$$\langle | V_4^0 | \rangle = 5940\beta = \left\{ \overset{+}{3} \ldots \vec{0} \right\}(V_4^0) \left\{ \overset{+}{3} \ldots \overset{-}{0} \right\}$$

this last matrix element can again be evaluated using an operator equivalent method since inside a manifold of constant $\underline{l}$ ($\underline{l}=3$ for f electrons)

$$\left\{ \overset{+}{3} \ldots \overset{-}{0} \right\}(V_4^0)\left\{ \overset{+}{3} \ldots \overset{-}{0} \right\} = \gamma \left[O_4^0(\text{for } \underline{l}=3,) + O_4^0 \, l=3, l_z=2 \rangle + \ldots \right]$$

$$= \gamma(180-420+60+360+60-420+180+180-420+60+360)$$

$$= 180\gamma$$

Finally consider the element $\{3\}(V_4^0)\{3\} = 180\gamma$, this is, of course, equal to $\langle \underline{l}=3,\ l_z=3 | 35z^4-30r^2z^2+3r^4 | \underline{l}=3, l_z=3 \rangle$

Using the fact that $| \underline{l}=3,\ l_z=3 \rangle$ = Normalizing Factor x $f(r)\ P_3^3(\cos\theta)e^{3i\phi}$,

$$\langle \underline{l}=3, l_z=3 | 35z^4-30r^2-z^2+3r^4 | \underline{l}=3, l_z=3 \rangle = \frac{8}{11}\bar{r}^4$$

Thus making use of all the relations derived:

$16380\,\alpha = 5940\,\beta = 180\,\gamma = 8/11\,\vec{r}^4$ giving

$$\alpha = \frac{8\bar{r}^4}{11 \cdot 16380} = \frac{2\bar{r}^4}{11 \cdot 15 \cdot 273}$$

hence for this particular example $B_4 = C_4 . r^4$ (2/11.15.273) For the ground state of rare earth ions, Stevens has tabulated all such relations. One final comment, in the previous discussion it has been assumed the multiplying factors associated with $V_4^o (V_6^o)$ and $V_4^4 (V_6^4)$ are the same, as Stevens points out, these factors, for same $V_\perp^m$, depend only on 1 and are independent of m, a consequence of the Wigner-Eckart theorem.

APPENDIX 3

As Wilson[85] has pointed out, the energy of some sample placed in a magnetic field is obtained from the relation:

$$TdS = dU + \sum_i Ai\ da_i$$

Ai being the generalised force exerted by the sample on its surroundings, corresponding to the generalised coordinate, ai. For a magnetically isotropic sample placed in a magnetic field Hx, the above equation in the usual notation, becomes, neglecting demagnetising effects:

$$dU = Tds + HxdMx$$

This leads to a free energy G given by:

$$G = U - TS - MxHx$$

from which the force exerted on the sample by the field in some z direction is given by

$$Fz = -\partial G/\partial z = Mx\,\partial Hx/\partial z$$

This holds whatever dependence the magnetisation has on the applied field. The experimental arrangement is

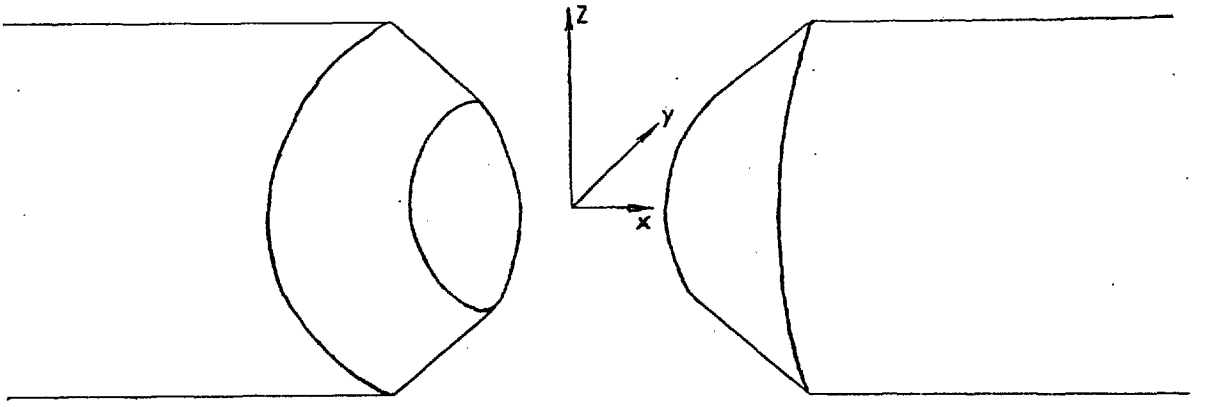

Clearly then, Hx >> Hy or Hz. Consequently if the body is not strictly isotropic it is still reasonable to assume that MxHx >> MyHy or MzHz. Neglect of demagnetising effects is not serious, as Appendix 6 demonstrates.

APPENDIX 4

The Wareham power unit used to supply the magnet current can be controlled 'internally' by a ten turn 10K helipot, and also has provision for an external control. In this case one was used which switched suitable resistors in place of the helipot.

When using the internal control the current must be manually swept up to or down from some value. Particularly during warm up, continually sweeping the current is a rather laborious and time consuming operation. Using the controller drawn below, the current can be reset from zero at practically the same value in less than five seconds.

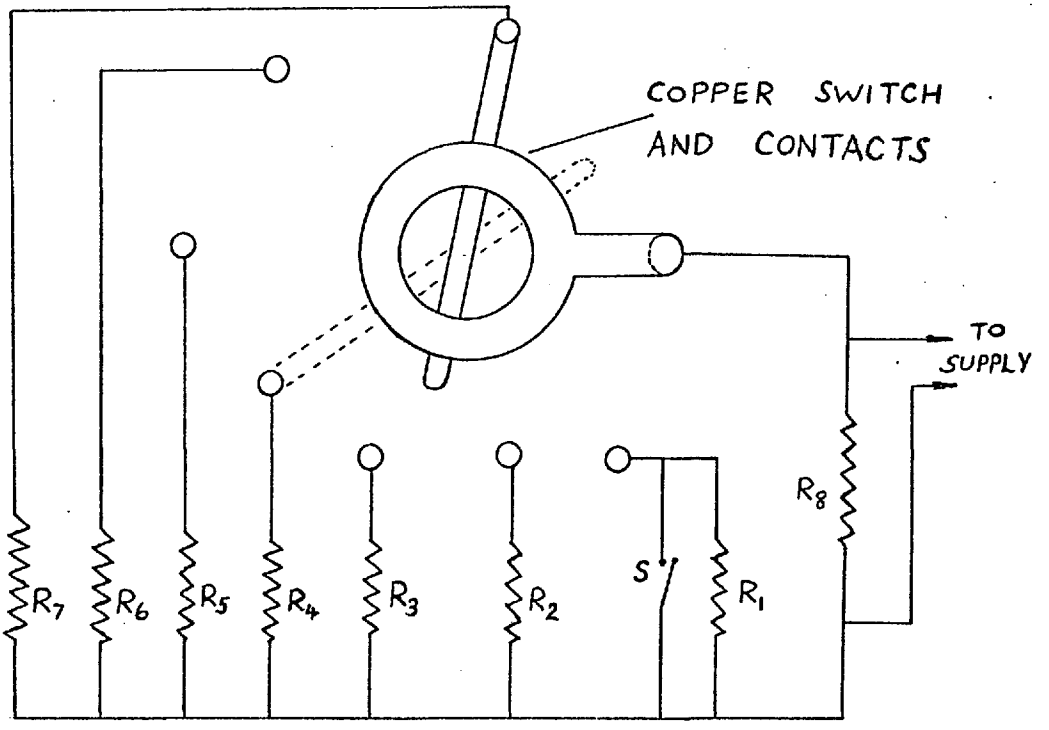

A unit of this type has the advantage that the supply is not even momentarily open circuited, since R_8 is always connected. In addition the current can only be reduced to zero from the lowest current setting i.e. R_1 and R_8 in parallel.

APPENDIX 5

A correction to the measured variation of the magnetic field due to the finite size of the flip coil can be made on the basis of an approximation in which the field gradient is assumed to be constant over the area of the flip coil.

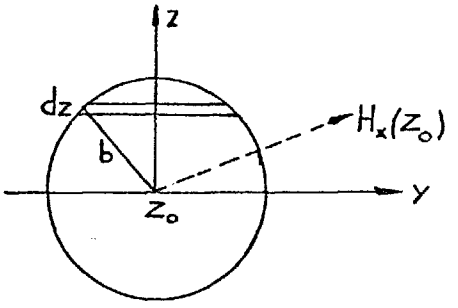

Flux through the coil

$$= 2b \int_{Z_o-b}^{Z_o+b} \sqrt{1-\frac{(Z-Z_o)^2}{b^2}}\, H_x(Z)\,dz$$

which is equated to the area of the coil multiplied by an average field $\bar{H}_x(Z_o)$:

$$\overline{H_x}(Z_o) = \frac{1}{\pi b^2} \int_{Z_o-b}^{Z_o+b} 2b \sqrt{1-\frac{(Z-Z_o)^2}{b^2}}\, H_x(Z)\,dz$$

Expanding $H_x(Z)$ in a Taylor Series about Z_o

$$H_x(Z) = H_x(Z_o) + (Z-Z_o)H_x'(Z_o) + \frac{(Z-Z_o)^2}{2} H_x''(Z_o) +$$

and noting that since $H_x'(Z_o)$ is assumed constant over the region of integration then the contribution to the

integrand from the term containing this quantity will be zero since $(Z-Z_o)$ is an odd function . Hence:

$$\overline{H_x(Z_o)} = \frac{1}{\pi b^2} \int_{Z_o-b}^{Z_o+b} 2b\sqrt{1-\frac{(Z-Z_o)^2}{b^2}} \cdot \left\{ H_x(Z_o) + \frac{(Z-Z_o)^2}{2!} H''_x(Z_o) \right\} dz$$

the first term simply gives $H_x(Z_o)$ multiplied by the area of the coil, hence

$$\overline{H_x(Z_o)} = H_x(Z_o) + \frac{b}{\pi} \int_{Z_o-b}^{Z_o+b} \frac{(Z-Z_o)^2}{b^2} H''_x(Z_o) \sqrt{1-\frac{(Z-Z_o)^2}{b^2}}\, dz$$

The final term above can be evaluated simply by putting $b \sin \theta = (Z-Z_o)$ etc, and the above equation becomes

$$\overline{H_x(Z_o)} = H_x(Z_o) + \frac{b^2}{8} H''_x(Z_o)$$

thus giving $H_x(Z_o) = \overline{H_x(Z_o)} - \frac{b^2}{8} \overline{H''_x(Z_o)}$

APPENDIX 6

Estimates of the couples produced by sample misalignment.

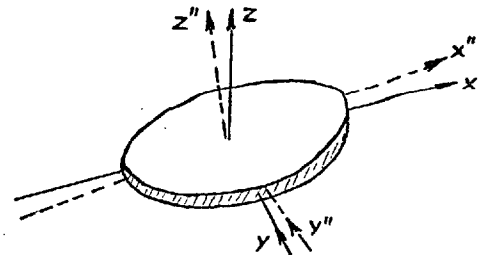

Consider a sample in the form of a disc of thickness 2a and area πb^2, oriented with respect to the field in the manner indicated above, i.e. (x,y,z) are fixed axes in the field direction, (x",y",z") refer to axes fixed in the sample. Perform a small rotation ϕ about z, followed by α about x', such that

$$(x,y,z) \xrightarrow{\phi} (x',y',z' = z) \xrightarrow{\alpha} (x'', = x', y'', z'')$$

with:

$H_x'' = H_x \cos\phi + H_y \sin\phi \simeq H_x \cos\phi$ since $H_x \gg H_y$ or H_z

$H_y'' = H_y \cos\phi \cos\alpha - H_x \sin\phi \cos\alpha - H_z \sin\alpha \simeq -H_x \sin\phi \cos\alpha$

$H_z'' = H_z \cos\phi + H_y \cos\phi \sin\alpha - H_x \sin\phi \sin\alpha \simeq 0$, since α and ϕ are small:

The contribution to the free energy (assuming $M = \chi H$) is:

$$= \chi \iiint_{\text{over sample}} (H_x''^2 + H_y''^2 + H_z''^2)\, dx''dy''dz''$$

$$\simeq \chi \iiint_{\text{sample}} (H_x''^2 + H_y''^2)\, dx''dy''dz''$$

Experimentally the dominant terms in the force come from the variation of H_x in z, hence expanding H_x'' and H_y'' in a power series about the centre of the sample thus:

$$H_x''(Z) = H_x''(0) + Z\left\{\frac{\partial H_x''}{\partial Z''}\right\} +$$

Then the above equation becomes:-

$$\chi \iiint_{\text{sample}} \left[H_x''(0)^2 + 2H_x''(0)\left(\frac{\partial H_x''}{\partial Z''}\right)Z + \left(\frac{\partial H_x''}{Z''}\right)^2 Z^2 + \text{similar terms in } H_y'' \right] dx''dy''dz'' =$$

$$\pi b^2 \chi \int_{-a}^{+a} \left[H_x''^2(0) + 2H_x''(0)\left(\frac{\partial H_x''}{\partial Z''}\right)Z + \left(\frac{\partial H_x''}{\partial Z''}\right)^2 Z^2 \ldots \right] dz''$$

the integration over dx" and dy" giving the area.

$$= \pi b^2 \chi \left[2a\left\{H_x''^2 + H_y''^2\right\} + \frac{2a^3}{3}\left\{\left(\frac{\partial H_x''}{\partial z''}\right)^2 + \left(\frac{\partial H_y''}{\partial z''}\right)^2\right\} \right]$$

the second term in the previous expression vanishing since it is an odd function: Hence contribution to the free energy

$$\simeq \text{Volume}\chi\left\{\left[H_x^2\cos^2\phi + H_x^2\sin^2\phi\cos^2\right] + \right.$$

$$\left. + \frac{a}{3}\left[\left(\frac{\partial H_x}{\partial 2}\right)^2\cos^2\phi + \left(\frac{\partial H_x}{\partial 2}\right)^2\sin^2\phi\sin^2\alpha\right]\right\}$$

Thus the torque due to misalignment $= -\frac{\partial(\text{Free energy})}{\partial \phi}$

$$\simeq \text{Volume}\chi\left[H_x^2 2\cos\phi\sin\phi(1-\cos^2\alpha) + \frac{2a}{3}\left(\frac{\partial H_x}{\partial z}\right)^2\cos\phi\sin\phi\right.$$
$$\left.(1-\cos^2\alpha)\right]$$

Using the tabulated data for the balance (D.Griffiths, Thesis)[77] a couple of one dyne cm is roughly equivalent in effect to a direct force of one dyne, thus:

$$\frac{\text{Tortional force}}{\text{Direct force}} = \frac{2\cos\phi\sin\phi(1-\cos^2\alpha)\left(H_x^2 + a/3\left(\frac{\partial H_x}{\partial z}\right)^2\right)}{H_x\,\partial H_x/\partial z}$$

Using $H_x = 5 \times 10^3$ gauss; $\partial H_x/\partial z = 9 \times 10^2$ gauss/cm; $\alpha = \phi = 5^\circ$ and $a = .05$ cms, the ratio $\simeq 3 \times 10^{-3}$, giving a 1/3% effect.

Demagnetizing effects

Following the above scheme, and using

$M_x'' = M_x \cos\phi + M_y \sin\phi$

$M_y'' = M_y \cos\phi \cos\alpha - M_x \sin\phi \cos\alpha - M_z \sin\alpha$

$M_z'' = M_z\cos\alpha + M_y \cos\phi \sin\alpha - M_x \sin\phi \sin\alpha$

Writing the contribution, via demagnetising effects, of these magnetisation to the free energy as :

$$N_x''M_x''^2 + N_y''M_y''^2 + N_z''M_z''^2$$

where the N's are the appropriate demagnetising factors and

$$N_x'' + N_y'' + N_z'' = 4\pi$$

For a thin disc arranged as indicated in the previous figure

$$N_x'' \simeq N_y'' \simeq 0: \quad N_z'' \simeq 4\pi$$

Hence Torque due to demagnetising fields $\simeq 8\pi M_x^2 \sin^2\alpha \cdot \sin\phi\cos\phi$ and the ratio

$$\frac{\text{Torque}}{\text{Force}} = \chi \cdot 8 \frac{H_x \sin^2\alpha \sin\phi\cos\phi}{\partial H_x/\partial z}$$

which is clearly vanishingly small.

APPENDIX SEVEN

Using equation (1.9) :

$$\chi = \frac{N}{kTB} \sum_i |\langle i|\mu_z|i\rangle|^2 e^{-E_i/kT} - \frac{2N}{B} \sum_{\substack{i,i' \\ i\neq i'}} \frac{|\langle i|\mu_z|i'\rangle|^2 e^{-E_i/kT}}{E_i - E_{i'}}$$

where $B = \sum_i e^{-E_i/kT}$

Expand all exponentials thus: $e^{-E_i/kT} = 1 - E_i/kT + \frac{1}{2}(\frac{E_i}{kT})^2$

The first term in the above expression for becomes:

$$\frac{N}{kT} \sum_i \frac{|\langle i|\mu_z|i\rangle|^2 (1-E_i/kT)}{(2J+1)(1 - \frac{1}{(2J+1)} \sum_i E_i/kT)} =$$

$$= \frac{N}{kT(2J+1)} \sum_i |\langle i|\mu_z|i\rangle|^2 (1-E_i/kT).(1-\frac{1}{(2J+1)} \sum_i E_i/kT)^{-1}$$

$$= \frac{N}{kT(2J+1)} \left\{ \sum_i |\langle i|\mu_z|i\rangle|^2 - \frac{1}{kT} \sum_i E_i |\langle i|\mu_z|i\rangle|^2 + \right.$$

$$\left. + \frac{1}{(2J+1)kT} \sum_i E_i . \sum_i |\langle i|\mu_z|i\rangle|^2 \right\}$$

and to terms of $O(\frac{1}{T^2})$, this becomes:-

$$= \frac{N}{kT(2J+1)} \sum_i |\langle i|\mu_z|i\rangle|^2 - \frac{N}{k^2T^2(2J+1)^2} \cdot$$

$$\left\{ (2J+1) \sum_i E_i |\langle i|\mu_z|i\rangle|^2 - \sum E_i \sum_i |\langle i|\mu_z|i\rangle|^2 \right\}$$

The second term in the expression for χ becomes:

$$-\frac{2N}{(2J+1)}\sum_{\substack{i\neq i'\\ i,i'}}\frac{|\langle i|\mu_z|i'\rangle|^2}{E_i-E_{i'}}\left(1-\frac{E_i}{kT}+\frac{1}{2}\left(\frac{E_i}{kT}\right)^2\right).$$

$$\left(1+\frac{\sum E_i}{kT(2J+1)}+\frac{\sum E_i^2}{(kT)^2(2J+1)}\right)$$

$$=-\frac{N}{(2J+1)}\left\{\sum_{i\neq i'}\frac{|\langle i|\mu_z|i'\rangle|^2}{E_i-E_{i'}}\left(1-\frac{E_i}{kT}+\frac{1}{2}\left(\frac{E_i}{kT}\right)^2-\right.\right.$$

$$\left.\left.-1+\frac{E_{i'}}{kT}-\frac{1}{2}\left(\frac{E_{i'}}{kT}\right)^2\right)\right\}\left(1+\frac{\sum E_i}{(2J+1)kT}+\frac{\sum E_i^2}{(2J+1)(kT)^2}\right)$$

$$=\frac{N}{(2J+1)}\sum_{i\neq i'}\frac{|\langle i|\mu_z|i'\rangle|^2}{kT}-$$

$$-\frac{N}{(2J+1)^2(kT)^2}\sum_{i\neq i'}\frac{(2J+1)(E_i+E_{i'})|\langle i|\mu_z|i'\rangle|^2}{2}$$

$$+\frac{N}{(2J+1)^2(kT)^2}\sum_{i\neq i'}|\langle i|\mu_z|i'\rangle|^2\cdot\sum_i E_i+\text{terms } O\left(\frac{1}{T^3}\right)$$

thus to terms of $O(\frac{1}{T^2})$:

$$=\frac{N}{(2J+1)}\sum_{i\neq i'}\frac{|\langle i|\mu_z|i'\rangle|^2}{kT}-\frac{N}{(2J+1)^2(kT)^2}\cdot$$

$$\left\{(2J+1)\sum_{i\neq i'}E_i|\langle i|\mu_z|i'\rangle|^2-\sum_{i\neq i'}E_i\cdot\sum_{i\neq i'}|\langle i|\mu_z|i'\rangle|^2\right\}$$

Combining the two sets of terms:

$$\chi \simeq \frac{N}{kT(2J+1)} \sum_{i,i'} |\langle i|\mu_z|i'\rangle|^2 - \frac{N}{(2J+1)^2(kT)^2} \cdot$$

$$\left\{(2J+1)\sum_{i,i'} E_i|\langle i|\mu_z|i'\rangle|^2 - \sum_{i,i'} E_i \sum_{i,i'}|\langle i|\mu_z|i'\rangle|^2\right\}$$

For $= \frac{C}{T+\Delta} \quad \frac{C}{T} - \frac{C\Delta}{T^2}$ ... then

$$\Delta = \frac{1}{k}\frac{\left\{(2J+1)\sum_{i,i'} E_i|\langle i|\mu_z|i'\rangle|^2 - (\sum_{i,i'} E_i).(\sum_{i,i'}|\langle i|\mu_z|i\rangle|^2\right\}}{(2J+1)\sum_{i,i'}|\langle i|\mu_z|i'\rangle|^2}$$

however $\langle i|\mu_z|i\rangle \alpha \langle i|J_z|i'\rangle$, and $\sum_{i,i'}|\langle i|J_2|i'\rangle|^2 E_i$

$= \sum_{i,i'}\langle i|J_2^2|i'\rangle E_i$ [109]

hence

$$\sum_{i,i'} E_i|\langle i|\mu_z|i'\rangle|^2 \alpha \sum_{i,i'} E_i\langle i|J_2^2|i\rangle$$

and for cubic symmetry at least

$$\sum_{i,i'} E_i\langle i|J_2^2|i'\rangle = \frac{1}{3}\sum_{i,i'} E_i\langle i|J_x^2+J_y^2+J_2^2|i'\rangle$$

$$= \frac{1}{3}\sum_{i,i'} E_i\langle i|\bar{J}^2|i'\rangle = \frac{J(J+1)}{3}\Sigma E_i$$

Clearly then, for cubic symmetry, Δ is zero.

APPENDIX EIGHT

A discussion of hyperfine effects. Neglecting the contribution associated with the nuclear term, i.e. since $g_I \sim 10^{-3}$.

In (I, J, F, M_F) representation the effective moment is found (in the approximation in which nuclear effects are neglected) by projecting $\underline{J}$ onto $\underline{F}$:

Thus:

$$\underline{\mu}eff = - g_J \mu_B \frac{(\underline{J}.\underline{F})}{\underline{F}} \underline{F}(\text{unit vector}) = - g_J \mu_B \frac{(\underline{J}.\underline{F})\ \underline{F}}{F(F+1)}$$

then

$$(\underline{\mu}eff)^2 = \underline{\mu}eff.\underline{\mu}eff = g^2 \mu_B^2 \frac{(\underline{J}.\underline{F})^2 \underline{F}.\underline{F}}{(F(F+1))^2} = \frac{(g\mu_B(\underline{J}.\underline{F}))^2}{F(F+1)}$$

In (I, J, M_I, M_J) representation, i.e. when the hyperfine coupling is broken, then:

$$\underline{\mu}eff = - g_J \mu_B \underline{J} \quad \text{and} \quad (\underline{\mu}eH)^2 = g^2 \mu_B^2 J(J+1)$$

Hence $$\frac{\mu eff(F)}{\mu\ eff(J)} = \sqrt{\frac{(\underline{J}.\underline{F})^2}{J(J+1)F(F+1)}}$$

The form of hyperfine coupling is usually represented as a $\underline{I}.\underline{J}$.

1. Positive 'a'

In the low temperature limit, this situation favours an anti-parallel $\underline{I}$ and $\underline{J}$

(a) $|J| > |I|$

In the lowest energy configuration:

$$F = J - I$$

then $2(\underline{J}.\underline{F}) = (\underline{F})^2 + (\underline{J})^2 - (\underline{I})^2 = F(F+1)+J(J+1)-I(I+1)$

$= (J-I)(J-I+1)+J(J+1)-I(I+1) = J^2-2JI+I^2+J-I+J^2$

$+ J-I^2-I = 2J^2-2JI+2J-2I = 2\{J(J-I)+(J-I)\}$

$= 2(J+1)(J-I) = 2(J+1)F$

hence $$\frac{\mu eff(F)}{\mu eff(J)} = \sqrt{\frac{(J+1)^2F^2}{J(J+1)F(F+1)}} = \sqrt{\frac{(J+1).F}{J\ (F+1)}} = \sqrt{\frac{1+1/J}{1+1/F}}$$

since $J > F$, in view of antiparallel coupling, then $1/F > 1/J$ $\therefore$ $\underline{\mu eff(F) < \mu eff(J)}$

(b) $|I| > |J|$

In the lowest energy configuration:

$$F = I - J$$

then $2\underline{J}.\underline{F} = (I-J)(I-J+1)+J(J+1)-I(I+1) = -2JF$

hence $$\frac{\mu eff(F)}{\mu eff(J)} = \sqrt{\frac{J^2F^2}{J(J+1)F(F+1)}} = \frac{1}{\sqrt{(1+\frac{1}{J})(1+\frac{1}{F})}}$$

$\therefore$ $\underline{\mu eff(F) < \mu eff(J)}$

2. Negative 'a'

Implies parallel coupling at the lowest temperature, and whether $|\underline{J}| > |\underline{I}|$ or the other way

$$F = J + I$$

$$2\underline{J}.\underline{F} = (J+I)(J+I+1) + J(J+1) - I(I+1) = 2J(F+1)$$

then $$\frac{\mu eff(F)}{\mu eff(J)} = \sqrt{\frac{JJ^2(F+1)^2}{J(J+1)F(F+1)}} = \sqrt{\frac{1 + 1/F}{1 + 1/J}}$$

Parallel coupling implies that $F > J$, hence $1/J > 1/F$

$$\therefore \quad \underline{\mu eff(F) < \mu eff(J)}$$

These results imply that the breakdown of hyperfine coupling should give rise to (M-H) curvature of the opposite sense to that observed.

Estimating the effect in Holmium

For Ho^{+++}, J=8, I=7/2[110], and 'a' is positive[111]. Then, in the above approximation :

$|F| = J-I = 9/2$ and $\mu eff(F)/\mu eff(J) = 9/\sqrt{88}$

- about a 4% effect.

However such an effect would have little chance of being observed due to the complicating effects of nuclear -4f electric quadrupole interaction.

REFERENCES

1. Messiah, A. : "Quantum Mechanics", Vol.1, p.67; North Holland (Amsterdam), 1964
2. Van Vleck, J.H.: "The Theory of Electric and Magnetic Susceptibilities", p.181 et.seq; Oxford University Press, 1932
3. Modified from: Kittel, C. : "Introduction to Solid State Physics", p.446; J.Wiley (New York), 1966
4. Mott, N.F. and Jones, H.: "The Theory of the Properties of Metals and Alloys", p.186; Dover (New York), 1936
5. Van Leeuwen, J.H. : Dissertation, Copenhagen, 1919, and J.de Physique; (6)2, 361, 1921
6. Landau, L.D. : Zeit.f.Phys; 64, 629, 1930
7. Peierls, R.E. : Zeit.f.Phys; 80, 786, 1933
8. Hebborn, J.E.,: Luttinger, J.M., Sondheimer, E.H. and Stiles, P.J. : J.Phys.Chem.Solids; 25, 741, 1964
9. Nakajima, S. : Adv.in Phys; 4, 363, 1955
10. Brillouin, L.; J.de Physique; 8, 74, 1927
11. Friedel, J. : Nuovo Cimento; 7, 287, 1958

12. Ziman, J.M. : "Electrons and Phonons", p.159; Clarendon Press, 1960

13. Koster, G.F. and Slater, J.C. : Phys.Rev; 96, 1208, 1954

14. Rojansky, V. : "Quantum Mechanics", p.222; Prentice Hall (New York), 1949

15. Blandin, A. and Friedel, J. : J.Phys.Rad; 20, Fig.2, 1959

16. Friedel, J.: Can.J.Phys; 34, 1190, 1956

17. Wolff, P.A. : Phys.Rev.; 124, 1030, 1961

18. Anderson, P.W.: Phys.Rev.; 124, 41, 1961

19. Kittel, C. : "Quantum Theory of Solids", p.113; J.Wiley (New York), 1963

20. Ziman, J.M.: "Theory of Solids", p.126; Cambridge University Press, 1964

21. Friedel, J. : Ann.Phys., 9, 166, 1954

22. Friedel, J. : Phil.Mag; 43, 153, 1952

23. de Casteljau, P. and Friedel, J. : J.Phys.Rad.; 17, 27, 1956

24. Kohn, W. and Vosko, S.H. : Phys.Rev.; 119, 912, 1960

25. Burcham, W.E. : "Nuclear Physics", p.516; Longmans (London), 1963

26. Cohen, M.H. and Reif, F.: "Solid state Physics", Vol.5, p.321; Academic Press (New York), 1957

27. Rowland, T.J.: Phys.Rev.; 119, 903, 1960

28. March, M.H. and Murray, A.M.: Proc.Roy.Soc.; A261, 119, 1961

29. Landau, L.D. and Lifshitz, E.M. : "Quantum Mechanics", p.38; Pergamon Press (London), 1965

30. Weiss, P. : J.Phys.Rad.; 4, 661, 1907

31. Dirac, P.A.M. : Proc.Roy.Soc., A123, 714, 1929

32. Stoner, E.C.: Proc.Roy.Soc.; A165, 372, 1938

33. Wolfarth, E.P.: Phil.Mag; 43, 374, 1951

34. Lidiard, A.B.: Proc.Roy.Soc., A224 , 161, 1954

35. Smart,J.S.:"Effective Field theories of Magnetism", Saunders (London), 1966

36. Zener, C. : Phys.Rev.; 81, 440, 1951

37. Yosida, K. : Phys.Rev.; 106, 893,1957

38. Kasuya, T.: Prog.Theor.Phys., 16, 45, 1956

39. Mitchell, A.H., Phys.Rev., 105, 1439, 1957

40. Frohlick, F. and Nabarro,F.R.N.; Proc.Roy.Soc., 115, 382, 1940

41. Ruderman, M.A. and Kittel, C.; Phys.Rev.; 96, 99, 1954

42. Freeman,A.J. and Watson, R.E.; Phys.Rev., 152, 566, 1966

43.
Ref.114, and Low, G.G.: Proc.International Conference on Magnetism (Nottingham, 1964); I.P.P.S. (London), 1965

44. de Gennes, P. : J.Phys.Rad.; 23, 630, 1962

45. Blandin, A. and Friedel, J. : J.Phys.Rad.; 20, 160, 1959

46. Caroli, B.: Thesis, University of Paris, 1966

47. Daniel, E. and Friedel, J. : Proc.Low.Temp.Conf. IX (Columbus), p.950; Plenum Press (New York) 1965

48. Sato,H., Kikuchi, R., and Arrott, A. : J.PHys.Chem. Solids; 10, 19, 1959

49. Opechowski, W. : Physica; 4, 181, 1937

50. Doniach, S. : to be published

51. de Gennes, P. : J.Phys.Rad.; 23, 510, 1962

52. Overhauser, A.W. : J.Phys.Chem.Solids, 13, 71, 1960

53. Marshall, W. : Phys.Rev.; 118, 1519, 1960

54. Klein, M. : Phys.Rev.Letters, 11, 408, 1963

55. Klein, M. and Brout, R. : Phys.Rev.; 132, 2412, 1963

56. Wigner, E.P. :"Group theory, and its application to the Quantum Mechanics of Atomic Spectra", Academic Press (New York), 1959

57. Bathe, H. : Ann.Phys., 3, 133, 1929

58. Bleaney, B. and Stevens, K.H.W. : Rep.Prog.Phys. 16, 108, 1953

59. Ref.57, and Overhauser, A.W. : Phys.Rev.; 101, 1702, 1956

60. For example, see, Tinkham,M. : "Group theory and Quantum Mechanics", p.133, McGraw-Hill (New York), 1964

61. Kramers, H. : Proc.Acad.Sci. Amsterdam; 33, 959, 1930

62. Stevens, K.H.W. : Proc.Phys.Soc., 65A, 209, 1952

63. Opechowski,W. : Physica; 7, 552, 1940

64. Rider, P.E., Gschneidner, K.A. and McMasters, O.D. Trans.Met.Soc.Aime; 233, 1488, 1965

65. Sugawara,T. : Soga, R. and Yamase, I. : J.Phys. Soc.(Japan); 19, 780, 1964

66. Bijvoet,J., de Hon.B., Dekker, J.A. and Van Beek, F. Solid State Comms; 3, 289, 1966

67. Arjas, S. and Dunmyre, G.R.; J. Less Common Metals; 10, 220, 1966

68. Lowin, R.J. : to be published

69. Bijvoet, J., et al: Ref.66; Figures 2(a) and (b)

70. Zimmerman, J.E., Arrot, A. and Shinozaki, S. Proc. 1966, Low Temp.Calorimetry Conf. (Helsinki)

71. Lounasmaa, O.V. : Phys.Rev., 128, 1136, 1962

72. Pickett, G.R. : Phys. Letters, 21, 618, 1966

73. Gainon, D., Donze, P. and Sierro, J. : Solid State Comms.; 5, 151, 1967

74. Kondo, J.; Prog.Theor.Phys., 34, 372, 1965

75. de Vroomen, A.R. and Potters, M.L.; Physica, 27, 1083, 1961

76. Foiles, C.L. : to be published

77. Griffiths, D. : Thesis, University of London, 1961

78. Hoare, F.E. and Matthews,J. : Proc.Roy.Soc., 212, 139, 1952

79. Hoare, F.E. and Walling,F. : Proc.Phys.Soc., 64B, 337, 1951

80. J. of Research (N.B.S.); 64A, 5, 1960

81. Clement, J.R. and Quinell, E.H., : Rev.Sci.Inst.; 23, 213, 1950

82. Powell, R.L., Brunch, M.D. and Corruccini, : Cryogenics, 139, 1961

83. "Rubber Handbook", p.1143; The Chemical Rubber Publishing Co. (Ohio), 1961

84. Wasink, J.H. : Thesis, University of London, 1964

85. Wilson, A.H. : "Thermodynamics and Statistical Mechanics", p.282; Cambridge University Press, 1960

86. Hurd, C.M. : J.Phys.Chem.Solids; 27 (No.9), 16,1966

87. Low, W. : "Paramagnetic Resonance in Solids", p.113; Academic Press (New York), 1960

88. Bleaney, B. and Scovil, H.E.D. : Proc.Phys.Soc; 64A, 204, 1951

89. Gschneidner, K.A. : "Rare Earth Alloys", p.280, D.Van Nostrand Company (New York), 1961

90. Owen, J., Brown, M.E., Knight, W.D., and Kittel, C. Phys.Rev; 102, 1501, 1956

91. du Chatenier, F.J. : Thesis, Leiden, 1965

92. Zimmerman, J.E. and Hoare, F.E. : J.Phys.Chem. Solids, 17, 52, 1960

93. Schmitt, R.N. and Jacobs, I.S. : J.Phys.Chem. Solids, 3, 324, 1957

94. Griffiths, D. and Coles, B.R. : Phys.Rev.Letters, 16, 1093, 1966

95. Kahle, H.G. : Zeit.f.Phys., 161,486, 1961

96. Lea, K.R., Leask, M.J.M. and Wolf, W.P. J.Phys.Chem.Solids, 23, 1381, 1962

97. Stevens, K.H.W. and Elliot, R.J. : Proc.Phys.Soc. 219A, 387, 1953

98. Dicke, R.H. and Wittke, J.P. : "Introduction to Quantum Mechanics", p.279; Addison-Wesley (Massachusetts), 1960

99. Bleaney, B. : Proc.Phys.Soc., 73, 979, 1959

100. Hirst, L.L. : to be published

101. Markowitz, D. and Kadanoff, L.P. : Phys.Rev., 131, 563, 1963

102. Abrikosov,A. and Gor'kov, L.P. : Soviet Phys. (Translation) - J.E.P.T., 10,593,1960

103. Bloembergen, N. J.App.Phys., 23,1379, 1952

104. Korringa, J. : Physica, 16, 601, 1950

105. See, for example, Orbach, R. : Proc.Phys.Soc., A264, 458, 1961; Bierig, R.W., Weber,M.J. and Warshaw, S.I. : Phys.Rev., 134,1504,1964

106. Modified from: Peter, M., Dupraz, J. and Cottet, H. to be published.

107. Modified from: Slichter, C.P. "Principles of Magentic Resonance", p.126; Harper and Row, (New York), 1964

108. Konyukhov, V.K., Pashimin, P.P. and Prokhorov,A.M., Soviet Phys. (Translation) - Solid State, 4, 175, 1962

109. Van Vleck, J.H. :"The Theory of Electric and Magnetic Susceptibilities", p.141; Oxford University Press, 1932

110. Ramsay, N. : "Molecular Beams", p.175; Clarendon Press, 1956

111. Al'Tshuler, S.A. and Kozyrev, B.M. : "Electron Paramagnetic Resonance", p.132; Academic Press (New York), 1964

112. Crangle, J. and Lyang, R.B. : Proc. Vth Rare Earth Conf. (1965).

113. Lyang, R.B., Thesis, University of Sheffield, 1963

114. Shaltiel, D., Wernick, J.H., Williams, H.J. and Peter, M. : Phys.Rev., 135, 1346, 1964

115. Schindler, A.I. and Coles. B.R. : Proc. International Conference on Magnetism (Boston, 1967); to be published.

116. Foiles, C.L.; to be published

117. Rice, M.J. : Proc.International Conference on Magnetism (Boston, 1967), to be published

118. Vogt, K. : Ann.Phys., 14, 1, 1932

119. Heine, V. : "The Fermi Surface", p.279, J.Wiley (New York), 1960

120. Allan, G. : Thesis, University of Paris, 1967

121. Hodges, L., Ehrenreich, H. and Lang, N.D., Phys.Rev., 152, 505, 1966

EFFECTIVE MOMENTS DERIVED FROM NOMINAL COMPOSITIONS

The compositions quoted in Chapter 7 are nominal. The effective moments derived from the high temperature slope of the inverse susceptibility versus temperature plots, using these compositions, are given below.

ALLOY	Effective Moment (in Bohr Magnetons)
Ag - 0.8 At.% Gd	8.0
Ag - 0.45 At.% Gd	7.6
Ag - 0.1 At. % Gd	8.0
Ag - 0.55 At. % Tb	9.5
Ag - 0.86 At.% Dy	10.8
Ag - 0.51 At.% Dy	10.9
Ag - 0.35 At.% Ho	10.2
Ag - 0.25 At.% Ho	11.3
Ag - 0.28 At.% Er	9.8
Ag - 1.0 At.% Er	9.8
Ag - 0.5 At.% Tm	7.6
Ag - 0.5 At.% Yb	diamagnetic
Au - 1.0 At.% Er	9.2
Au - 0.3 At.% Tm	7.7
Au - 1.0 At.% Yb	4.3